

Characterization of the Interactions Between High Velocity Jets and Fluidized Particles

(Spine Title: Interactions of High Velocity Jets and Fluidized Particles)

(Thesis format: Integrated-Article)

by

Jennifer McMillan

Graduate Program in Engineering Science
Department of Chemical and Biochemical Engineering

Submitted in partial fulfillment
of the requirements for the degree of
Doctor of Philosophy

Faculty of Graduate Studies
The University of Western Ontario
London, Ontario
November 2006

© Jennifer McMillan 2006



Library and
Archives Canada

Bibliothèque et
Archives Canada

Published Heritage
Branch

Direction du
Patrimoine de l'édition

395 Wellington Street
Ottawa ON K1A 0N4
Canada

395, rue Wellington
Ottawa ON K1A 0N4
Canada

Your file Votre référence

ISBN: 978-0-494-50497-0

Our file Notre référence

ISBN: 978-0-494-50497-0

NOTICE:

The author has granted a non-exclusive license allowing Library and Archives Canada to reproduce, publish, archive, preserve, conserve, communicate to the public by telecommunication or on the Internet, loan, distribute and sell theses worldwide, for commercial or non-commercial purposes, in microform, paper, electronic and/or any other formats.

The author retains copyright ownership and moral rights in this thesis. Neither the thesis nor substantial extracts from it may be printed or otherwise reproduced without the author's permission.

AVIS:

L'auteur a accordé une licence non exclusive permettant à la Bibliothèque et Archives Canada de reproduire, publier, archiver, sauvegarder, conserver, transmettre au public par télécommunication ou par l'Internet, prêter, distribuer et vendre des thèses partout dans le monde, à des fins commerciales ou autres, sur support microforme, papier, électronique et/ou autres formats.

L'auteur conserve la propriété du droit d'auteur et des droits moraux qui protègent cette thèse. Ni la thèse ni des extraits substantiels de celle-ci ne doivent être imprimés ou autrement reproduits sans son autorisation.

In compliance with the Canadian Privacy Act some supporting forms may have been removed from this thesis.

Conformément à la loi canadienne sur la protection de la vie privée, quelques formulaires secondaires ont été enlevés de cette thèse.

While these forms may be included in the document page count, their removal does not represent any loss of content from the thesis.

Bien que ces formulaires aient inclus dans la pagination, il n'y aura aucun contenu manquant.

THE UNIVERSITY OF WESTERN ONTARIO
FACULTY OF GRADUATE STUDIES

CERTIFICATE OF EXAMINATION

Joint-Supervisor

Dr. Cedric Briens

Joint-Supervisor

Dr. Franco Berruti

Supervisory Committee

Dr. Edward Chan

Examiners

Dr. Amarjeet Bassi

Dr. Shahzad Barghi

Dr. Jerzy Floryan

Dr. Ted Knowlton

The thesis by

Jennifer McMillan

entitled:

**Characterization of the Interactions Between High Velocity Jets and
Fluidized Particles**

is accepted in partial fulfillment of the
requirements for the degree of
Doctor of Philosophy

Date _____

Chair of the Thesis Examination Board

ABSTRACT

The research work presented in this investigation deals with experimental and modeling studies involving the injection of high velocity gas-liquid and gas-only jets into fluidized beds. These types of jets occur in many industrial applications, and in particular, the heavy oil upgrading process of fluid bed coking.

High velocity gas attrition nozzles are used in the fluid coking process to control the particle size in the reactor. Different high velocity attrition nozzles and operating conditions were tested in order to determine the effects of fluidization velocity, nozzle size, nozzle geometry, bed material and attrition gas properties on the grinding efficiency. An empirical correlation was also developed to estimate the grinding efficiency.

Using the data from the attrition nozzle study, a model was developed to describe particle attrition when a sonic velocity gas jet was injected into a fluidized bed. The model predicts the particle size distribution of ground particles, the particle breakage frequency and the proportion of original particles in the bed which were not ground.

Different high velocity attrition nozzle designs which promoted particle entrainment and mixing were tested to improve the grinding efficiency. The highest grinding efficiencies were obtained with a new design, a shroud that was placed around the nozzle. A draft tube placed downstream of the nozzle also greatly increased the grinding efficiency.

The draft tube was applied to a gas-liquid injection nozzle in order to improve the mixing between injected liquids and fluidized particles. During the fluid coking process uniform contact between the liquid feed droplets and entrained particles is essential for high yields. A quick method has been developed that uses thermal tracers to characterize the solid-liquid mixing.

This measurement technique was then applied to a new technology which consists of a downer with a mixing chamber located at its entrance. The quality of mixing between injected liquid feed and circulating solid particles in a downer mixing chamber was measured for different mixing chamber geometries.

To achieve the best results, a mixing chamber should provide a stable liquid-solid dispersion. A novel technique was developed in which the signals from tribo-electric probes were analyzed to determine the stability of the flow in the downer.

Keywords:

fluidized bed, fluid coking, sonic velocity jets, solids entrainment, particle attrition, solid-liquid mixing, draft tube mixer, shroud, downer, mixing chamber, tribo-electric probes

CO-AUTHORSHIP

The journal articles written from the present thesis work are listed below, and the individual contributions of all members are indicated.

Chapter 2

Article Title: High Velocity Attrition Nozzles in Fluidized Beds
Authors: Jennifer McMillan, Cedric Briens, Franco Berruti, and Edward Chan
Status: Submitted to <i>Powder Technology</i> (2006).
This article was written by Jennifer McMillan who also conducted all of the experimental work and performed the data analysis. The work was jointly supervised by Cedric Briens, Franco Berruti and Edward Chan. Various drafts of the article were reviewed by Cedric Briens and Franco Berruti.

Chapter 3

Article Title: Modeling the Particle Attrition Mechanism of a Sonic Gas Jet Injected into a Fluidized Bed
Authors: Jennifer McMillan, Cedric Briens, Franco Berruti, and Edward Chan
Status: Submitted to <i>Chemical Engineering Science</i> (2006).
This article was written by Jennifer McMillan who also conducted all of the experimental work and performed the data analysis. The data was analyzed using a program written by Cedric Briens. The work was jointly supervised by Cedric Briens, Franco Berruti and Edward Chan. Various drafts of the article were reviewed by Cedric Briens and Franco Berruti.

Chapter 4

Article Title: Methods of Improving Particle Attrition in Fluidized Beds
Authors: Jennifer McMillan, Craig Hulet, Cedric Briens, and Franco Berruti
Status: Unpublished (pending patent)
This article was written by Jennifer McMillan who also conducted all of the experimental work and performed the data analysis. Craig Hulet had the original idea for the shroud, which was used in this paper. Craig Hulet also assisted in some of the experimental work. The work was jointly supervised by Cedric Briens and Franco Berruti. Various drafts of the article were reviewed by Cedric Briens and Franco Berruti.

Chapter 5

Article Title: Characterization of the Contact Between Liquid Spray Droplets and Particles in a Fluidized Bed
Authors: Jennifer McMillan, David Zhou, Siva Ariyapadi, Cedric Briens, Franco Berruti and Edward Chan
Status: Published in <i>Industrial and Engineering Chemistry Research</i> 44 , 4931-4939 (2005).
This article was written by Jennifer McMillan who also conducted all of the experimental work and performed the data analysis. The thermal tracer measurement technique used in this study was developed by Jennifer McMillan. David Zhou assisted in the experimental work, and a model developed by Siva Ariyapadi was used to predict the flux of solids entering the jet. Programs written by Cedric Briens were used to analyze the data. The work was jointly supervised by Cedric Briens, Franco Berruti and Edward Chan. Various drafts of the article were reviewed by Cedric Briens and Franco Berruti.

Chapter 6

Article Title: Measurement Techniques to Characterize the Contact Between Injected Liquid and Circulating Solids in a Downer Mixing Chamber
Authors: Jennifer McMillan, David Zhou, Mohammad Saberian, Cedric Briens, and Franco Berruti
Status: Published in <i>Powder Technology</i> 161 , 175-184 (2006).
This article was written by Jennifer McMillan who also conducted all of the experimental work and performed the data analysis. The thermal tracer measurement technique used in this study was developed by Jennifer McMillan. David Zhou assisted in the experimental work, and Mohammad Saberian provided general guidance. Programs written by Cedric Briens were used to analyze the data. The work was jointly supervised by Cedric Briens and Franco Berruti. Various drafts of the article were reviewed by Cedric Briens and Franco Berruti.

Chapter 7

Article Title: Flow Stability in a Downer Mixing Chamber
Authors: Jennifer McMillan, Cedric Briens, and Franco Berruti
Status: Published in <i>Chemical Engineering and Processing</i> 45 , 798-805 (2006).
This article was written by Jennifer McMillan who also conducted all of the experimental work and performed the data analysis. Programs written by Cedric Briens were used to analyze the data. The work was jointly supervised by Cedric Briens and Franco Berruti. Various drafts of the article were reviewed by Cedric Briens and Franco Berruti.

Appendix A

Article Title: Visualization of the Effect of a Shroud on Entrainment of Fluidized Solids into a Gas Jet
Authors: Craig Hulet, Jennifer McMillan, Cedric Briens, Franco Berruti and Edward Chan
Status: Unpublished (pending patent and review/approval by Syncrude Canada Ltd.)
The study was performed after a suggestion by Cedric Briens and Franco Berruti. Craig Hulet and Jennifer McMillan conducted the set-up and acquisition jointly. Craig Hulet performed the qualitative analysis of the results and wrote the manuscript. Various drafts of the article were reviewed by Cedric Briens and Franco Berruti.

Appendix B

Article Title: Measurement Technique for the On-Line Detection of Fines in a Fluidized Bed
Authors: Matthew Dawe, Jennifer McMillan, Cedric Briens, and Franco Berruti
Status: Unpublished (pending patent)
This work was supervised by Cedric Briens and Franco Berruti. All experiments were performed by Matthew Dawe and Jennifer McMillan. The correlation development was conducted jointly by Matthew Dawe and Jennifer McMillan, with suggestions from Cedric Briens and Franco Berruti. The manuscript was written jointly by Matthew Dawe and Jennifer McMillan. Various drafts of the article were reviewed by Cedric Briens and Franco Berruti.

ACKNOWLEDGEMENTS

I wish to extend my sincere thanks and gratitude to my supervisors and mentors Dr. Cedric Briens and Dr. Franco Berruti. They kindly and generously gave of their time and expertise to assist me with my research. Their support and guidance throughout my studies was invaluable and truly appreciated. Being a member of the Western Fluidization Group (WFG) has been a very positive experience and has provided me with many unique opportunities for which I am extremely grateful.

I would also like to thank Dr. Edward Chan for his advice and support during my internship at Syncrude Canada Limited's Research Facility. His enthusiasm, knowledge and the valuable insights he provided into the world of industry enhanced my development as a professional engineer and were very much appreciated.

I am grateful for the financial support from Syncrude Canada Ltd. and the Ontario Graduate Scholarship Program. Thanks also to the Natural Sciences and Engineering Research Council (NSERC) for an Industrial Postgraduate Scholarship (IPS-2), which allowed me to gain valuable work experience in an industrial setting.

Special thanks to Clayton Cook and the University Machine Services for all of their help with my experimental equipment. Thank you also to Stephen and Jim from Stores, The Electronics Shop, and the Information and Technology Group for their assistance during my research. I would also like to mention my appreciation for all of the help and support that the Faculty and Staff members of the Department of Chemical and Biochemical Engineering have provided.

I also wish to acknowledge my colleagues from the Western Fluidization Group. I sincerely thank Matt, Siva, David, Mohammad, Peter, Craig, Sarah, Federica, Mike and Katherine who all helped me during the course of my research work.

Finally, I would especially like to thank my family who has always supported and encouraged me in all of my endeavours.

DEDICATIONS

This thesis is dedicated to my family.

TABLE OF CONTENTS

CERTIFICATE OF EXAMINATION	ii
ABSTRACT.....	iii
CO-AUTHORSHIP	v
ACKNOWLEDGEMENTS.....	ix
DEDICATIONS.....	x
TABLE OF CONTENTS.....	xi
LIST OF TABLES.....	xvi
LIST OF FIGURES	xvii
LIST OF APPENDICES.....	xxiii
NOMENCLATURE	xxiv

Chapter 1: Introduction

1.1 Applications of the Injection of High Velocity Jets into Fluidized Beds.....	1
1.1.1 Applications Involving Gas Injection into Fluidized Beds.....	2
1.1.2 Applications Involving Gas-Liquid Injection into Fluidized Beds.....	3
1.2 The Fluid Coking Process.....	5
1.2.1 Background Information.....	5
1.2.2 Motivation for Research.....	7
1.3 Interactions Between High Velocity Jets and Fluidized Particles - Literature Review.....	9
1.3.1 Gas Jets in Fluidized Beds.....	9
1.3.1.1 Modeling Particle Attrition.....	12
1.3.1.2 Methods of Improving Particle Attrition.....	14
1.3.2 Liquid Injection into Conventional Fluidized Beds.....	17
1.4 Research Objectives.....	21
1.5 References.....	24

Chapter 2: High Velocity Attrition Nozzles in Fluidized Beds

2.1 Introduction.....	31
2.2 Experimental Set-Up.....	35

2.3 Results and Discussion.....	39
2.4 Conclusion.....	54
2.5 Nomenclature.....	55
2.6 References.....	55

Chapter 3: Modeling the Particle Attrition Mechanism of a Sonic Gas Jet Injected into a Fluidized Bed

3.1 Introduction.....	58
3.2 Experimental.....	61
3.2.1 Model Development.....	64
3.2.2 Model Calculation Procedure.....	70
3.3 Results and Discussion.....	76
3.4 Conclusions.....	88
3.5 Nomenclature.....	89
3.6 References.....	90

Chapter 4: Methods of Improving Particle Attrition in Fluidized Beds

4.1 Introduction.....	92
4.2 Experimental Set-Up.....	94
4.2.1 Attrition Tests.....	94
4.2.1.1 Nozzle Designs.....	96
4.2.2 Solids Entrainment Tests.....	100
4.3 Results and Discussion.....	102
4.4 Conclusion.....	117
4.5 Acknowledgements.....	118
4.6 Nomenclature.....	118
4.7 References.....	118

Chapter 5: Characterization of the Contact Between Liquid Spray Droplets and Particles in a Fluidized Bed

5.1 Introduction.....	120
-----------------------	-----

5.2 Experimental Setup.....	123
5.2.1 Theory.....	127
5.3 Results and Discussion.....	129
5.4 Conclusion.....	141
5.5 Acknowledgements.....	141
5.6 Nomenclature.....	141
5.7 References.....	142

Chapter 6: Measurement Techniques to Characterize the Contact Between Injected Liquid and Circulating Solids in a Downer Mixing Chamber

6.1 Introduction.....	144
6.2 Experimental Set-Up.....	146
6.2.1 Temperature Method.....	150
6.2.2 Tribo-Electric Method.....	151
6.3 Results and Discussion.....	155
6.4 Conclusion.....	164
6.5 Acknowledgements.....	164
6.6 Nomenclature.....	164
6.7 References.....	166

Chapter 7: Flow Stability in a Downer Mixing Chamber

7.1 Introduction.....	169
7.2 Experimental Set-Up.....	171
7.2.1 Tribo-Electric Measurement Procedure.....	173
7.3 Results and Discussion.....	175
7.3.1 Raw Signals.....	175
7.3.2 Cross Correlation.....	180
7.3.3 Standard Deviations.....	181
7.3.4 Power Spectrum.....	182
7.3.5 Correlation Dimension.....	183
7.3.6 Hölder Exponent.....	184
7.3.7 Time Averaged Solids Dispersion Over the Downer Cross Section.....	184

7.3.8 Time Averaged Liquid-Solid Dispersion Over the Downer Cross Section.....	186
7.4 Conclusion.....	189
7.5 Acknowledgements.....	190
7.6 Nomenclature.....	190
7.7 References.....	191

Chapter 8: General Discussion

8.1 Key Contributions and Links Between Chapters.....	193
8.1.1 Chapter 2.....	193
8.1.2 Chapter 3.....	194
8.1.3 Chapter 4.....	195
8.1.4 Chapter 5.....	196
8.1.5 Chapter 6.....	198
8.1.6 Chapter 7.....	199
8.1.7 Appendix A.....	199
8.1.8 Appendix B.....	200
8.1.9 Appendix C.....	200
8.2 Comparison Between the Downer and the Draft Tube Mixer.....	201
8.3 Nomenclature.....	203
8.4 References.....	204

Chapter 9: Conclusions and Recommendations

9.1 Conclusions.....	206
9.2 Recommendations.....	209

Appendix A: Visualization of the Effect of a Shroud on Entrainment of Fluidized Solids into a Gas Jet

A.1 Introduction.....	211
A.1.1 Theory.....	212
A.2 Materials and Methods.....	214
A.3 Results and Discussion.....	216
A.3.1 Free Jet.....	219
A.3.2 Shrouded Jet.....	219
A.4 Concluding Remarks.....	220
A.5 Acknowledgements.....	220
A.6 Nomenclature.....	220
A.7 References.....	221

Appendix B: Measurement Technique for the On-Line Detection of Fines in a Fluidized Bed

B.1 Introduction.....	223
B.2 Experimental Setup.....	224
B.3 Results and Discussion.....	226
B.4 Conclusion.....	231
B.5 Nomenclature.....	231
B.6 References.....	232

Appendix C: Solid-Liquid Mixing Results Obtained with a Shrouded Gas-Liquid Nozzle

C.1 Introduction.....	233
C.2 Experimental Setup and Theory.....	233
C.3 Results and Discussion.....	234
C.4 Nomenclature.....	247
C.5 References.....	247

Appendix D: Copyright Permission.....249

CURRICULUM VITAE.....	256
-----------------------	-----

LIST OF TABLES

Table 2.1: Experimental Test Conditions.....	39
Table 2.2: Gas Properties.....	43
Table 4.1: ANOVA Results Comparing the Relative Solids Entrainment for the Type C, Shrouded and Type A Nozzles at a Gas Flowrate of 0.01 kg/s.....	116
Table 5.1: Summary of Measurement Locations and Mixing Indices.....	130
Table 6.1: Mixing Indices for 4-Nozzle Configurations.....	156
Table 6.2: Mixing Indices for 8-Nozzle Configurations.....	156
Table 8.1: Table of Data Comparing Downer to Draft Tube.....	201
Table A.1: Differences Between Free Jet and Shrouded Jet.....	220
Table C.1: Summary of Mixing Indices for Nozzle Y with a Draft Tube.....	235
Table C.2: Comparison Between Nozzle X and Y.....	236

LIST OF FIGURES

Figure 1.1: The Fluid Coking Process.....	7
Figure 1.2: Laval Nozzle.....	12
Figure 1.3: Target System from Dunlop (1958).....	15
Figure 1.4: Concentric Ring Target System from Siegel et al. (1978).....	15
Figure 1.5: Alpine Jet Mill.....	16
Figure 1.6: Confined Jet Intersection from Henderson et al. (1996).....	17
Figure 1.7: Draft tube from Smith et al. (1992).....	17
Figure 2.1: Experimental Set-Up.....	36
Figure 2.2: Type A Nozzle.....	37
Figure 2.3: Type B Nozzle.....	37
Figure 2.4: Type C Nozzle.....	38
Figure 2.5: Effect of Geometry on Grinding Efficiency; Silica Sand; Air; $d_n = 2.4$ mm; $U_g = 0.065$ m/s.....	40
Figure 2.6: Effect of Nozzle Scale on Grinding Efficiency; Silica Sand; Air; Type C Nozzle; $U_g = 0.065$ m/s.....	41
Figure 2.7: Effect of Solid Properties on Grinding Efficiency; Air; $d_n = 2.4$ mm; Type A Nozzle; $U_g = 0.065$ m/s.....	42
Figure 2.8: Effect of Gas Properties and Nozzle Scale on Grinding Efficiency; Silica Sand; Type C Nozzle; $U_g = 0.065$ m/s.....	44
Figure 2.9: Effect of Gas Properties and Nozzle Type on Grinding Efficiency; Silica Sand; $d_n = 2.4$ mm; $U_g = 0.065$ m/s.....	45
Figure 2.10: Effect of Fluidization on Grinding Efficiency; Silica Sand; Air.....	46
Figure 2.11: Effect of Velocity on Grinding Efficiency.....	47
Figure 2.12: Experimental Versus Calculated Grinding Efficiency; Coke; Air; $U_g = 0.065$ m/s.....	49
Figure 2.13: Experimental Versus Calculated Grinding Efficiency; Silica Sand; Type A Nozzle; $U_g = 0.065$	50
Figure 2.14: Experimental Versus Calculated Grinding Efficiency; Silica Sand; Type B Nozzle; $U_g = 0.065$ m/s.....	51
Figure 2.15: Experimental Versus Calculated Grinding Efficiency; Silica Sand; Type C Nozzle.....	52

Figure 2.16: Effect of Temperature on Grinding Efficiency; Silica Sand; Type A Nozzle; $d_n = 2.4$ mm; $P = 300$ psig; Helium.....	54
Figure 3.1: Experimental Equipment.....	61
Figure 3.2: Type A Nozzle.....	63
Figure 3.3: Type B Nozzle.....	63
Figure 3.4: Type C Nozzle.....	63
Figure 3.5: Particle Breakage Mechanism.....	65
Figure 3.6: Coke Particles Before Grinding Process (Magnification: 100X).....	66
Figure 3.7: Coke Particles After Grinding Process (Magnification: 100X).....	67
Figure 3.8: Size Distributions for Limit to Fineness Test.....	68
Figure 3.9a: Model Calculation Procedure Flow Diagram.....	71
Figure 3.9b: Probability Model Procedure for Calculating β	73
Figure 3.10: Comparison of Experimental and Calculated Size Distribution of Ground Particles. $D_N = 2.4$ mm, Type A Nozzle, $V_g = 6.5$ cm/s, $M_{\text{solids}} = 160$ kg.....	77
Figure 3.11: Comparison of Experimental and Calculated Size Distribution of Ground Particles. $D_N = 4.6$ mm, Type C Nozzle, $V_g = 10$ cm/s, $M_{\text{solids}} = 13$ kg.....	78
Figure 3.12: Effect of Grinding Time on F_m	79
Figure 3.13: Effect of Fluidization Velocity on F_m	80
Figure 3.14: Effect of Nozzle Diameter on F_m	81
Figure 3.15: Effect of Nozzle Geometry on F_m	82
Figure 3.16: Effect of Bed Mass on F_m	83
Figure 3.17: Effect of Draft Tube on F_m	84
Figure 3.18: Effect of Nozzle Enhancements on F_m	85
Figure 3.19: Breakage Frequency Versus Grinding Efficiency.....	86
Figure 3.20: Comparison Between Experimental and Calculated Breakage Frequency...	88
Figure 4.1: Experimental Equipment.....	95
Figure 4.2: Base Case Straight Tube Attrition Nozzle (Type C Nozzle).....	96
Figure 4.3: Target Configuration.....	97
Figure 4.4: Cup Configuration.....	97
Figure 4.5: Draft Tube Configuration.....	98

Figure 4.6: Shroud Configuration.....	98
Figure 4.7: Nozzle Inserts Configuration.....	99
Figure 4.8: Spiral Flow Configuration.....	99
Figure 4.9: Laval Type Nozzle (Type A Nozzle).....	100
Figure 4.10: Experimental Setup for Entrainment Tests.....	101
Figure 4.11: Effect of Target on Grinding Efficiency.....	103
Figure 4.12: Effect of Cup on Grinding Efficiency.....	104
Figure 4.13: Effect of Draft Tube on Grinding Efficiency.....	105
Figure 4.14: Effect of 44 mm Diameter Shroud on Grinding Efficiency.....	106
Figure 4.15: Effect of Nozzle Scale on Grinding Efficiency.....	107
Figure 4.16: Effect of Nozzle Inserts on Grinding Efficiency.....	108
Figure 4.17: Effect of Spiral Flow on Grinding Efficiency.....	109
Figure 4.18: Comparison of Grinding Efficiencies for Various Nozzle Enhancements..	110
Figure 4.19: Comparison of Size Distributions of Ground Particles: Draft Tube versus Free Jet.....	111
Figure 4.20: Comparison of Size Distributions of Ground Particles: Shroud versus Free Jet.....	112
Figure 4.21: Comparison of Particle Breakage Frequency, F_m	113
Figure 4.22: Comparison of Relative Solids Entrainment for Different Nozzle Types...	114
Figure 4.23: Effect of Particle Inertia and Entrainment Location on Velocity.....	117
Figure 5.1: Experimental Set-Up.....	124
Figure 5.2: Injection Nozzle.....	124
Figure 5.3: Holder Used to Align Draft Tube with Injection Nozzle and to Position Thermocouples Inside the Draft Tube.....	126
Figure 5.4: Dimensions of Draft Tube and Locations of Positions A, B and C.....	127
Figure 5.5: Comparison of the Coefficient of Variation Obtained with the Experimental Data and Model Data for Various LT for the Draft Tube.....	129
Figure 5.6: L/S Distribution at Locations A, B and C in the Draft Tube.....	133
Figure 5.7: Comparison of L/S Distribution for Free Jet and Draft Tube.....	135
Figure 5.8: Cumulative Distribution of Liquid for Draft Tube $\ell = 1.27$ cm.....	136

Figure 5.9: Cumulative Distribution of Liquid for Draft Tube $\ell = 2.54$ cm.....	137
Figure 5.10a: Cumulative Distribution of Liquid for $L_T = 3.27$ cm.....	138
Figure 5.10b: Cumulative Distribution of Liquid for $L_T = 5.27$ cm.....	138
Figure 5.10c: Cumulative Distribution of Liquid for $L_T = 7.27$ cm.....	139
Figure 5.11: Reproducibility of Data: Cumulative Distribution of Liquid for Draft Tube $\ell = 6.35$ cm.....	140
Figure 6.1: Experimental Apparatus.....	147
Figure 6.2: Orifice Dimensions.....	148
Figure 6.3: Mixing Chamber.....	149
Figure 6.4: Spray Nozzle.....	150
Figure 6.5: Cumulative Liquid Distribution for Configuration #1 – Comparison Between Temperature and Tribo-Electric Techniques.....	155
Figure 6.6: Contour Plots for 4-Nozzle Configurations.....	158
Figure 6.7: Contour Plots of 8-Nozzle Configurations.....	159
Figure 6.8: Cumulative Plots for 4-Nozzle Configurations Using the Circular Orifice Plate.....	160
Figure 6.9: Cumulative Liquid Distribution for 8-Nozzle Configurations Using the Circular Orifice Plate.....	161
Figure 6.10: Contour Plots for 4-Nozzle Configurations Using Tribo-Electric Measurements.....	162
Figure 6.11: Cumulative Distribution Plots for 4-Nozzle Configurations Using Tribo- Electric Method.....	163
Figure 7.1: Mixing Chamber.....	172
Figure 7.2: Mixing Chamber Configuration.....	172
Figure 7.3: Gas-Liquid Injection Nozzle.....	173
Figure 7.4: Probe Locations.....	174
Figure 7.5: Raw Data for Base Case 5% Water.....	176
Figure 7.6: Raw Data for Replicate Run #5.....	177
Figure 7.7: Raw Data for High F_s Case.....	178
Figure 7.8: Raw Data for Low F_s Case.....	179

Figure 7.9: Standard Deviation vs Chunk Length for Each Probe of Replicate Run #1.....	182
Figure 7.10: Power Spectrum for Replicate Run #1.....	183
Figure 7.11: Contour Plot of W_s for Run #1.....	184
Figure 7.12: Contour Plot of W_s for Run #2.....	184
Figure 7.13: Cumulative Solid Distribution.....	185
Figure 7.14: Contour Plot of L/S for Run #1.....	186
Figure 7.15: Contour Plot of L/S for Run #2.....	186
Figure 7.16: Cumulative Liquid Distribution for Replicate Runs.....	187
Figure 7.17: Cumulative Liquid Distribution for Different Startup Conditions.....	188
Figure 7.18: Cumulative Liquid Distribution for 1 Second Chunk Intervals for Run #1.....	189
 Figure 8.1: Cumulative Liquid Distribution for the Free Jet, Draft Tube and Downer...	203
 Figure A.1: Illustration of a Typical Turbulent Submerged Jet.....	212
Figure A.2: Side View of 2.5D Fluidized Bed Used for the Half-Jet Study.....	215
Figure A.3: Half-Jet Nozzle Assembly Showing the Glass Plate, Nozzle and Semi-Cylindrical Shroud.....	216
Figure A.4: Illustration of Entrainment into Horizontal Gas Jet (a) Without Shroud and (b) With Shroud.....	219
 Figure B.1: Schematic Diagram of Fluidized Bed System.....	225
Figure B.2: Simplified Overhead View of Triboelectric Probe Setup.....	226
Figure B.3: Effect of Fluidization Velocity on Triboelectric Signal: $d_{psm} = 132 \mu m$	227
Figure B.4: Effect of Particle Diameter on Triboelectric Signal: $V_g = 0.065 \text{ m/s}$	228
Figure B.5: Effect of Particle Diameter on the Average Triboelectric Signal: $V_g = 0.065 \text{ m/s}$	228
Figure B.6: Comparison Between Experimental and Calculated Results.....	230
Figure B.7: Comparison Between Experimental and Calculated Results Including the Results of Two Critical Tests.....	231
 Figure C.1: Dimensions of Draft Tube and Locations of Positions A, B and C.....	234

Figure C.2: Contour Plots of the L/S Distribution Within the Draft Tube at Locations A, B and C for the Type Y Nozzle.....	238
Figure C.3: Contour Plots of the L/S Distribution Within the Free Jet for the Type Y and Type X Nozzles.....	242
Figure C.4: Cumulative Distribution of Liquid Within the Draft Tube $\ell = 25.4$ mm for the Type Y Nozzle.....	244
Figure C.5a: Cumulative Distribution of Liquid for a Free Jet at $L_T = 96.2$ mm.....	245
Figure C.5b: Cumulative Distribution of Liquid for a Free Jet at $L_T = 116.2$ mm.....	246
Figure C.5c: Cumulative Distribution of Liquid for a Free Jet at $L_T = 136.2$ mm.....	247

LIST OF APPENDICES

Appendix A: Visualization of the Effect of a Shroud on Entrainment of Fluidized Solids into a Gas Jet.....	211
Appendix B: Measurement Technique for the On-Line Detection of Fines in a Fluidized Bed.....	223
Appendix C: Solid-Liquid Mixing Results Obtained with a Shrouded Gas-Liquid Nozzle.....	233
Appendix D: Copyright Permission.....	249

NOMENCLATURE

ΔA_i	Area (m^2)
A_p	Characteristic area (m^2)
ALR	Air-to-liquid ratio
C_D	Drag coefficient (-)
$c_{p,L}$	Specific heat capacity of liquid (kJ/kg $^{\circ}$ C)
$c_{p,S}$	Specific heat capacity of solids (kJ/kg $^{\circ}$ C)
C_v	Coefficient of variation (-)
d	Diameter of nozzle (mm)
d_N	Nozzle diameter (mm)
d_o	Orifice diameter (m)
$d_{P,large}$	Diameter of larger daughter particle (m)
$d_{P,o}$	Diameter of original mother particle (m)
$d_{P,small}$	Diameter of smaller daughter particle (m)
$d_{Pam,a}$	Arithmetic mean diameter of attritable particles (m)
$d_{Pam,o}$	Arithmetic mean diameter of original particles (m)
$d_{Pam,e-cal}$	Arithmetic mean diameter of calculated ground particles (m)
$d_{Pam,e-exp}$	Arithmetic mean diameter of experimentally ground particles (m)
$d_{Pam,o}$	Arithmetic mean diameter of original particles (m)
$d_{Psm,e-exp}$	Sauter mean diameter of experimentally ground particles (m)
$d_{Psm,e-cal}$	Sauter mean diameter of calculated ground particles (m)
d_t	Diameter of draft tube (m)
D_S	Diameter of shroud (mm)
D_T	Diameter of draft tube (mm)
F	Particle breakage rate (number of particles/s)
F_D	Drag Force (N)
F_L	Liquid mass flowrate (kg/s)
$F_{L,exp}$	Global experimental liquid mass flowrate (kg/s)
F_m	Particle breakage rate (mass of particles/s)
F_S	Solids mass flowrate (kg/s)
$F_{S,exp}$	Global experimental solids mass flowrate (kg/s)
i	Tribo signal
K	Attrition constant (s^2/m^2)
ℓ	Distance from nozzle tip to draft tube (mm)
L	Length of draft tube (mm)
L_C	Location where jet contacts draft tube wall (mm)
L_S	Length of shroud (mm)
L_T	Chapter 4: Length of draft tube; Chapter 5: Distance from nozzle to location where measurements were taken (mm)
L_{Tip}	Distance from nozzle tip to base of shroud (mm)
L/S	Liquid to solid ratio (-)
m_o	Mass flowrate of jet gas (kg/s)
M	Molecular weight (kg/mole)
M_{solids}	Mass of solids in the bed (kg)
n	Sample size

n_o	Number of original particles in the bed
N	Chapter 3: Number of particle breaks (-); Chapter 5: Number of data points within cross-section (-)
P_o	Upstream pressure (psig)
P^*	Critical pressure (psig)
r	Population size
R	Chapter 1: Jet attrition rate (kg/s); Chapters 2, 3: Gas constant (N.m/moles/K)R
R_a	Jet attrition rate (kg/s)
R_{xy}	Cross-correlation coefficient (-)
S_x	Sample standard deviation
S_y	Population standard deviation
t	Chapter 2, 3: Grinding time (s); Chapter 7: Time (s)
T	Temperature (K)
T_{Lin}	Initial temperature of liquid (K)
T_{Sin}	Initial temperature of solids (K)
U	Gas velocity at nozzle throat (m/s)
U_o	Equivalent gas velocity at nozzle throat (m/s)
$U_{sound,eq}$	Equivalent speed of sound (m/s)
U_g	Fluidization velocity (m/s)
U_h	Velocity through holes (m/s)
U_{mf}	Minimum fluidization velocity (m/s)
V_g	Fluidization velocity (cm/s)
W_L	Liquid mass flux (kg/m ² s)
W_S	Solids mass flux (kg/m ² s)
W_{stat}	W statistic
$x_{i,a}$	Number fraction of attritable particles (-)
$x_{i,e-cal}$	Number fraction of calculated ground particles (-)
$x_{i,o}$	Number fraction of original particles (-)
x_o	Axial distance at which a particle enters the jet (m)
\bar{X}	Sample mean
y	Tribo-electric signal (V)
\bar{Y}	Population mean

Greek Letters

α	Chapter 1: Exponent for gas velocity (-); Chapter 2: Solid coefficient (-)
β	Chapter 2: Geometry coefficient (-); Chapter 3: Proportion of original particles that have not been ground (%); Chapter 6: Tribo-electric exponent (-)
γ	Grinding symmetry coefficient (-)
δ	L/S correction factor (-)
η	Grinding efficiency (m ² /kg)
κ	Isentropic expansion factor (-)

λ	Tribo-electric signal constant ($\text{kg/Vm}^2\text{s}$)
μ	Chapter 2, 3: Viscosity (Ns/m^2); Chapter 6: Average
ρ_o	Gas density at bed conditions (kg/m^3)
ρ	Gas density at nozzle throat (kg/m^3)
σ	Standard deviation
σ_{abs}	Absolute deviation
σ_x	Sample standard deviation
σ_y	Population standard deviation
τ	Time lag of the cross-correlation function (s)

Subscripts

i	Location in cross-section of downer
freq1.6	Frequency of 1.6 Hz
freq8.6	Frequency of 8.6 Hz
wav1	Wavelet coefficient of the 1 st octave
wav2	Wavelet coefficient of the 2 nd octave
wav4	Wavelet coefficient of the 4 th octave
wav7	Wavelet coefficient of the 7 th octave
wavn1	Normalized wavelet coefficient of the 1 st octave
wavn3	Normalized wavelet coefficient of the 3 rd octave
wavn5	Normalized wavelet coefficient of the 5 th octave
wavn6	Normalized wavelet coefficient of the 6 th octave
wavn10	Normalized wavelet coefficient of the 10 th octave
0	0 wt% water in ethanol
5	5 wt% water in ethanol
10	10 wt% water in ethanol
99%comp	Using a 99% compression ratio

CHAPTER 1

INTRODUCTION

The research work presented in this investigation deals with experimental and modeling studies involving the injection of high velocity gas and gas-liquid jets into fluidized beds. These types of jets occur in many industrial applications, and in particular, the heavy oil upgrading process of fluid bed coking.

The following chapter discusses applications involving gas and gas-liquid injection into fluidized beds. The fluid coking process is one application which uses both gas and gas-liquid injection. A key motivational factor for this work is to improve the operation of the fluid coking process, and therefore, a brief description of the current fluid coking process is also presented. A review of recent studies involving high velocity injection into fluidized beds follows. Finally, an overview of the research objectives will be outlined.

1.1 Applications of the Injection of High Velocity Jets into Fluidized Beds

A fluidized bed consists of a bed of small, solid particles that are suspended and kept in motion by an upward flow of gas. The gas is introduced into the vessel via either a grid plate distributor or a sparger distributor. Fluidized beds can be run in either the conventional, or the circulating mode. Circulating fluidized beds can be operated as either a riser or a downer. The reactor is called a riser when the gas and solids flow co-currently upwards. Conversely, the reactor is called a downer when the gas and solids flow co-currently downwards. Fluidized bed reactors are often used for applications that require the contacting of particulates with gases and/or liquids. Fluidized beds are ideal for these applications because of the rapid solids mixing that occurs as a result of the fluid behaviour of the solids (Werther, 2001). Fluidized beds operate at near isothermal conditions, have excellent heat and mass transfer rates, and provide good solids mixing. Fluidized beds are commonly used in the pharmaceutical, chemical and refining industries, where these types of advantages are extremely important. A large number of industrial processes utilize fluidized beds where horizontal or vertical jets are used to inject reactants, agglomerating reagents, or are used for grinding and particle attrition.

The injection of high velocity gas jets into fluidized beds occurs in such processes as fluidized bed coal combustion and fluid coking, where steam jets are used to control the size of the fluidized particles. High velocity gas jets are also used in jet mills, which are used to grind materials such as toners, high purity ceramics, foodstuffs, ultra-fine metal oxides, pharmaceutical powders, pigments, polymer powders and ultra-fine particles for powder coating.

The injection of high velocity gas-liquid jets into fluidized beds is encountered in applications such as gas-phase polymerization reactions, fluid catalytic cracking (FCC), and fluid coking.

1.1.1 Applications Involving Gas Injection into Fluidized Beds

Fluidized bed coal combustion is one application in which the injection of high velocity gas-only jets is used. In this process, coal is burned in a hot fluidized bed of inert material, which consists of sand, ash and limestone. The coal is introduced into the bed at several feeding points. An upward flow of air enters through the distributor plate, fluidizes the particles, and is used for combustion, which takes place in a vertical chamber or furnace at temperatures between 800 and 900°C. Cyclones separate the gaseous combustion products from the solid material. This solid material is then reintroduced into the furnace and the gaseous combustion products exit the cyclone and enter a convection section where they pass through a heat exchanger. Either baghouse filters or electrostatic precipitators are used to remove the ash from the flue gas. High velocity air jets are used to inject secondary air into the fluidized bed. This secondary air allows for staged combustion to occur which decreases the NO_x emissions. In addition, the secondary air injection allows for the more efficient combustion of volatiles, as it supplies more air and provides intense mixing in the freeboard (Oka, 2004).

High velocity gas jets are also commonly used in jet mills, which are used for particle size reduction in industrial applications. A common type of jet mill is a fluidized bed jet mill, in which several gas jets are located around the periphery of a grinding chamber and are directed towards a single point in the chamber. The particles are introduced either from the top or the bottom of the chamber and are fluidized, causing them to circulate throughout the bed. A grinding region is formed in the fluidized bed

where the gas jets intersect, and the particles impact against each other, thus reducing their size. The efficiency of these fluidized bed jet mills can be improved by placing targets downstream of the jets, providing a surface for the particles to impact against (Rhodes, 1990).

1.1.2 Applications Involving Gas-Liquid Injection into Fluidized Beds

Contrary to particle grinding, an application that uses liquid injection into fluidized beds is the granulation process. In this process, large liquid droplets are injected into a fluidized bed. The liquid droplets adhere to several smaller solid particles, which result in granules (Sherrington and Oliver, 1981; Pacek and Nienow, 1991). The shear forces in the fluidized bed break the weak agglomerates and the strong agglomerates survive. The wet granules are then dried to produce a stable product. A similar procedure is used in the coating process, however a higher fluidization velocity is maintained in order to achieve enough shear to break the granules and result in a finely coated product (Henderson et al., 1996).

Another application which uses high velocity liquid injection into fluidized beds is the production of polyethylene. The gas-phase production of low-density polyethylene (LDPE) is an example where the injection of liquid reactants has greatly improved the process efficiency. This polymerization process is exothermic and rapid heat removal is extremely important since the reactor operates near the sintering temperature of the solid product. Normally, the heat from the reaction is removed by circulating a large flowrate of gas out of the reactor, through an external heat exchanger and back to the fluidized bed. However, in this process, the recirculation flowrate is limited in order to avoid excessive entrainment of the bed particles, which could deposit on the surfaces of the external heat exchanger. This problem was overcome by a novel operation, called the supercondensed mode, which involves the injection of liquid reactants, which remove the heat of reaction by evaporative cooling (Jiang et al., 1997). There are two methods which are used to inject the liquid. In the first method ethylene and co-monomers enter the fluidized bed reactor through the distributor, and come into contact with the fine catalyst seed particles. In the second method spray nozzles are used to inject the liquid directly

into the bed. The reactor is maintained at temperatures of 77 - 100°C and at a pressure of 20 bars (Bhruns, 2002).

Fluid catalytic cracking (FCC) is another application which uses gas-liquid injection into fluidized beds. FCC is a petrochemical operation used to convert heavy hydrocarbons with boiling points greater than 350°C to lighter products by cracking them over a catalyst at temperatures of approximately 500°C. In a typical FCC unit, hot catalyst particles from the regenerator, with an average diameter of 70 µm, are conveyed into a riser reactor. The heavy feedstock is injected via several spray nozzles positioned around the circumference, near the riser base. Steam is used to atomize the feedstock and to convey the catalyst particles. The catalyst particles contact the spray droplets and transfer their heat to vaporize the liquid. The liquid vaporization causes a volume expansion, which results in a relatively short residence time of between 1 and 4 seconds. This residence time is ideal for the gas-phase cracking reactions, while at the same time minimizes over-cracking. An important aspect of the FCC process is the liquid injection, which greatly affects the product composition. Newton (1998) found that an ideal FCC feed injector should produce small droplets with a narrow size distribution, cover a wide area of the riser cross-section and provide good mixing between the spray droplets and the catalyst. Droplet size is extremely important as large droplets heat up slowly and could lead to unwanted coking reactions, and excessively small droplets tend to over-crack and produce dry gas.

The fluid coking process is one application, which uses the injection of both high velocity gas jets and high velocity gas-liquid jets into a fluidized bed. The fluid coking process is used for the primary upgrading of bitumen and residual oils and uses a non-catalytic, thermal conversion technique to upgrade bitumen extracted from oil sands to produce crude oil. The fluid coking process uses both high velocity gas attrition nozzles to control particle size in the bed, and high velocity gas-liquid nozzles to disperse the feed into the bed. One key motivation for this work is to improve the fluid coking process by better understanding the interactions between these jets and the fluidized particles. Therefore, a summary of the Syncrude fluid coking process follows.

1.2 The Fluid Coking Process

1.2.1 Background Information

The oil sands, located in Western Canada, contain one of the largest known hydrocarbon deposits in the world. Bitumen, a thick, sticky black form of crude oil is contained in the ground as a mixture of sand, water, and clay and is a highly viscous substance with a large carbon-to-hydrogen ratio. Bitumen makes up about 10-12% of the actual oil sands found in Alberta, the remainder being 80-85% mineral matter and 4-6% water (Government of Alberta-Energy, 2006). The total amount of bitumen contained in the Albertan oil sands is approximately 1.7 trillion barrels, of which 175 billion barrels are currently recoverable, and 315 billion are ultimately recoverable, once the necessary technology has been developed (Syncrude Canada Ltd., 2006). When the bitumen is separated from the sand and other materials, the remaining fraction contains 50 – 60 wt% vacuum residue. Vacuum residue is the fraction of petroleum that does not distill under vacuum, and typically has a normal boiling point of over 525°C (Gray, 1994). The high boiling point is the result of long chain hydrocarbon molecules that are present in the bitumen. Due to the existence of these long chain hydrocarbon molecules, bitumen cannot be processed in oil refineries in its raw form, and must undergo an extensive upgrading process to break the carbon-carbon bonds before it can be marketed.

Coking, a thermal conversion process, which produces carbon-rich solid coke, distillable liquids, and light ends, has been found to be the most feasible method to achieve the carbon-carbon bond breakage in bitumen. Coking is preferable over other methods such as hydro-conversion, since it is much more efficient (Gray, 1994). There are two main types of coking: delayed coking and fluid coking.

Delayed coking is the most common method used to upgrade bitumen. This process is a semi-batch process that uses long liquid-phase residence times. The feed is heated to approximately 500°C and enters one of two insulated vessels referred to as the coke drums. As the reaction occurs, vapour products are withdrawn from the reactor, and coke accumulates on the walls of the drum. Once the first drum is full of coke, the feed is switched to the second drum, and the coke is drilled out of the first drum (Gray, 1994).

The other type of coking is the fluid coking process, which was developed by Exxon in the mid-1950s. The fluid coking process has been shown to be superior to the delayed coking operation due to its continuous operation, reduced residence times of cracked vapours, subsequent higher yield of distillates, and its reduced coke production (Gray, 1994). Syncrude Canada Ltd. is a world-leader in fluid coking and operates three of the largest fluid cokers in the world. Currently, Syncrude produces approximately 240 000 barrels per day of high quality, light, sweet crude oil (Syncrude Canada Ltd., 2006).

In Syncrude's fluid coking operation, two vessels are used simultaneously, the fluid bed reactor and the fluid bed burner, as shown in Figure 1.1. The fluidized bed reactor is used to contact hot coke particles with preheated bitumen, which is injected through high velocity gas-liquid feed nozzles. The bitumen feed is mixed with atomization steam and enters the reactor at approximately 350°C. The feed contacts the hot coke particles that are fed into the reactor from the top. The thermal cracking reaction takes place on the surface of these coke particles at a temperature of approximately 530°C. The cracked vapours rise up the reactor and cyclones located at the top of the vessel remove entrained coke particles and return them to the dense bed of the reactor. The condensable vapour products pass through a scrubber and are then further processed downstream. The "cold" coke is withdrawn from the bottom of the reactor and transported to the burner, after passing through a stripping section, where it is contacted with steam to remove any adsorbed hydrocarbons. In the burner section the coke deposited on the particles by the cracking reaction is burnt off by reheating the coke particles. The "hot" coke is then pneumatically conveyed back to the top of the coker.

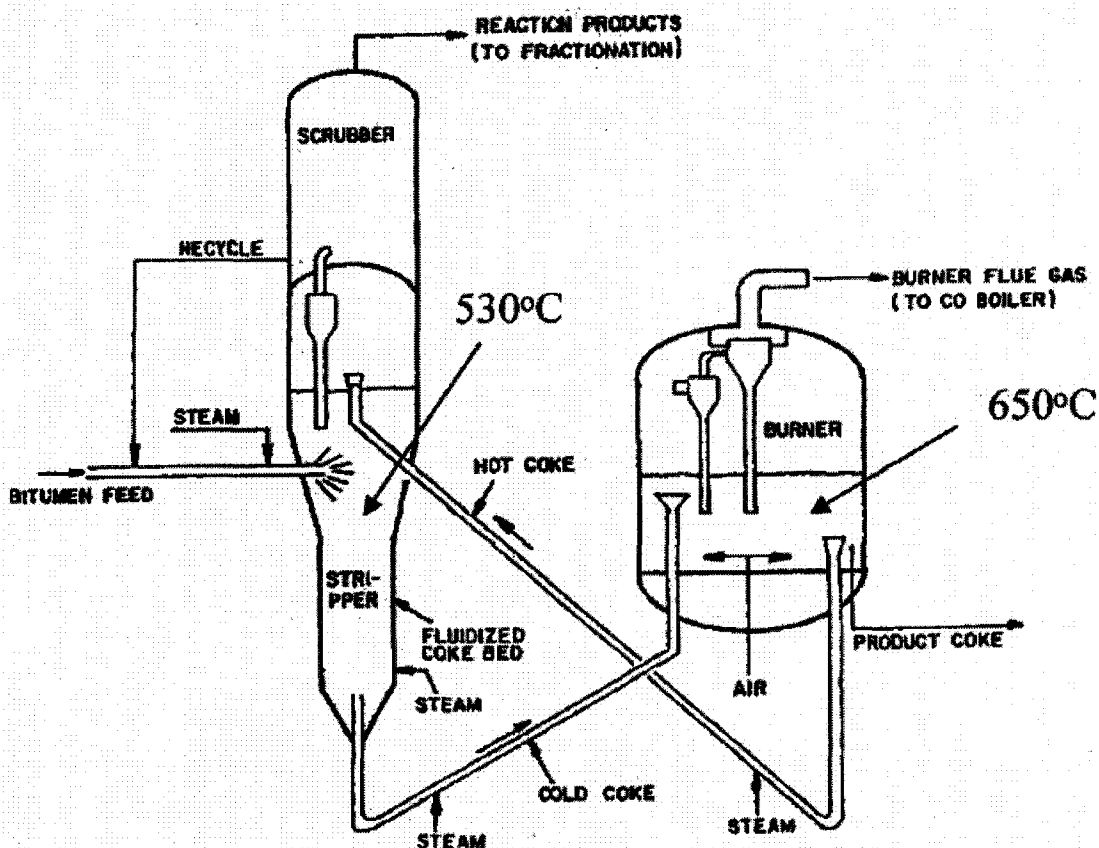


Figure 1.1: The Fluid Coking Process (House et al., 2004)

1.2.2 Motivation for Research

As mentioned previously, the motivation for the research contained in this dissertation is derived from the Syncrude fluid coking process. Syncrude is conducting research aimed at improving the efficiency of its fluid cokers due to the high worldwide demand for oil, high market prices, and the quantity of the reserves in Canada's oil sands.

In the fluid coking process, the particle size of the coke is of great importance. If too many fine particles with a diameter less than $50\text{ }\mu\text{m}$ exist, agglomeration will occur and result in poor fluidization. Conversely, an excess of large particles with a diameter greater than $600\text{ }\mu\text{m}$ results in slugging and poor circulation. During the fluid coking process, there is a gradual increase in the size of the coke particles due to the fact that coke is formed and deposited on the surface of the coke particles during the reaction. The coke is formed at a rate which is proportional to the surface area available, and a

uniform thickness of coke is formed on each particle, regardless of size. In addition to particle growth due to the reaction, agglomerates are also formed when several coke particles stick together. In order to control the size of the particles in the fluid bed, steam is injected into the reactor section through high velocity gas-only attrition nozzles, which contain an expansion section and operate at sonic conditions. These nozzles cause the particles to grind, thus decreasing the particle size. Although some of the coke produced during the reaction is burned out in the burner section, there is still a large excess of coke, and if attrition nozzles are not used the average particle size in the reactor would continue to increase. Currently, attrition nozzles require a large quantity of steam, and account for a large percentage of the total steam usage in the fluid coker. Improving the efficiency of the attrition nozzles would reduce steam consumption, which would allow for more throughput to the reactor. The gas velocity in the coker is limited by entrainment, and therefore, if less steam is used in the attrition nozzles, more hydrocarbons can be put through the reactor.

Along with attrition, another crucial step in the fluid coking process is the initial interaction of the liquid jet spray and the fluidized particles. The fluid coking process requires good contact of the liquid droplets and particles in order to achieve efficient cracking and high yields. A poor initial distribution of the liquid feed on the particles can cause a thick liquid film to form on the solids surface, imposing a high resistance to mass and heat transfer, resulting in the formation of undesirable secondary products. To avoid slow cracking and prevent heat or mass transfer limitations, the feedstock must contact a large number of particles quickly and uniformly. The greater the number of hot coke particles with which the liquid comes into contact, the better the dispersion of the liquid on the surface of the particles, and the better the yield. Gray (1994) found that the ideal liquid-to-solid ratio (L/S) for the fluid coking process is below 0.1 g/g, based on mass transfer limitations. Gray (1994) had originally thought that the liquid would spread on the surface of the individual particles and then remain as individual particles in the fluidized bed. However, Ariyapadi et al. (2003a) showed that most of the liquid was trapped within the agglomerates. Therefore, House et al. (2004) modeled the effect on product yields of heat transfer limitations within the agglomerate. House et al. (2004) found that heat transfer limitations become limiting at reaction temperatures if the

particles do not contact the liquid quickly enough for the reaction to proceed at an optimal rate. It was found that the L/S should be as low as possible and preferably below approximately 0.06 g/g to avoid the formation of stable agglomerates. Currently, the fluid coking operation is being shifted towards higher throughput due to the high market oil prices. As a result, the interaction between the feed spray and coke particles is even more important.

1.3 Interactions Between High Velocity Jets and Fluidized Particles - Literature Review

1.3.1 Gas Jets in Fluidized Beds

Gas jets are extremely important in the operation of fluidized beds. There have been numerous studies of both high velocity gas jets and low velocity gas jets in fluidized beds. Studies on low velocity gas jets in particular have been very extensive. Many early studies examined low velocity, subsonic jets issuing from gas distributors (Zenz, 1968; Behie et al., 1970; Merry, 1975). Massimilla (1985) has written a review of the considerable amount of early work that exists on the interactions between low velocity gas jets and fluidized beds. More recently, Hong et al. (1997) and Al-Sherehy et al. (2004) studied the jet penetration length and gas dispersion when gas jets were injected into a fluidized bed.

Most of the work done involving high velocity jets in fluidized beds is based on the theory of turbulent jets by Abromovich (1963) (De Michelle et al., 1976; Xuerub et al., 1991a, 1991b). When a high velocity jet is injected into a fluidized bed, the fluidization gas is drawn towards the jet due to the pressure differential between the expanding jet and the turbulent shear layers that are created at the jet/bed interface. If the flowrate of entrained gas is large enough it will draw particles towards the jet. It has been observed that the majority of the entrainment occurs at the nozzle tip (Felli, 2002; Xuereb et al., 1991a, b; Merry, 1971). Particle size and density as well as gas jet properties, will affect the entrainment rate of particles (Ariyapadi, 2003a).

One important aspect of injecting high velocity gas jets into fluidized beds is particle attrition. There are two main modes of attrition: abrasion and fragmentation. Abrasion occurs when very fine pieces are removed from the surface of the particle, thus

producing many fines, while the particle size distribution of the original particles remains unchanged. Alternatively, fragmentation occurs when a particle breaks into pieces of similar size and the size distribution of the original particles decreases (Werther and Rappenhagen, 1999). There are two main variables that affect the attrition process in a fluidized bed. The first is the particle properties such as shape, surface roughness and strength. The second is the properties of the environment such as the fluidization velocity, and operating pressure of the attrition gas (Patel et al., 1986).

A number of researchers have studied the effects of particle properties and fluidized bed operating conditions on particle attrition. This attrition was the result of particle interactions with gas jets issuing from the distributor plate and with gas bubbles in the bulk of the bed (Blinichev et al., 1968; Lin et al., 1980; Aroostoopour and Chen, 1983; Patel et al., 1986; Stein et al., 1998; Werther and Rappenhagen, 1999). For example, Lin et al. (1980) studied elutriation and attrition in a fluidized bed and found that the rate of attrition was a function of the excess gas velocity ($U_g - U_{mf}$), and that the particle diameter had little effect on the attrition rate. They found that the majority of the attrition occurred in the bubble wakes and an empirical correlation for estimating the rate of fines generation was presented.

Several studies have been published focusing on the effects of gas properties on the attrition of particles in fluidized beds when injecting subsonic jets (Chen et al., 1980; Pacek and Nienow, 1991; Werther and Xi, 1993; Ghadiri et al., 1994; Wu et al., 1999; Boerefijn et al., 2000; Bentham et al., 2004). All of these studies have found that the attrition rate was dependent on the velocity of the jet. Most recently, Bentham et al. (2004) analyzed particle breakage in a single jet region in a fluidized bed in order to determine the role of jet hydrodynamics and material properties. They found that the breakage mechanism in a fluidized bed jet involves the entrainment of particles from the dense phase region surrounding the jet into the dilute jet core. Once in this region, particles were accelerated by the gas jet and collided with each other as well as impacting on the dense phase at the top of the jet. The breakage of the particles was also successfully predicted as a function of the jet velocity and exhibited a strong sensitivity to changes in jet angle and gas flow rate.

The gas velocity in the distributor holes has a strong effect on the attrition rate. The attrition rate is usually given by an expression such as:

$$R \propto U_h^\alpha \quad (1.1)$$

Where U_h is the gas velocity through the distributor holes. For velocities below 100 m/s, the exponent α ranges from 1.2 to 3 (Chen et al., 1980; Shamlou, 1990; Werther and Xi, 1993; Ghadiri et al., 1994; Davuluri and Knowlton, 1998). For higher velocities, up to 250 m/s, results are less clear. Stein et al. (1998) and Wu et al. (1999) found an exponent α of 1, whereas Bentham et al. (2004) reported an exponent that varied from 2.6 to 5.6 depending on the nature of the particles.

There is no consensus on the effect of the grid hole diameter on the attrition rate. Ghadiri et al. (1994) report that increasing the hole diameter reduced the attrition rate. Wu et al. (1999) found that the hole diameter did not affect attrition. Davuluri and Knowlton (1998), Stein et al. (1998) and Werther et al. (1993) reported that the attrition rate was proportional to the hole diameter raised to an exponent of 1.4, 1 and 2, respectively.

It has also been found that the gas density affects the attrition rate. Davuluri and Knowlton (1998) found that the attrition rate was proportional to the gas density raised to an exponent of 1.4, while Shamlou et al. (1990) reported that it was directly proportional to the gas density.

Most of the studies mentioned above involve the use of subsonic jets. However, few studies have been published on the use of very high velocity jet attrition in fluidized beds. Many jet attritors operate with sonic or supersonic velocities, and velocities much higher than 100 m/s at the nozzle exit are used. Dunlop et al. (1958) describe a fluidized bed jet attritor for the attrition of coke particles in fluid cokers. However, they did not provide any information on the effects of variables such as jet velocity, nozzle size or nozzle shape.

Although not mentioned in the publications, most of the experimental research on jet grinding is believed to have been done using straight tube nozzles. Only one experimental research work has been done using a nozzle with the contraction-expansion geometry typical of Laval nozzles, as shown in Figure 1.2 (Benz et al., 1996).

Under subsonic conditions the gas flow accelerates through the converging section of the nozzle, reaching its maximum speed at the throat. The flow then decelerates through the diverging section before exiting the nozzle. However, during supersonic flow the diverging section acts as a nozzle and accelerates the flow, while the converging section acts as a diffuser and decelerates the flow. When the ratio of the pressure at the exit of the nozzle to the upstream pressure (P_2/P_0) is less than the critical pressure ratio (P^*/P_0), according to Equation 1.2, the flow will be subsonic in the converging section of the nozzle, sonic at the nozzle throat, and supersonic in the diverging section of the nozzle. During supersonic flow, if the nozzle exit pressure, P_2 , is greater than the ambient discharge pressure, P_3 , shock waves will occur outside of the nozzle. However, if the exit pressure, P_2 , is less than the ambient discharge pressure, P_3 , the shock waves will occur within the expanding portion of the nozzle.

$$\frac{P^*}{P_0} = \left(\frac{2}{\kappa + 1} \right)^{\kappa/(\kappa-1)} \quad (1.2)$$

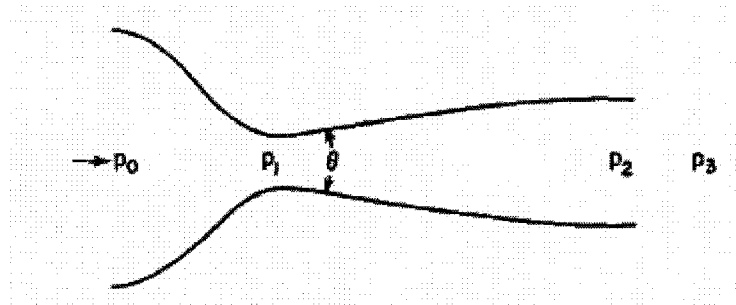


Figure 1.2: Laval Nozzle (Perry and Green, 1997)

Nozzle geometry may be an important parameter which affects the grinding rate. Investigations on jet grinding characteristics using nozzles with an expansion section and operating at sonic conditions are needed.

1.3.1.1 Modeling Particle Attrition

An important aspect of particle attrition is the understanding and modeling of the particle breakage mechanisms. Previously, several studies have been done which focus on modeling attrition in a fluidized bed in the absence of an injection nozzle. Ray et al. (1987) proposed a “surface-reaction” model which states that the attrition rate is

proportional to the particle surface area. Levenspiel et al. (1968) developed a model for particles of changing or unchanging sizes and used a first-order shrinkage rate to represent particle attrition. However, this model did not consider the roles of fines or the original particles that remained intact after the attrition process. Merrick and Highley (1974) developed a mathematical model of a fluidized bed process which assumed a first-order correlation for size reduction, and a critical particle size for elutriation. This model was used to predict the elutriation rate and mean bed particle size in a system. They found that the mass attrition rate of a component was proportional to the excess gas velocity, the mass of solids and the mass fraction of the component smaller than a certain radius.

Austin (1971) developed a model introduced by Epstein (1948) and Reid (1965) to estimate the particle size distribution of ground particles after a known grinding time, given the initial size distribution. A cumulative breakage distribution function gave the size distribution of the new fragments created, and a selection function was defined as the fraction of particles broken per unit time. These breakage and selection functions became the standard parameters used to describe the grinding process.

Many researchers have modeled the grinding process in a fluidized jet mill (Gommeren et al., 1996, Benz et al., 1996; Berthiaux and Dodds, 1999; Berthiaux et al., 1999 and Gommeren et al. 2000, Han, 2002). Berthiaux and Dodds (1999) and Berthiaux et al. (1999) modeled the grinding process in a fluidized bed jet mill with batch and continuous operation, respectively. A new parameter, the residual fraction, was introduced in order to characterize the grinding kinetics. The residual fraction represented the performance of the grinding process and characterized the proportion of particles which were not ground.

Han et al. (2002) proposed a combined discrete element method and computational fluid dynamic numerical model for particle grinding in a jet mill. The particle motion in the gas flow was simulated by applying the Reynolds-averaged Navier-Stokes equations. The model proposed by the authors was in strong agreement with experimental values and was found to be suitable to predict the size distributions of the ground particles. They concluded that the particle feed rate, the angle of the particle feed

nozzle and the air feed rate were the most important parameters in governing the particle breakage in the jet mill.

Ghadiri et al. (1994) used the single particle impact breakage model from Donsi et al. (1980) to calculate the particle velocity at the tip of the jet. They combined this model with a correlation for solids entrainment into the jet to obtain the fluidized bed jet attrition rate. The model can predict the dependence of the attrition rate on both the orifice gas velocity and the orifice size.

The models previously developed for jet attritors are quite complex and require many empirical parameters that have to be experimentally determined (Baddour and Briens, 2006). Baddour and Briens (2006) developed a simple, two-parameter model to describe jet milling of carbon nanotubes. However, as all the other models, it applies only to small fluidized beds where there is intense solids mixing. It does not apply to processes such as fluid coking, where solids mixing may be a limiting factor and impact on the attrition rate and product size distribution.

1.3.1.2 Methods of Improving Particle Attrition

There are several methods that can be used to improve particle attrition in fluidized beds. Simple jet attrition can be enhanced through the use of a target, opposing jets or a draft tube accelerator. Some studies also combine several of these techniques to further enhance attrition. Werther and Xi (1993) found that jet orientation had a major effect on attrition. Horizontal and upward jets had similar attrition rates, however downward jets provided attrition rates that were 50% larger.

Yates et al. (1991) found that interacting jets significantly enhanced attrition only when they were interacting near a wall. Arastoopour et al. (1983) reported that the interaction of grid jets with the column wall made a significant contribution to attrition.

Dunlop et al. (1958) found that grinding was enhanced by placing a target plate in the fluidized bed, on which the attrition jet impacted. Their implementation was rather complex since solids were supplied into the nozzle tube upstream of the fluidized bed, so that they could be fully accelerated before entering the bed, as shown in Figure 1.3. Dunlop et al. (1958) found that target grinding and regular jet grinding had similar power requirements, but target grinding produced a smaller proportion of undesirable very fine

particles. However, they recommended regular jet grinding for fluid cokers since it was simpler in equipment and operation, and did not suffer from target erosion problems.

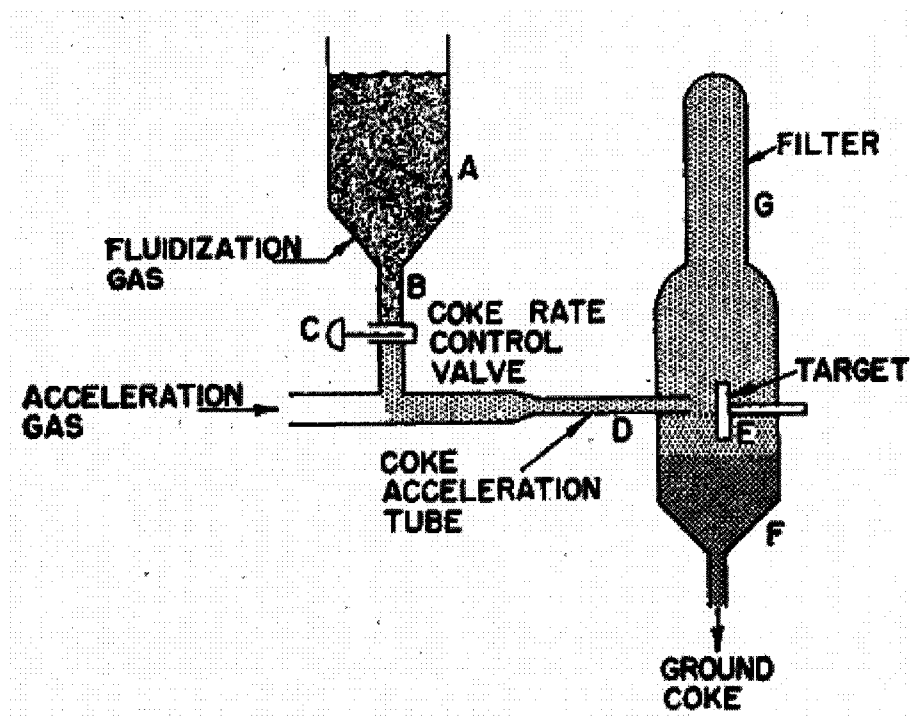


Figure 1.3: Target System from Dunlop (1958)

Siegel et al. (1978) reduced the production of very fine particles with an attrition apparatus consisting of a succession of rings, coaxial with the nozzle. The ring hole size decreased gradually as the axial distance from the nozzle increased, as shown in Figure 1.4.

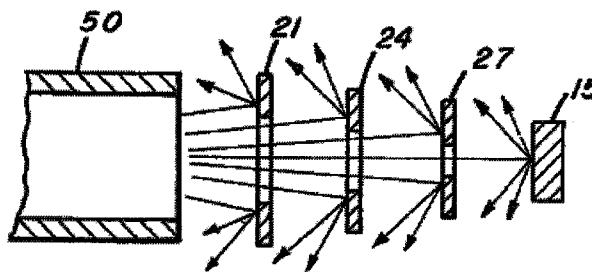


Figure 1.4: Concentric Ring Target System from Siegel et al. (1978)

Smith et al. (1992) found that a target improved jet attrition rates, while an inclined target did not provide any benefit. In addition, spherical targets were more effective than flat targets. Tasirin et al. (1999) stressed that it was important to provide a

large enough distance between nozzle and target, to allow for sufficient particle acceleration. They found that a jet and flat plate target combination required half the power of opposing jets to achieve the same grinding, confirming the results provided by Henderson et al. (1996).

Tasirin et al. (1999) found that two vertical opposing jets achieved roughly the same grinding rates as two identical, non-interacting vertical jets. However, using two horizontal opposing jets was not attractive since they achieved roughly the same grinding rate as a single horizontal nozzle (Tasirin et al., 1999). Commercial fluidized jet mills from Alpine corporation, described by Berthiaux et al. (1999a, 1999b) and Godet-Morand et al. (2002), use 3 intersecting jets that are inclined with an angle of about 45 degrees with the horizontal plane, as shown in Figure 1.5.

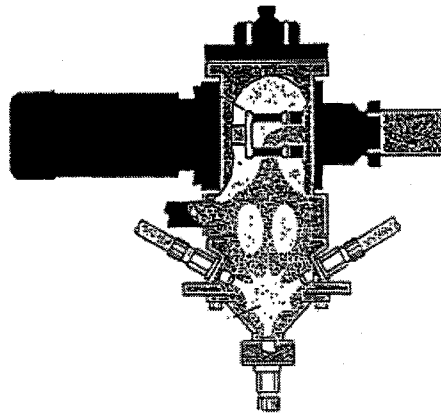


Figure 1.5: Alpine Jet Mill

Henderson et al. (1996) improved upon the Alpine design by placing a target in the region where the three jets intersect. The target consists of a hollow vertical tube, of circular or triangular cross-section, with holes of appropriate size to allow the jets to penetrate, as shown in Figure 1.6. The jets interact in a confined space, which enhances attrition. Gommeren et al. (1996) describe a spiral jet mill that uses several angled jets to make the fluidized bed spin at high speed. This enhances attrition through friction of the particles on the bed wall, while simultaneously acting as a classifier by preventing the entrainment of large particles.

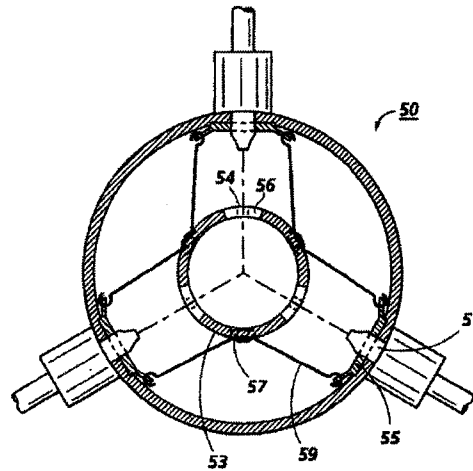


Figure 1.6: Confined Jet Intersection from Henderson et al. (1996)

Smith et al. (1992) proposed the use of a draft tube downstream and coaxial with the attrition nozzle, shown in Figure 1.7. Its purpose was to accelerate the particles entrained into the jet by maintaining a high gas velocity over a significant distance. There may be other modifications and designs of attrition nozzles, not yet investigated, that could improve the grinding efficiency of particles in a fluidized bed.

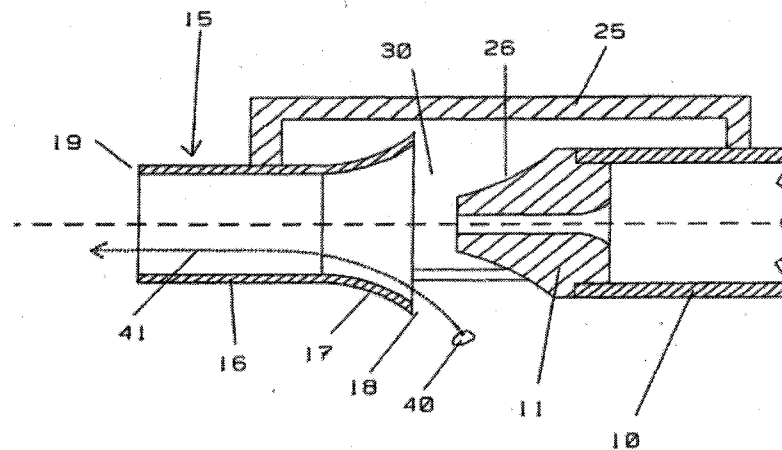


Figure 1.7: Draft tube from Smith et al. (1992)

1.3.2 Liquid Injection into Conventional Fluidized Beds

In addition to gas jets in fluidized beds, there have been several studies conducted that consider the interaction of evaporative liquid jets in fluidized beds. Leclerc et al. (1991a, 1991b) developed a method to characterize the contact between a vaporizing

liquid and particles in a fluidized bed by measuring the vaporization rate of the injected liquid. They also proposed a new model to predict the formation of agglomerates when liquid droplets larger than bed particles were injected into a hot fluidized bed. More recently, Leclerc et al. (2004) developed a new experimental method that was based on quenching the bed and recovering the agglomerates. From the analysis of the liquid phase of these agglomerates the fraction of remaining liquid was determined.

There are several other measurement techniques that have been used to measure evaporative liquid jets in fluidized beds. The use of temperature measurements has been used in the past to investigate the injection of evaporative liquid jets into fluidized beds. Smith and Nienow (1982) used an X-ray technique to study evaporation of a solvent sprayed vertically into a fluidized bed. In addition, bed temperature profiles were measured by radially navigating thermocouples at vertical intervals along the bed. They detected low-temperature regions within the liquid jet in which the majority of evaporation was assumed to occur. Similarly, Shakhova and Minaev (1973) injected liquid horizontally into a fluidized bed granulator and studied the spray zone by taking temperature measurements in the cross-section of the jet at different axial locations. They determined that most of the evaporation of the solution occurs at the end of the injector. Zhu et al. (2000) also used a thermocouple measuring technique to determine the evaporation length of the vertical jet and found that variations in the solids concentration can shorten the evaporation length due to turbulent mixing and phase interactions.

There have been several studies done which focus on the modeling of evaporative liquid jets in fluidized beds. Bruhns and Werther (2004) experimentally studied the mechanism of liquid injection into a fluidized bed by using local temperature measurements, suction probes, and capacitance probes to characterize the liquid injection. They used the information obtained by these three methods to model the mechanism of the injection. Wang and Zhu (2003) also developed a model for hydrodynamic mixing of evaporating spray jets in dilute gas-solids pipe flows and studied the effect of solids loading, inlet gas velocity, and spray mass. They acquired temperature measurements along the spray jet axis to obtain an averaged mixture temperature, which represented the phase-weighted temperature of all three phases. The measured temperature depended on

the local heat balance of the thermocouple from the turbulent thermal convection, the heat transfer due to droplet collisions and evaporation, and the heat transfer due to the solids collisions. From the results, information regarding each phase of gas, solids and droplets was obtained. Mirgain et al. (2000) modeled the vaporization of feedstock droplets sprayed into a fluid cracker. Both the homogenous vaporization of the droplets in the gas phase and the heterogeneous vaporization of the droplets as they collide with catalyst particles were modeled. However, droplet evaporation is a key factor in the phase mixing and flow characteristics of these evaporating spray jets, and these methods cannot be adapted to applications with a non-vaporizing liquid.

Several studies have been done that explore horizontal injection of non-evaporative gas-liquid jets into conventional fluidized beds. Ariyapadi et al. (2003b) used digital X-ray imaging to study the internal flow structure of liquid jets injected into fluidized beds and determined the jet expansion angle and penetration distance. In another study done by Ariyapadi et al. (2003a), a model to determine the entrainment rate of solids and gas into a gas-liquid jet injected into a fluidized bed of fine particles was developed. In addition, Felli (2002) developed and validated a technique to measure this entrainment rate. Gray (2002) determined that the key relationships that govern the behaviour of wet particles in coking processes are the Stokes number of the particles, the thickness of the liquid films, and the diameter and surface roughness of the particles. He concluded that to obtain a uniform thin film on the coke particles there must be an efficient mechanism for distributing the feed on a bed of coke after the feed has been injected, and that the feed contacts only a portion of the coke in the bed. Knapper et al. (2003) used copper naphthenate as a tracer for measuring the dispersion of liquid feed jet into a hot fluidized bed of coke. Although there were numerous particle-particle collisions in the fluidized bed, they found that the transfer of liquid feed among the particles was poor. However, at higher L/S values it has been shown that heat transfer, as opposed to mass transfer, is the limiting process (House, 2004).

In order to improve this transfer, Chan et al. (2004) have devised a draft tube mixer that is positioned co-axially downstream of an atomization nozzle and enhances the contact between the liquid spray droplets and the fluidized particles. Hulet et al. (2003) studied the entrainment and stability of a horizontal gas-liquid jet in a fluidized bed with

a draft tube located downstream of the injection nozzle. They found that the optimal distance for entrainment occurred at a point when the liquid jet was touching the draft tube wall near its centre. House et al. (2004) proposed a model to illustrate the importance of the initial liquid-solid mixing on coker yields and developed an experimental technique to quantitatively determine the quality of the initial liquid-solid mixing. Tests were done using a conventional nozzle and a nozzle with a draft tube mounted co-axially downstream, similar to the one used by Hulet et al. (2003). The use of the draft tube was shown to greatly improve the liquid-solid mixing by increasing the amount of wetted solids and creating a more uniform initial liquid-solid mixture.

Another technology that can be used to improve the quality of mixing between injected liquid and fluidized particles is a downer equipped with a mixing chamber. Spray nozzles are widely used to inject atomized feeds in industrial circulating fluidized bed reactors such as FCC risers (Skouby, 1999; Chang et al., 2001; Gao et al., 2001; Gupta and Subba Rao, 2001; Tafreshi et al., 2002). However, these types of reactors could presumably be replaced by downers. Briens et al. (1997) and Mirgain et al. (1998) evaluated a gas-solids mixing chamber, which consisted of gas-liquid injector nozzles that could be oriented in both the vertical and horizontal plane. The sprays from the gas injector nozzles were contacted with down flowing solids in a mixing chamber. They found that very good contact between injected gas and circulating solids could be achieved with certain mixing chamber geometries. This type of system can also be applied to the case when liquid spray nozzles are used.

Gas-liquid spray nozzles are not typically used in the published studies of downer reactors. There has been extensive literature published on gas-solid mixing behaviour when gas is injected into downer reactors (Berg et al., 1989; Zheng et al., 1992; Johnston et al., 1999; Namkung and Kim, 2000; Brust and Wirth 2004a, 2004b; Zhang et al., 2004). There have also been several studies conducted that consider the interaction of evaporative liquid jets in gas-solid risers (Schuurmans, 1980; Skouby, 1999; Liu, 2003). However, as mentioned previously, droplet evaporation is a key factor in the phase mixing and flow characteristics of evaporating spray jets, and the same methods cannot be adapted to applications with a non-vaporizing liquid. Currently, there have been no

studies done which investigate the interaction between liquid jets and circulating solids in a downer reactor.

1.4 Research Objectives

1. **OPTIMIZE THE OPERATING CONDITIONS OF EXISTING SONIC VELOCITY ATTRITION NOZZLES.** For some industrial applications, controlling the size distribution of the particles in a fluid bed is extremely important in order to avoid poor fluidization. One method to control the size of the particles in the bed is to use attrition nozzles, which inject high velocity gas jets into the bed creating high shear regions and grinding particles together. Different high velocity attrition nozzles and operating conditions were investigated in order to determine the effects of fluidization velocity, nozzle size, nozzle geometry, bed material and attrition gas properties on the grinding efficiency. An empirical correlation was also developed to estimate the grinding efficiency, and its predictions were validated using the experimental data. Chapter 2 discusses this study.
2. **DEVELOP A PARTICLE ATTRITION MODEL.** An important aspect of particle attrition studies is the understanding and modeling of the particle breakage mechanisms. A simple model, with a minimum of empirical parameters, was developed to describe the attrition mechanism when a sonic velocity gas jet is used to grind particles in a fluidized bed and to account for the effect of solids mixing. The model predicts the particle size distribution of ground particles, the particle breakage frequency and the proportion of original particles in the bed which were not ground. The results from the model were verified with experimental data. An important application of the model would be to use the particle breakage frequency to predict the attrition results in different bed sizes. The results of this study are presented in Chapter 3.
3. **IMPROVE PARTICLE GRINDING EFFICIENCY WITH NEW TYPES OF ATTRITION NOZZLES.** Simple jet attritors require large amounts of gas to grind the particles effectively. If these attrition jets were improved, they may be able to

achieve the same attrition rates while operating at a much lower gas flowrate. Simple jet attrition can be enhanced through the use of a target (Dunlop et al., 1958; Tasirin et al., 1999), opposing jets (Tasirin et al., 1999; Yates et al., 1991) or a draft tube accelerator (Smith et al., 1992). However, there may be other modifications and designs of attrition nozzles, not yet investigated, that could improve the grinding efficiency of particles in a fluidized bed. Nozzle designs which enhance attrition by promoting the entrainment into the gas jet of particles, and accelerating them to high speed have been developed and tested in order to determine which ones result in the greatest increase in grinding efficiency. The results from this study are presented in Chapter 4. Videos of a half-jet with and without a nozzle shroud were taken in order to understand the flow patterns of gas and solids when a shroud is present. This study is described in Appendix A. In addition, a novel technique was developed using tribo-electric probes to measure the proportion of fines in a gas-solid fluidized bed. Details of this study can be found in Appendix B.

4. **USE NOVEL TECHNOLOGIES TO IMPROVE THE SOLID-LIQUID MIXING QUALITY WHEN GAS-LIQUID JETS ARE INJECTED INTO A FLUIDIZED BED.** The principles of some of the technologies used to improve particle attrition in a simple gas-solid system have been applied to a more complicated gas-liquid-solid system. A measurement technique was required to characterize the solid-liquid contact when a gas-liquid jet was injected into a fluidized bed. As a result, a technique was developed to determine the local, instantaneous quality of solid-liquid mixing when a gas-liquid spray jet was injected horizontally into a fluidized bed. Chan et al. (2004) have devised a draft tube mixer similar to the one used in the attrition nozzle study, that is positioned co-axially downstream of an atomization nozzle and enhances the contact between the liquid spray droplets and the fluidized particles. The liquid-solid mixing when a conventional spray nozzle was injected into the bed is compared to the results obtained when a draft tube was located co-axially downstream of the spray nozzle. The details of this study are illustrated in Chapter 5.

In another study, an additional piece was added to the tip of the injection nozzle to simulate the shroud apparatus that was also previously used in the attrition nozzle study. The results obtained using the shrouded nozzle were compared to the results

obtained with the nozzle used in Chapter 5. Details of this study are presented in Appendix C.

5. **STUDY A REVOLUTIONARY NEW TECHNOLOGY TO IMPROVE SOLID-LIQUID MIXING QUALITY.** Previously, tests were conducted when a draft tube was placed downstream of the injection nozzle. This draft tube was designed to improve the mixing between sprayed droplets and fluidized particles. However, there may be another innovative technology that could improve the mixing even more. Tests were performed in a downer equipped with a mixing chamber at its entrance, in which liquid was sprayed through nozzles and contacted with circulating solids. An efficient method was developed to determine the local quality of solid-liquid mixing on a short time scale. The measurement technique used two types of measurements in order to obtain the cross-sectional distribution of liquid-to-solid ratios. First, temperature measurements were used to characterize the solid/liquid distribution and, second, tribo-electric probes were used to obtain the local solids fluxes. These techniques were used to determine the mixing chamber geometries which provided the best solid-liquid mixing. The results of this investigation are provided in Chapter 6.
6. **DEVELOP A MEASUREMENT TECHNIQUE TO MEASURE THE STABILITY OF THE SOLID-LIQUID FLOW.** To achieve the best mixing results, the mixing chamber should provide a stable solid-liquid dispersion. Therefore, a measurement technique to measure the stability of the solid-liquid flow in the downer was required. Previous studies have investigated the stability of liquid sprays into conventional fluidized beds. However, there have not been any studies done which investigated the stability of gas-liquid jets injected into a circulating fluidized bed. A novel technique was developed to determine the stability of the flow in the downer, which applies the tribo-electric technique that was previously used to characterize the solid-liquid contact. The tribo-electric probes were used to obtain the local solids flowrates and their signals were then analyzed to determine the stability of the solids flow. A variety of different startup conditions and injection liquids were tested to determine

their effects on the stability of the system. The results from this study are discussed in Chapter 7.

1.5 References

- Abromovich, G., *The Theory of Turbulent Jets*, Massachusetts: M.I.T. Press, 1963.
- Al-Sherehy, F., Grace, J., Adris, A., “Gas Mixing and Modeling of Secondary Gas Distribution in a Bench-Scale Fluidized Bed”, *AIChE J.*, **50**, 922 – 936 (2004).
- Arastoopour, M., Chen, C., “Attrition of Char Agglomerates”, *Powder Technol.*, **36**, 99-106 (1983).
- Ariyapadi, S., Berruti, F., Briens, C., Griffith, P., Hulet, C., “Modeling the Injection of Gas-Liquid Jets into Fluidized Beds of Fine Particles”, *Can. J. Chem. Eng.*, **81**, 891 – 899, (2003a).
- Ariyapadi, S., Holdsworth, D., Norley, C., Berruti, F., Briens, C., “Digital X-Ray Imaging Technique to Study the Horizontal Injection of Gas-Liquid Jets into Fluidized Beds”, *Int. J. Chem. React. Eng.*, **1** (A56), 1114 (2003b).
- Austin, L., “A Review: Introduction to the Mathematical Description of Grinding As a Rate Process”, *Powder Technol.*, **5**, 1-17, (1971).
- Baddour, C., Briens, C., “Modeling the Grinding Process of Carbon Nanotubes”, Manuscript Submitted to *AIChE J.*, (2006).
- Behie, L., Bergougnou, M., Baker, C., Bulani, W., “Jet Momentum Dissipation at a Grid of a Large Gas Fluidised Bed”, *Can. J. Chem. Eng.*, **48**, 158 – 161 (1970).
- Bentham, A., Kwan, C., Boerefijn, R., Ghadiri, M., “Fluidised-Bed Jet Milling of Pharmaceutical Powders”, *Powder Technol.*, **161**, 233-238 (2004).
- Benz, M., Herold, H., Ulfik, B., “Performance of a Fluidized Bed Jet Mill as a Function of Operating Parameters”, *Int. J. Miner. Process.*, **44-45**, 507-519 (1996).
- Berg, D., Briens, C., Bergougnou, M., “Reactor Development for the UltrapYROLYSIS Process”, *Can. J. Chem. Eng.*, **67**, 96-101 (1989).
- Berthiaux, H., Dodds, J. “Modelling Fine Grinding in a Fluidized Bed Opposed Jet Mill. Part I: Batch Grinding Kinetics”, *Powder Technol.* **106**, 78-87 (1999).
- Berthiaux, H., Chiron, C., Dodds, J., “Modelling Fine Grinding in a Fluidized Bed Opposed Jet Mill. Part II: Continuous Grinding Kinetics”, *Powder Technol.*, **106**, 88-97 (1999).

- Blinichev, V., Strel'tsov, V., Lebedeva, E., "An Investigation of the Size Reduction of Granular Materials During Their Processing In Fluidized Beds", *Int. Chem. Eng.* **8**, 615-618 (1968).
- Briens, C., Mirgain, C., Bergougnou, M., Del Pozo, M., Loutaty, R., "Evaluation of Gas-Solids Mixing Chamber Through Cross Correlation and Hurst's Analysis", *AIChE J.*, **43**, 1469-1479 (1997).
- Bruhns, S. "On the mechanism of Liquid Injection into Fluidized Bed Reactors", *PhD Thesis*, Technical University of Hamburg-Harburg, Germany (2002).
- Bruhns, S., Werther, J., "On the Mechanism of Liquid Injection into Fluidized Bed Reactors", *Fluidization XI*, U. Arena, R. Chirone, M. Miccio, P. Salatino, (Eds.) Engineering Conferences International, Brooklyn, NY: 2004, pp. 67 – 74.
- Brust, H., Wirth, K., "Gas/Solids Mixing-Behaviour in the Entrance Region of a Downer and its Effect on the Residence Time Distribution of the Gas", *Fluidization XI*, U. Arena, R. Chirone, M. Miccio, P. Salatino, (Eds.), Engineering Foundation, New York, 2004a, pp. 371 – 378.
- Brust, H., Wirth, K., "Residence Time Behaviour of Gas in a Downer Reactor", *Ind. Eng. Chem. Res.*, **43**, 5796-5801 (2004b).
- Boerefijn, R., Gudde, N., Ghadiri, M., "Review of Attrition of Fluid Cracking Catalyst Particles", *Adv. Powder Tech.*, **11**, 145-174 (2000).
- Chan, E., McDougall, S., Knapper, B., "Nozzle/Mixer Assembly", *United States Patent*: 7 025 874 (2004).
- Chang, S., Lottes, S., Zhou, C., Bowman, B., Petrick, M., "Numerical Study of Spray Injection Effects on the Heat Transfer and Product Yields of FCC Riser Reactors", *J. Heat Trans.*, **123**, 544-555 (2001).
- Chen, T., Sishtla, C., Punwani, D., Arastoopour, H., "A Model for Attrition In Fluidized Beds", in: J. Grace, J. Matsen, (Eds.), *Fluidization*, Engineering Foundation, New York, NY: 1980, pp. 445 – 452.
- Davuluri, R., Knowlton, T., "Development of a Standard Attrition Test Procedure", in: L.-S. Fan, T. Knowlton, (Eds.), *Fluidization IX*, Engineering Foundation, New York, NY: 1998, pp. 333 – 340.
- De Michele, G., Elia, A., Massimilla, L., "The Interaction Between Jets and Fluidized Beds", *Ing. Chim. Ital.*, **12**, 155 – 162 (1976).
- Donsi, G., Massimilla, L., Colantuoni, L., "The Dispersion of Axi-Symmetric Gas Jets in

- Fluidized Beds”, *Fluidization*, J. Grace, J. Matsen, (Eds.), Plenum Press: New York, NY, 1980, pp.297 – 304.
- Dunlop, D., Griffin, L., Moser, J., “Particle Size Control in Fluid Coking”, *Chem. Eng. Prog.*, **54**, 39-43 (1958).
- Epstein, B., “Logarithmico-Normal Distribution in Breakage of Solids”, *Ind. Eng. Chem.*, **40**, 2289-2291, (1948).
- Felli, V., “Solids Entrainment From a Fluidized Bed into a Gas-Liquid Jet”. *MESc Thesis*, The University of Western Ontario, (2002).
- Gao, J., Xu, C., Lin, S., Yang, G., Guo, Y., “Simulations of Gas-Liquid-Solid 3-Phase Flow and Reaction in FCC Riser Reactors”, *AIChE J.*, **47**, 677-692 (2001).
- Ghadiri, M., Cleaver, J., Tuponogov, V., Werther, J., “Attrition of FCC Powder in the Jetting Region of a Fluidized Bed”, *Powder Technol.*, **80**, 175-178 (1994).
- Godet-Morand, L., Chamayou, A., Dodds, J., “Talc Grinding in an Opposed Air Jet Mill: Start-up, Product Quality and Production Rate Optimization”, *Powder Technol.* **128**, 306– 313 (2002).
- Gommeren, H., Heitzmann, D., Kramer, H., Heiskanen, K., Scarlett, B., “Dynamic Modeling of a Closed Loop Jet Mill”, *Int. J. of Min. Proc.*, **44-45**, 497-506, (1996).
- Gommeren, H., Heitzmann, D., Moolenaar, J., Scarlett, B., “Modelling and Control of a Jet Mill Plant”, *Powder Technol.* **108**, 147-154, (2000).
- Government of Alberta-Energy, <<<http://www.energy.gov.ab.ca/100.asp>>>, (2006)
- Gray, M., “Upgrading Petroleum Residues and Heavy Oils”, Marcel Dekker, New York, NY, 1994.
- Gray, M., “Fundamentals of Bitumen Coking Processes Analogous to Granulations: A Critical Review”, *Can. J. Chem. Eng.*, **80**, 393 – 401 (2002).
- Gupta, A., Subba Rao, D., “Model for the Performance of a Fluid Catalytic Cracking (FCC) Riser Reactor: Effect of Feed Atomization”, *Chem. Eng. Sci.*, **56**, 4489-4503 (2001).
- Han, T., Kalman, H., Levy, A., “DEM Simulation of Particle Comminution in Jet Milling”, *Trans. Soc. Min. Eng. of AIME*, **247**, 309, (2002).
- Henderson, K., Smith, L., Silva, P., “Throughput Efficiency Enhancement of Fluidized Bed Jet Mill”, *United States Patent*, 5 562 253 (1996).

- Hong, R., Li, H., Li, H., Wang, Y., "Studies on the Inclined Jet Penetration Length in a Gas-Solid Fluidized Bed", *Powder Technol.*, **92**, 205 – 212 (1997).
- House, P., Saberian, M., Briens, C., Berruti, F., Chan, E., "Injection of a Liquid Spray into a Fluidized Bed: Particle-Liquid Mixing and Impact on Fluid Coker Yields", *Ind. Eng. Chem.*, **43**, 5663 – 5669 (2004).
- Hulet, C., Briens, C., Berruti, F., Chan, E., Ariyapadi, S., "Entrainment and Stability of a Horizontal Gas-Liquid jet in a Fluidized Bed", *Int. J. Chem. React. Eng.*, **1** (A60), 1127, (2003).
- Jiang, Y., McAuley, K., Hsu, J., "Heat Removal from Gas-Phase Polyethylene Reactors in the Supercondensed Mode", *Ind. Eng. Chem. Res.*, **37**, 1176 – 1180 (1997).
- Johnston, P., De Lasa, Zhu, H., "Axial Flow Structure in the Entrance Region of a Downer Fluidized Bed: Effects of the Distributor Design", *Chem. Eng. Sci.*, **54**, 2161-2173 (1999).
- Knapper, B., Gray, M., Chan, E., Mikula, R., "Measurement of Efficiency of Distribution of Liquid Feed in a Gas-Solid Fluidized Bed Reactor", *Int. J. Chem. React. Eng.*, **1**(A35), 1035 (2003).
- Leclerc, K., Briens, C., Gauthier, T., Bergougnou, M., Bayle, J., Guigon, P., "Liquid Vaporization in a Fluidized Bed", *Ind. Eng. Chem. Res.*, **40**, 5415 - 5420 (2001a).
- Leclerc, K., Briens, C., Gauthier, T., Bayle, J., Bergougnou, M., Guigon, P., "Experimental Study of Droplet Vaporization in a Fluidized Bed," *Can. J. Chem. Eng.*, **79**, 866 – 873 (2001b).
- Leclerc, K., Briens, C., Gauthier, T., Bergougnou, M., Bayle, J., Guigon, P., "Experimental Measurement of Droplet Vaporization Kinetics in a Fluidized Bed", *Chem. Eng. Process.*, **43**, 693 – 699 (2004).
- Levenspiel, O., Kunii, D., Fitzgerald, T., "The Processing of Solids of Changing Size in Bubbling Fluidized Beds", *Powder Technol.*, **2**, 87-96 (1968).
- Lin, L., Sears, J., Wen, C., "Elutriation and Attrition of Char from a Large Fluidized Bed", *Powder Technol.*, **27**, 105-115 (1980).
- Massimilla, L., "Gas Jets in Fluidized Beds", *Fluidization*, J. Davidson, R. Clift, D. Harrison, (Eds.), Academic Press: London, 1985, pp. 133 – 172.
- Merrick, D., Highley, J., "Particle Size Reduction and Elutriation in a Fluidized Bed Process", *AIChE Symp. Ser.*, **70**, 366 (1974).

- Merry, J., "Penetration of a Horizontal Gas Jet into a Fluidised Bed", *Trans. Instn. Chem. Engrs.*, **49**, 189 – 195 (1971).
- Merry, J., "Penetration of Vertical Jets into Fluidized Beds", *AIChE J.*, **21**, 507 – 510 (1975).
- Mirgain, C., Briens, C., Del Pozo, M., Loutaty, R., Bergougnou, M., "New Technique for the Evaluation of a Circulating Fluidized Bed Mixing Chamber with a Central Solids Jet", *Powder Technol.*, **96**, 202-210 (1998).
- Mirgain, C., Briens, C., Del Pozo, M., Loutaty, R., Bergougnou, M., "Modeling of Feed Vaporization in Fluid Catalytic Cracking", *Ind. Eng. Chem. Res.*, **39**, 4392 – 4399 (2000).
- Namkung, W., Kim, S., "Radial Gas Mixing in a Circulating Fluidized Bed", *Powder Technol.*, **113**, 23-29 (2000).
- Newton, D., "How BP Makes Use of Its X-Ray Imaging Facility to Support Developments in Fluidized Bed Processes", *Proceedings of the 1998 AIChE Annual Meeting*, (1998).
- Oka, S. "Fluidized Bed Combustion", M. Dekker: New York, 2004.
- Pacek, A., Nienow, A., "Application of Jet Grinding to Fluidised Bed Granulation", *Powder Technol.*, **65**, 305-310 (1991).
- Patel, K., Nienow, A., Milne, I., "Attrition of Urea in a Gas-Fluidised Bed", *Powder Technol.*, **47**, 257-261 (1986).
- Perry, R., Green, D., (Eds.) *Perry's Chemical Engineers' Handbook, 7th Ed.* New York: McGraw-Hill, 1997, p. 6-23.
- Ray, Y., Jiang, T., Jiang, T., "Particle Population Model for a Fluidized Bed with Attrition", *Powder Technol.*, **52**, 35-48, (1987).
- Reid, K., "A Solution to the Batch Grinding Equation", *Chem. Eng. Sci.*, **20**, 953-963, (1965).
- Rhodes, M., *Principles of Powder Technology*, John Wiley & Sons: Toronto, 1990.
- Schuurmans, H., "Measurements in a Commercial Catalytic Cracking Unit", *Ind. Eng. Chem. Proc. Des. Dev.*, **19**, 267-271 (1980).

- Siegel, H., Olson, J., "Impact Target for Fluid Energy Mills", *United States Patent* 4 089 472, (1978).
- Shakhova, N., Minaev, G., "Investigation of the Temperature Field in the Spray Zone of a Granulator with a Fluidized Bed", *Int. Chem. Eng.*, **13** (1), 65 - 68 (1973).
- Shamlou, P., Liu, Z., Yates, J., "Hydrodynamic Influences on Particle Breakage in Fluidized Beds", *Chem. Eng. Sci.*, **45**, 809-817 (1990).
- Sherrington, P., Oliver, R., *Granulation*, Heyden: London, UK, 1981.
- Skouby, D., "Hydrodynamic Studies in a 0.45m Riser with Liquid Feed Injection" *AIChE Symp.*, **95**, 67-70 (1999).
- Smith, P., Nienow, A., "On Atomising a Liquid Into a Gas Fluidized Bed", *Chem. Eng. Sci.*, **37** (6), 950 - 954 (1982).
- Smith, L., Mastalski, H., "Throughput Efficiency Enhancement of Fluidized Bed Jet Mill", *United States Patent*, 5 133 504 (1992).
- Stein, M., Seville, J., Parker, D., "Attrition of Porous Glass Particles in a Fluidised Bed", *Powder Technol.*, **100**, 242-250 (1998).
- Syncrude Canada Ltd., <<<http://www.syncrude.ca>>>, (2006)
- Tafreshi, Z., Kirpalani, D., Bennett, A., McCracken, T., "Improving the Efficiency of Fluid Cokers by Altering Two-Phase Feed Characteristics", *Powder Technol.*, **125**, 234-241 (2002).
- Tasirin, S., Geldart, D., "Experimental Investigation on Fluidized Bed Jet Grinding", *Powder Technol.* **105**, 337-341 (1999).
- Wang, X., Zhu, C., "Concentric Evaporating Spray Jets in Dilute Gas-Solids Pipe Flows", *Powder Technol.*, **129**, 59 - 71 (2003).
- Werther, J., Xi, W., "Jet Attrition of Catalyst Particles in Gas Fluidized Beds", *Powder Technol.*, **76**, 39-46 (1993).
- Werther, J., Rappenhagen, J., "Catalyst Attrition in Fluidized-Bed Systems", *AIChE J.*, **45**, 2001-2010 (1999).
- Werther, J., "Fluidized-Bed Reactors", *Ullmann's Encyclopedia of Industrial Chemistry*, Wiley-VCH: Weinheim, 2001.

- Wu, S., Baeyens, J., Chu, C., "Effect of the Grid-Velocity on Attrition in Gas Fluidized Beds", *Can. J. Chem. Eng.*, **77**, 738-744 (1999).
- Xuereb, C., Laguerie, C., Baron, T., "Etude du Comportement de Jets Continus Horizontaux ou Inclines Introduits Dans un Lit Fluidise Par un Gaz. I : Morphologie des Jets", *Powder Technol.*, **67**, 43 – 56 (1991a).
- Xuereb, C., Laguerie, C., Baron, T., "Etude du Comportement de Jets Continus Horizontaux ou Inclines Introduits Dans un Lit Fluidise Par un Gaz. II : Profiles de Vitesse du Gaz Dans Les Jets Horizontaux", *Powder Technol.*, **64**, 271 – 283 (1991b).
- Yates, J., Cobbinah, S., Cheesman, D., Jordan, S., "Particle Attrition in Fluidized Beds Containing Opposing Jets", *AIChE Symposium Series* **87**, 13-19 (1991).
- Zenz, F., "Bubble Formation and Grid Design", *I. Chem. E. Symp. Series*, **30**, 136-139 (1968).
- Zhang, M., Qian, Z., Yu, H., Wei, F., "Gas-Solid Flow Behaviours in a 0.42 m Diameter CFB Downer with Nozzle Gas Injection", *Fluidization XI*, U. Arena, R. Chirone, M. Miccio, P. Salatino, (Eds.), Engineering Foundation, New York 2004, pp. 323 – 330.
- Zheng, Q., Wei, X., Fei, L., "Experimental Study on Radial Gas Dispersion and its Enhancement in Circulating Fluidized Beds", *Fluidization VII*, O. Potter D. Nicklin, (Eds.), Engineering Foundation, New York, 1992, pp. 285-293.
- Zhu, C., Wang, X., Fan, L.-S., "Effect of Solids Concentration on Evaporative Liquid Jets in Gas-Solid Flows", *Powder Technol.*, **111**, 79 – 82 (2000).

CHAPTER 2

High Velocity Attrition Nozzles in Fluidized Beds

Jennifer McMillan¹, Cedric Briens¹, Franco Berruti¹, Edward Chan²

¹*Department of Chemical and Biochemical Engineering
The University of Western Ontario
1151 Richmond Street
London, Ontario, Canada, N6A 5B9*

²*Syncrude Canada Ltd.
Edmonton Research Centre
9421-17 Avenue
Edmonton, Alberta, Canada T6N 1H4*

2.1 Introduction

Gas-solid fluidized beds are used in many applications such as polyethylene production, drying, coating, granulation, fluid catalytic cracking and fluid coking. One application in particular, the fluid coking process, uses thermal cracking to upgrade bitumen extracted from oil sands to produce synthetic crude oil. During the fluid coking process there is a gradual increase in the size of the coke particles due to the formation and deposition of coke, a reaction byproduct, on the surface of the particles during the reaction. In addition to particle growth due to the reaction, agglomerates are also formed when several coke particles stick together as a result of poor feed distribution. Controlling the particle size of the coke within the fluid coker is of great importance, since large particles will result in slugging and poor circulation. Conversely, if too many fine particles with a diameter less than 70 microns exist, agglomeration will occur and lead to poor fluidization (Dunlop et al., 1958). In order to control the size of the particles in the fluidized bed, steam is injected into the reactor section through attrition nozzles. The high velocity gas jets issuing from each of these nozzles entrain bed particles and accelerate them to a high speed; because of their inertia, these particles slam on slow

moving bed particles near the jet tip, causing breakage and, thus, reducing the particle size.

Currently attrition nozzles require a large quantity of steam. Improving the efficiency of the attrition nozzles would reduce steam consumption, which could allow more throughput to the reactor.

There are two main modes of attrition: abrasion and fragmentation. Abrasion occurs when very fine pieces are removed from the surface of the particle, thus producing many fines, while the particle size distribution of the mother particles remains unchanged. Alternatively, fragmentation occurs when a particle breaks into pieces of similar size (Werther and Rappenhagen, 1999). There are two main variables that affect the attrition process in a fluidized bed. The first is the particle properties such as shape, surface roughness and strength. The second is the properties of the environment such as the fluidization velocity, and operating pressure of the attrition gas (Patel et al., 1986).

A number of researchers have studied the effects of particle properties and fluidized bed operating conditions on particle attrition resulting from particle interactions with gas jets issuing from the distributor plate and with gas bubbles in the bulk of the bed (Werther and Rappenhagen, 1999; Patel et al., 1986; Arastoopour and Chen, 1983; Blinichev et al., 1968; Lin et al., 1980; Stein et al., 1998). For example, Lin (1980) studied elutriation and attrition in a fluidized bed and found that the rate of attrition was a function of the excess gas velocity ($U_g - U_{mf}$), and that the particle diameter had little effect on the attrition rate. They found that the majority of the attrition occurred in the bubble wakes and an empirical correlation for estimating the rate of fines generation was presented.

Several studies have been published focusing on the effects of injecting subsonic jets on the attrition of particles in fluidized beds (Pacek and Nienow, 1991; Wu et al., 1999; Benthams et al., 2004; Boerefijn et al., 2000; Werther and Xi, 1993; Chen et al., 1980; Ghadiri et al., 1994). All of these studies have found that the attrition rate was dependent on the velocity of the jet. Most recently, Benthams et al. (2004) analyzed particle breakage in a single jet region in a fluidized bed in order to determine the role of jet hydrodynamics and material properties. They found that the breakage mechanism in a fluidized bed jet involves the entrainment of particles from the dense phase region

surrounding the jet into the dilute jet core. Once in this region, particles were accelerated by the gas jet and collided with each other as well as impacting on the dense phase at the top of the jet. The breakage of the particles was also successfully predicted as a function of the jet velocity and exhibited a strong sensitivity to changes in jet angle and gas flow rate.

The majority of the publications have found that the attrition rate can be described by a power law function of the attrition jet velocity. Werther and Xi (1993) studied grid jet attrition, and suggested a model which considered the efficiency of the process by relating the surface energy created by the process to the kinetic energy which was spent to produce the surface area. For a jet issuing from an orifice, having a diameter d_0 , with a velocity of u_0 into a gas fluidized bed, the following correlation of the jet attrition rate was presented:

$$R_a = K \rho d_0^2 u_0^3 = K' m_0 u_0^2 \quad (2.1)$$

where the attrition constant K or K' described the material property. Their measurements showed good agreement between theory and experiment. The effect of jet attrition depended on whether the jet was issuing into a fluidized bed or into a non-aerated bed. The jet attrition rate of an upward jet was equal to that of a horizontal jet, whereas the attrition rate of a downward jet was significantly higher. However, relatively small nozzle diameters and gas velocities were tested.

Chen et al. (1980) obtained attrition data in a fluidized bed with a single jet mounted in a porous plate distributor and developed a model to predict the particle size distribution and amount of fines generated from a jet in fluidized beds. A similar correlation:

$$R_a \propto m_0 u_0^2 \quad (2.2)$$

was proposed and confirmed by experiments using different types of particles. Their theoretical analysis was based on the assumption that jet impingement was the only significant cause of attrition. The fines generation rate was assumed to be proportional to energy received per unit time and excess surface area.

Ghadiri et al. (1994) found that, in general, correlations for the attrition rate can be represented by:

$$R_a \propto u_0^n d_0^h \quad (2.3)$$

They found that the fitted exponent on the orifice gas velocity, n , covered a very wide range from 1 to 5.8, and that the exponent on the orifice diameter, h , was 2. Ghadiri et al. (1994) also concluded that particle size and material properties have a strong influence on this exponent.

It has also been found that the gas density affects the attrition rate. Davuluri and Knowlton (1998) found that the attrition rate was proportional to the gas density raised to an exponent of 1.4, while Shamlou et al. (1990) reported that it was directly proportional to the gas density.

Very few recent studies have been conducted using high velocity attrition jets in fluidized beds (Dunlop et al., 1958; Forsythe and Hertwig, 1949; Tasirin and Geldart, 1999). Dunlop et al. (1958) found that the equilibrium distribution of particle sizes in a fluid coker was influenced by the size of the small particles added and by the ratio of large to small particles. A high velocity gas jet was injected into the bed of fluidized particles and the grinding was found to be a direct function of the horsepower, as estimated by assuming an adiabatic expansion of the gas.

Forsythe and Hertwig (1949) developed a standard test based on a single submerged air jet at high air velocities for the assessment of attrition for various types of catalysts. A 0.39 mm diameter nozzle was used which injected gas at a sonic velocity of 340 m/s. They found that microspheroidal particles had considerably better attrition resistance than ground catalysts because of their improved particle shape. Also, the presence of fine particles in the catalyst reduced the rate of attrition of the coarser particles.

Although not mentioned in the publications, most of the experimental research on jet grinding is believed to have been done using straight tube nozzles. Only one experimental research work has been done using a nozzle with the contraction-expansion geometry typical of Laval nozzles (Benz et al., 1996). Nozzle geometry may be an important parameter which affects the grinding rate. Also, there are no publications involving jet grinding done under sonic conditions at the nozzle orifice. Investigations on jet grinding characteristics using nozzles with an expansion section and operating at sonic conditions are needed.

The objective of this study was to optimize the operating conditions of existing sonic velocity attrition nozzles and to develop an empirical correlation in order to predict the grinding efficiency. Different types of attrition nozzles were tested in order to determine the effect of nozzle geometry on the grinding efficiency and attrition gas consumption. Various exit diameters were also tested in order to determine the effect of nozzle scale on the grinding efficiency and attrition gas consumption. The nozzle operating pressure and the bed fluidization velocities were varied in order to determine their effects on the grinding efficiency. Finally, different types of particles and attrition gases were tested in order to determine the effect of the solid and gas properties on the grinding efficiency.

2.2 Experimental Set-Up

Experiments were conducted in a fluidized bed with a height of 3.2 m and a rectangular cross section of 1 m by 0.3 m, as shown in Figure 2.1. The particles filled the column to a height of approximately 0.3 m and were fluidized with air at various fluidization velocities. Entrained particles were separated from the gas stream by two cyclones in series. Particles from the primary cyclone were continuously returned to the fluidized bed by a dipleg. Particles from the secondary cyclone were collected after each run: under most of the studied conditions, their contribution to the new particle surface was negligible.

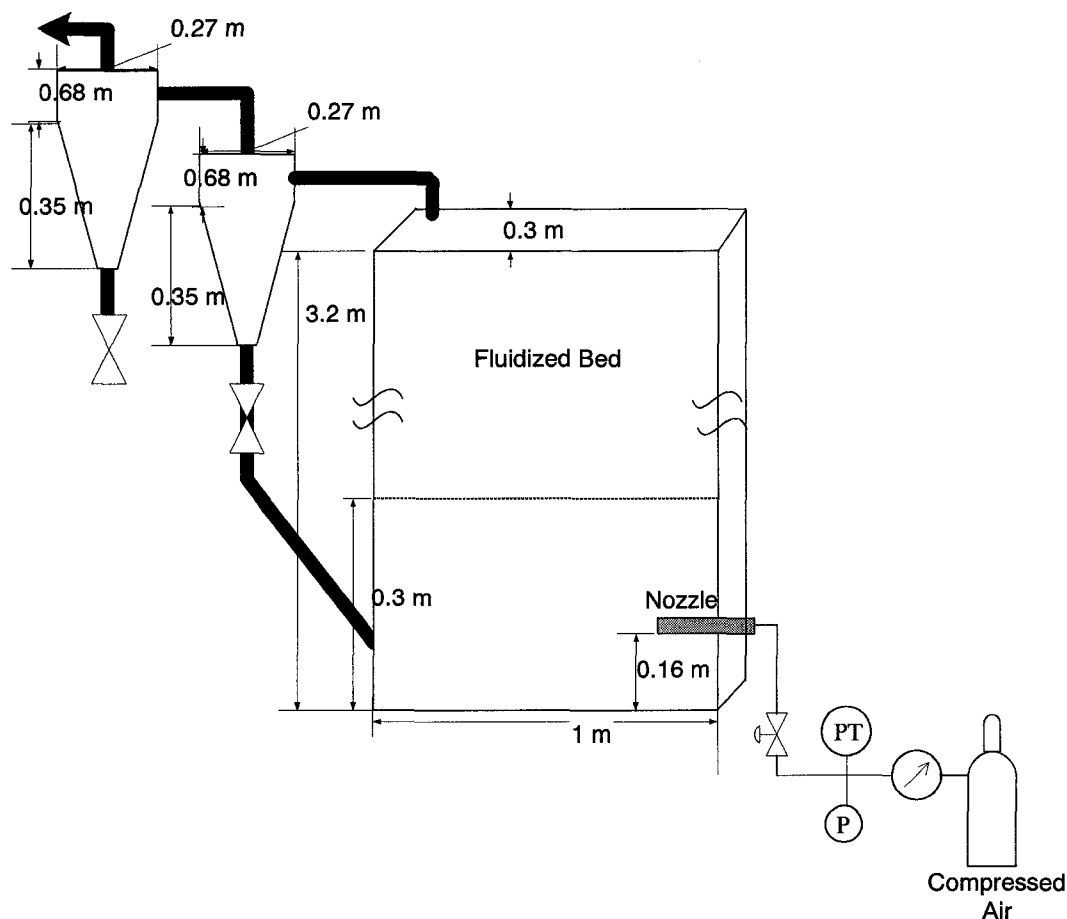


Figure 2.1: Experimental Set-Up

The attrition nozzle was placed inside the bed at a distance of 0.16 m above the gas distributor, and injected gas horizontally into the fluidized particles in order to grind the particles. A constant gas mass flowrate from a high-pressure cylinder was supplied to the injection nozzle during the grinding process. Adjusting the pressure of the cylinder controlled the gas flowrate to the nozzle. Prior calibration provided the relationship between applied pressure and mass flowrate for each nozzle. The mass gas flowrate was verified after each run by comparing the cylinder pressure which was measured by a transducer connected to a data acquisition system.

After each injection, the fluidization gas was stopped in order to slump the bed. The fluidization gas was then turned on again at a velocity just above the minimum bubbling velocity for approximately 5 minutes in order to mix the particles (separate experiments indicated that background particle attrition in the fluidized bed, in the

absence of an attrition jet, was negligible when compared to the attrition observed with the nozzles). A sample of solids was taken from the bed before and after each run and analyzed using a Malvern laser diffraction apparatus in order to obtain the size distribution and the specific surface area created during the grinding process.

Three different types of attrition nozzles were tested in order to determine the effect of nozzle geometry on the grinding efficiency and attrition gas consumption. The first nozzle, Type A, was a convergent-divergent, Laval-type nozzle, similar to the nozzles used by Benz et al. (1996). The second nozzle, Type B, was a uniquely shaped nozzle which was similar to Type A, but contained a 10 mm straight section at the tip of the nozzle. The third nozzle type tested, Type C, was a simple straight tube nozzle with a 25.4 mm long straight tube located at the nozzle tip. Figures 2.2, 2.3, and 2.4 show nozzles A, B and C, respectively. Type C nozzles with various exit diameters, d_N , were tested in order to determine the effect of nozzle scale on the grinding efficiency and attrition gas consumption. The nozzles that were tested had diameters, d_N , of 4.3 mm, 2.4 mm, 1.7 mm, and 1.2 mm.

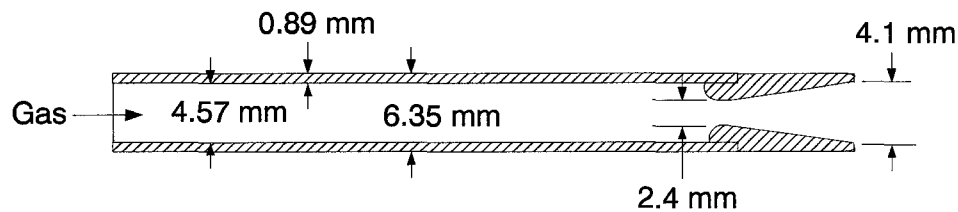


Figure 2.2: Type A Nozzle

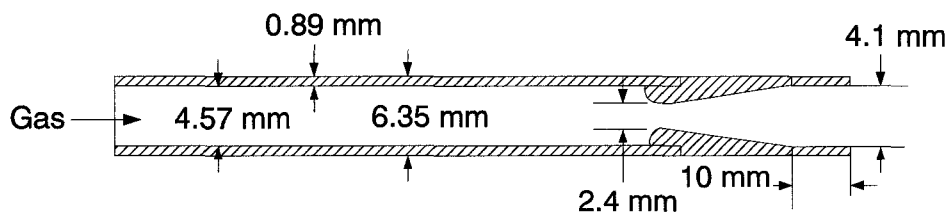


Figure 2.3: Type B Nozzle

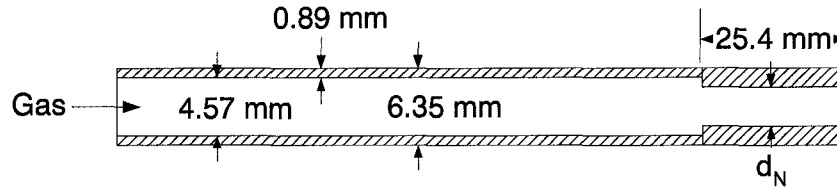


Figure 2.4: Type C Nozzle

Two different types of particles were tested: coke with an original Sauter mean diameter of 135 μm , and silica sand with an initial Sauter mean diameter of 190 μm . In addition, different types of attrition gases: carbon dioxide, argon, air, helium, and different combinations of air/helium mixtures were tested in order to determine the effect of gas properties on the grinding efficiency, such as density, viscosity, and the equivalent speed of sound. The equivalent speed of sound was calculated using equation 2.4, which takes into account the fact that the temperature of the gas changes (Perry and Green, 1997).

$$U_{\text{sound, eq}} = \sqrt{\frac{RT\gamma}{M} \left(\frac{2}{\gamma+1} \right)^{\left(\frac{\gamma+1}{\gamma-1} \right)}} \quad (2.4)$$

Various gas flowrates were tested by changing the upstream pressure. A summary of the experimental test conditions is shown in Table 2.1.

Table 2.1: Experimental Test Conditions

Type of Solids	Attrition Gas	Nozzle Type	Nozzle Diameter (d _N) (mm)	Upstream Pressure (psig)	Fluidization Velocity (U _R) (m/s)
Coke	Air	A	2.4	300,250,200,150,100	0.065
Coke	Air	B	2.4	300,250,200,150,100	0.065
Coke	Air	C	2.4, 1.7, 1.2	300,250,200,150,100	0.065
Silica Sand	Air	A	2.4	300,250,200,150,100	0.065
Silica Sand	Helium	A	2.4	300	0.065
Silica Sand	Argon	A	2.4	300	0.065
Silica Sand	Carbon Dioxide	A	2.4	300	0.065
Silica Sand	0.77Helium/0.23Air	A	2.4	345	0.065
Silica Sand	0.5Helium/0.5Air	A	2.4	345	0.065
Silica Sand	0.33Helium/0.67Air	A	2.4	345	0.065
Silica Sand	Air	B	2.4	300,250,200,150,100	0.065
Silica Sand	Helium	B	2.4	300	0.065
Silica Sand	Air	C	4.3	100	0.065
Silica Sand	Air	C	4.3	300	0.065, 0.12, 0.18
Silica Sand	Helium	C	4.3	100, 300	0.065
Silica Sand	0.77Helium/0.23Air	C	4.3, 2.4	345	0.065
Silica Sand	0.5Helium/0.5Air	C	4.3, 2.4	345	0.065
Silica Sand	0.33Helium/0.67Air	C	4.3, 2.4	345	0.065
Silica Sand	Argon	C	4.3, 2.4	300	0.065
Silica Sand	Carbon Dioxide	C	4.3, 2.4	300	0.065
Silica Sand	Air	C	2.4	250,200,150,100	0.065
Silica Sand	Air	C	2.4	300	0.065, 0.075, 0.09, 0.12, 0.18
Silica Sand	Helium	C	2.4	100, 300	0.065
Silica Sand	Air	C	1.7, 1.2	300,250,200,150,100	0.065
Silica Sand	Helium	C	1.7, 1.2	300	0.065

2.3 Results and Discussion

In order to compare the results from all of the tests, a grinding efficiency was calculated, which was defined as the amount of new surface area created per mass of attrition gas used:

$$\eta = \frac{\text{new particle surface created by attrition}}{\text{mass of required attrition gas}} = \frac{\frac{m^2}{s}}{\frac{kg}{s}} = \frac{m^2}{kg} \quad (2.5)$$

This definition was chosen, as the objective was to achieve maximum grinding, while using a minimum amount of attrition gas. Experiments were conducted with the Type A,

B and C nozzles at different air flowrates in order to determine the effect of nozzle geometry on the grinding efficiency in silica sand. Figure 2.5 shows a plot of the grinding efficiency versus the upstream pressure. Higher grinding efficiencies were obtained at higher gas flowrates, and the highest grinding efficiencies were obtained with the Type A nozzle, followed by the Type B and then Type C nozzle. The venturi-like expansion section of the Type A nozzle increased the momentum of the gas and as a result less gas was required to achieve the same grinding efficiency as a straight-tubed nozzle of equal size. Although better than the Type C nozzle, the extra section of straight tube located at the tip of the Type B nozzle had a detrimental effect on the efficiency of the original, Type A nozzle. The straight tube section reduced the expansion of the jet at the nozzle tip and therefore, reduced the size of the dilute cavity created within the fluidized bed. As a result, fewer particles were entrained and accelerated within the jet, thus decreasing the grinding efficiency.

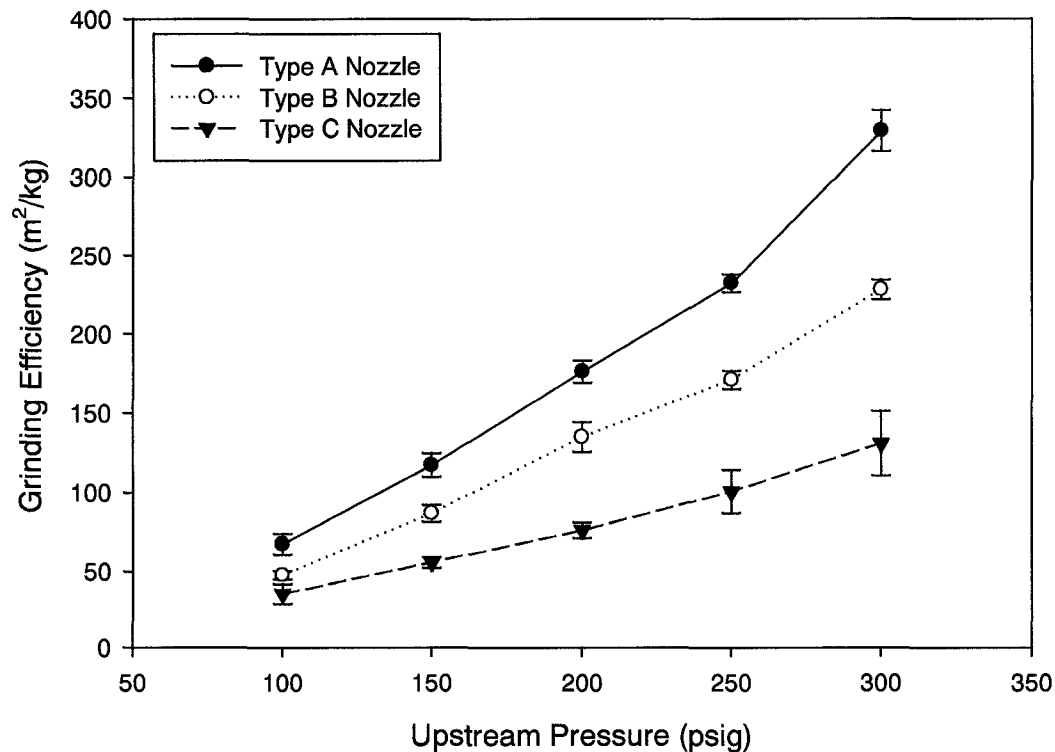


Figure 2.5: Effect of Geometry on Grinding Efficiency; Silica Sand; Air; $d_n = 2.4$ mm; $U_g = 0.065$ m/s (Error Bars Show the Standard Deviation)

In order to determine the effect of scale on the grinding efficiency, tests were done using Type C nozzles of different diameters in silica sand. Air was used as the attrition gas, and the upstream pressure was varied in order to obtain results at various attrition gas flowrates. These results are shown in Figure 2.6. The grinding efficiency increased as both the upstream pressure and nozzle diameter were increased. Larger diameter nozzles create a longer dilute cavity within the fluid bed and as a result the entrained particles are accelerated to a higher velocity before they impact with each other and the remaining particles in the dense phase of the bed.

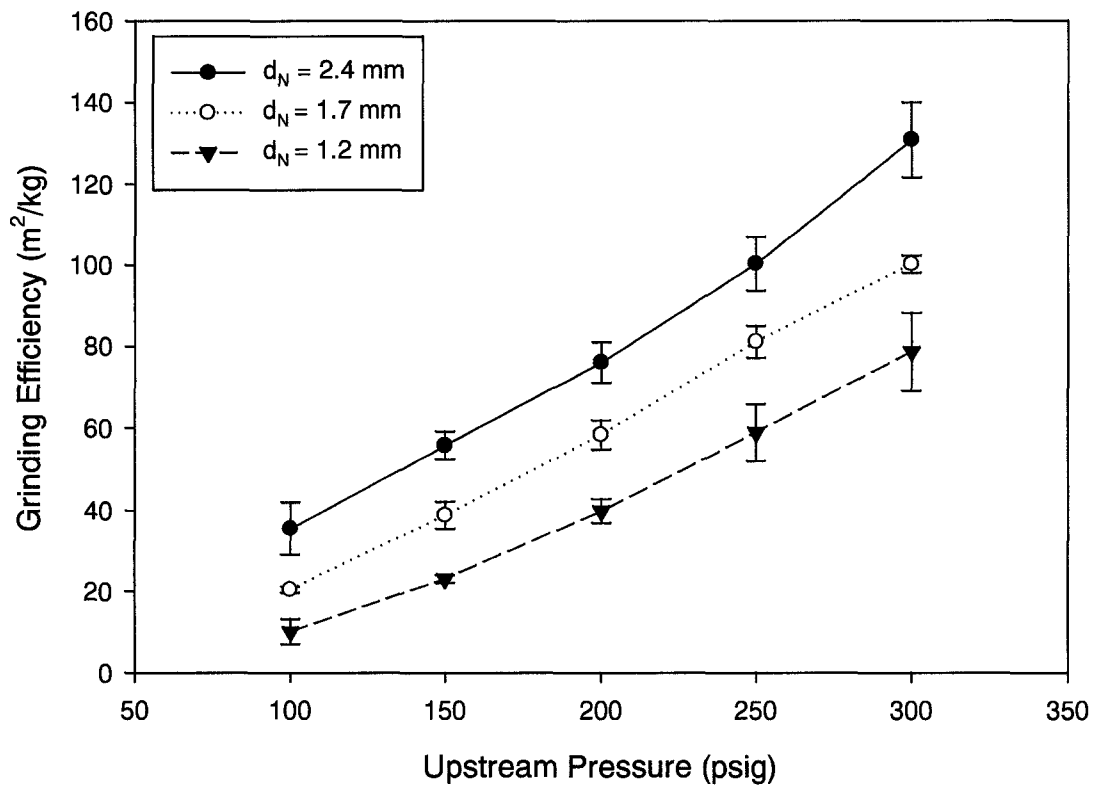


Figure 2.6: Effect of Nozzle Scale on Grinding Efficiency; Silica Sand; Air; Type C Nozzle; $U_g = 0.065$ m/s (Error Bars Show the Standard Deviation)

The effect of solids properties on the grinding efficiency was also determined. Tests were performed in coke using the Type A, B and C nozzles, as well as different scales of Type C nozzles. Figure 2.7 shows the effect of changing the solids on the

grinding efficiency for the Type A nozzle. The same trends were seen when the Type B and Type C nozzles were used. The silica sand resulted in slightly higher grinding efficiencies than the coke. However, similar trends were observed when either silica sand or coke was used.

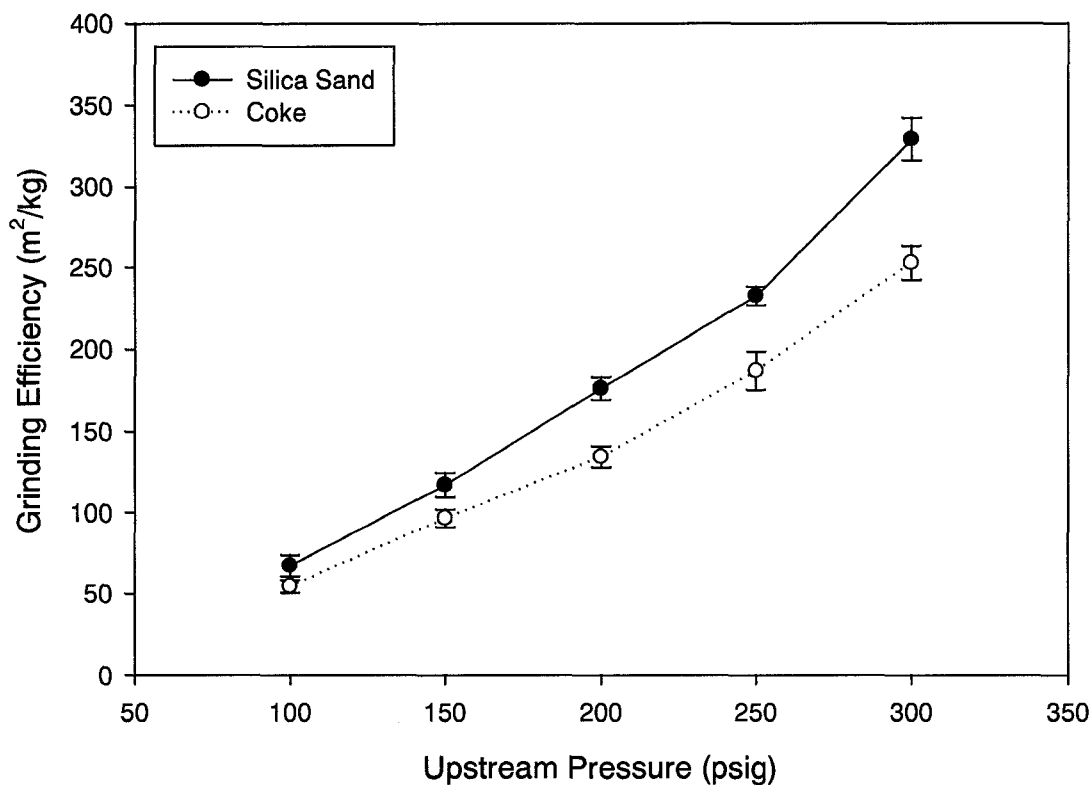


Figure 2.7: Effect of Solid Properties on Grinding Efficiency; Air; $d_n = 2.4$ mm; Type A Nozzle; $U_g = 0.065$ m/s (Error Bars Show the Standard Deviation)

The effect of changing the attrition gas properties was also studied. Various gases with a wide range of densities, equivalent speeds of sound and viscosities, were tested with the 2.4 mm and 4.3 mm Type C nozzles. Table 2.2 summarizes the gas properties for the seven different attrition gases used.

Table 2.2: Gas Properties

Gas (Molar Fraction)	Molar Mass, M (g/mol)	Density at fluidized bed conditions, ρ (kg/m ³)	Equivalent Speed of Sound, $U_{\text{sound,eq}}$ (m/s)	Viscosity, μ (kg/m's)
Carbon Dioxide	44	1.8	158	1.5×10^{-5}
Air	29	1.19	200	1.8×10^{-5}
Argon	40	1.64	181	2.2×10^{-5}
0.33Helium/0.67Air	21	0.85	242	1.8×10^{-5}
0.5Helium/0.5Air	16	0.67	274	1.8×10^{-5}
0.77Helium/0.23Air	10	0.4	362	1.8×10^{-5}
Helium	4	0.16	571	1.8×10^{-5}

Figure 2.8 shows the effect of nozzle scale and gas properties on the grinding efficiency. The grinding efficiencies obtained with the 4.3 mm diameter nozzle were always significantly higher than the grinding efficiencies obtained with the smaller scale nozzles. Also, lower density gases with higher equivalent speeds of sound tended to give larger grinding efficiencies.

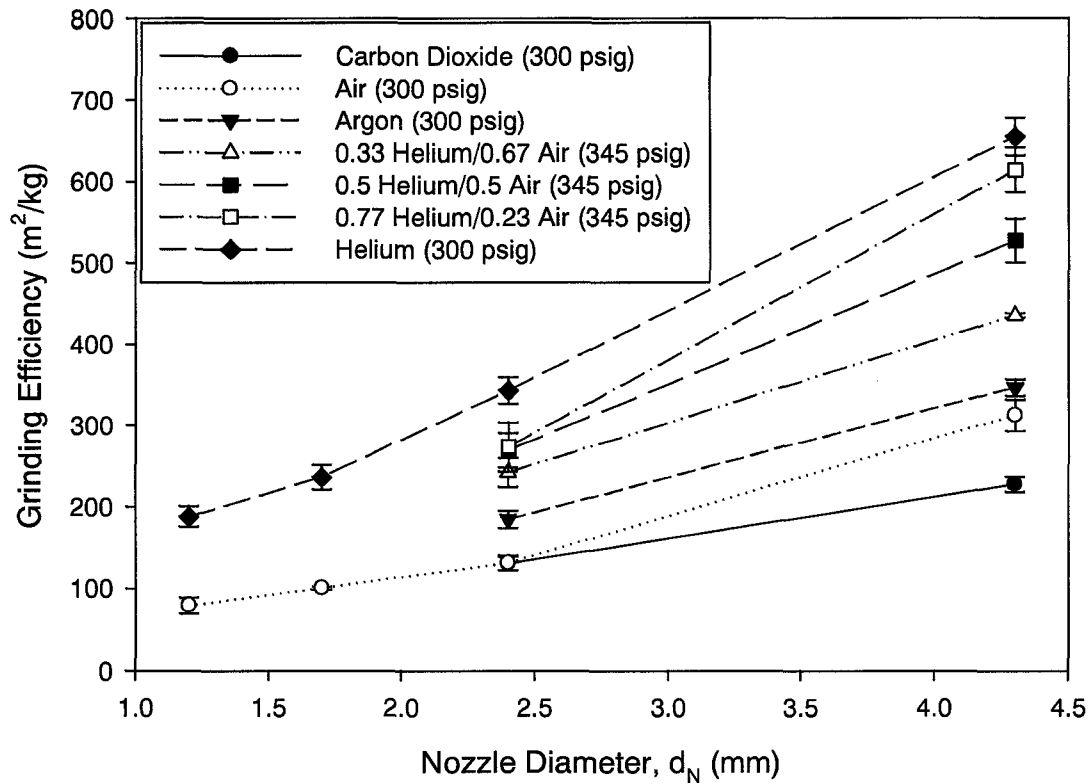


Figure 2.8: Effect of Gas Properties and Nozzle Scale on Grinding Efficiency; Silica Sand; Type C Nozzle; $U_g = 0.065$ m/s (Error Bars Show the Standard Deviation)

Results were also obtained with the Type A and B nozzles using different attrition gases in order to determine the effect of nozzle geometry and gas properties on the grinding efficiency. Figure 2.9 shows a plot of the grinding efficiency versus nozzle type for different gases. The Type A nozzle always had a higher grinding efficiency than the Type B nozzle which had a higher grinding efficiency than the Type C nozzle. Once again, lower density gases with higher equivalent speeds of sound resulted in higher grinding efficiencies.

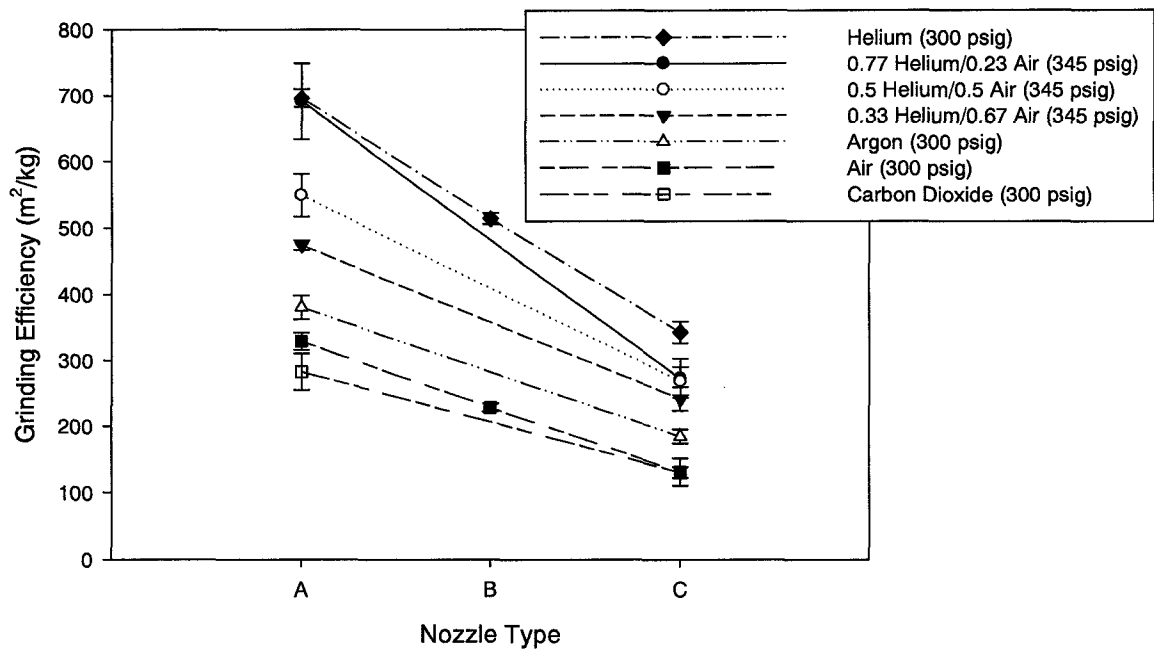


Figure 2.9: Effect of Gas Properties and Nozzle Type on Grinding Efficiency; Silica Sand; $d_n = 2.4$ mm; $U_g = 0.065$ m/s (Error Bars Show the Standard Deviation)

The effect of fluidization velocity on the grinding efficiency was also studied. The minimum fluidization velocities for coke and silica sand are 0.011 m/s and 0.025 m/s, respectively. The majority of the runs were performed at a fluidization velocity of 0.065 m/s, which is well above the minimum fluidization velocity for both types of particles. Runs were performed at higher fluidization velocities using the 2.4 mm and 4.3 mm diameter Type C nozzles at operating pressures of 100 psig and 300 psig. Velocities of 0.075, 0.09, 0.12, and 0.18 m/s were tested. Figure 2.10 shows the grinding efficiencies obtained at various fluidization velocities. The grinding efficiencies were increased when the fluidization velocity was increased. There was no significant in-bed attrition, in the absence of the attrition nozzle, even at the highest fluidization velocity. The effect of the fluidization velocity is, therefore, due to its impact on the attrition nozzle jet. Hulet et al. (2003) studied the effect of fluidization velocity on the mass flowrate of entrained solids into a jet and found that it increased with increasing fluidization velocity. A larger solids entrainment rate increases the number of high

velocity particles impacting slow moving particles at the tip of the jet, thus enhancing particle attrition.

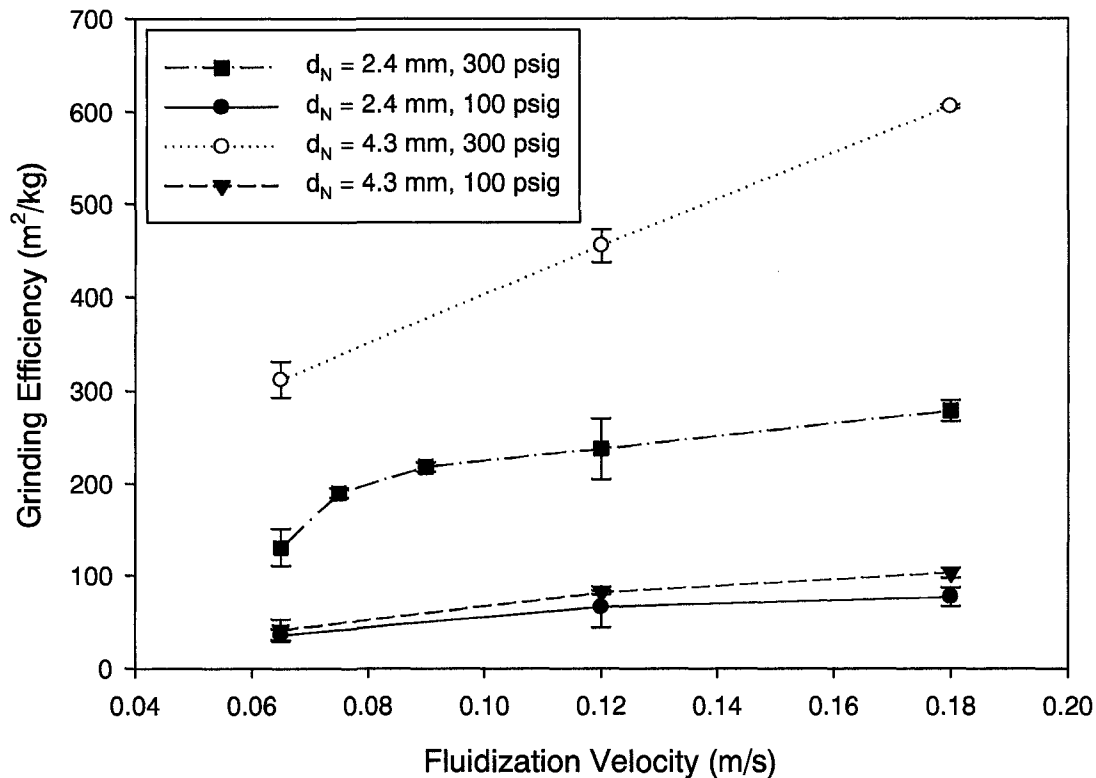


Figure 2.10: Effect of Fluidization on Grinding Efficiency; Silica Sand; Air (Error Bars Show the Standard Deviation)

The effect of sonic flow on the grinding efficiency was also determined. Tests were performed at gas velocities near the equivalent speed of sound in air (200 m/s), and the experimental grinding efficiencies were measured. Figure 2.11 shows a plot of attrition gas velocity versus experimental grinding efficiency (note that for clarity, the velocity was reported as the equivalent gas velocity at the nozzle throat, or the ratio $U_0 = (\rho U)/\rho_0$, where ρ_0 is the gas density at bed conditions). At velocities below 185 m/s, the grinding efficiency increases as the velocity increases. However, once the velocity approaches sonic conditions, there is a drop in effectiveness, which could be due to the expansion of the gas at the nozzle tip. However, once the velocity reaches 201 m/s, and

the velocity exceeds the equivalent speed of sound, the grinding efficiencies once again begin to increase as the velocity increases. Therefore, it appears that nearing sonic conditions has a detrimental effect on grinding efficiency. Although increasing the mass flowrate beyond sonic conditions has a beneficial effect on the grinding efficiency, the grinding efficiency remains lower than it would have been if the trend established well below sonic conditions had been extrapolated to higher velocities. In practice, it is still beneficial to operate well beyond sonic conditions. Therefore, excluding the results shown in Figure 2.11, all other results presented in this paper were obtained under conditions where sonic flow at the nozzle throat existed.

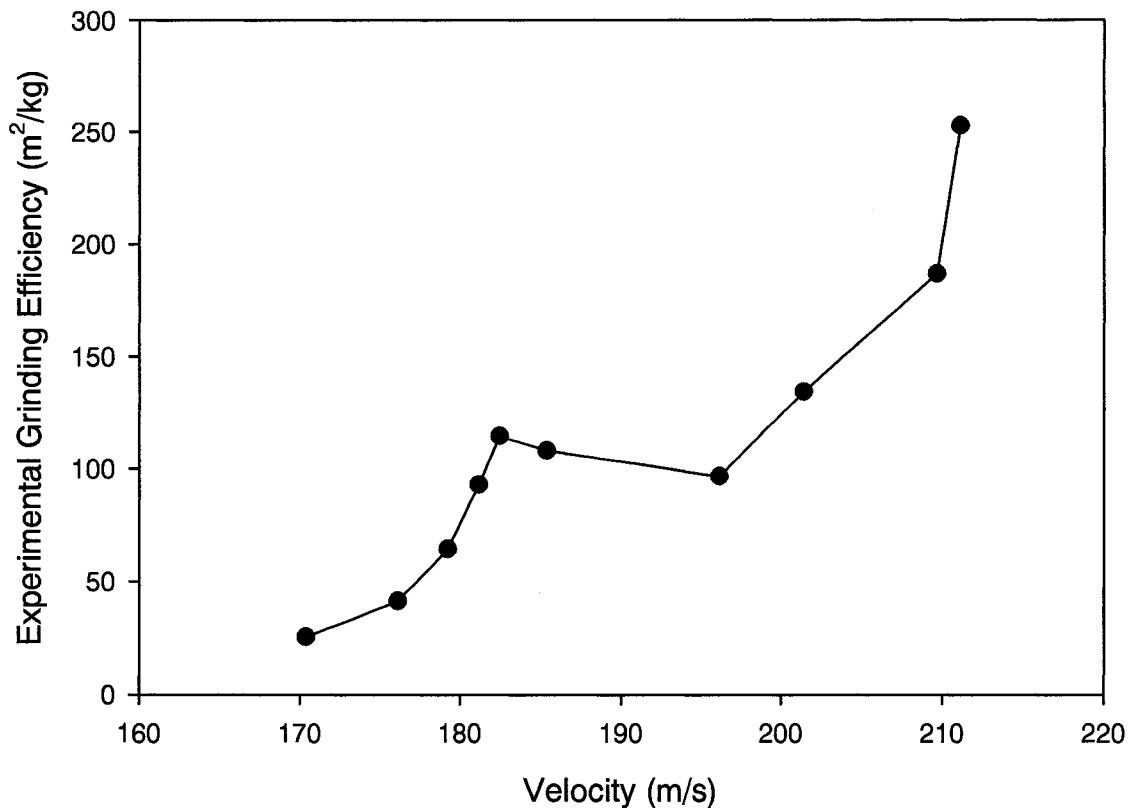


Figure 2.11: Effect of Velocity on Grinding Efficiency

An empirical correlation was developed in order to estimate the grinding efficiency. The correlation takes into account the solid properties, nozzle geometry, nozzle scale, gas properties and fluidization velocity. The following expression was used to predict the grinding efficiency:

$$\eta = 7.81 \times 10^{-7} \alpha \beta d_N^{1.131} U_{\text{sound,eq}}^{0.55} (\rho U_{\text{sound,eq}}^2)^{1.635} \left(\frac{U_g - U_{mf}}{U_{mf}} \right)^{0.494} \quad (2.6)$$

Where:

α = Solid coefficient

Silica: $\alpha = 1$

Coke: $\alpha = 0.8$

β = Geometry coefficient

Type A Nozzle: $\beta = 2.09$

Type B Nozzle: $\beta = 1.55$

Type C Nozzle: $\beta = 1$

Hutchings (1993) reviewed the physical mechanisms involved in grinding and concluded that quantitative, model-based predictions of the effect of particle properties on grinding are not feasible as there are many factors that affect grinding. As a result, a general solid coefficient, α , was used in Equation 2.6. Figure 2.12 shows a comparison of the experimental versus the calculated grinding efficiencies for tests done using coke, including results which were not presented earlier in this publication.

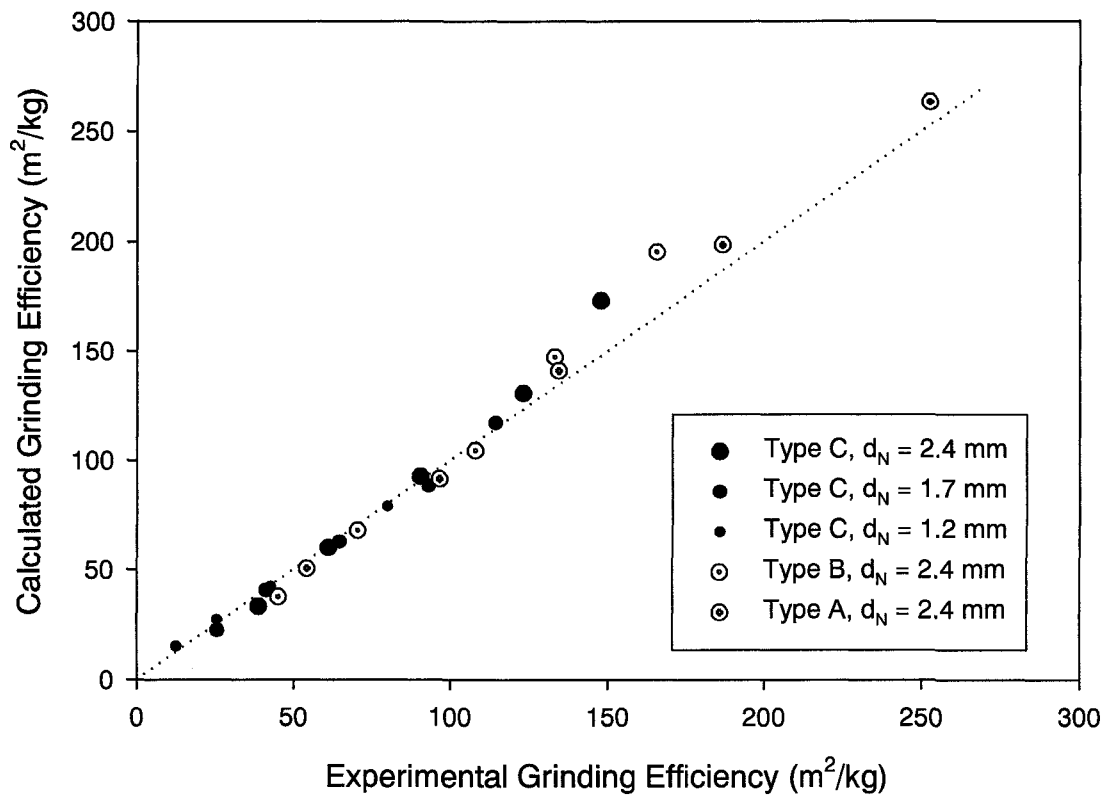


**Figure 2.12: Experimental Versus Calculated Grinding Efficiency; Coke; Air;
 $U_g = 0.065$ m/s**

Figures 2.13, 2.14, and 2.15 show a comparison of the experimental versus the calculated grinding efficiencies for tests done using silica sand for nozzle Types A, B and C, respectively. In all cases there was excellent agreement between calculated and experimental results.

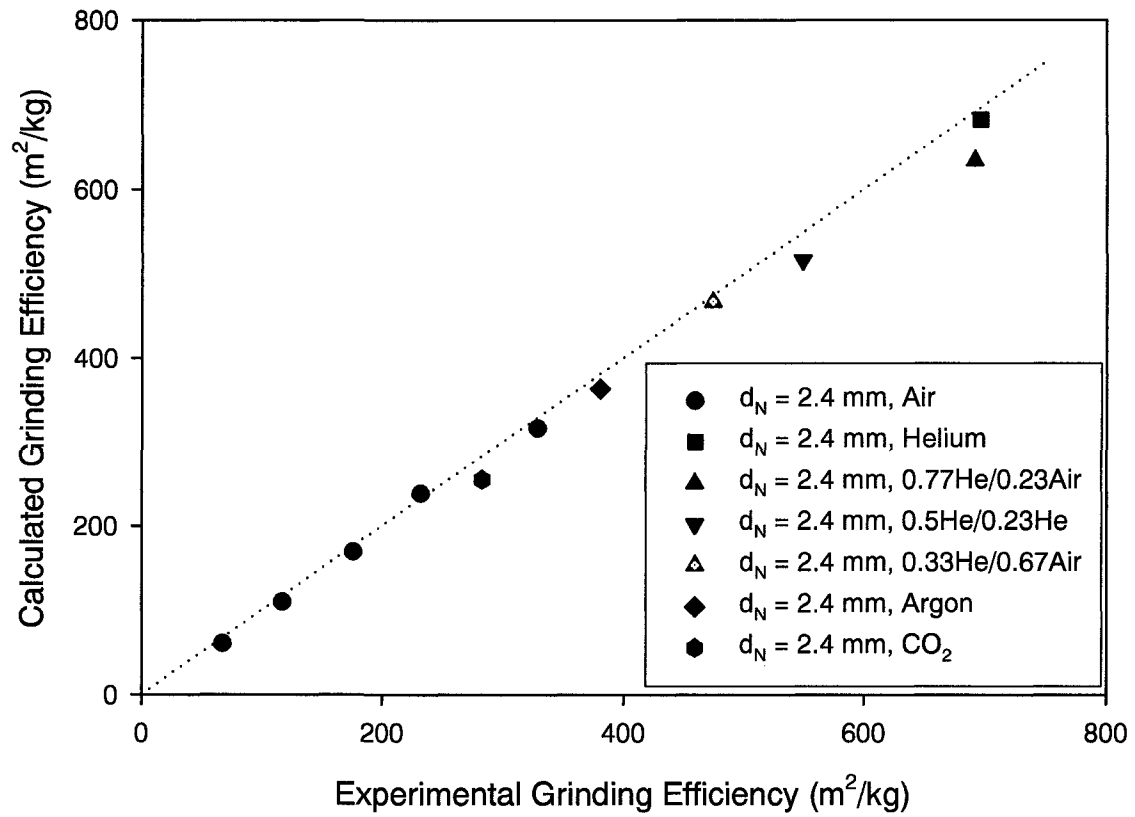


Figure 2.13: Experimental Versus Calculated Grinding Efficiency; Silica Sand; Type A Nozzle; $U_g = 0.065 \text{ m/s}$

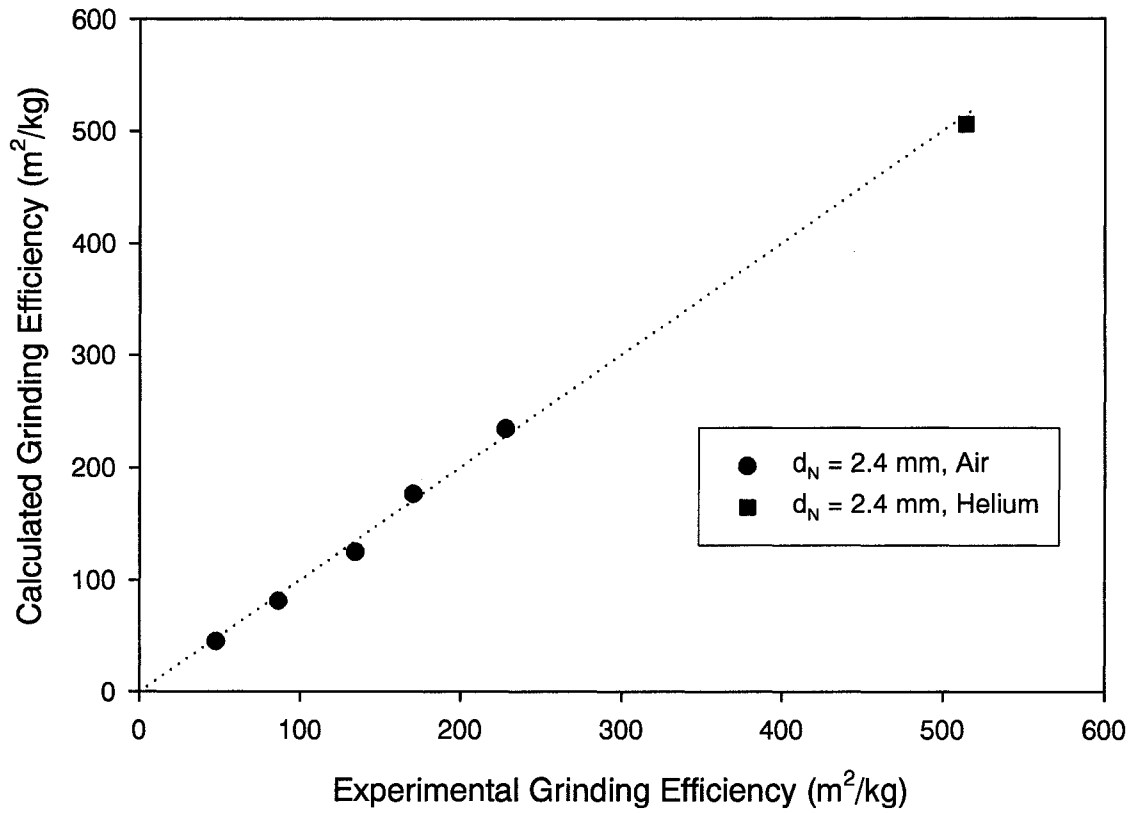


Figure 2.14: Experimental Versus Calculated Grinding Efficiency; Silica Sand; Type B Nozzle; $U_g = 0.065$ m/s

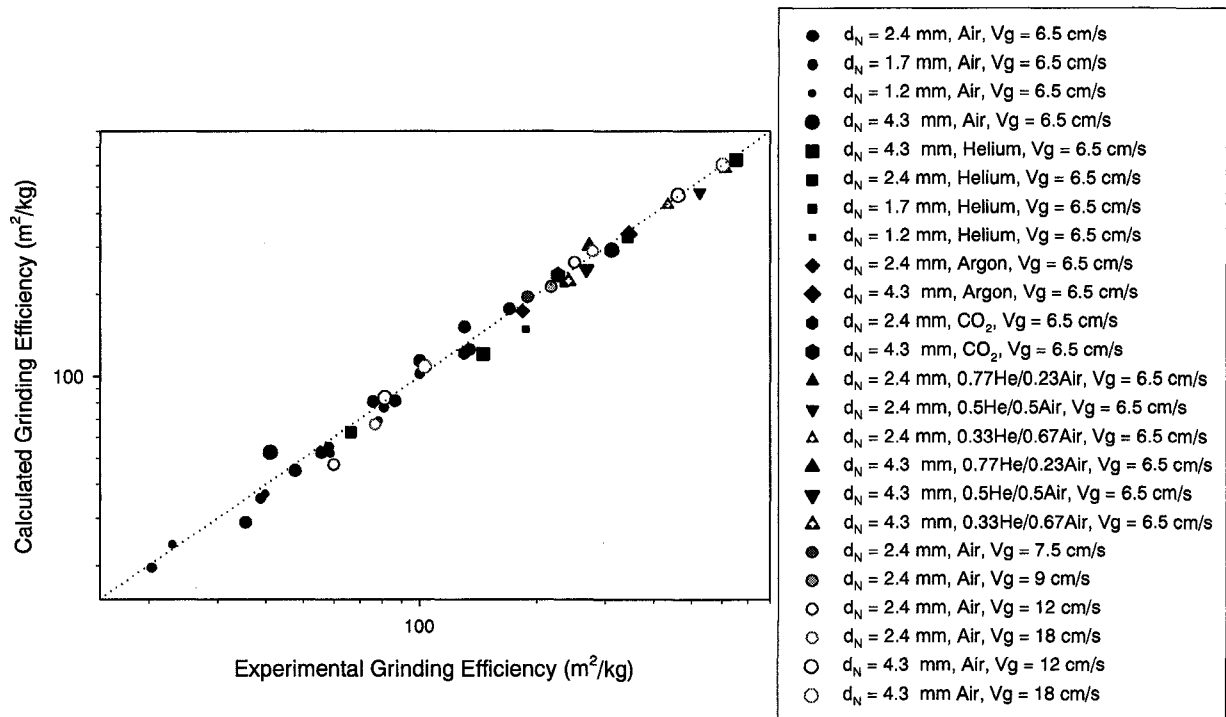


Figure 2.15: Experimental Versus Calculated Grinding Efficiency; Silica Sand; Type C Nozzle

The last term in Equation 2.6 is the ratio of the excess fluidization air to the minimum fluidization velocity. Both the experimental and calculated results showed that at higher fluidization velocities the grinding efficiency was increased. This suggests that, when the excess fluidization gas was increased, more particles were entrained into the jet and had a higher probability of grinding with each other and with particles located in the dense phase surrounding the jet cavity, thus resulting in an increased grinding efficiency.

The two main gas properties that were taken into account in the correlation were the gas density at the tip of the nozzle and the equivalent speed of sound. It was assumed that the effect of the upstream pressure was fully accounted for by the density of the attrition gas. Several different gases with different viscosities were tested and it was shown that the viscosity of the gas had little effect on the grinding efficiency.

Larger diameter nozzles with an expansion region at the nozzle tip, operated with gases with high equivalent speeds of sound, resulted in the highest grinding efficiencies because these conditions gave higher gas momentums. The particles that had a

significant chance of attriting were entrained near the tip of the nozzle, where the velocity and momentum of the gas was the highest. Particles that were entrained into the jet further downstream were moving more slowly, and their impact velocities were small and did not make a significant contribution to the attrition rate.

The term ρU^2 from Equation 2.6 refers to the energy input to the system and can be considered proportional to the drag force near the nozzle tip. The initial acceleration of the particles into the jet cavity can be assumed to be in Newton's Regime. As a result, the coefficient of discharge (C_D) is independent of the gas viscosity and is equal to 0.43. The drag force is equal to:

$$F_D = 0.5C_D A_p (\rho U^2) \quad (2.7)$$

This indicates that the most significant contribution to the energy input is ρU^2 . Similarly, the most significant contribution to the acceleration in the jet is the scale of the nozzle (d_N).

The correlation (Equation 2.6) was also used to determine the effect of gas temperature on the grinding efficiency. The grinding efficiencies were calculated at various temperatures for the scale that produced the best grinding results at room temperature: the 2.4 mm diameter, Type A nozzle using helium as the attrition gas at an upstream pressure of 300 psig and a fluidization velocity of 0.065 m/s. The percent increase in grinding efficiency was plotted versus the temperature, and the results are shown in Figure 2.16. As the gas temperature increases the grinding efficiency improves significantly.

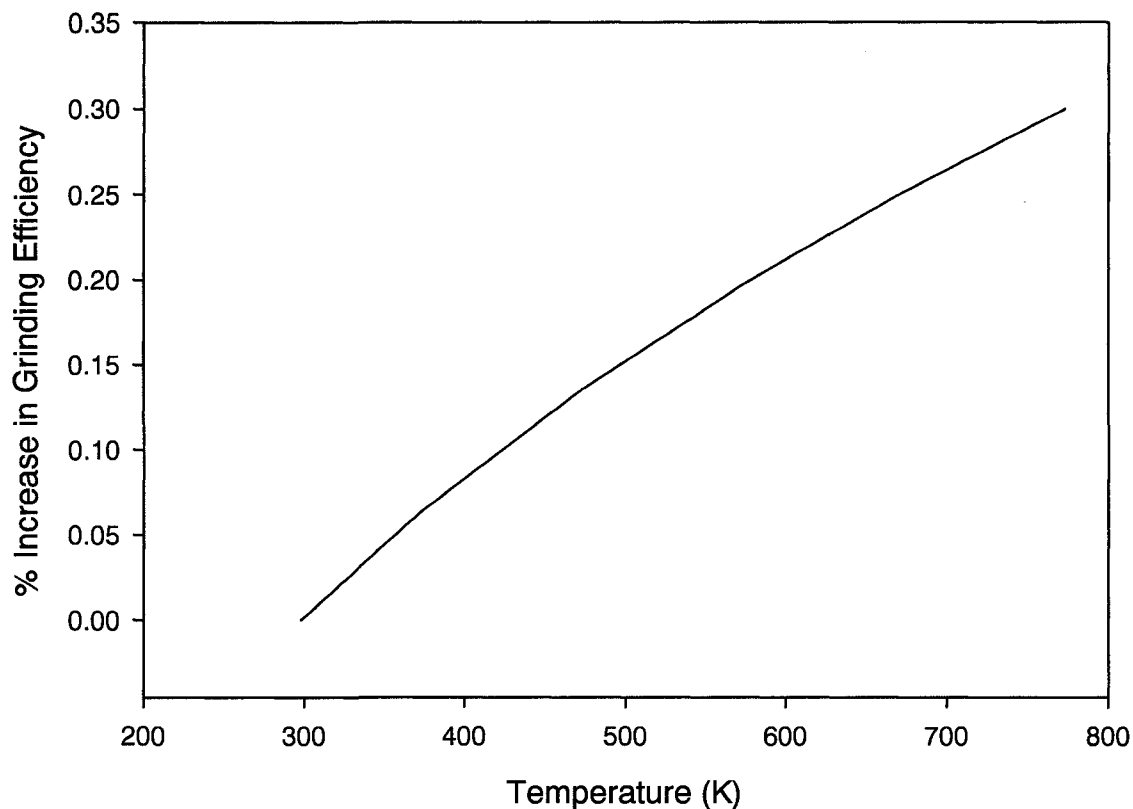


Figure 2.16: Effect of Temperature on Grinding Efficiency; Silica Sand; Type A Nozzle; $d_n = 2.4$ mm; $P = 300$ psig; Helium

2.4 Conclusion

A high velocity attrition nozzle was injected into a gas-solid fluidized bed in order to study the particle attrition. Different high velocity attrition nozzles were tested in order to determine the effects of fluidization velocity, nozzle size, nozzle geometry, bed material and attrition gas properties on the grinding efficiency. An empirical correlation was developed for nozzles operating at sonic conditions at the nozzle throat, which took into account solid properties, nozzle scale, nozzle geometry, fluidization velocity and gas properties, and was able to accurately predict the grinding efficiencies. Changing the attrition gas did have a significant effect on the attrition rate. Larger diameter nozzles with an expansion region at the tip, operating at high flowrates using lower density gases with higher equivalent speeds of sound, resulted in the highest grinding efficiencies.

2.5 Nomenclature

A_p	Characteristic area (m^2)
C_D	Drag coefficient (-)
F_D	Drag Force (N)
d_N	Nozzle diameter (m)
d_o	Orifice diameter (m)
m_o	Mass flowrate of jet gas (kg/s)
M	Molecular weight (kg/mole)
K	Attrition constant (s^2/m^2)
R	Gas constant (N.m/moles/K)
R_a	Jet attrition rate (kg/s)
T	Temperature (K)
U	Gas velocity at nozzle throat (m/s)
U_o	Equivalent gas velocity at nozzle throat (m/s)
$U_{sound,eq}$	Equivalent speed of sound (m/s)
U_g	Fluidization velocity (m/s)
U_{mf}	Minimum fluidization velocity (m/s)

Greek Letters

α	Solid coefficient (-)
β	Geometry coefficient (-)
η	Grinding efficiency (m^2/kg)
μ	Viscosity (Ns/ m^2)
ρ_o	Gas density at bed conditions (kg/m^3)
ρ	Gas density at nozzle throat (kg/m^3)

2.6 References

- Arastoopour, M., Chen, C., "Attrition of Char Agglomerates", *Powder Technol.*, **36**, 99-106 (1983).
- Bentham, A., Kwan, C., Boerefijn, R., Ghadiri, M., "Fluidised-Bed Jet Milling of Pharmaceutical Powders", *Powder Technol.*, **161**, 233-238 (2004).
- Benz, M., Herold, H., Ulfik, B., "Performance of a Fluidized Bed Jet Mill as a Function of Operating Parameters, *Int. J. Miner. Process.*, **44-45**, 507-519 (1996).
- Blinichev, V., Strel'tsov, V., Lebedeva, E., "An Investigation of the Size Reduction of Granular Materials During Their Processing In Fluidized Beds", *Int. Chem. Eng.* **8**, 615-618 (1968).
- Boerefijn, R., Gudde, N., Ghadiri, M., "Review of Attrition of Fluid Cracking Catalyst Particles", *Adv. Powder Tech.*, **11**, 145-174 (2000).

- Chen, T., Sishtla, C., Punwani, D., Arastoopour, H., "A Model for Attrition In Fluidized Beds", in: J. Grace, J. Matsen, (Eds.), *Fluidization*, Engineering Foundation, New York, NY: 1980, pp. 445 – 452.
- Davuluri, R., Knowlton, T., "Development of a Standard Attrition Test Procedure", in: L.-S. Fan, T. Knowlton, (Eds.), *Fluidization IX*, Engineering Foundation, New York, NY: 1998, pp. 333 – 340.
- Dunlop, D., Griffin, L., Moser, J., "Particle Size Control in Fluid Coking", *Chem. Eng. Prog.*, **54**, 39-43 (1958).
- Forsythe, W., Hertwig, W., "Attrition Characteristics of Fluid Cracking Catalysts", *Ind. Eng. Chem.*, **41**, 1200-1206 (1949).
- Ghadiri, M., Cleaver, J., Tuponogov, V., Werther, J., "Attrition of FCC Powder in the Jetting Region of a Fluidized Bed", *Powder Technol.*, **80**, 175-178 (1994).
- Hulet, C., Briens, C., Berruti, F., Chan, E., Ariyapadi, S., "Entrainment and Stability of a Horizontal Gas-Liquid Jet in a Fluidized Bed", *Int. J. Chem. React. Eng.* **1**, 1127-1140 (2003).
- Hutchings, I., "Mechanisms of Wear in Powder Technology: A Review", *Powder Technol.*, **76**, 3-13 (1993).
- Lin, L., Sears, J., Wen, C., "Elutriation and Attrition of Char from a Large Fluidized Bed", *Powder Technol.*, **27**, 105-115 (1980).
- Pacek, A., Nienow, A., "Application of Jet Grinding to Fluidised Bed Granulation", *Powder Technol.*, **65**, 305-310 (1991).
- Patel, K., Nienow, A., Milne, I., "Attrition of Urea in a Gas-Fluidised Bed", *Powder Technol.*, **47**, 257-261 (1986).
- Perry, R., Green, D., (Eds.) *Perry's Chemical Engineers' Handbook, 7th Ed.* New York: McGraw-Hill, 1997, p. 6-23.
- Shamlou, P., Liu, Z., Yates, J., "Hydrodynamic Influences on Particle Breakage in Fluidized Beds", *Chem. Eng. Sci.*, **45**, 809-817 (1990).
- Stein, M., Seville, J., Parker, D., "Attrition of Porous Glass Particles in a Fluidised Bed", *Powder Technol.*, **100**, 242-250 (1998).
- Tasirin, S., Geldart, D., "Experimental Investigation on Fluidized Bed Jet Grinding", *Powder Technol.*, **105**, 337-341 (1999).

Werther, J., Xi, W., "Jet Attrition of Catalyst Particles in Gas Fluidized Beds", *Powder Technol.*, **76**, 39-46 (1993).

Werther, J., Rappenhagen, J., "Catalyst Attrition in Fluidized-Bed Systems", *AIChE J.*, **45**, 2001-2010 (1999).

Wu, S., Baeyens, J., Chu, C., "Effect of the Grid-Velocity on Attrition in Gas Fluidized Beds", *Can. J. Chem. Eng.*, **77**, 738-744 (1999).

CHAPTER 3

Modeling the Particle Attrition Mechanism of a Sonic Gas Jet Injected into a Fluidized Bed

Jennifer McMillan¹, Cedric Briens¹, Franco Berruti¹, Edward Chan²

*¹Department of Chemical and Biochemical Engineering
The University of Western Ontario
1151 Richmond Street
London, Ontario, Canada, N6A 5B9*

*²Syncrude Canada Ltd.
Edmonton Research Centre
9421-17 Avenue
Edmonton, Alberta, Canada T6N 1H4*

3.1 Introduction

Fluidized bed jet attritors use high velocity gas jets to grind fluidized particles. Because grinding is autogenous, there is no contamination of the ground product by fragments from grinding surfaces, as in most other grinders. Jet mills are, therefore, used to grind materials such as toners, high purity ceramics, foodstuffs, ultrafine metal oxides, pharmaceutical powders, pigments, polymer powders and ultrafine particles for powder coating (Alpine, 2006). Jet milling can also be used to grind carbon nanotubes (Baddour and Briens, 2006). Jet attritors are also applied in fluidized bed processes such as fluidized bed coal combustion, where they grind the sorbent particles to maximize the adsorption efficiency of sulfur oxides, and fluid coking.

The fluid coking process uses thermal cracking to upgrade bitumen extracted from oil sands to produce synthetic crude oil. During the fluid coking process there is a gradual increase in the size of the coke particles due to the fact that coke is formed and deposited on the surface of the particles during the reaction. In addition to particle growth due to the reaction, agglomerates are also formed when several coke particles stick together. Controlling the particle size of the coke within the fluid coker is of great

importance, since large particles will result in slugging and poor circulation. Conversely, if too many fine particles with a diameter less than 70 microns exist, agglomeration will occur and result in poor fluidization (Dunlop, 1958). In order to control the size of the particles in the fluidized bed, steam is injected into the reactor section through attrition nozzles. The high velocity gas jet issuing from these nozzles entrains bed particles and accelerates them to a high speed. Due to their inertia, these particles slam on slow moving bed particles near the jet tip, causing breakage and thus, reducing the particle size.

An important aspect of particle attrition is the understanding and modeling of the particle breakage mechanisms. Austin (1971) developed a model introduced by Epstein (1948) and Reid (1965) to estimate the particle size distribution of ground particles after a known grinding time, given the initial size distribution. A cumulative breakage distribution function gave the size distribution of the new fragments created, and a selection function was defined as the fraction of particles broken per unit time. These breakage and selection functions became the standard parameters used to describe the grinding process.

Many researchers have modeled the grinding process in a fluidized jet mill (Gommeren et al., 1996, Benz et al., 1996; Berthiaux and Dodds, 1999; Berthiaux et al., 1999 and Gommeren et al. 2000, Han, 2002). Berthiaux and Dodds (1999) and Berthiaux et al. (1999) modeled the grinding process in a fluidized bed jet mill with batch and continuous operation, respectively. A new parameter, the residual fraction, was introduced in order to characterize the grinding kinetics. The residual fraction represented the performance of the grinding process and characterized the proportion of particles which were not ground.

Han et al. (2002) proposed a combined discrete element method and computational fluid dynamic numerical model for particle grinding in a jet mill. The particle motion in the gas flow was simulated by applying the Reynolds-averaged Navier-Stokes equations. The model proposed by the authors was in strong agreement with experimental values and was found to be suitable to predict the size distributions of the ground particles. They concluded that the particle feed rate, the angle of the particle feed

nozzle and the air feed rate were the most important parameters in governing the particle breakage in the jet mill.

Ghadiri et al. (1994) used the single particle impact breakage model from Donsi et al. (1980) to calculate the particle velocity at the tip of the jet. They combine this model with a correlation for solids entrainment into the jet to obtain the fluidized bed jet attrition rate. The model can predict the dependence of the attrition rate on both the orifice gas velocity and the orifice size.

Previously, several studies have been done which focus on modeling attrition in a fluidized bed in the absence of an injection nozzle. Ray et al. (1987) proposed a “surface-reaction” model which states that the attrition rate is proportional to the particle surface area. Levenspiel et al. (1968) developed a model for particles of changing or unchanging sizes and used a first-order shrinkage rate to represent particle attrition. However, this model did not consider the roles of fines and the post-attrition mother particles.

Merrick and Highley (1974) developed a mathematical model of a fluidized bed process which assumed a first-order correlation for size reduction, and a critical particle size for elutriation. This model was used to predict the elutriation rate and mean bed particle size in a system. They found that the mass attrition rate of a component was proportional to the excess gas velocity, the mass of solids and the mass fraction of the component smaller than a certain radius.

The models previously developed for jet attritors are quite complex and require many empirical parameters that have to be experimentally determined (Baddour and Briens, 2006). Baddour and Briens (2006) developed a simple, two-parameter model to describe jet milling of carbon nanotubes. However, as all the other models, it applies only to small fluidized beds where there is intense solids mixing. It does not apply to processes such as fluid coking, where solids mixing may be a limiting factor and impact on the attrition rate and product size distribution.

The objective of this study was to develop a simple model, with a minimum of empirical parameters, to describe the attrition mechanism when a sonic velocity gas jet is used to grind particles in a fluidized bed and to account for the effect of solids mixing.

3.2 Experimental

To obtain data to verify the results from the model, experiments were conducted in a fluidized bed column with a height of 3.2 m and a rectangular cross section of 1 m by 0.3 m, as shown in Figure 3.1. Two different types of particles were tested: coke with a Sauter mean diameter of 135 μm , and silica sand with a Sauter mean diameter of 190 μm . The particles filled the column to a height of approximately 0.3 m and were fluidized with air at various fluidization velocities. Entrained particles were separated from the gas stream by two cyclones in series. Particles from the primary cyclone were continuously returned to the fluidized bed by a dipleg. Particles from the secondary cyclone were collected after each run: under most of the studied conditions, their contribution to the new particle surface was negligible. In order to determine the effects of scale, a smaller fluidized bed column with a height of 0.84 m and rectangular cross section of 0.5 m by 0.1 m was also used. This bed was filled with 13 kg of coke to a height of 0.23 m.

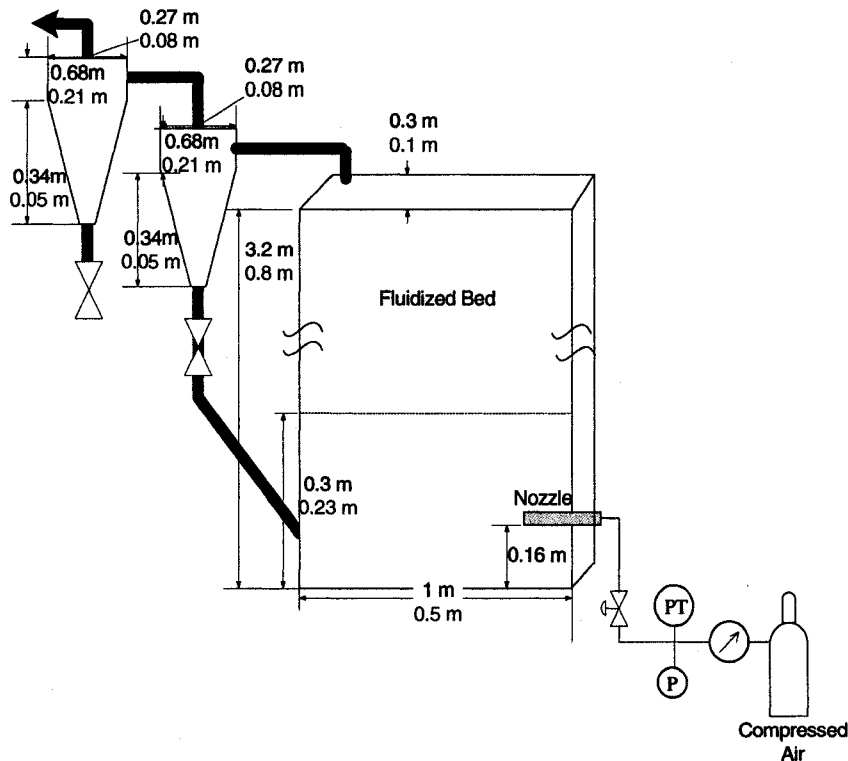


Figure 3.1: Experimental Equipment

In both systems the attrition nozzle was placed inside the bed at a distance of 0.16 m from the gas distributor and injected gas horizontally into the fluidized particles. A constant gas mass flowrate from a high-pressure cylinder was supplied to the injection nozzle during the grinding process. Adjusting the pressure of the cylinder controlled the gas flowrate to the nozzle. Prior calibration provided the relationship between applied pressure and mass flowrate for each nozzle. The mass gas flowrate was verified after each run from the evolution in the cylinder pressure, which was measured with a transducer connected to a data acquisition system.

After injection, the fluidization gas was stopped in order to slump the bed. The fluidization gas was turned on again at a velocity just above the minimum bubbling velocity for approximately 5 minutes in order to mix the particles. Separate experiments indicated that background particle attrition in the fluidized bed, in the absence of an attrition jet, was negligible when compared to the attrition observed with the nozzles. A sample of solids was taken from the bed before and after each run and analyzed using a Malvern laser diffraction apparatus in order to obtain the size distribution of the particles before and after the grinding process.

Three different types of attrition nozzles were tested in order to determine the effect of nozzle geometry on the grinding efficiency and attrition gas consumption. The first nozzle, designated as Type A, was a convergent-divergent, Laval-type nozzle, similar to the nozzles used by Benz et al., 1996. The second nozzle, Type B, was a uniquely shaped nozzle which was similar to Type A, but contained a 10 mm straight section at the tip of the nozzle. The third nozzle type tested, Type C, was a simple straight tube nozzle. Nozzles A, B and C are shown in Figures 3.2, 3.3 and 3.4, respectively. Type C nozzles with various exit diameters were tested in order to determine the effect of nozzle scale on the grinding efficiency and attrition gas consumption. The nozzles that were tested had tip diameters, d_N (see Figure 3.2), of 4.3 mm, 2.4 mm, 1.7 mm, and 1.2 mm.

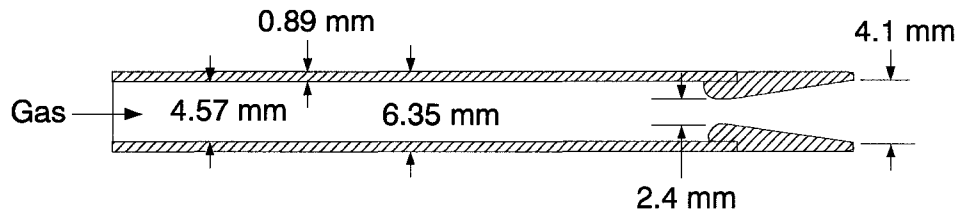


Figure 3.2: Type A Nozzle

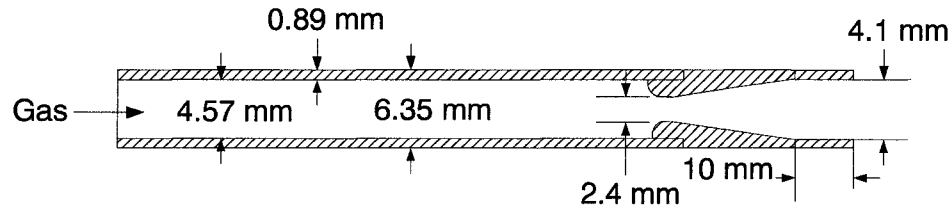


Figure 3.3: Type B Nozzle

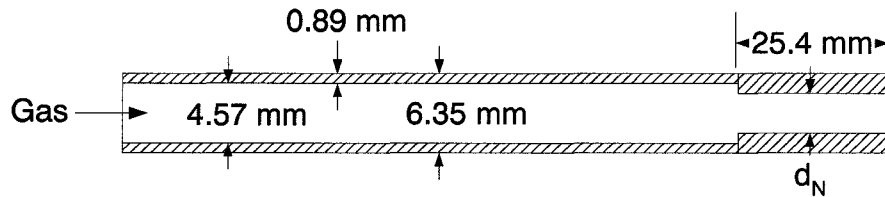


Figure 3.4: Type C Nozzle

Different gas flowrates and various types of attrition gases (carbon dioxide, argon, air, helium, and different combinations of air/helium mixtures) were tested in order to determine the effect of gas properties on the grinding efficiency, such as density, viscosity, and the equivalent speed of sound. The equivalent speed of sound was calculated using Equation 3.1, which takes into account the fact that the temperature of the gas changes (Perry and Green, 1997).

$$U_{\text{sound equivalent}} = \sqrt{\frac{RT\kappa}{M} \left(\frac{2}{\kappa+1} \right)^{\frac{\kappa+1}{\kappa-1}}} \quad (3.1)$$

Different fluidization velocities and grinding times were also used to determine their effects on the particle attrition rate. In addition, various attrition nozzle enhancements were used in order to increase the grinding efficiency. A target, draft tube, shroud, nozzle inserts, and spiral flow were used in conjunction with the attrition nozzle to determine their effects on the particle breakage rate. Details of these designs can be found in a study done by McMillan et al. (2006a).

In order to compare the results from all of the tests, a grinding efficiency was calculated, which was defined as the amount of new surface area created per mass of attrition gas used:

$$\eta = \frac{\text{new particle surface created by attrition}}{\text{mass of required attrition gas}} = \frac{\frac{m^2}{s}}{\frac{kg}{s}} = \frac{m^2}{kg} \quad (3.2)$$

This definition was chosen, as the objective was to achieve maximum grinding, while using a minimum amount of attrition gas.

3.2.1 Model Development

The model presented in this study predicts the particle breakage frequency, the proportion of particles which have not been ground, and the size distribution of the product, after grinding with a sonic velocity attrition jet in a fluidized bed for a determined period of time.

The proposed model assumes that one mother particle breaks into two daughter particles of different size, as shown in Figure 3.5.

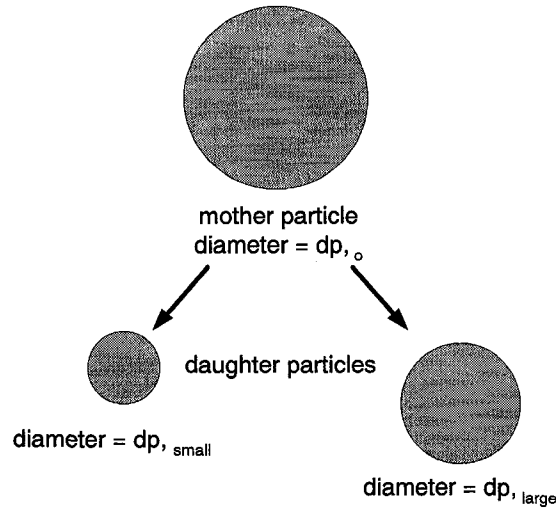


Figure 3.5: Particle Breakage Mechanism

A symmetry coefficient, γ , is introduced which represents the ratio of the volume of the small daughter particle to the volume of the large daughter particle. For example the two daughter particles will be equally sized if $\gamma = 1$. The diameter of the small and large daughter particles can be defined by Equations 3.3 and 3.4, respectively.

$$d_{p,small} = \frac{d_{p,o}}{\sqrt[3]{\frac{1}{\gamma} + 1}} \quad (3.3)$$

$$d_{p,large} = \frac{d_{p,o}}{\sqrt[3]{\gamma + 1}} \quad (3.4)$$

It was found that the grinding symmetry coefficient, γ , remained approximately constant throughout the grinding process, as well as between runs. Therefore, the value of γ was kept constant at 0.8.

There are two main modes of attrition: abrasion and fragmentation. Abrasion occurs when very fine pieces are removed from the surface of the particle, thus producing many fines, while the particle size distribution of the mother particles remains unchanged. Alternatively, fragmentation occurs when a particle breaks into pieces of similar size. Since the grinding symmetry coefficient is fairly high (approximately equal to 80%), and the mother particle is splitting into two particles of fairly equal size, the

primary attrition mechanism occurring in the bed is fragmentation, as opposed to abrasion. Photographs were taken of the particles before and after the grinding process using a Scanning electron microscope, at a magnification of 100X. Figures 3.6 and 3.7 show the results before and after grinding, respectively. The ground particles are significantly smaller than the original mother particles suggesting that the particles had been split several times during the attrition process. In addition, the daughter particles have sharp, jagged edges. This finding confirms that fragmentation is the primary attrition mechanism: if abrasion were occurring, the daughter particles would be much smoother.

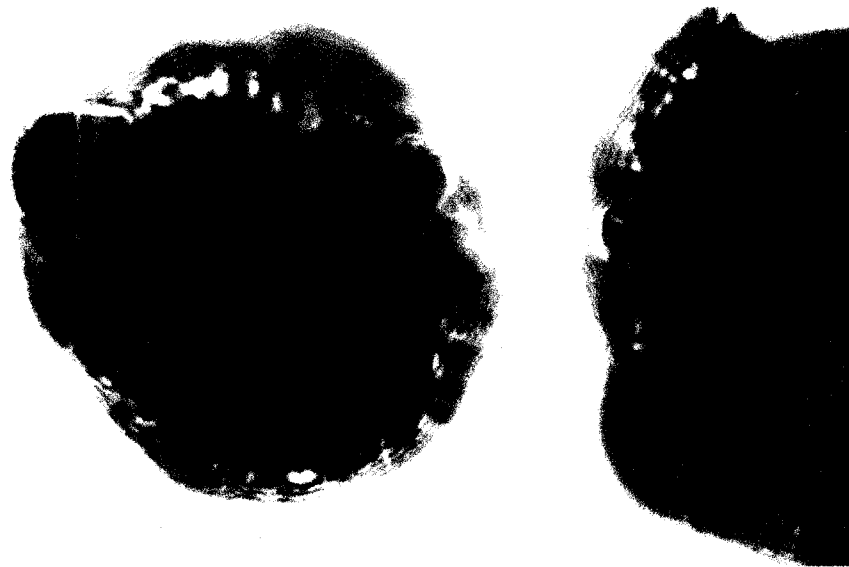


Figure 3.6: Coke Particles Before Grinding Process (Magnification: 100X)



Figure 3.7: Coke Particles After Grinding Process (Magnification: 100X)

In addition, the smallest diameter particle that could split into two daughter particles was determined by performing a limit to fineness test. Air was injected into the bed through a sonic velocity attrition nozzle for an extended period of time in order to grind the particles to their minimum size. Samples were taken from the bed at various time intervals in order to determine the size distribution and the Sauter mean diameter of the particles in the bed. It was found that after 15 hours of grinding, a limit occurred, where the average particle size in the bed stopped decreasing even after more attrition gas was injected into the bed. Figure 3.8 shows the size distributions of the particles in the bed as the particles are reduced from a Sauter mean diameter of 121 μm to a Sauter mean diameter of 48 μm .

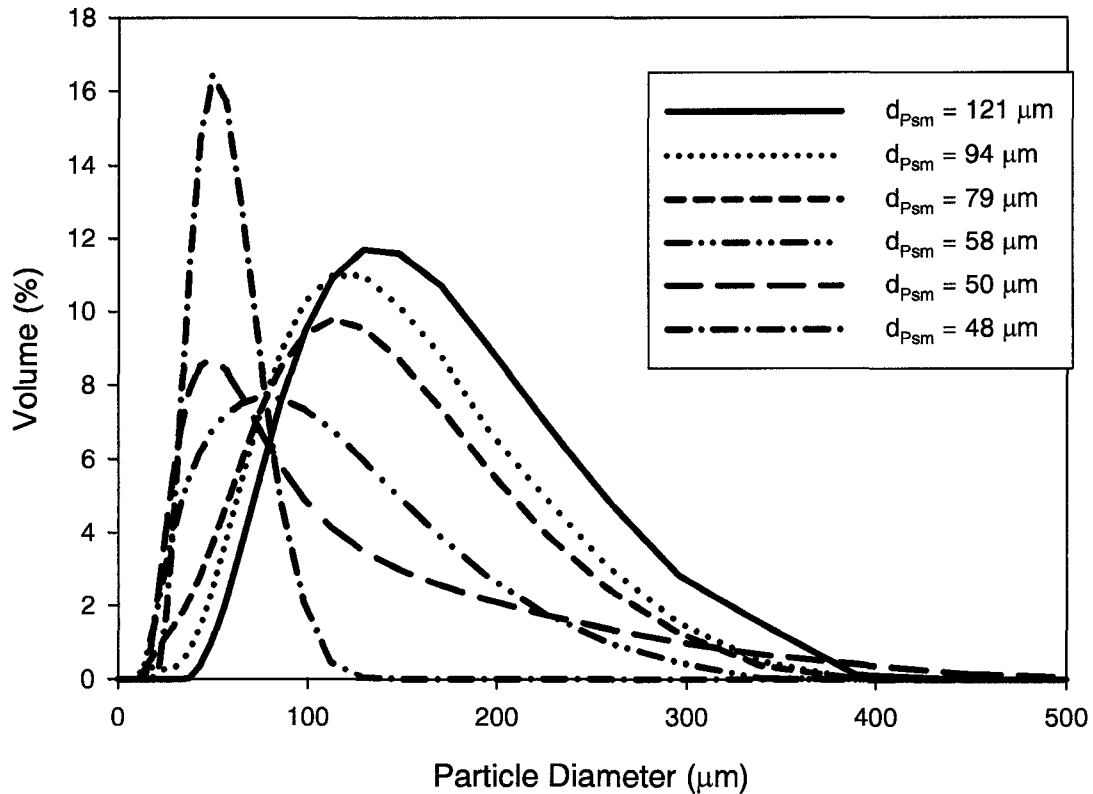


Figure 3.8: Size Distributions for Limit to Fineness Test

As can be seen in Figure 3.8, the minimum particle size in the bed is approximately $14 \mu m$. Using Equation 3.3, the size of the mother particle required to create a daughter particle with a diameter of $14 \mu m$ was calculated to be $18 \mu m$. As a result, it was assumed that particles with a diameter less than $18 \mu m$ were unable to split.

Each split of a mother particle into two daughter particles increases the number of particles in the bed by a value of one, and the total number of breaks during the grinding process is defined as N . The particle breakage frequency, F , is determined from the total number of breaks and the grinding time, t . The particle breakage frequency, F , is a result of both the solids entrainment rate into the jet cavity and the extent of micro-mixing within this jet. The majority of the particle attrition occurs at the tip of the gas jet where entrained particles traveling at high speed, impact particles in the dense phase of the bed. Entrained particles start near the jet boundary, where the gas velocity is small and

migrate through micro-mixing to the high velocity central region. As both the entrainment rate, and the impact velocity of the entrained particles at the tip of the jet increase, the particle breakage frequency, F , also increases.

$$F = \frac{N}{t} \quad (3.5)$$

Some particles are never exposed to the attrition jet during the grinding process, even if the mixing in the fluidized bed is perfect. Therefore, a parameter β , was introduced. It represents the proportion of original mother particles that have not been ground, assuming that the particles in the bed are perfectly mixed.

The value of β can be calculated from a probability model, as shown in the next section. The proportion of original particles that have not been ground, β , depends on the amount of macro-mixing in the fluidized bed. If excellent macro-mixing exists, fewer particles will be left intact, and the value of β will be decreased.

In order to determine the governing solids mixing mechanism in the bed, the solids mixing time in the jet was compared to the total solids mixing rate in the bed. The jet mixing time was calculated by taking the ratio of the total mass of solids in the bed to the flowrate of entrained solids into the jet. Hulet et al. (2005) performed tests with gas jets under similar conditions and found the entrainment rate of solids into the attrition jet to be approximately 0.105 kg/s.

$$t_{mix_jet} = \frac{M_{bed}}{F_{s,entrained}} \quad (3.6)$$

Using Equation 3.6, the jet mixing time was found to be 123 s.

The circulation rate of solids in the bed was calculated by taking the ratio of the total mass of solids in the bed to the flowrate of solids mixed in the bed. The flowrate of solids mixed was estimated from the assumptions that the wakes of the gas bubbles issuing from the jet carry solids upwards in the bed, away from the jet region, that the wake volume is 30% of the bubble volume and that the wake density is approximately the same as the bed density.

$$F_{s,mixed_bed} = \frac{0.3 * F_{g,nozzle} * \rho_{bed}}{\rho_{g,bed}} \quad (3.7)$$

$$t_{mix_bed} = \frac{M_{bed}}{FS_{mixed_bed}} \quad (3.8)$$

Using Equation 3.8 it was found that the mixing time was 17.2s, which means that the bubbles can carry approximately 7 times more solids than the amount of solids that can be entrained by the jet. Therefore, the particles that are ground by the jet are quickly removed from the jetting region by the bubbles, and as a result, the bed is extremely well mixed.

3.2.2 Model Calculation Procedure

Figure 3.9a shows a flow diagram depicting the model calculation procedure. The model assumes that n_0 particles are present in the bed before grinding. These particles can be divided into two groups: attritable particles, and non-attritable particles. The proportion of non-attritable particles, β , corresponds to the particles that never enter the grinding region of the fluidized bed and, therefore, remain intact. The attritable particles represent the particles in the grinding region of the bed. The total number of non-attritable particles in the bed is equal to $n_0\beta$, and the total number of attritable particles originally in the bed is equal to $n_0(1-\beta)$.

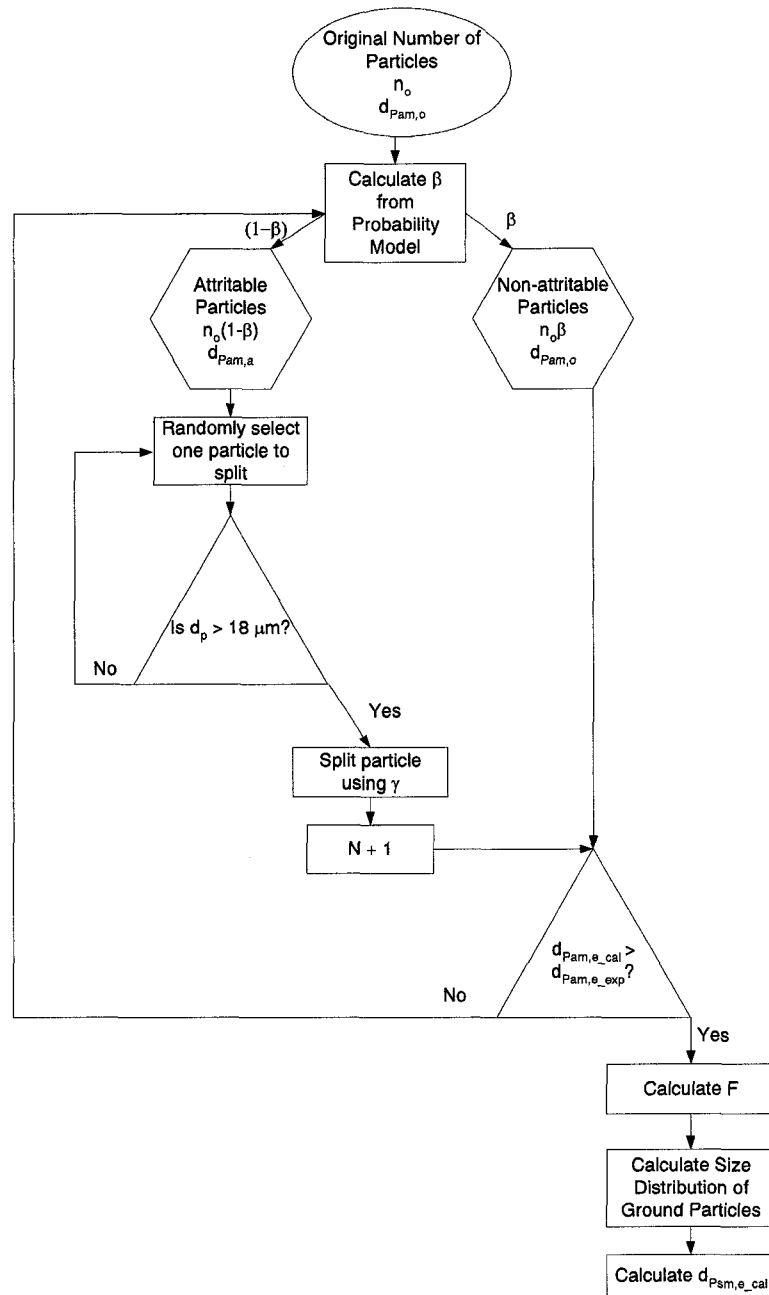


Figure 3.9a: Model Calculation Procedure Flow Diagram

The first step of the calculation procedure is to calculate, from the known experimental size distributions, the arithmetic mean diameters of the particles before and after grinding; $d_{Pam,o}$ and d_{Pam,e_exp} , respectively. The Sauter mean diameter of the

experimentally ground particles, d_{psm,e_exp} , was also calculated from the given size distribution.

Next, β , the proportion of non-attributable particles, is determined using a probability model which assumes that the fluidized bed is perfectly mixed, and therefore all of the particles in the bed are equally likely to be ground. This probability model takes into account the fact that either a fresh unground particle, or a particle that has already been ground, can split into two daughter particles, and then β is calculated for a given breakage frequency, F , and grinding time, t . Figure 3.9b shows a flow diagram depicting the probability model calculation procedure for determining the value of β .

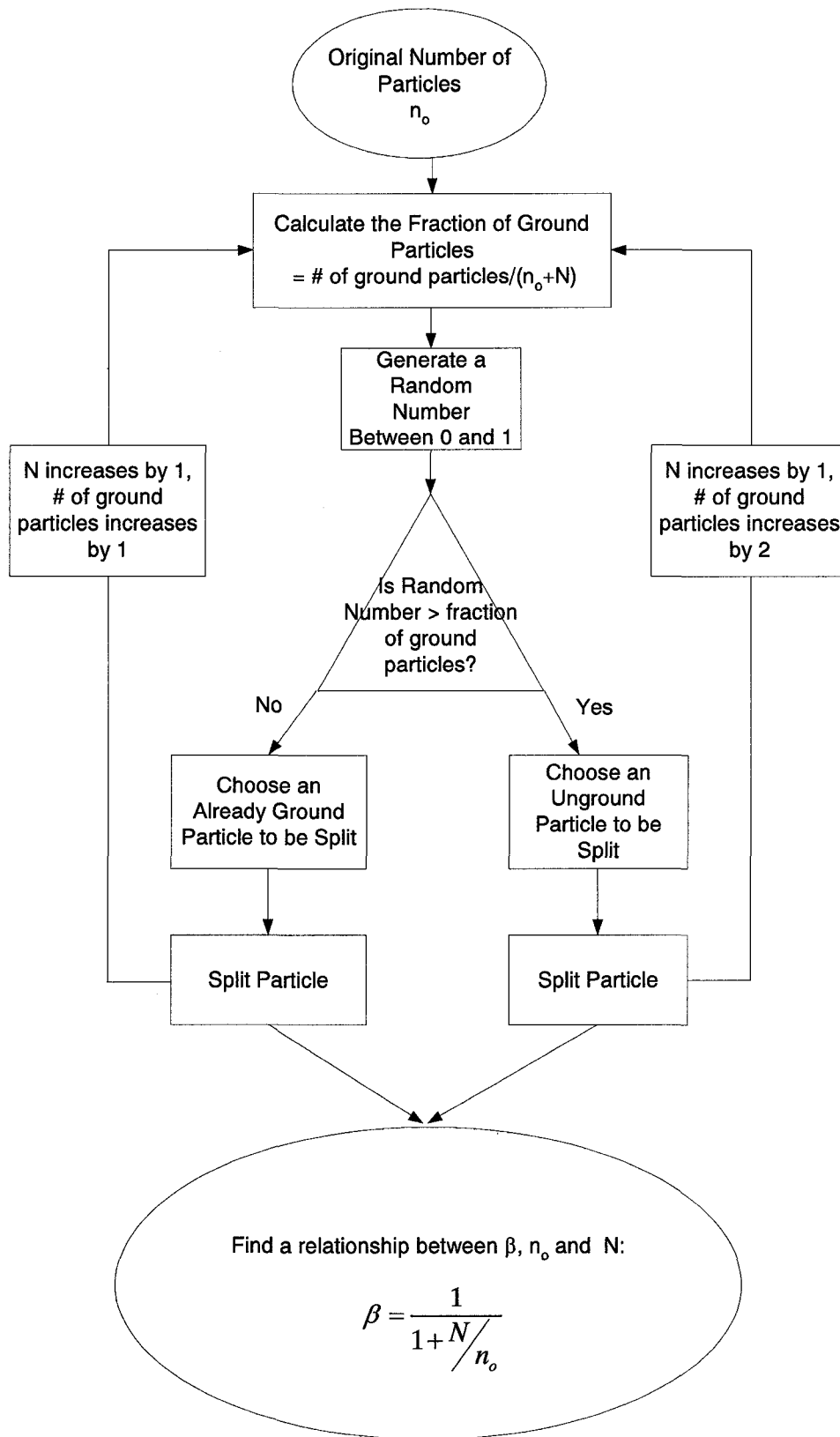


Figure 3.9b: Probability Model Procedure for Calculating β

First, the fraction of ground particles is calculated:

$$\text{fraction of ground particles} = \frac{\text{number of ground particles}}{(n_o + N)} \quad (3.9)$$

Second, it is decided if the particle chosen to be split is an unground particle, or a particle that has already been ground. A random number is obtained from a uniform distribution in the range from zero to unity. If this random number is less than the fraction of ground particles in the bed, then it is assumed that an unground particle is chosen to be split. If this random number is greater than the fraction of ground particles in the bed, then it is assumed that a particle that has already been ground is chosen to split. Therefore, at the beginning of the attrition process when there are more unground particles in the bed than ground particles, the probability that an unground particle will be chosen to split is much higher than the probability that a ground particle will be chosen. However, as the attrition process proceeds, the probability that a ground particle is chosen to be split becomes higher. If an unground particle is chosen to split then the number of ground particles in the bed increases by 2 and the number of particles in the bed increases by 1. If an already ground particle is chosen to be split, then the number of ground particles in the bed increases by 1 and the total number of particles in the bed increases by 1. Then the fraction of unground particles in the bed, β is recalculated. This procedure was repeated several thousands of times, in order to simulate the grinding process and a relationship between β , N and n_o was determined. The following equation was obtained in order to estimate β for the case that the fluidized bed is perfectly mixed:

$$\beta = \frac{1}{1 + N/n_o} \quad (3.10)$$

As can be seen in Equation 3.10, in order to calculate the value of β , the number of breaks, N , is required. The arithmetic mean diameter of the particles in the bed decreases as the number of breaks increases. The number of breaks, N , is determined by picking random particles from the bed and splitting them until the arithmetic mean

diameter matches the arithmetic mean diameter of the experimentally measured ground particles.

Referring back to Figure 3.9a, particles from the attritable region of the bed are selected using a random number obtained from a uniform distribution in the range from zero to unity. If a random particle with a size of 18 μm or smaller is selected, it is assumed that this particle does not grind. If the particle chosen is larger than 18 μm , it is split into two daughter particles, and their diameters are determined using the grinding symmetry coefficient, γ . The total number of particles in the bed is then increased by a value of one and, as a result the final number of particles in the bed after grinding is equal to $n_o + N$. Particles were randomly selected to be broken 100 times before the arithmetic mean diameter at the end of the grinding process, d_{Pam,e_cal} , was calculated. The average particle diameter was calculated by taking the average of the ground particles from the attritable region of the bed, $d_{Pam,a}$, and the non-attritable particles, $d_{Pam,o}$, whose size did not change during the grinding process.

$$\begin{aligned}
 d_{Pam,e_cal} &= \frac{1}{N + n_o} \sum_{i=1}^{N+n_o} d_{Pi,e_cal} \\
 (N + n_o)d_{Pam,e_cal} &= \sum_{i=1}^{n_o\beta} d_{Pi,o} + \sum_{i=1}^{N+n_o(1-\beta)} d_{Pi,a} \\
 (N + n_o)d_{Pam,e_cal} &= n_o\beta d_{Pam,o} + [N + n_o(1-\beta)]d_{Pam,a} \\
 d_{Pam,e_cal} &= \frac{n_o\beta d_{Pam,o} + [N + n_o(1-\beta)]d_{Pam,a}}{(N + n_o)} \quad (3.11)
 \end{aligned}$$

If after 100 splits, the arithmetic mean diameter of the product, d_{Pam,e_cal} , was still greater than the arithmetic mean diameter of the measured ground particles, d_{Pam,e_exp} , another set of 100 randomly selected particles were split to further decrease the average particle diameter. Once the arithmetic mean diameter of the calculated ground particles, d_{Pam,e_cal} , became less than the arithmetic mean diameter of the experimentally ground particles, d_{Pam,e_exp} , the value of N , the number of particle breaks, and F , the particle breakage frequency, were determined. The size distribution of the final product was also calculated. To obtain the average distribution, the average of the number fraction from

the attritable region of the bed and the number fraction from the unground particles from the non-attritable region was calculated, using a procedure similar to the procedure for calculating the average particle size in Equation 3.11.

$$x_{i,e_cal} = \frac{n_o \beta x_{i,o} + [N + n_o(1 - \beta)] x_{i,a}}{(N + n_o)} \quad (3.12)$$

At the end of the calculation procedure, the proportion of unground particles, β , particle breakage frequency, F , and the final size distribution of the ground particles were known.

3.3 Results and Discussion

The model was used to predict the size distribution of the ground particles, as well as the particle breakage frequency, F , and the proportion of non-attritable particles, β , for various experimental conditions. Typical examples of the comparison between the experimental size distribution and the calculated size distribution of the ground particles are shown in Figures 3.10 and 3.11, for two different cases. Both figures show that there is excellent agreement between the cumulative volume percent of the experimentally ground particles and the cumulative volume percent of the ground particles predicted from the model.

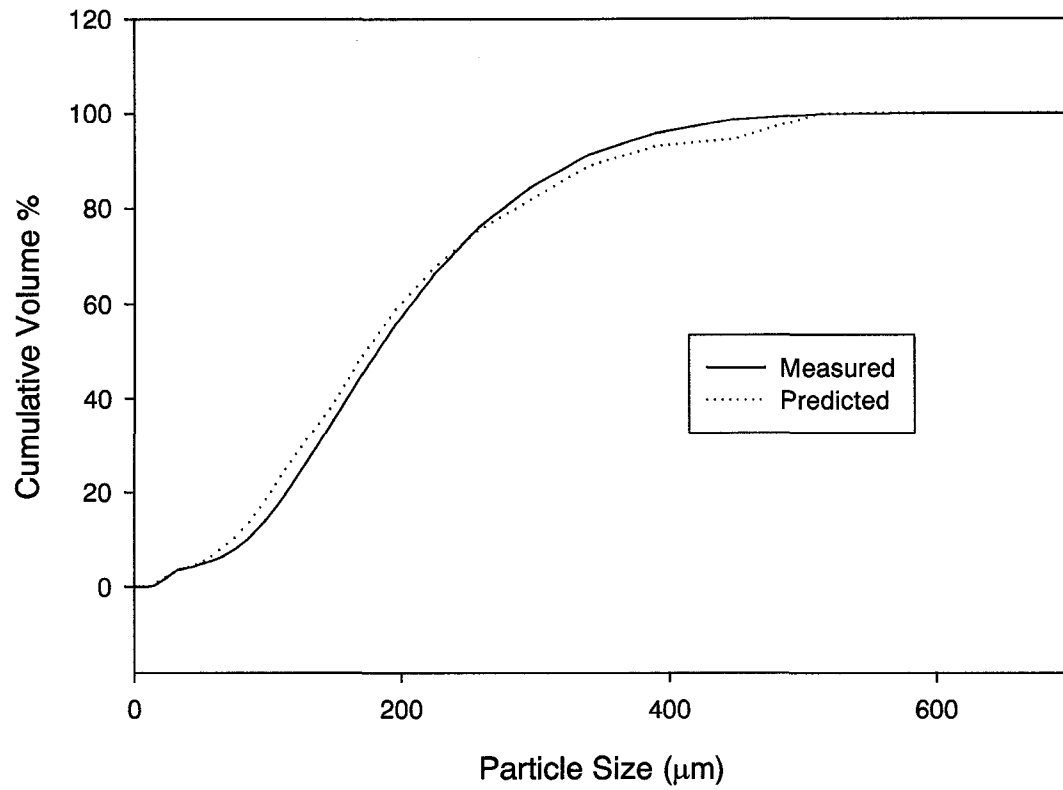


Figure 3.10: Comparison of Experimental and Calculated Size Distribution of Ground Particles. $D_N = 2.4$ mm, Type A Nozzle, $V_g = 6.5$ cm/s, $M_{\text{solids}} = 160$ kg

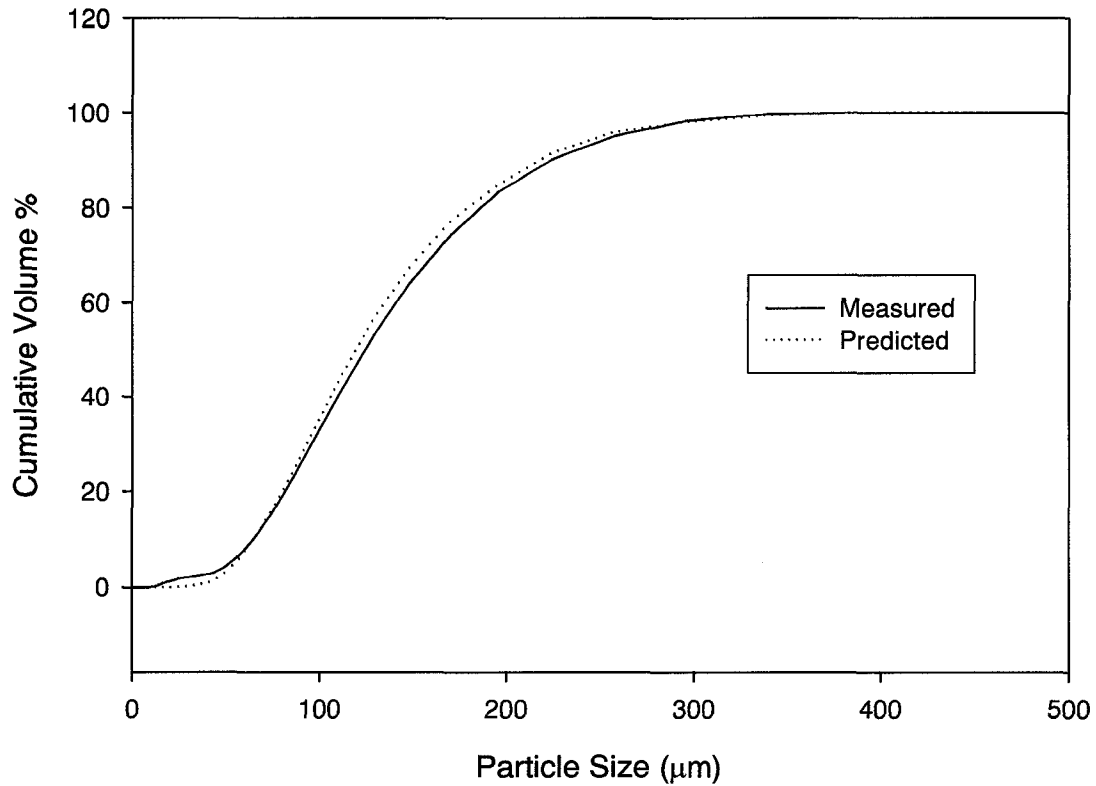


Figure 3.11: Comparison of Experimental and Calculated Size Distribution of Ground Particles. $D_N = 4.6$ mm, Type C Nozzle, $V_g = 10$ cm/s, $M_{\text{solids}} = 13$ kg

The particle breakage frequency can also be expressed in terms of mass of particles broken per unit time, F_m . The effect of various operating conditions and nozzle designs on the value of F_m was also determined. Figure 3.12 shows the effect of the grinding time, t , on F_m . The mass of particles broken per second remains approximately constant as the grinding time increases.

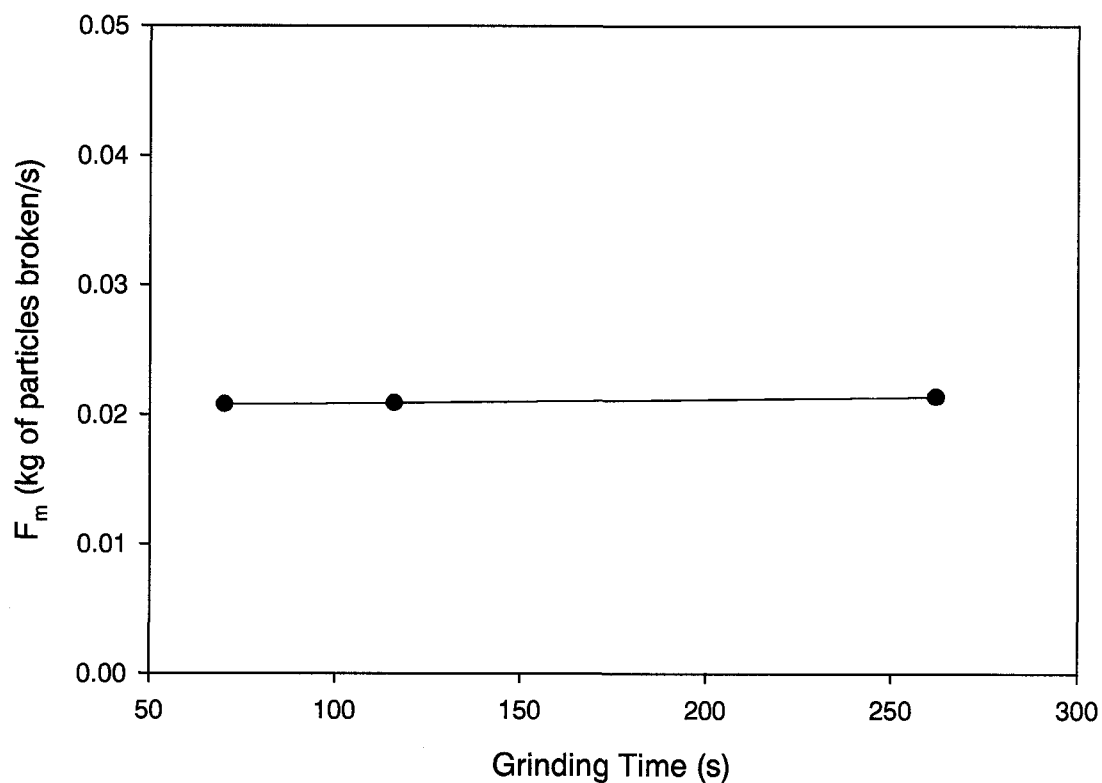


Figure 3.12: Effect of Grinding Time on F_m

The effect of fluidization velocity on F_m was also determined, as shown in Figure 3.13. As the fluidization velocity is increased, a greater mass of particles is broken per unit time. The increased fluidization velocity helps to entrain more particles into the jet cavity, thus promoting particle attrition.

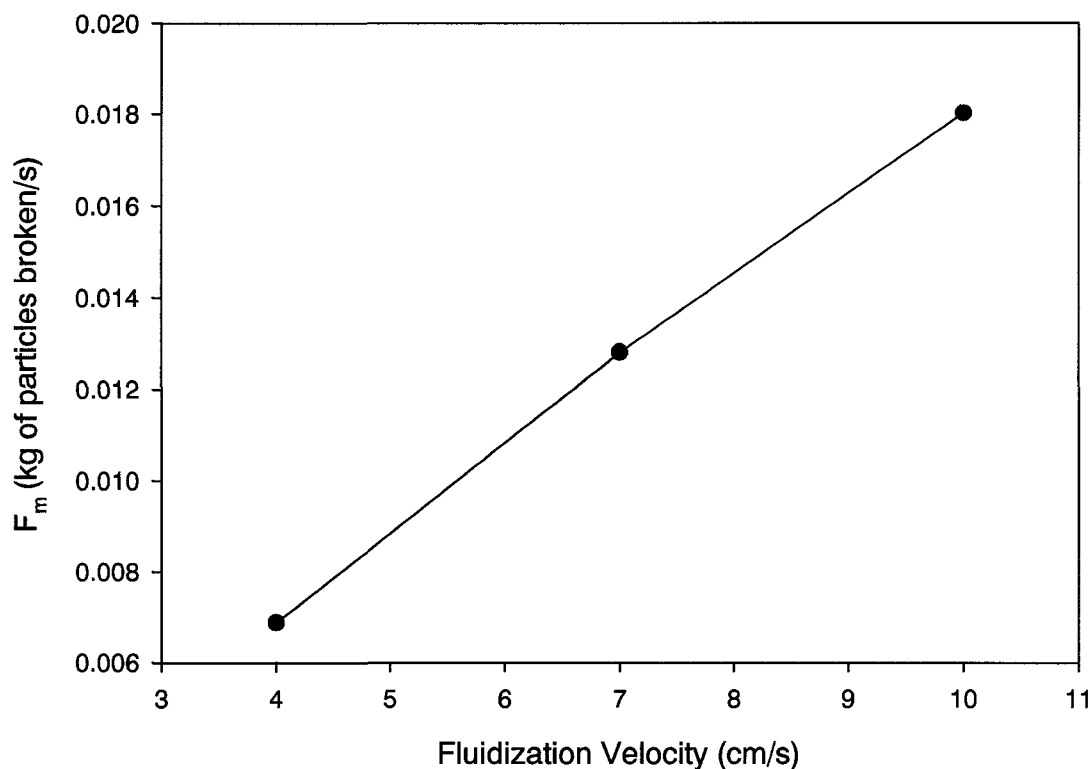


Figure 3.11: Effect of Fluidization Velocity on F_m

Figure 3.14 illustrates the effect of nozzle diameter on F_m . As the nozzle diameter was changed, the mass velocity (upstream pressure) was kept constant. Therefore, a larger mass flowrate was injected through the larger diameter nozzles, which provided these jets with more energy. The larger diameter nozzles also create a larger cavity within the fluidized bed and, as a result more particles can be entrained into the jet. This larger volume of entrained particles then impact with the dense region of stagnant particles at the tip of the jet and increase the particle breakage frequency, F_m .

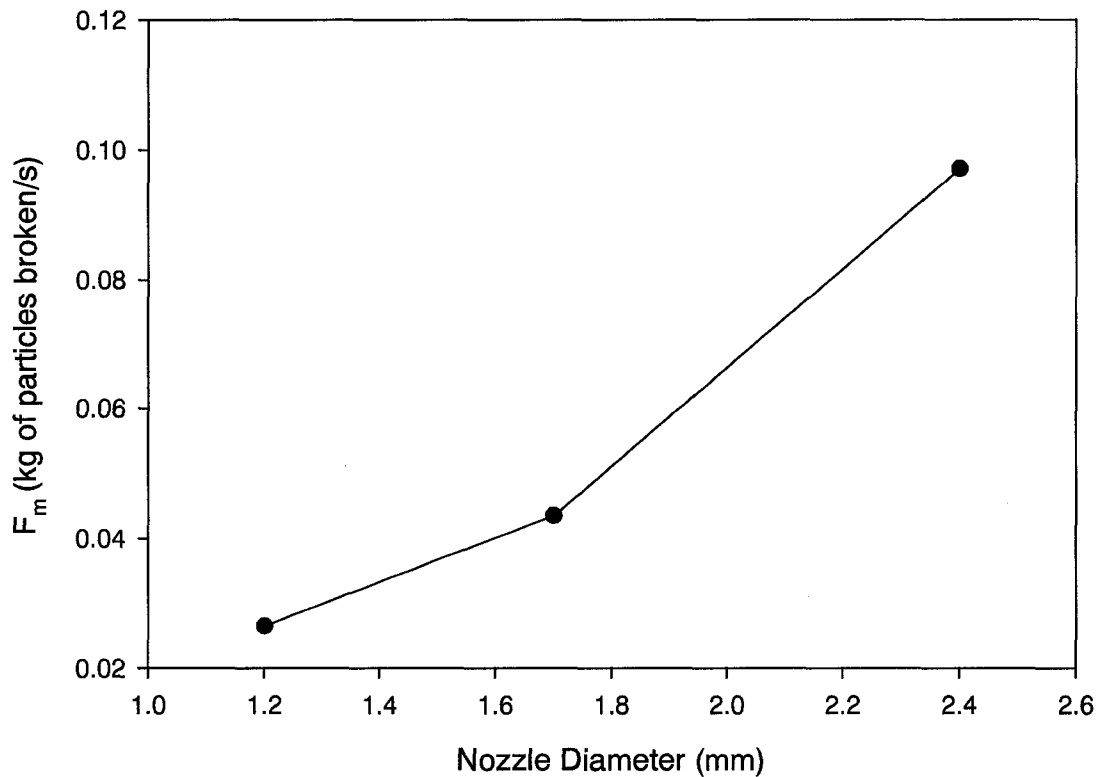


Figure 3.14: Effect of Nozzle Diameter on F_m

The effect of nozzle geometry on the particle breakage frequency is shown in Figure 3.15. The profiled shape of the Type A nozzle increases the expansion angle of the gas exiting the attrition nozzle and, as a result more particles can be entrained near the tip of the nozzle where the gas velocity is high. These accelerated particles have a higher probability of attriting and therefore, help to increase the particle breakage frequency. The Type B nozzle grinds significantly fewer particles. The additional straight section located at the tip of the nozzle decreases the expansion angle of the jet issuing into the fluidized bed, and thus decreases the amount of particles that can be entrained into the jet.

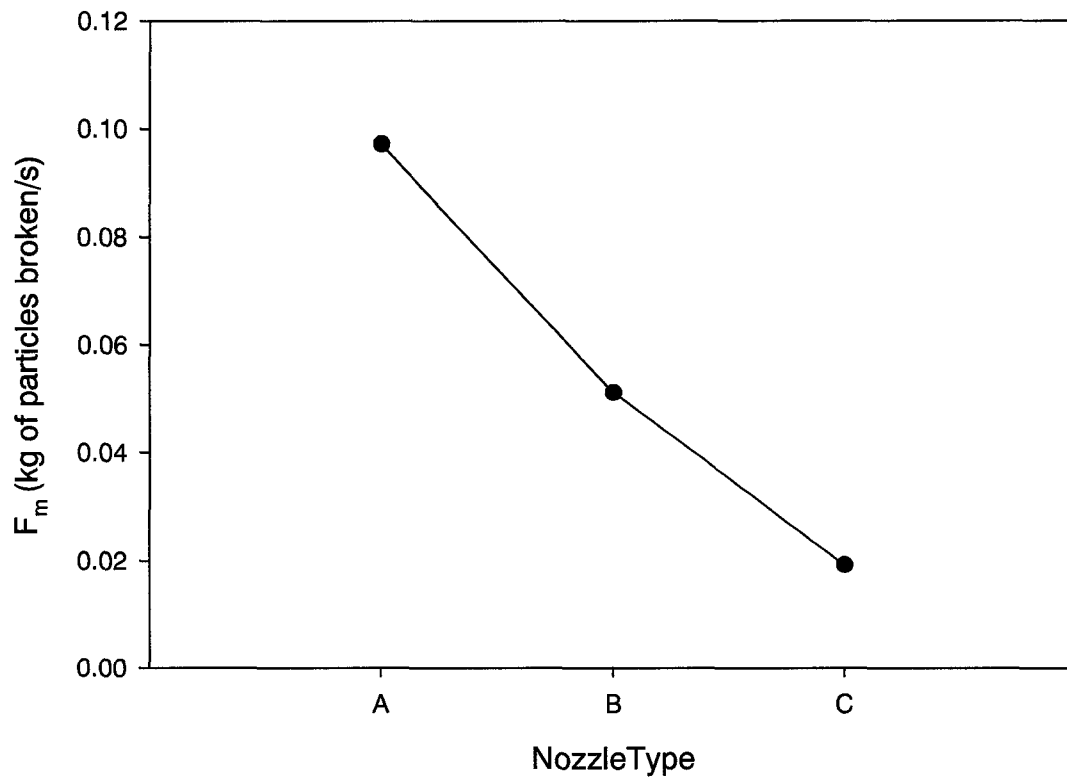


Figure 3.15: Effect of Nozzle Geometry on F_m

The effect of the mass of bed material was also determined by comparing the results obtained in a fluidized bed containing 77 kg of coke, to the results obtained in a fluidized bed containing 13 kg of coke. As shown in Figure 3.16, the particle breakage frequency, F_m , was approximately the same for both beds: for a given solid, it depends primarily only on the nozzle geometry, its operating conditions and the fluidization velocity. This means that if F_m is determined for a given nozzle and solids in a small bed, it can be used to predict the results of attrition in a larger bed.

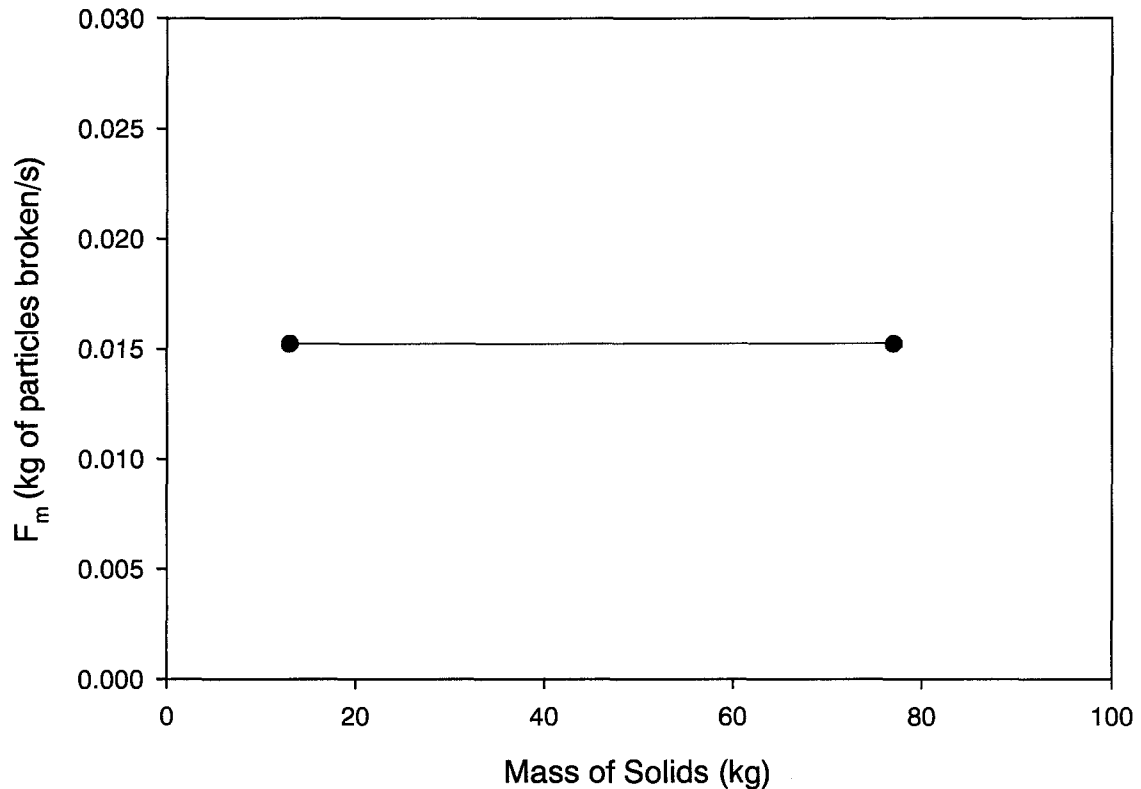


Figure 3.16: Effect of Bed Mass on F_m

The effect of placing a draft tube at various distances downstream of the attrition nozzle was also determined, and the results are shown in Figure 3.17. The particle breakage frequency increases as the distance between the nozzle tip and the draft tube, ℓ , is increased, up to 38 mm. Once the distance between the draft tube and nozzle is increased beyond 38 mm, the breakage frequency begins to decrease. The draft tube enhances the migration of particles from the low velocity peripheral region to the high velocity central region of the jet. Particles in the central region are accelerated to higher velocities and are much more likely to fragment when hitting the dense bed particles at the tip of the jet. The increased mixing and acceleration of the particles results in an increase in the particle breakage rate. The greater the distance between the nozzle and draft tube, the greater the number of particles entrained, and the greater the proportion of attrited particles. However, when the distance between the nozzle and draft tube is too

large, the enhancing effects of the draft tube are no longer observed because particles entrained further downstream in the jet have a lower momentum, and therefore decrease the particle breakage frequency. Nevertheless, in all cases with the draft tube, the breakage frequency is higher than in the free jet case.

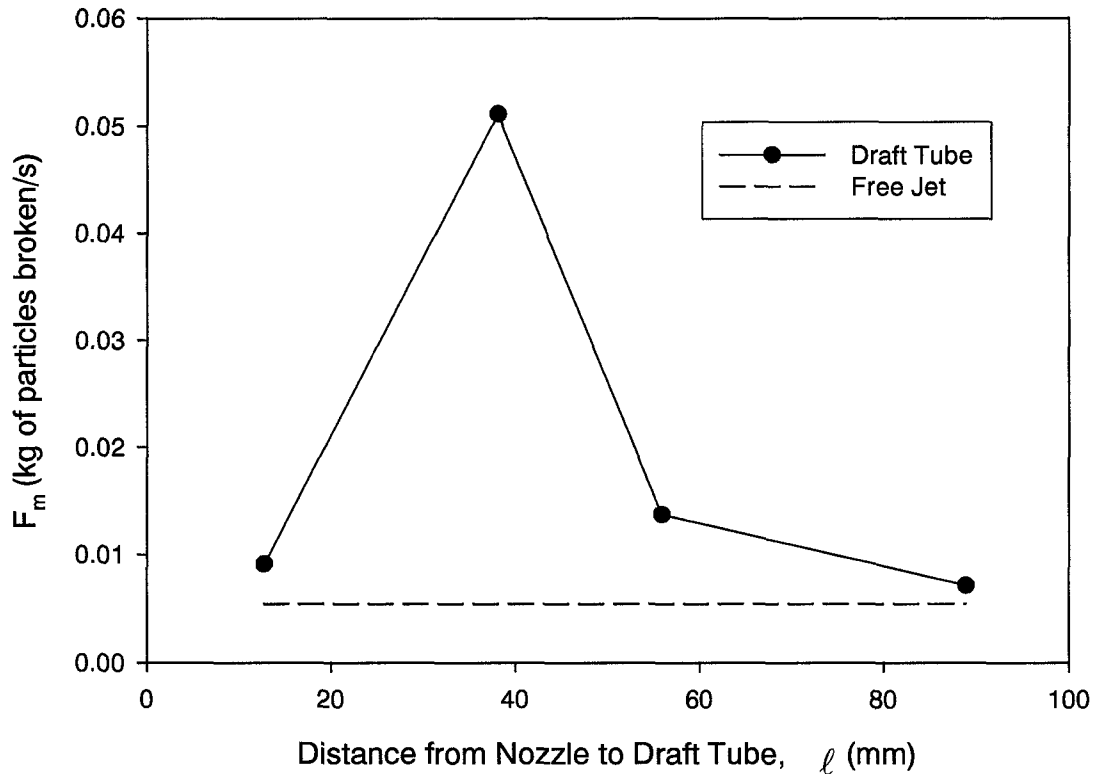


Figure 3.17: Effect of Draft Tube on F_m

Figure 3.18 shows a summary of the F_m values for various nozzle designs. Nozzle enhancements such as the draft tube, shroud, and nozzle inserts which increase the grinding efficiency result in higher values of F_m . These nozzle enhancements increase the particle breakage rate. The highest particle attrition rate is achieved when the draft tube and shroud are used in conjunction with each other.

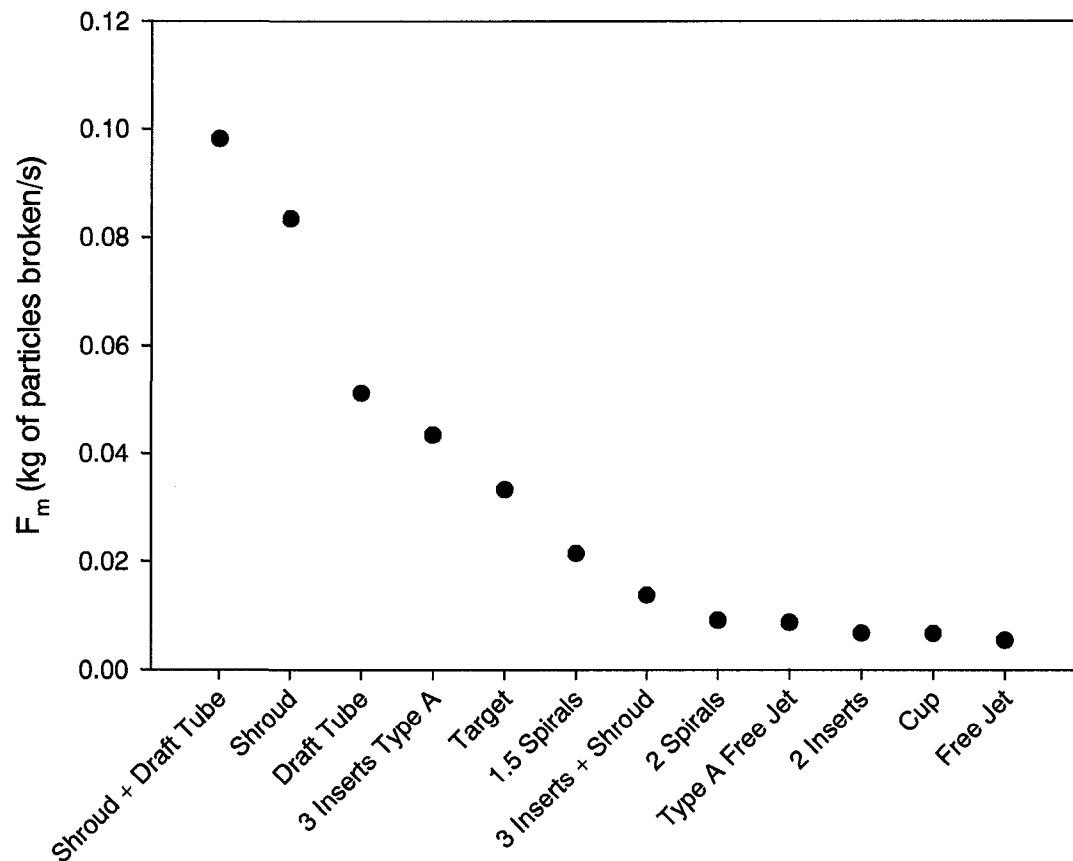


Figure 3.18: Effect of Nozzle Enhancements on F_m

To determine the relationship between the grinding efficiency and the parameters calculated from the model, the particle breakage frequency, F_m , was plotted against the grinding efficiencies calculated from Equation 3.2. The particle breakage frequency increases proportionally with the grinding efficiency, as can be seen in Figure 3.19.

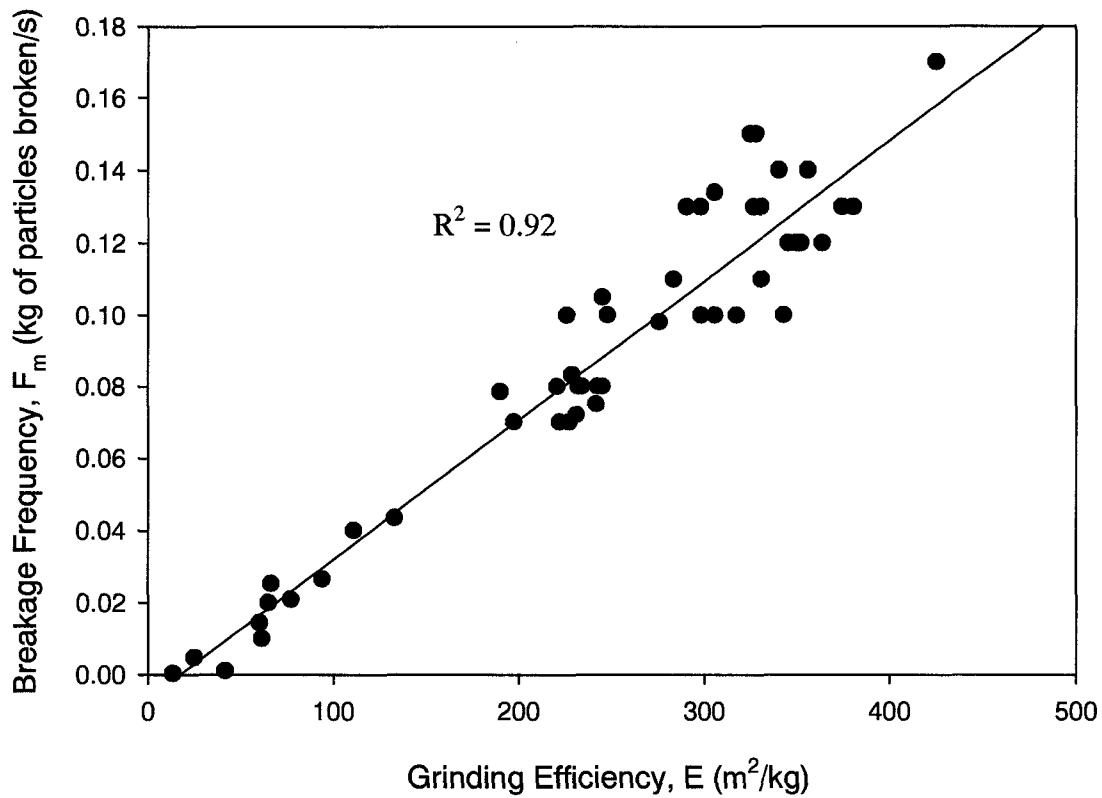


Figure 3.19: Breakage Frequency Versus Grinding Efficiency

In a previous study by McMillan et al. (2006b) a correlation was developed to estimate the grinding efficiency which took into account the nozzle diameter, attrition gas density, equivalent speed of sound of the gas, and the percent excess fluidization velocity. The particle breakage frequency was also correlated using these parameters, and β . β is determined by first calculating N , which is equal to the product of the particle breakage frequency, F , and the grinding time. Then n_o is calculated by dividing the mass of solids in the bed by the average mass of one particle. Finally, Equation 3.10 is used to calculate β . Since β is obtained from F , an equation that requires a solution by trial and error can be obtained, and the following correlation was developed.

$$F_m = 3.33 \times 10^{-7} \alpha \beta^{-1.406} d_N^{2.918} U_{\text{sound},eq}^{0.434} (\rho U_{\text{sound},eq}^2)^{0.306} \left(\frac{V_g - U_{mf}}{V_g} \right)^{0.278} \quad (3.13)$$

Where α is the nozzle geometry coefficient and has a value of 2.52, 1.87 and 1 for the Type A, B and C nozzles, respectively. Each parameter in Equation 3.13 has an impact on the mass of particles that are broken in the bed. A large proportion of particles remain unground in the bed if the β term is large, and therefore, the mass of particles broken will be smaller. If the nozzle diameter is increased, the mass of particles broken will also increase. The equivalent speed of sound takes into account implications for the effect of gas properties and temperature, the gas density term takes into account the effect of upstream pressure and the last term takes into account the effect of fluidization velocity. The experimental versus calculated number of particles broken per mass of attrition gas was plotted in Figure 3.20. There was good agreement between the experimental and calculated values. The particle breakage frequency is closely correlated with the attrition nozzle properties and bed operating conditions.

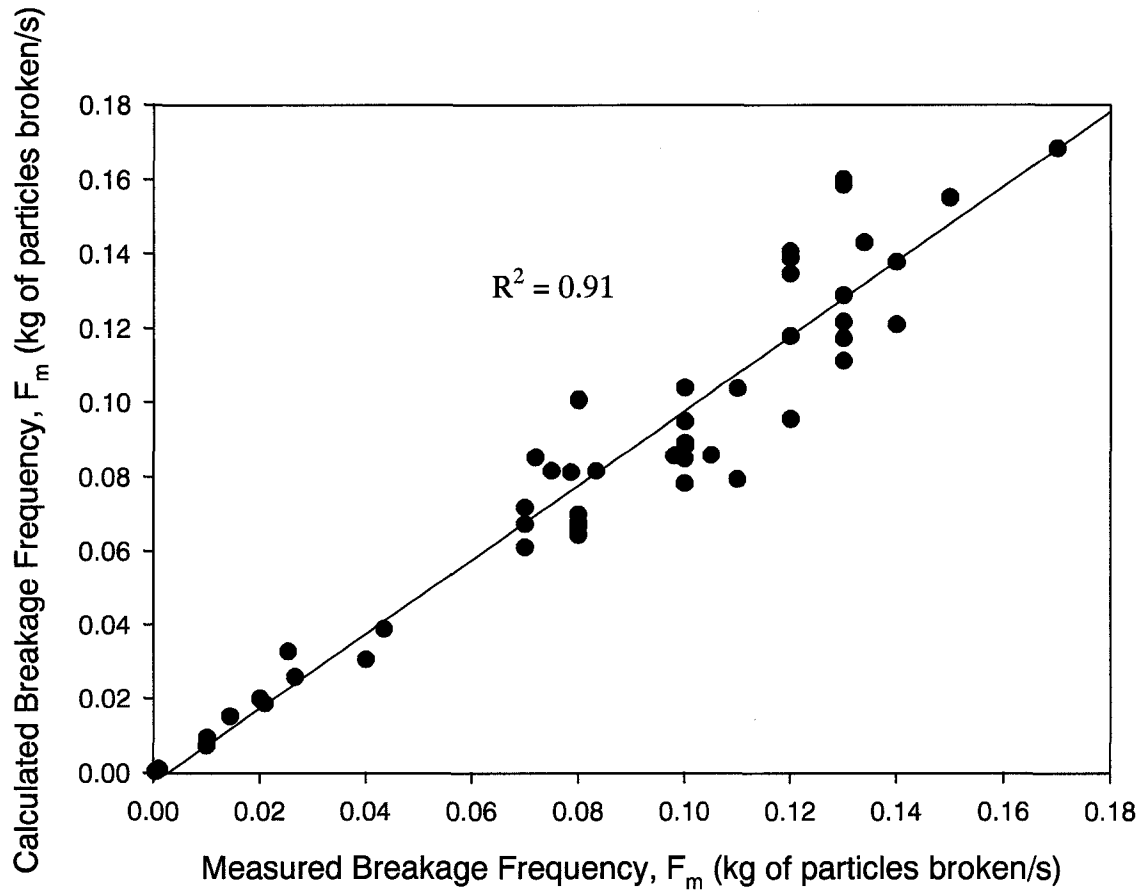


Figure 3.20: Comparison Between Experimental and Calculated Breakage Frequency

3.4 Conclusions

A model has been developed which predicts the particle breakage rate, the proportion of original particles that were not ground, and the size distribution of particles in a fluidized bed after they have been ground by the injection of a sonic velocity gas jet. The results were verified using experimental data obtained using various nozzle designs and different operating conditions. The particle breakage rate increased as the fluidization velocity and nozzle diameter were increased. Nozzle designs which resulted in an increase in particle entrainment and higher grinding efficiencies also resulted in an increase in particle breakage frequency. The mass of particles broken per unit time remained constant as the grinding time, the mass of solids in the bed and the column size

increased. Therefore, once F_m is known for a given nozzle design, it can be used to predict the attrition results in larger beds.

3.5 Nomenclature

$d_{p,large}$	Diameter of larger daughter particle (m)
$d_{p,o}$	Diameter of original mother particle (m)
$d_{p,small}$	Diameter of smaller daughter particle (m)
$d_{Pam,a}$	Arithmetic mean diameter of attritable particles (m)
$d_{Pam,o}$	Arithmetic mean diameter of original particles (m)
$d_{Pam,e-cal}$	Arithmetic mean diameter of calculated ground particles (m)
$d_{Pam,e-exp}$	Arithmetic mean diameter of experimentally ground particles (m)
$d_{Pam,o}$	Arithmetic mean diameter of original particles (m)
$d_{Psm,e-exp}$	Sauter mean diameter of experimentally ground particles (m)
$d_{Psm,e-cal}$	Sauter mean diameter of calculated ground particles (m)
d_N	Nozzle diameter (mm)
E	Grinding efficiency (m^2/kg)
F	Particle breakage rate (number of particles/s)
F_m	Particle breakage rate (mass of particles/s)
ℓ	Distance from nozzle tip to draft tube (mm)
M	Molecular weight (kg/mole)
M_{solids}	Mass of solids in the bed (kg)
N	Number of particle breaks (-)
n_o	Number of original particles in the bed
R	Gas constant (N.m / moles / K)
T	Temperature (K)
t	Grinding time (s)
U_{mf}	Minimum fluidization velocity (cm/s)
$U_{sound, eq}$	Equivalent speed of sound (m/s)
V_g	Fluidization velocity (cm/s)
$x_{i,a}$	Number fraction of attritable particles (-)
$x_{i,e-cal}$	Number fraction of calculated ground particles (-)
$x_{i,o}$	Number fraction of original particles (-)

Greek Letters

β	Proportion of original particles that have not been ground (%)
γ	Grinding symmetry coefficient (-)
η	Grinding efficiency (m^2/kg)
κ	Isentropic expansion factor (-)
ρ	Density of gas (kg/m^3)

3.6 References

- Alpine, <<<http://www.hosokawa.co.uk/flash/afg.html>>>, (2006)
- Austin, L., "A Review: Introduction to the Mathematical Description of Grinding As a Rate Process", *Powder Technol.*, **5**, 1-17 (1971).
- Baddour, C., Briens, C., "Modeling the Grinding Process of Carbon Nanotubes", Manuscript Submitted to *AIChE J.*, (2006).
- Benz, M., Herold, H., Ulfik, B., "Performance of a Fluidized Bed Jet Mill as a Function of Operating Parameters", *Int. J. Min.Proc.*, **44-45**, 507-519 (1996).
- Berthiaux, H., Dodds, J. "Modelling Fine Grinding in a Fluidized Bed Opposed Jet Mill. Part I: Batch Grinding Kinetics", *Powder Technol.* **106**, 78-87 (1999).
- Berthiaux, H., Chiron, C., Dodds, J., "Modelling Fine Grinding in a Fluidized Bed Opposed Jet Mill. Part II: Continuous Grinding Kinetics", *Powder Technol.*, **106**, 88-97 (1999).
- Donsi, G., Massimilla, L., Colantuoni, L., "The Dispersion of Axi-Symmetric Gas Jets in Fluidized Beds", *Fluidization*, J. Grace, J. Matsen, (Eds.), Plenum Press: New York, NY, 297 - 304 (1980).
- Dunlop, D., Griffin, L., Moser, J., "Particle Size Control in Fluid Coking", *Chem. Eng. Prog.*, **54**, 39-43 (1958).
- Epstein, B., "Logarithmico-Normal Distribution in Breakage of Solids", *Ind. Eng. Chem.*, **40**, 2289-2291 (1948).
- Ghadiri, M., Cleaver, J., Tuponogov, V., Werther, J., "Attrition of FCC Powder in The Jetting Region of a Fluidized Bed", *Powder Technol.*, **80**, 175-178 (1994).
- Gommeren, H., Heitzmann, D., Kramer, H., Heiskanen, K., Scarlett, B., "Dynamic Modeling of a Closed Loop Jet Mill", *Int. J. of Min. Proc.*, **44-45**, 497-506 (1996).
- Gommeren, H., Heitzmann, D., Moolenaar, J., Scarlett, B., "Modelling and Control of a Jet Mill Plant", *Powder Technol.* **108**, 147-154 (2000).
- Han, T., Kalman, H., Levy, A., "DEM Simulation of Particle Comminution in Jet Milling", *Trans. Soc. Min. Eng. of AIME*, **247**, 309 (2002).
- Hulet, C., Briens, C., Berruti, F., Chan, E., Ariyapadi, S., "Entrainment and Stability of a Horizontal Gas-Liquid Jet in a Fluidized Bed", *Int. J. Chem. React. Eng.* **1**, A60 (2003).

- Levenspeil, O., Kunii, D., Fitzgerald, T., "The Processing of Solids of Changing Size in Bubbling Fluidized Beds", *Powder Technol.*, **2**, 87-96 (1968).
- McMillan, J., Briens, C., Berruti, F., "Methods of Improving Particle Attrition in Fluidized Beds", (2006a). Unpublished (pending patent application and review/approval by Syncrude Canada Ltd.)
- McMillan, J., Briens, C., Berruti, F., "High Velocity Attrition Nozzles in Fluidized Beds", Submitted to *Powder Technol.*, (2006b).
- Merrick, D., Highley, J., "Particle Size Reduction and Elutriation in a Fluidized Bed Process", *AIChE Symp. Ser.*, **70**, 366 (1974).
- Perry, R., Green, D., (Eds.) *Perry's Chemical Engineers' Handbook*, 7th Ed. New York: McGraw-Hill, 1997, p. 6-23.
- Ray, Y., Jiang, T., Jiang, T., "Particle Population Model for a Fluidized Bed with Attrition", *Powder Technol.*, **52**, 35-48 (1987).
- Reid, K., "A Solution to the Batch Grinding Equation", *Chem. Eng. Sci.*, **20**, 953-963, (1965).
- Rowe, P., Partridge, B., Cheney, A., Henwood, G., Lyall, E., "Mechanisms of Solids Mixing in Fluidised Beds", *Inst. Chem. Eng. Trans.*, **43** (9), T271-T286 (1965).

CHAPTER 4

Methods of Improving Particle Attrition in Fluidized Beds

Jennifer McMillan, Craig Hulet, Cedric Briens, Franco Berruti

*Department of Chemical and Biochemical Engineering
The University of Western Ontario
1151 Richmond Street
London, Ontario, Canada, N6A 5B9*

4.1 Introduction

Fluidized bed jet attritors use high velocity gas jets to grind fluidized particles. Because grinding is autogenous, there is no contamination of the ground product by fragments from grinding surfaces, as in most other grinders. Jet mills are, therefore, used to grind materials such as toners, high purity ceramics, foodstuffs, ultrafine metal oxides, pharmaceutical powders, pigments, polymer powders and ultrafine particles for powder coating (Alpine, 2006). Jet milling can also be used to grind carbon nanotubes (Baddour and Briens, 2006). Jet attritors are also applied in fluidized bed processes such as fluidized bed coal combustion, where they grind the sorbent particles to maximize the adsorption efficiency of sulfur oxides, and fluid coking.

The fluid coking process, for example, uses thermal cracking to upgrade bitumen extracted from oil sands to produce synthetic crude oil. During the fluid coking process there is a gradual increase in the size of the coke particles due to the formation and deposition of coke byproduct on the surface of the particles during the reaction. In addition to particle growth due to the reaction, agglomerates are also formed when several coke particles stick together as a result of the injection of the liquid bitumen feed. Controlling the particle size of the coke within the fluid coker is of great importance, since large particles will result in slugging and poor circulation. Conversely, if too many fine particles with a diameter less than 70 microns exist, agglomeration will occur and result in poor fluidization (Dunlop, 1958). In order to control the size of the particles in the fluid coker, steam is injected into the reactor section through attrition nozzles. The high velocity gas jet issuing from these nozzles entrains bed particles and accelerates

them to a high speed. Due to their inertia, these particles slam on slow moving bed particles near the jet tip, causing breakage and, thus, reducing the particle size.

Currently attrition nozzles require a large proportion of the total steam consumed by the fluid cokers. If attrition nozzles could be improved to achieve the same attrition rates with a much lower steam flowrate, the production rate of synthetic crude from the fluid cokers could be greatly increased. Simple jet attrition can be enhanced through the use of a target, opposing jets or a draft tube accelerator.

The use of a target to enhance particle attrition has been studied fairly extensively. Dunlop et al. (1958) found that grinding was enhanced by impacting the attrition jet on a target plate, which was placed in the fluidized bed. However, their implementation was complex since solids were supplied into the nozzle tube upstream of the fluidized bed, in order to be fully accelerated before entering the bed. Dunlop et al. (1958) also found that target grinding and regular jet grinding had similar power requirements, but that target grinding produced a smaller proportion of undesirable excessively fine particles. However, a major problem associated with target grinding is erosion of the target itself. This problem was avoided by Siegel et al. (1978), who reduced the production of very fine particles with an attrition apparatus consisting of a succession of rings. These rings were coaxial with the nozzle, and the ring hole size decreased gradually as the distance from the nozzle increased. Smith et al. (1992) also determined that a target improved jet attrition rates. They found that spherical targets were more effective than flat targets, and that an inclined target did not provide any benefit. Tasirin et al. (1999) stressed that it was important to provide a large enough distance between the nozzle and the target, to allow for sufficient particle acceleration. They found that a jet and flat plate target combination required half the power of opposing jets to achieve the same grinding, confirming the results obtained by Henderson et al. (1996).

Opposing jets have also been studied to determine their effects on particle attrition. Tasirin et al. (1999) found that two vertical opposing jets achieved roughly the same grinding rates as two identical, non-interacting vertical jets. Using two horizontal opposing jets was not advantageous as they achieved roughly the same grinding rate as a single horizontal nozzle (Tasirin et al., 1999). When two opposing jets were used, the region between them had a much lower particle concentration, which lead to fewer

particle–particle collisions. Yates et al. (1991) measured particle attrition in the overlapping region between opposing vertical jets and found that the attrition rate varied according to whether the gases were discharged in the centre of the bed or close to the walls. The opposing jets only had a significant influence on attrition in the region close to the walls. Commercial fluidized jet mills from Alpine corporation, described by Berthiaux et al. (1999a, 1999b) and Godet-Morand et al. (2002), use three intersecting jets that are inclined with an angle of about 45 degrees with the horizontal plane. Henderson et al. (1996) improved upon the Alpine design by placing a target in the region where the three jets intersect. The target consisted of a hollow vertical tube, with a circular or triangular cross-section, and holes to allow the jets to penetrate. As a result, the jets interacted within the confined volume, thus enhancing the attrition. Gommeren et al. (1996) described a spiral jet mill that uses several angled jets to make the fluidized bed spin at high speed. This type of mill enhances attrition through friction of the particles on the bed wall, while preventing the entrainment of large particles.

Another method which can be used to enhance particle attrition is the use of a draft tube (Chan et al., 2004). Smith et al. (1992) proposed the use of a draft tube downstream and coaxial with the attrition nozzle. The purpose of the draft tube is to accelerate the particles entrained into the jet by maintaining a high gas velocity over a significant distance.

There may be other modifications and designs of attrition nozzles, not yet investigated, that could improve the grinding efficiency of particles in a fluidized bed. The objective of this study is to test different sonic velocity attrition nozzles and determine which nozzle configurations result in the greatest increase in grinding efficiency. Nozzle designs which enhance attrition by promoting the entrainment into the gas jet of particles, and accelerating them to high speed have been developed and tested.

4.2 Experimental Set-Up

4.2.1 Attrition Tests

Attrition experiments were conducted in a fluidized column with a height of 0.84 m and a rectangular cross section of 0.5 m by 0.1 m, as shown in Figure 4.1. The solids

were coke particles with a density of 1400 kg/m^3 and a Sauter-mean diameter of $135 \text{ }\mu\text{m}$, which filled the column to a height of approximately 0.23 m . The bed was fluidized with air at a velocity of 10 cm/s and the entrained particles were separated from the gas stream by a cyclone.

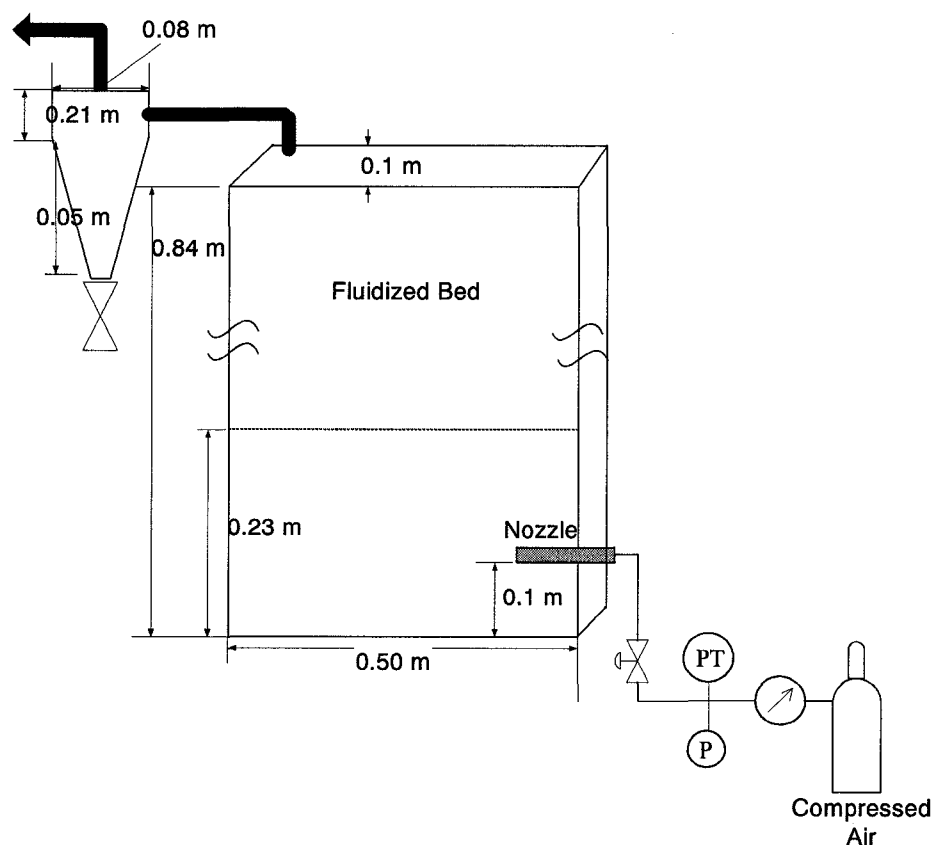


Figure 4.1: Experimental Equipment

The attrition nozzle was placed inside the bed at a distance of 0.1 m from the gas distributor, and injected gas horizontally into the fluidized particles in order to grind the particles. A constant gas mass flowrate from a high-pressure cylinder was supplied to the injection nozzle during the grinding process. Adjusting the pressure of the cylinder controlled the gas flowrate to the nozzle. Prior calibration provided the relationship between applied pressure and mass flowrate for each nozzle (the nozzle acted as a sonic orifice). The mass gas flowrate was verified after each run from the variation in the cylinder pressure that was measured by a transducer connected to a data acquisition system.

After injection, the fluidization gas was stopped in order to slump the bed. The fine particles collected in the cyclone were then returned to the bed. The fluidization gas was turned on again at a velocity just above the minimum bubbling velocity for approximately five minutes, in order to mix the particles. Previous experiments indicated that background particle attrition in the fluidized bed, in the absence of an attrition jet, was negligible when compared to the attrition observed with the nozzles (McMillan et al., 2006a). A sample of solids was taken from the bed before and after each run and analyzed using a Malvern laser diffraction apparatus to obtain the size distribution and the specific surface area created during the grinding process.

4.2.1.1 Nozzle Designs

Several different types of attrition nozzle designs were tested to determine the effect of nozzle geometry on the grinding efficiency. Each nozzle design was compared to a base case free jet nozzle. The base case nozzle used in this study, the Type C nozzle, was a simple straight tube nozzle with an exit diameter of 4.6 mm, as shown in Figure 4.2.

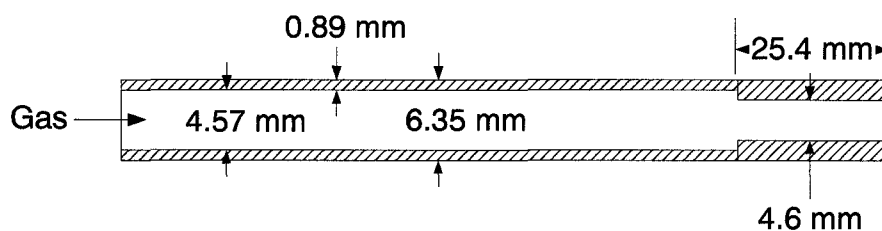


Figure 4.2: Base Case Straight Tube Attrition Nozzle (Type C Nozzle)

One method of improving the grinding efficiency is to place objects downstream of the attrition nozzle. A circular target constructed of stainless steel, with a diameter of 50 mm was placed downstream of the nozzle, as shown in Figure 4.3. Tests were performed with the target located at distances from the nozzle tip, ℓ , of 25 mm, 38 mm, 51 mm, 63 mm, 89 mm, 102 mm and 127 mm.

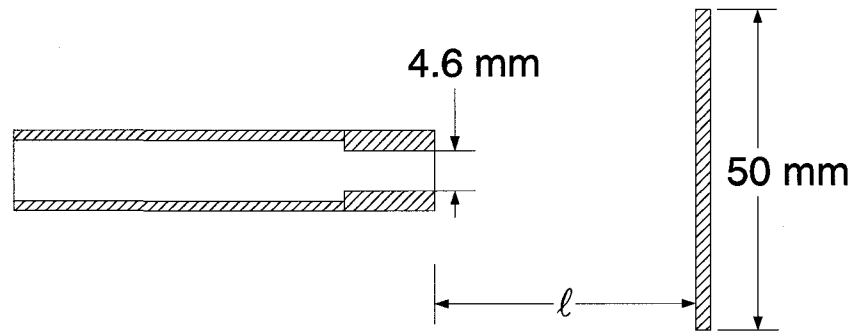


Figure 4.3: Target Configuration

Similar to the target, a stainless steel cup with an internal diameter of 50 mm and a depth of 25 mm was placed downstream of the attrition nozzle. The objective of the cup was to reduce target erosion by forming a dense layer of particles on which the high velocity particles entrained into the jet would impact. The cup contained two 3 mm by 20 mm slots which allowed solids to enter and exit, as shown in Figure 4.4. Tests were performed with the cup at distances from the nozzle tip, ℓ , of 63 mm and 102 mm.

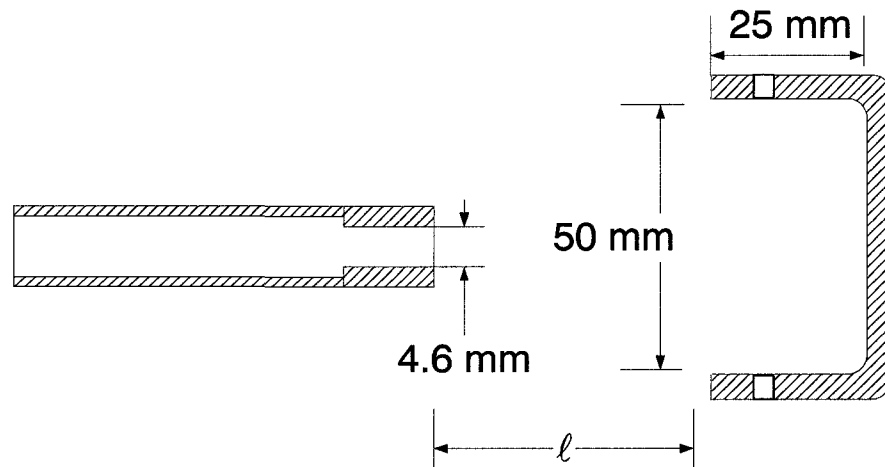


Figure 4.4: Cup Configuration

A third object, which was used to increase the grinding efficiency, was a draft tube. A stainless steel tube with a length (L_T) of 50 mm and a diameter (D_T) of 25 mm was placed coaxially downstream of the injection nozzle, as shown in Figure 4.5. The

distance between the draft tube and injection nozzle, ℓ , was varied. Distances of 13 mm, 38 mm, 56 mm and 89 mm were tested.

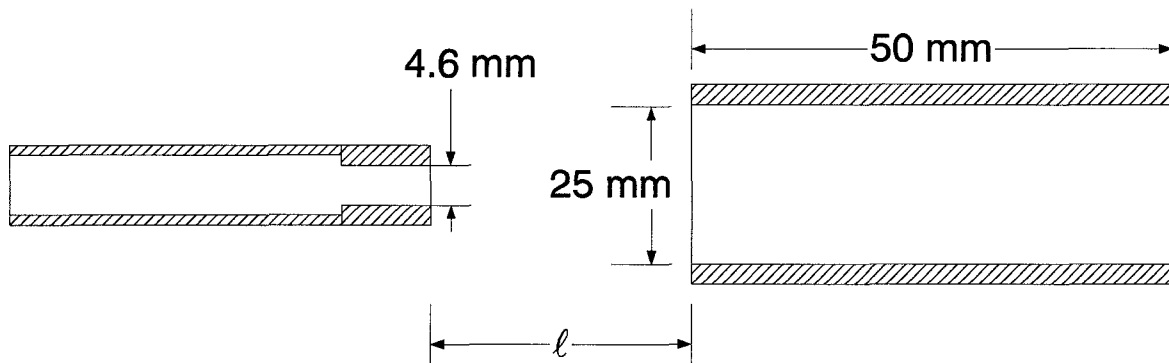


Figure 4.5: Draft Tube Configuration

Another method of improving the grinding efficiency was to place a shroud around the nozzle. A Lexan shroud with a diameter (D_S) of 44 mm was placed around the tip of the injection nozzle, as shown in Figure 4.6. The distance between the tip of the nozzle and the base of the shroud (L_{Tip}) was 6 mm. Two shrouds were tested: one with a length (L_S) of 50 mm and the other with a length (L_S) of 19 mm.

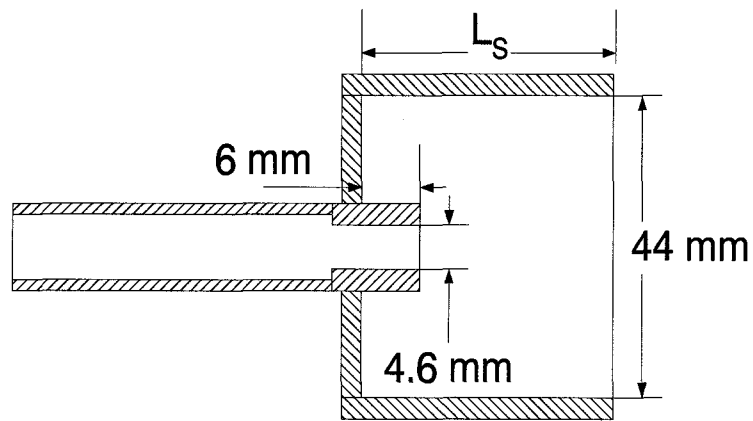


Figure 4.6: Shroud Configuration

Internals were also added to the attrition nozzle in order to improve the grinding efficiency. Inserts that consisted of rods, 1 mm in diameter and 25.4 mm in length, were placed around the circumference of the exit of the attrition nozzle. Nozzles with 2, 3 and 4 inserts were tested. Figure 4.7 depicts a nozzle with 3 inserts.

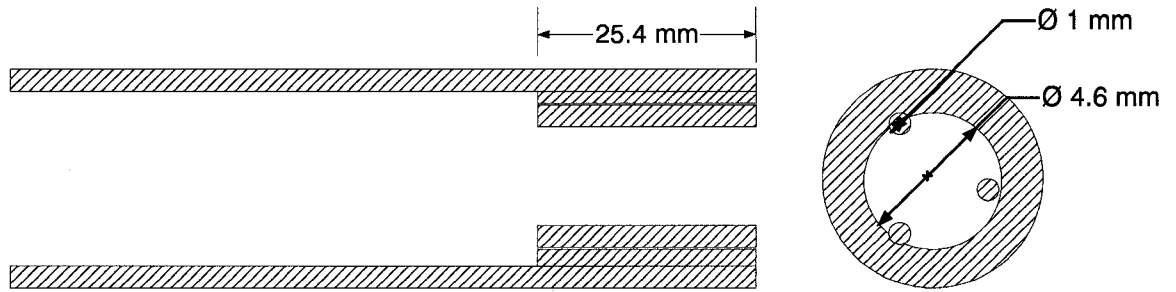


Figure 4.7: Nozzle Inserts Configuration

The final method used to improve the grinding efficiency was to force the gas exiting the attrition nozzle to flow in a spiral pattern. A 1 mm thick twisted stainless steel plate, 4 mm wide and 230 mm long, was placed inside the nozzle, as shown in Figure 4.8. Spirals with 1.5, 2, and 5 turns were tested.

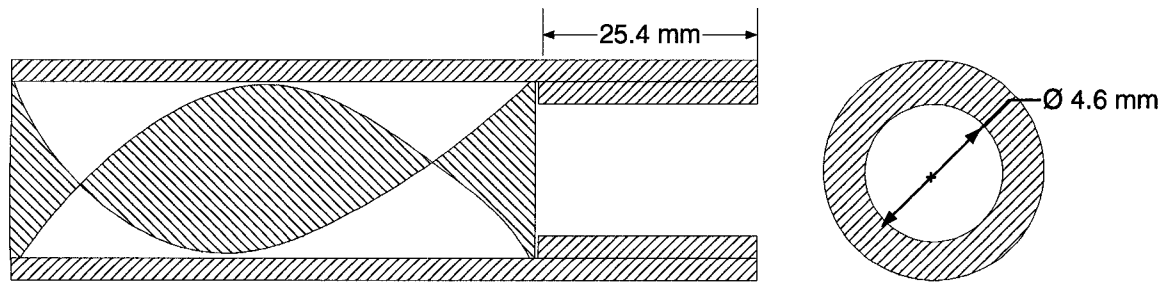


Figure 4.8: Spiral Flow Configuration

Various combinations of the above mentioned nozzle designs were also tested. The shroud, draft tube, nozzle inserts, spiral flow, and target were all used in conjunction with each other. An additional nozzle geometry, tested previously by McMillan et al. (2006) was tested with the shroud, draft tube and nozzle inserts. This nozzle, the Type A nozzle, was a convergent-divergent, Laval-type nozzle, similar to the nozzles used by Benz et al. (1996), as shown in Figure 4.9.

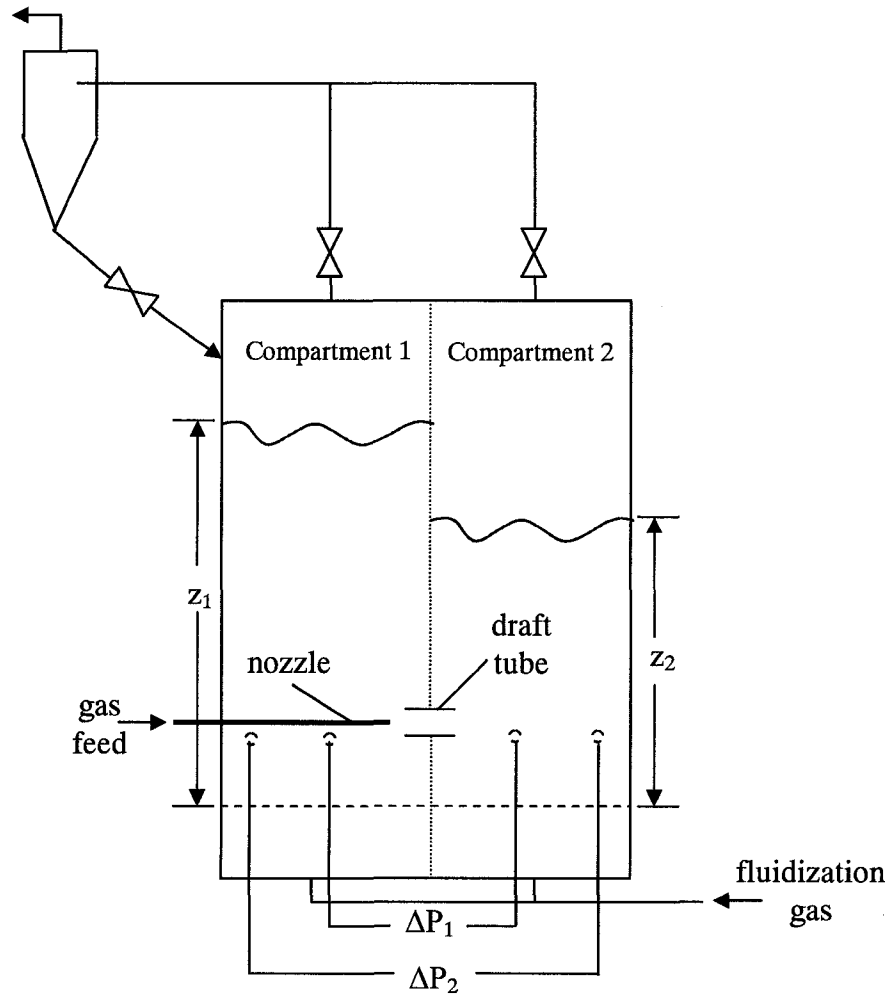


Figure 4.10: Experimental Setup for Entrainment Tests

If z_1 and z_2 are the heights of the two fluidized bed compartments, and ΔP_{12} , the pressure drop between them, the solids mass flow rate between the two compartments can be expressed as:

$$F_s = \frac{A_b}{2g} \frac{d(\Delta P_{12})}{dt} \quad (4.1)$$

Equation 4.1 assumes that friction loss at the wall of the draft tube is minimal. The bed levels were adjusted by closing one of the two ball valves located downstream of the gas exits, in the freeboard region. Two pressure transducers were wall mounted close to the draft tube, along its axis and measured ΔP_{12} . In order to measure the entrainment, the gas jet was injected into the fluidized bed through a nozzle located in compartment 1 and separated by a distance of 25.4 mm from the draft tube. By closing the ball valve

(V₂) on the right side of the freeboard region, compartment 2 was pressurized, and as a result the height in compartment 2 was greater than the height in compartment 1 ($z_1 < z_2$). Once the desired pressure difference was achieved, the ball valve was opened and the data acquisition started. The pressure transducers continuously measure ΔP_{12} . During this process, at a particular instant in time, a condition existed where $\Delta P_{12} = 0$. At this point, the entrainment of solids through the draft tube was purely a function of the jet momentum, and thus the slope of ΔP_{12} versus time at $\Delta P_{12} = 0$ was directly related to the solids entrainment as given in Equation 4.1. The entrainment rates for the 3 types of nozzles tested were obtained at various gas flowrates. For these tests it was intended to simulate the entrainment in a free jet injected into a fluidized bed, and therefore the draft tube diameter was large enough to minimize the interaction of the jet with its walls.

4.3 Results and Discussion

To compare the results from all of the tests, a grinding efficiency was calculated, defined as the amount of new surface area created per mass of attrition gas used:

$$\eta = \frac{\text{new particle surface created by attrition}}{\text{mass of attrition gas}} = \frac{\frac{m^2}{s}}{\frac{kg}{s}} = \frac{m^2}{kg} \quad (4.2)$$

This definition was chosen, as the objective was to achieve maximum grinding, while using a minimum amount of attrition gas.

The grinding efficiencies for each nozzle design were compared to the value obtained using the free jet base case nozzle. Figure 4.11 shows the results obtained when the target was placed downstream of the nozzle. For all cases, when the target was used the grinding efficiency was higher than the efficiency obtained with the free jet. The target provided a hard surface on which the particles could grind, thus increasing the grinding rate. In addition, the grinding efficiencies increased as the distance from the nozzle to the target was increased, up to a distance of 63.5 mm. The greater the distance between the nozzle and the target, the greater the volume of particles entrained into the jet, causing the grinding efficiency to increase. However, when the distance between the nozzle and the target was greater than 63.5 mm the grinding efficiency began to decrease

as the energy of the jet began to dissipate and the velocity of the entrained particles decreased. Although the results obtained with the target are superior to the free jet, there still exists the disadvantage of target erosion.

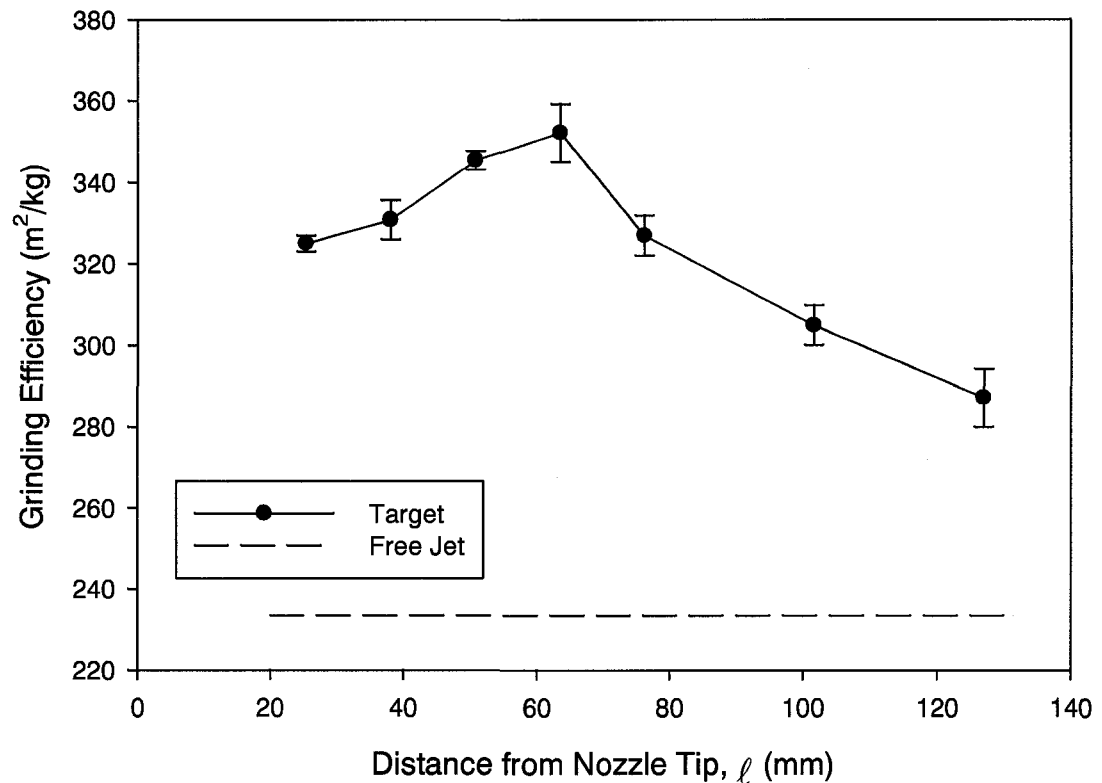


**Figure 4.11: Effect of Target on Grinding Efficiency
(Error Bars Show the Standard Deviation)**

To achieve increased grinding efficiencies, while reducing the amount of erosion, a cup-shaped target was placed downstream of the nozzle. The cup causes entrained solids to impact on a dense layer of particles instead of the metal surface of the target. Figure 4.12 shows the grinding efficiencies obtained when the cup was used. The grinding efficiencies obtained with the cup are significantly lower than the grinding efficiencies obtained with the target at the corresponding distances. Although the cup was equipped with slots to enable renewal of solids, the amount of solids exposed to the grinding area was significantly lower than when the target was used.

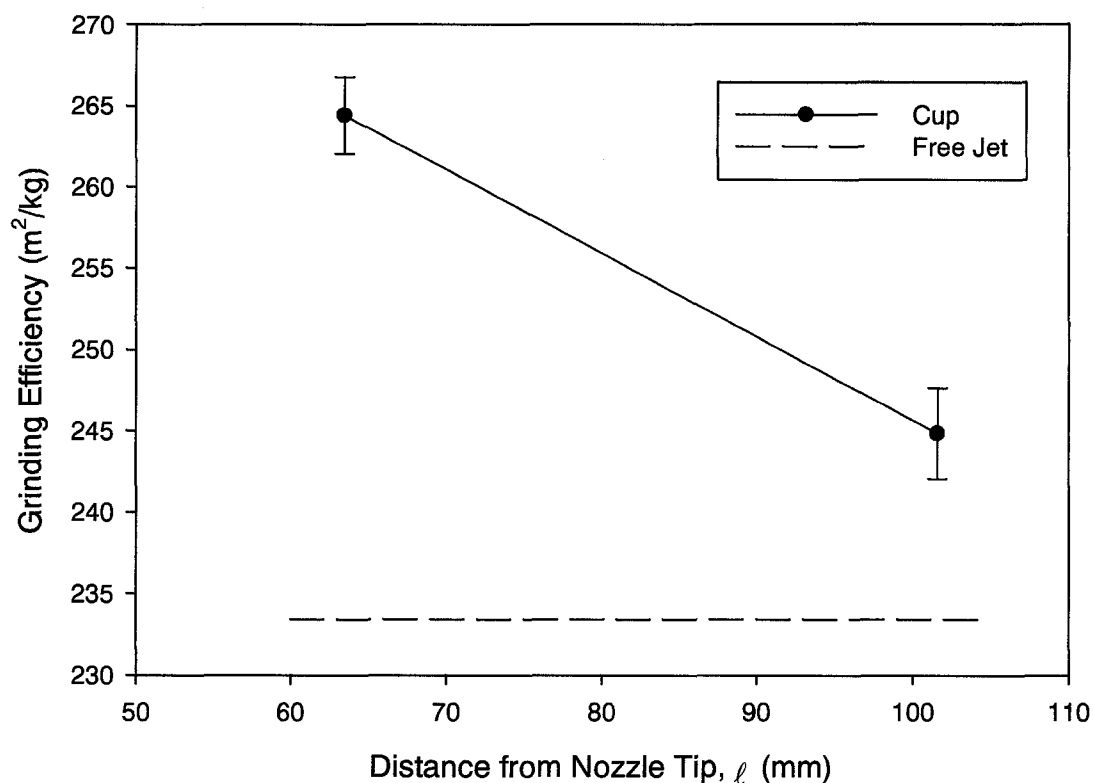


**Figure 4.12: Effect of Cup on Grinding Efficiency
(Error Bars Show the Standard Deviation)**

Figure 4.13 shows the results obtained when the draft tube was placed downstream of the nozzle. The use of a draft tube greatly enhanced the grinding. As the distance between the nozzle and the draft tube was increased, the grinding efficiency also increased. The amount of solids entrained into the jet increased as the axial distance from the nozzle was increased and as a result more solids entered the draft tube. The draft tube enhanced the migration of particles from the low velocity peripheral region to the high velocity central region of the jet. Particles in the central region were accelerated to higher velocities and were much more likely to fragment when hitting the dense bed particles at the tip of the jet. The increased mixing and acceleration of the particles resulted in an increased grinding efficiency.

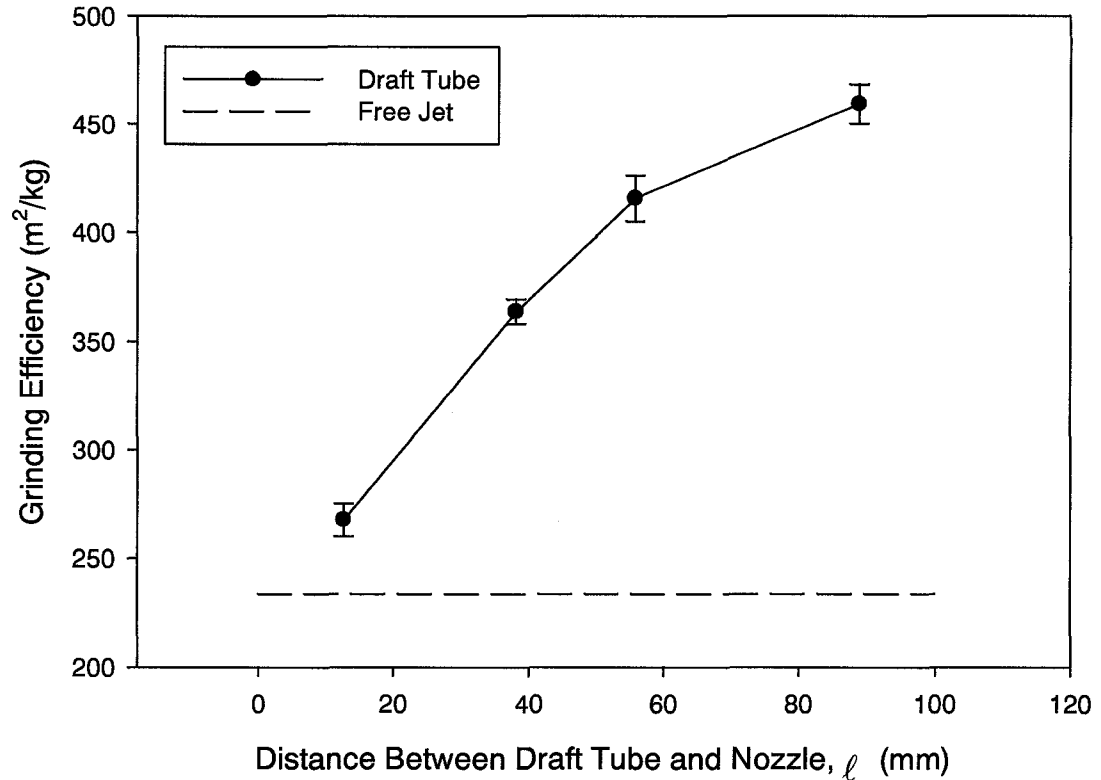


Figure 4.13: Effect of Draft Tube on Grinding Efficiency (Error Bars Show the Standard Deviation)

In addition to placing objects downstream of the nozzle, additions to the nozzle were used to increase the grinding efficiency. Figure 4.14 shows the results of the grinding efficiencies obtained when a shroud was placed on the tip of the injection nozzle. The grinding efficiencies obtained when a shroud was placed on the tip of the injection nozzle were higher than the free jet case, especially when the 19 mm long shroud was used. The shroud enhanced solids entrainment into the jet by creating a dense region of non-fluidized solids near the tip of the injection nozzle. The particles were constantly being entrained into the jet and replenished with fresh solids. One of the reasons why the 19 mm shroud performed better than the 51 mm shroud could be due to the fact that the shorter shroud allowed more solids to be entrained into the jet. The distance between the inside diameter of the shroud and the periphery of the jet was greater for the shorter shroud. When the 51 mm shroud was used, the diameter of the gas

jet at the exit of the shroud was only slightly smaller than the diameter of the shroud itself, thus restricting the space for solids to flow into the shroud and allowing fewer solids to be entrained into the jet.

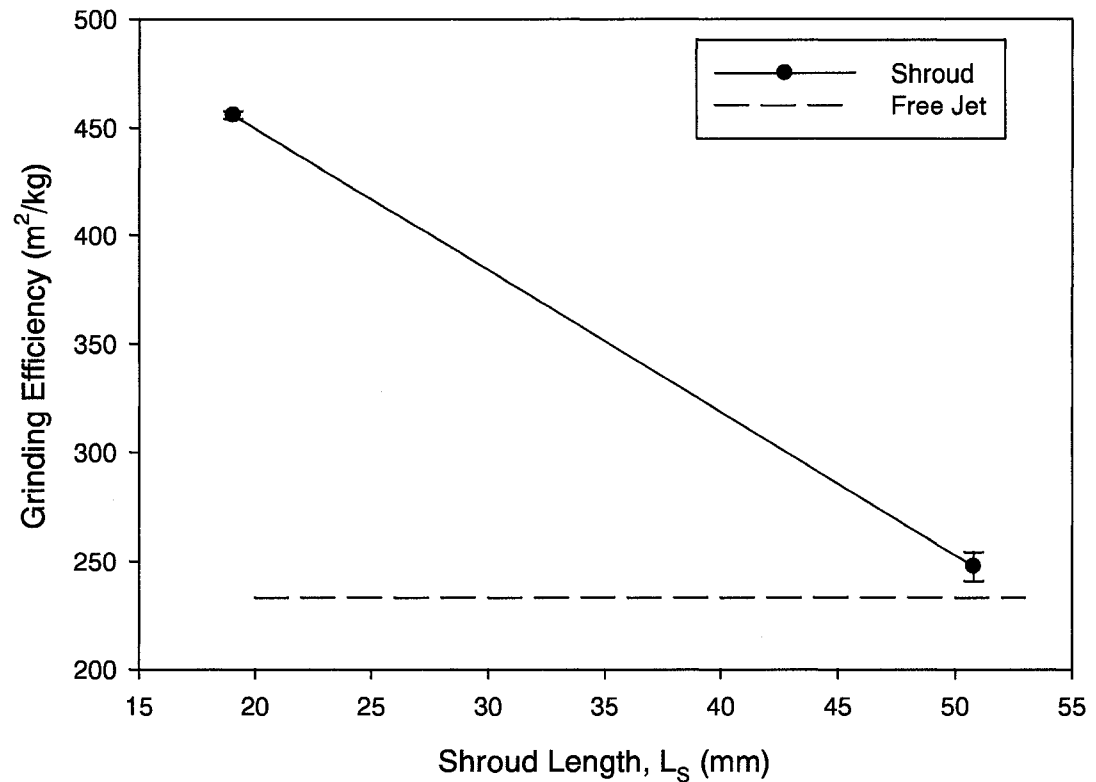


Figure 4.14: Effect of 44 mm Diameter Shroud on Grinding Efficiency (Error Bars Show the Standard Deviation)

The effect of nozzle scale on the grinding efficiencies was determined for three cases: free jet, shroud and draft tube. The results are shown in Figure 4.15. Similar large relative benefits in grinding efficiency were achieved with both the shroud and the draft tube, independently of the nozzle scale. The 4.6 mm diameter nozzle resulted in a much higher grinding efficiency than the 2.4 mm diameter nozzle. Similar trends were seen for each nozzle scale: the use of either a shroud or a draft tube increased the grinding efficiency considerably. This suggests that the effects on grinding efficiency of increasing the nozzle size and adding either a shroud or a draft tube were additive.

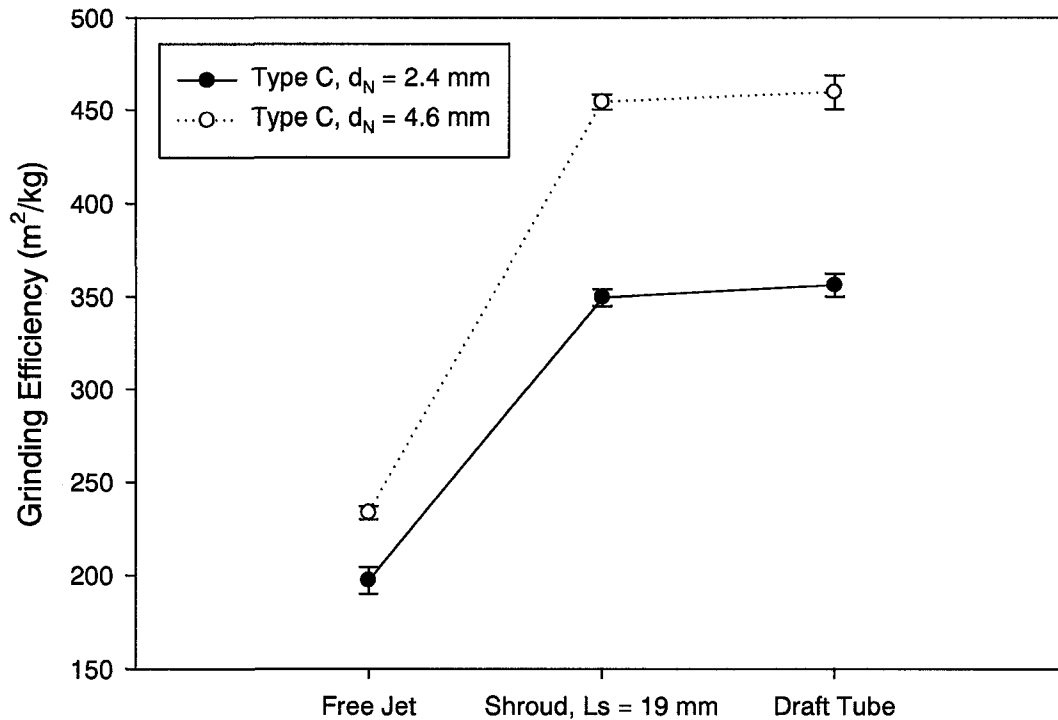
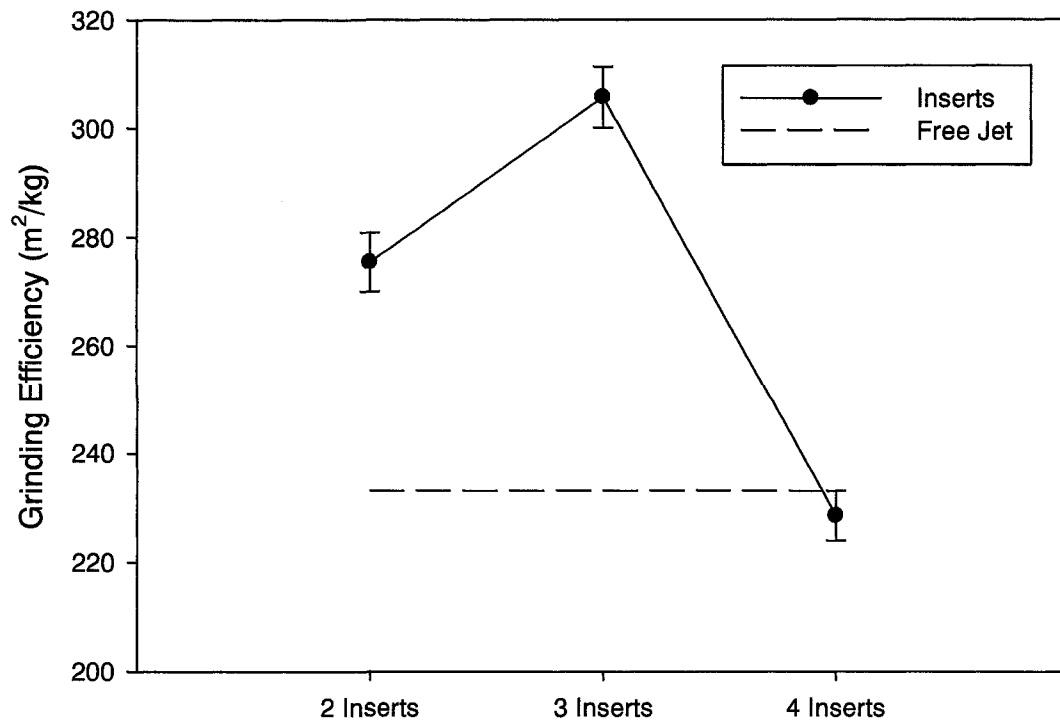


Figure 4.15: Effect of Nozzle Scale on Grinding Efficiency (Error Bars Show the Standard Deviation)

Nozzle internals were also used to enhance the grinding efficiency. Figure 4.16 shows the results obtained when 2, 3 and 4 inserts were placed in the nozzle tip to enhance attrition. The grinding efficiency increases above the free jet value when 2 and 3 inserts were used. The inserts changed the shape of the jet exiting the nozzle and created a larger surface area between the jet boundary and the fluidized bed, thus increasing the entrainment rate into the jet. The inserts also helped to destabilize the boundary between the jet and the fluidized particles by creating vortices at the exit of the nozzle, thus increasing the particle entrainment. The grinding efficiency increased as the number of inserts was increased, up to 3 inserts. When 4 inserts were used, the grinding efficiency decreased below the value obtained with the free jet. The 4 inserts occupied a large area of the nozzle cross-section and the nozzle behaved as though it were a smaller diameter free jet, thus reducing the benefits of the inserts.



**Figure 4.16: Effect of Nozzle Inserts on Grinding Efficiency
(Error Bars Show the Standard Deviation)**

Another internal used to enhance the grinding efficiency was a twisted metal plate which caused the gas exiting the nozzle to travel in a spiral pattern. As the number of turns in the plate decreased, the grinding efficiency increased, as shown in Figure 4.17. The more gradual the turn of the spiral plate the shorter the distance the gas had to travel before reaching the nozzle exit. As a result, the gas exiting the nozzle when the 5 turn spiral was used had traveled a longer distance than the 1.5 turn spiral, therefore reducing the kinetic energy of the gas.

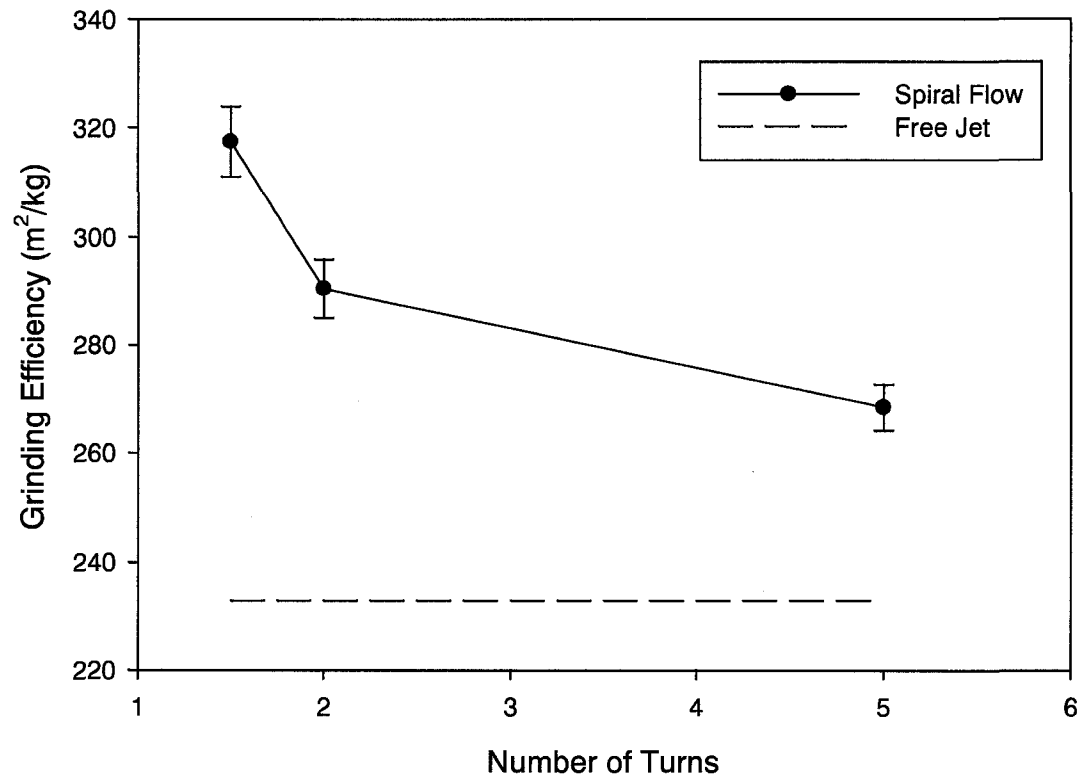


**Figure 4.17: Effect of Spiral Flow on Grinding Efficiency
(Error Bars Show the Standard Deviation)**

Various combinations of the above mentioned nozzle designs were tested together to determine if the grinding efficiency could be increased even further. The 19 mm length shroud was used in conjunction with the draft tube which was placed 88.9 mm from the nozzle tip. When the shroud and draft tube were used simultaneously there was not a significant improvement over either the draft tube or shroud case. A movie was taken with a half cylindrical configuration, so that the axis of both the nozzle and the shroud axes were on a transparent wall (Hulet et al., 2006). Without the shroud, particles were entrained over the whole first half of the jet cavity. The draft tube then helped redistribute entrained solids from low velocity peripheral regions to the high velocity central region. With the shroud, most of particles appeared to be entrained near the nozzle tip and the draft tube was not needed to transfer particles to the high velocity

central region. Both the increase in entrainment rate and the improved solids mixing contributed to increasing the grinding efficiency when the shroud was used.

The nozzle with 3 inserts was used in conjunction with the shroud, draft tube, 1.5 turn spiral and a profiled, Laval type nozzle, which was tested previously by McMillan et al. (2006a) and was found to increase the grinding efficiency over the simple straight tube nozzle. For each of these cases the grinding efficiency was greater than the results obtained when these enhancements were used with the base case nozzle. However, the effects were not additive, which suggests that the mechanism that improved attrition when the inserts were used, was also partly the mechanism that improved attrition when the shroud, draft tube, spiral flow and profiled nozzle were used. Figure 4.18 shows a summary of the grinding efficiencies obtained with each of the nozzle configurations.

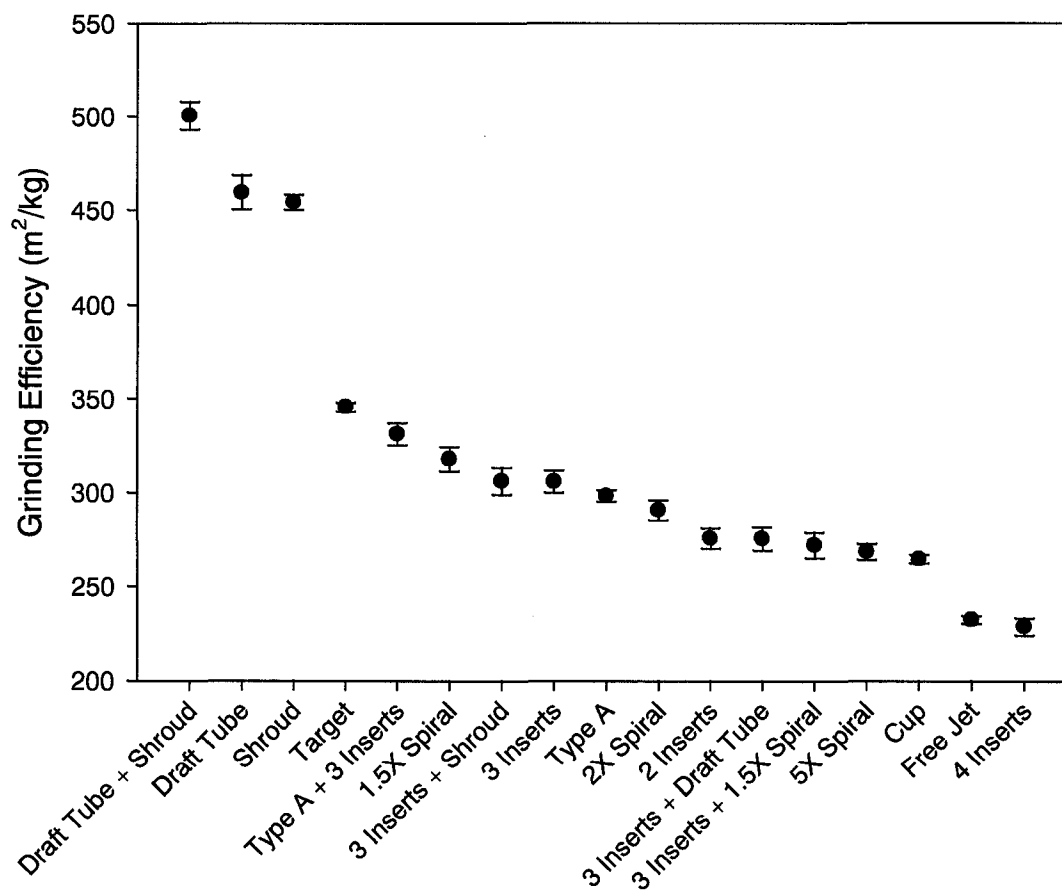


Figure 4.18: Comparison of Grinding Efficiencies for Various Nozzle Enhancements (Error Bars Show the Standard Deviation)

To illustrate the impact of the draft tube and shroud, the size distributions of the ground particles for each were compared to the size distribution of the ground particles obtained with the free jet base case. Figures 4.19 and 4.20 show a comparison of the size distributions when the draft tube and shroud were used, respectively. For both cases the size distribution of ground particles was similar to the size distribution of ground particles obtained with the free jet base case. This suggests that the draft tube and shroud do not increase the grinding efficiency by creating more fine particles, but by increasing the fraction of particles broken in the bed.

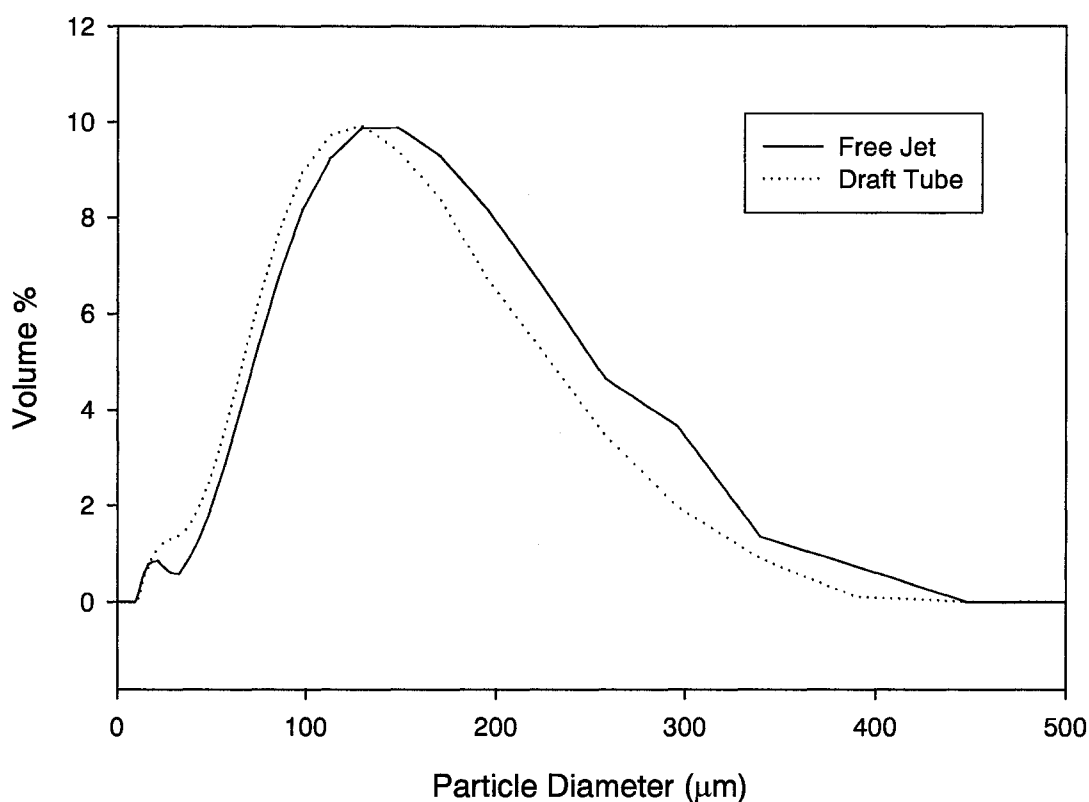


Figure 4.19: Comparison of Size Distributions of Ground Particles: Draft Tube versus Free Jet

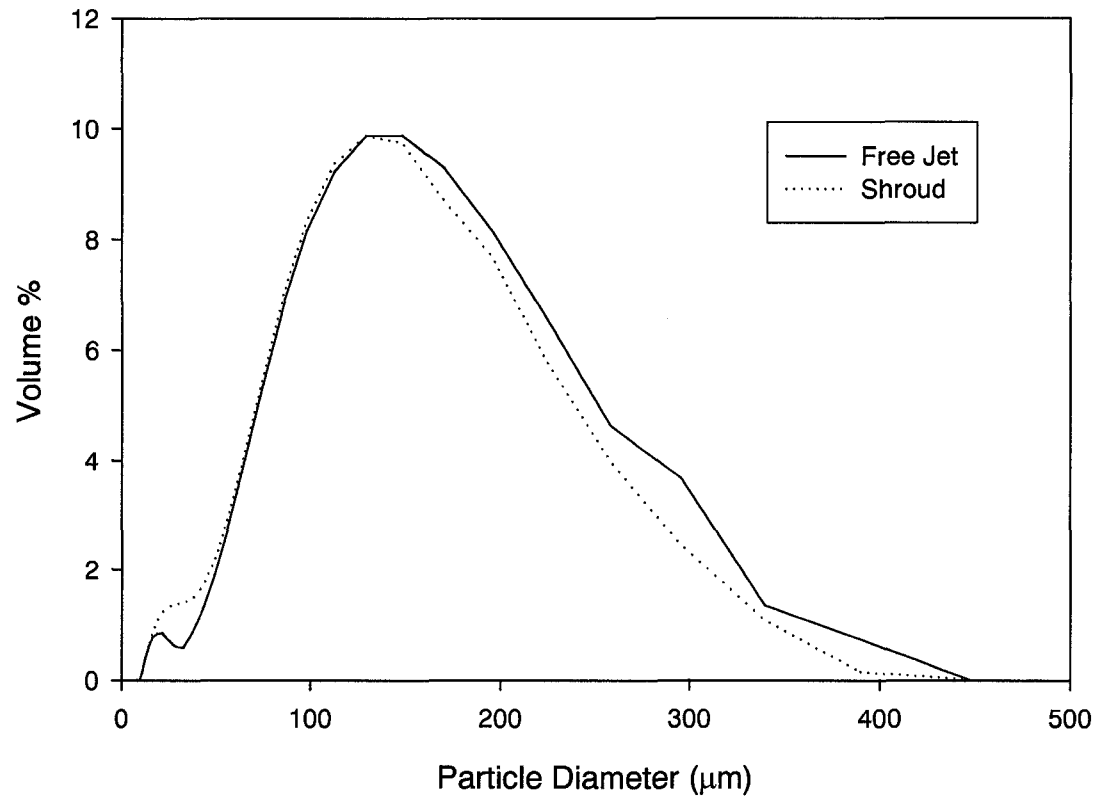


Figure 4.20: Comparison of Size Distributions of Ground Particles: Shroud versus Free Jet

In addition, a model developed by McMillan et al. (2006b) was used to verify that the attrition mechanism did not change when either the draft tube or shroud were used. The model predicts 2 parameters, the proportion of unground particles in the fluidized bed, β , and the grinding symmetry coefficient, γ , which represents the ratio of the volume of the small daughter particle to the volume of the large daughter particle. When compared to the free jet base case, the proportion of unground particles in the bed, β , was significantly lower for both the draft tube and shroud cases. β is calculated assuming that the fluidized bed is perfectly mixed, and is related to the particle breakage frequency, F , by the following equations:

$$F = \frac{N}{t} \quad (4.3)$$

$$\beta = \frac{1}{1 + N/n_o} \quad (4.4)$$

The model then uses β to predict the particle breakage frequency, F_m , the mass of particles broken per second. As seen in Figure 4.21, the particle breakage frequency was significantly higher for the draft tube and shroud cases, when compared to the free jet base case. For the cases when either the draft tube or shroud are used, significantly more particles are broken per unit time, and consequently the proportion of unground particles in the bed decreases, thus reducing the value of β . In addition, various values of γ , the grinding symmetry coefficient, were tested for all three cases. The value of γ did not change when either the draft tube, or shroud were used; all three cases had a grinding symmetry coefficient of approximately 0.8. Since the grinding symmetry coefficient is fairly high, and the mother particle is splitting into two particles of fairly equal size, the use of a shroud or a draft tube does not change the primary attrition mechanism occurring in the bed, which is fragmentation, as opposed to abrasion.

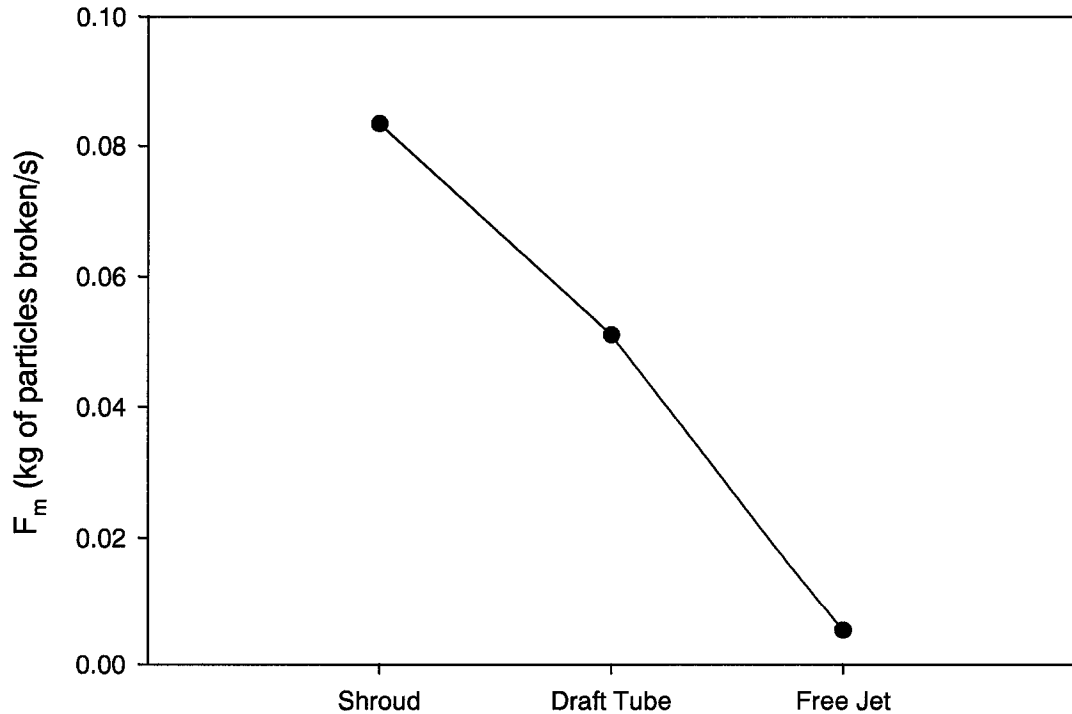


Figure 4.21: Comparison of Particle Breakage Frequency, F_m

To determine the effects of solids entrainment on the grinding efficiency, the solids entrainment rate was measured for 3 types of nozzles: the Type C nozzle, the Type A nozzle and the shrouded nozzle. The entrainment rate for each nozzle type was determined at several different gas flowrates that were within the range of flowrates used in the attrition tests, and three replicate runs were conducted at each condition. The relative solids entrainment for each nozzle was determined by normalizing the results by the solids entrainment rate obtained with the Type C nozzle at the same nozzle gas flowrate. Figure 4.22 shows a plot of the relative solids entrainment versus gas flowrate, and includes 95% confidence intervals.

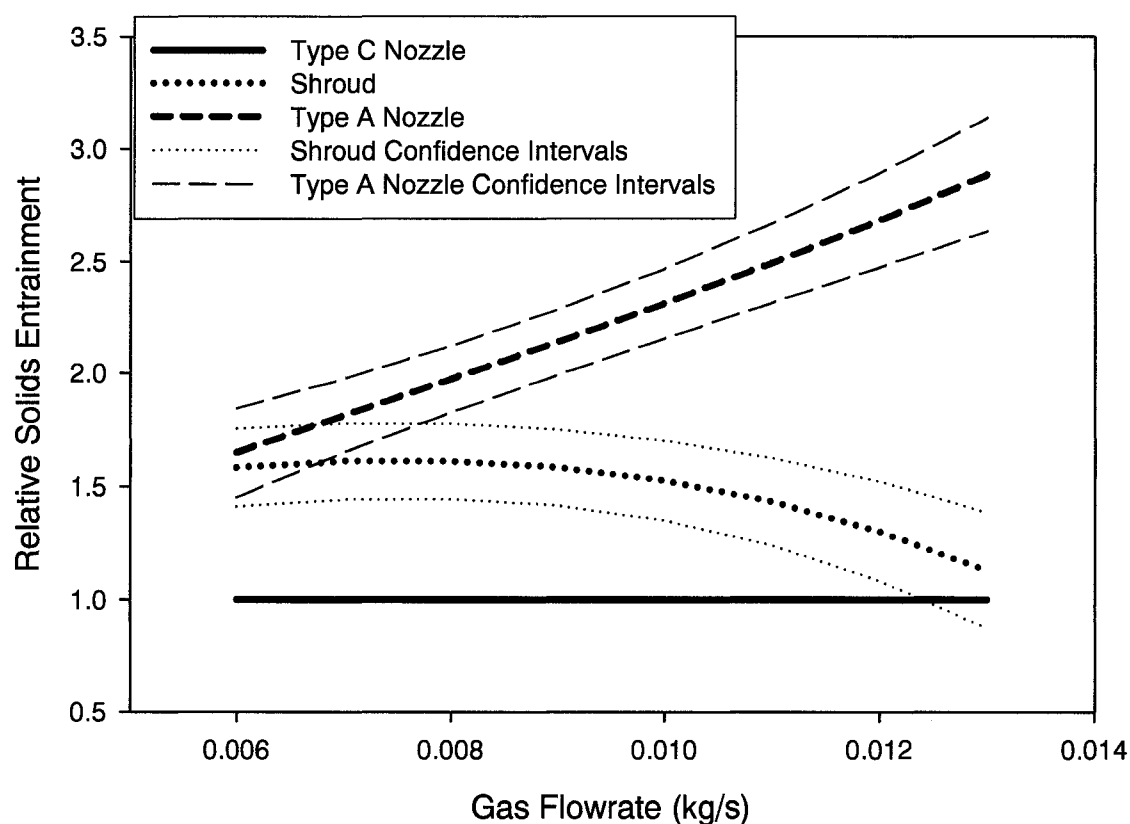


Figure 4.22: Comparison of Relative Solids Entrainment for Different Nozzle Types

As seen in Figure 4.22, the Type A nozzle entrains more solids than the shrouded nozzle. However, according to Figure 4.18, the shrouded nozzle has a higher grinding efficiency than the Type A nozzle. This suggests that the reason why the shroud is

superior to the Type A nozzle is not that it entrains more solids, but that it entrains solids as far upstream as possible, so that they are accelerated to higher velocities, and therefore grind more effectively. This corresponds with what was observed in the shroud movies (Hulet et al., 2006), as a dense region of solids were formed close to the nozzle tip and were entrained into the jet near the high velocity region of the nozzle exit.

In addition, to eliminate the possibility that the difference in solids entrainment for each nozzle type was the result of an error in the measurement, an analysis of variance (ANOVA) was performed. There are two hypotheses that can be tested using ANOVA: the null hypothesis and the alternative hypothesis. The null hypothesis states that there is no difference in the means of the groups. The alternate hypothesis states that there are significant differences among the individual means. Sets of data comparing the solids entrainment for the Type C, Shrouded, and Type A nozzles at a gas flowrate of 0.01 kg/s, were analyzed. Each of these data points corresponds to an average value obtained from three repeated experiments. Table 4.1 summarizes the results of the analysis, which includes the average relative solids entrainment, the overall variance, the variance between groups and the variance within groups. The value for α was set to 0.05, which corresponds to a % 95 confidence interval in the results. The F value corresponds to the ratio of the variance between the groups to the variance within groups. If the F value is greater than the critical F value (F_{crit}), then the null hypothesis can be rejected, which indicates that there is a significant statistical difference in the mean values. As shown in Table 4.1, the F value is greater than the corresponding critical value, F_{crit} , and therefore it is possible to reject the null hypothesis, which indicates that there is a significant statistical difference in the mean values which is not attributed to measurement error. The p value represents the probability of falsely rejecting the null hypothesis. Traditionally if p is less than 0.05, it is assumed that the null hypothesis can be rejected. In this case the p value was significantly lower than 0.05, which indicates that the probability of falsely rejecting the null hypothesis is extremely small. Therefore, it can be concluded that there is a statistical difference in the average relative entrainment values for the three nozzle types which is not attributed to experimental error.

Table 4.1: ANOVA Results Comparing the Relative Solids Entrainment for the Type C, Shrouded and Type A Nozzles at a Gas Flowrate of 0.01 kg/s

	Group 1 Type C Nozzle	Group 2 Shroud	Group 3 Type A Nozzle
Average	1	1.52	2.31
Overall Variance	0.012	0.030	0.025
Variance Between Groups		1.31	
Variance Within Groups		0.022	
F		58.9	
F _{crit}		5.14	
p		0.0001	
α		0.05	

Figure 4.23 illustrates the importance of particle inertia and the significance of the axial location at which the particles are entrained into the jet. The velocity along the jet centre line was calculated for both the injected gas, and an entrained particle. Velocities were compared for cases when the particle entered the jet at various distances along the axis of the jet (x_0). As seen in Figure 4.23, particles which entered the jet close to the tip of the nozzle reached a higher maximum velocity than particles that entered the jet further downstream where the jet momentum was lower. For example, at an axial distance of 0.8 m the kinetic energy of a particle that was entrained into the jet 0.15 m downstream of the nozzle tip is 52% lower than the kinetic energy of a particle that was entrained at the nozzle tip. This explains why the shrouded nozzle had a higher grinding efficiency than the Type A nozzle. The shrouded nozzle increased the particle entrainment close to the nozzle tip where the jet momentum was higher, causing the particles to reach a higher maximum velocity, thus increasing the particle grinding efficiency.

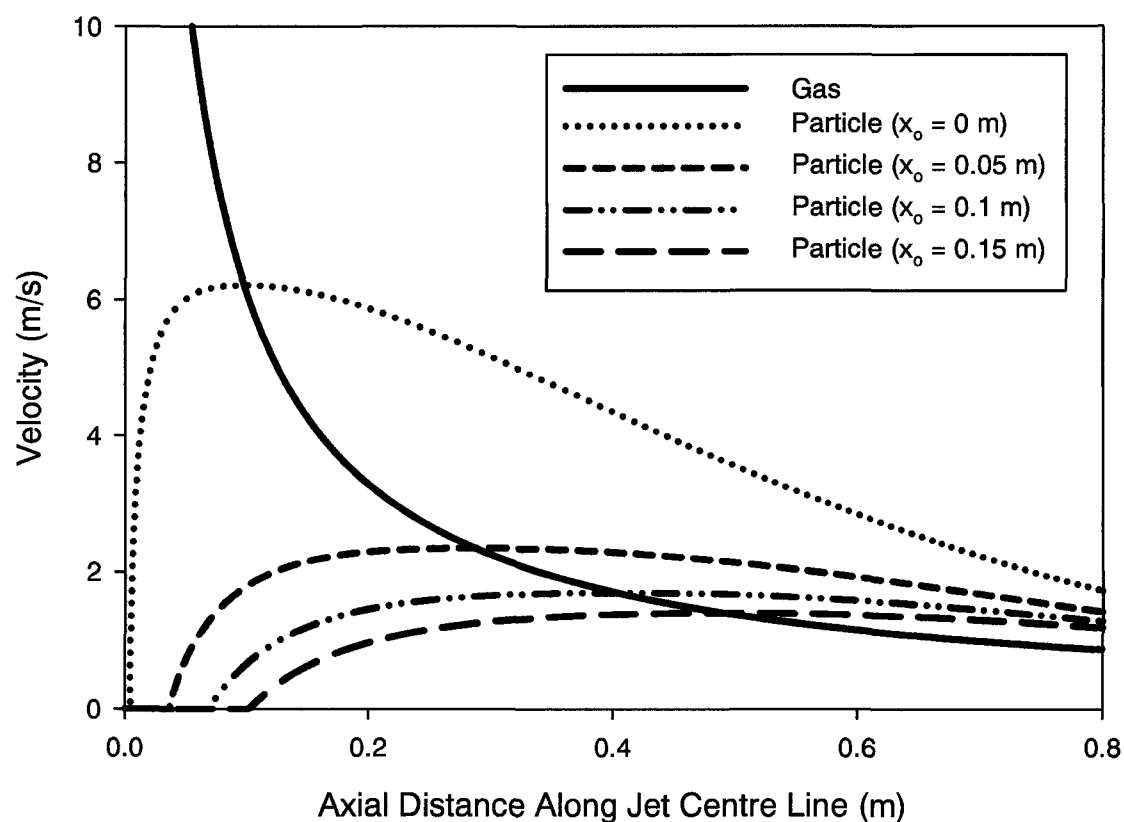


Figure 4.23: Effect of Particle Inertia and Entrainment Location on Velocity

4.4 Conclusion

A significant increase in the grinding efficiency was observed when either a target, draft tube, shroud, nozzle inserts, or spiral flow was used to enhance particle entrainment and mixing. The greater the number of high velocity particles entrained into the jet, the greater the number of collisions with the solids in the dense phase of the bed located at the tip of the jet, and the greater the attrition rate. Although the average solids entrainment into the jet was a significant factor contributing to the grinding efficiency for each nozzle type, other factors such as the mechanism of solids entrainment into the jet, and the location at which the solids were entrained played a significant role. The best grinding efficiencies were obtained when the shroud and draft tube were used in conjunction with each other. The best results, without the addition of internals to the bed,

were obtained with the Laval-type nozzle equipped with 3 nozzle inserts. However, the nozzle enhancements used in this study have yet to be optimized. The size and geometry of each nozzle design may be improved to increase the grinding efficiencies even further.

4.5 Acknowledgements

Thank you to the Natural Sciences and Engineering Research Council (NSERC) for Discovery Grants to Professors Cedric Briens and Franco Berruti, as well as a Collaborative Research Development Grant. Financial support from an NSERC Industrial Postgraduate Scholarship (IPS-2) is also greatly appreciated. Special thanks to the University Machine Services for their help with the experimental apparatus.

4.6 Nomenclature

D_S	Diameter of shroud (mm)
D_T	Diameter of draft tube (mm)
F_m	Particle breakage frequency (kg of particles broken/s)
L_S	Length of shroud (mm)
L_T	Length of draft tube (mm)
L_{Tip}	Distance from nozzle tip to base of shroud (mm)
ℓ	Distance from nozzle tip (mm)
x_o	Axial distance at which a particle enters the jet (m)

Greek Letters

β	Proportion of unground particles (%)
γ	Grinding symmetry coefficient (-)
η	Grinding efficiency (m^2/kg)

4.7 References

- Alpine, <<<http://www.hosokawa.co.uk/flash/afg.html>>>, (2006)
- Baddour, C., C. Briens, "Modeling the Grinding Process of Carbon Nanotubes", Submitted to *AIChE J.*, (2006).
- Benz, M., Herold, H., Ulfik, B., "Performance of a Fluidized Bed Jet Mill as a Function of Operating Parameters." *Int. J. Miner. Process.* **44-45**, 507-519 (1996).
- Berthiaux, H., Dodds, J., "Modelling Fine Grinding in a Fluidized Bed Opposed Jet Mill. Part I: Batch Grinding Kinetics", *Powder Technol.* **106**, 78-87 (1999a).

- Berthiaux, H., Chiron, C., Dodds, J., "Modelling Fine Grinding in a Fluidized Bed Opposed Jet Mill. Part II: Continuous Grinding Kinetics", *Powder Technol.* **106**, 88-97 (1999b).
- Chan, E., McDougall, S., Knapper, B., "Nozzle/Mixer Assembly", *United States Patent*: 7 025 874 (2004).
- Dunlop, D., Griffin, L., Moser, J., "Particle Size Control in Fluid Coking." *Chem. Eng. Prog.* **54**(8), 39-43 (1958).
- Felli, V., "Solids Entrainment From a Fluidized Bed into a Gas-Liquid Jet". *MESc Thesis*, The University of Western Ontario, (2002).
- Godet-Morand, L., Chamayou, A., Dodds, J., "Talc Grinding in an Opposed Air Jet Mill: Start-up, Product Quality and Production Rate Optimization", *Powder Technol.* **128**, 306– 313 (2002).
- Gommeren, H., Heitzmann, D., Kramer, H., Heiskanen, K., Scarlett, B., "Dynamic Modeling of a Closed Loop Jet Mill", *Int. J. Miner. Process.* **44-45**, 497-506 (1996).
- Henderson, K., Smith, L., Silva, P., "Throughput Efficiency Enhancement of Fluidized Bed Jet Mill", *United States Patent*: 5 562 253, (1996).
- Hulet, C., McMillan, J., Briens, C., Berruti, F., Chan, E., "Visualization of the Effect of a Shroud on Entrainment of Fluidized Solids into a Gas Jet", *Draft* (2006).
- McMillan, J., Briens, C., Berruti, F., "High Velocity Attrition Nozzles in Fluidized Beds", Submitted to *Powder Technol.*, (2006a).
- McMillan, J., Briens, C., Berruti, F., "Modeling the Particle Attrition Mechanism When a Sonic Gas Jet is Injected into a Fluidized Bed", Submitted to *Chem. Eng. Sci.*, (2006b).
- Siegel, H., Olson, J., "Impact Target for Fluid Energy Mills", *United States Patent*: 4 089 472, (1978).
- Smith, L., Mastalski, H., "Throughput Efficiency Enhancement of Fluidized Bed Jet Mill", *United States Patent*: 5 133 504, (1992).
- Tasirin, S., Geldart, D., "Experimental Investigation on Fluidized Bed Jet Grinding", *Powder Technol.* **105**, 337-341 (1999).
- Yates, J., Cobbinah, S., Cheesman, D., Jordan, S., "Particle Attrition in Fluidized Beds Containing Opposing Jets", *AIChE Symposium Series* **87**, n 281, 13-19 (1991).

CHAPTER 5

Characterization of the Contact Between Liquid Spray Droplets and Particles in a Fluidized Bed

Jennifer McMillan¹, David Zhou¹, Siva Ariyapadi¹, Cedric Briens¹, Franco Berruti¹,
Edward Chan²

*¹Department of Chemical and Biochemical Engineering
The University of Western Ontario
1151 Richmond Street
London, Ontario, Canada, N6A 5B9*

*²Synchrude Canada Ltd.
Edmonton Research Centre
9421-17 Avenue
Edmonton, Alberta, Canada T6N 1H4*

5.1 Introduction

The injection of gas-liquid jets into gas-solid fluidized beds is encountered in many petrochemical operations such as fluid coking, fluid catalytic cracking (FCC) and gas-phase polymerization reactions. In the fluid coking process, steam and bitumen are injected into a fluidized bed of hot coke particles. Uniform contact of the liquid droplets and entrained particles is essential for high yields. To prevent slow cracking and to avoid heat or mass transfer limitations, the bitumen must contact a large number of coke particles quickly and uniformly. Therefore, the greater the number of hot coke particles with which the liquid comes into contact and the better the dispersion of the liquid both on the surface and between the particles, the better the yield. Gray (1994) found that the ideal liquid-to-solid ratio (L/S) for the fluid coking process is below 0.1g/g, based on mass transfer limitations. House et al. (2004) considered the effect of heat transfer

limitations, which becomes limiting at reaction temperatures if the particles do not contact the liquid quickly enough for the reaction to proceed at an optimal rate, and found that the L/S should be as low as possible and preferably below approximately 0.06 to avoid the formation of stable agglomerates. Ariyapadi et al. (2003a), House et al. (2004) and Knapper et al. (2003) have all shown that currently in the fluid coking process, the bitumen is poorly distributed among the coke particles. As a result, more studies are required to improve the mixing between the liquid feed and the fluidized particles.

There have been several studies conducted that consider the interaction of evaporative liquid jets in fluidized beds. Leclerc et al. (2001a, 2001b) developed a method to characterize the contact between a vaporizing liquid and particles in a fluidized bed by measuring the vaporization rate of the injected liquid. They also proposed a new model to predict the formation of agglomerates when liquid droplets larger than bed particles were injected into a hot fluidized bed. More recently, Leclerc et al. (2004) developed a new experimental method that is based on quenching the bed and recovering the agglomerates. From the analysis of the liquid phase of these agglomerates the fraction of remaining liquid was determined.

The use of temperature measurements has been used in the past to investigate the injection of evaporative liquid jets into fluidized beds. Smith and Nienow (1982) used an X-ray technique to study evaporation of a solvent sprayed vertically into a fluidized bed. In addition, bed temperature profiles were measured by radially navigating thermocouples at vertical intervals along the bed. They detected low-temperature regions within the liquid jet in which the majority of evaporation was assumed to occur. Similarly, Shakhova and Minaev (1973) injected liquid horizontally into a fluidized bed granulator and studied the spray zone by taking temperature measurements in the cross-section of the jet at different axial locations. They determined that most of the evaporation of the solution occurs at the end of the injector. Zhu et al. (2000) also used a thermocouple measuring technique to determine the evaporation length of the vertical jet and found that variations in the solids concentration can shorten the evaporation length due to turbulent mixing and phase interactions. Bruhns and Werther (2004) experimentally studied the

mechanism of liquid injection into a fluidized bed by using local temperature measurements, suction probes, and capacitance probes to characterize the liquid injection. They used the information obtained by these three methods to model the mechanism of the injection. Wang and Zhu (2003) also developed a model for hydrodynamic mixing of evaporating spray jets in dilute gas-solids pipe flows and studied the effect of solids loading, inlet gas velocity, and spray mass. They acquired temperature measurements along the spray jet axis to obtain an averaged mixture temperature, which represented the phase-weighted temperature of all three phases. The measured temperature depended on the local heat balance of the thermocouple from the turbulent thermal convection, the heat transfer due to droplet collisions and evaporation, and the heat transfer due to the solids collisions. From the results, information regarding each phase of gas, solids and droplets was obtained. However, droplet evaporation is a key factor in the phase mixing and flow characteristics of these evaporating spray jets, and these methods cannot be adapted to applications with a non-vaporizing liquid.

Several studies have been done that explore horizontal injection of non-evaporative gas-liquid jets into fluidized beds. Ariyapadi et al. (2003b) used digital X-ray imaging to study the internal flow structure of liquid jets injected into fluidized beds and determined the jet expansion angle and penetration distance. In another study done by Ariyapadi et al. (2003a), a model to determine the entrainment rate of solids and gas into a gas-liquid jet injected into a fluidized bed of fine particles was developed. In addition, Felli (2002) developed and validated a technique to measure this entrainment rate. Gray (2002) determined that the key relationships that govern the behaviour of wet particles in coking processes are the Stokes number of the particles, the thickness of the liquid films, and the diameter and surface roughness of the particles. He concluded that to obtain a uniform thin film on the coke particles there must be an efficient mechanism for distributing the feed on a bed of coke after the feed has been injected, and that the feed contacts only a portion of the coke in the bed. Knapper et al. (2003) used copper naphthenate as a tracer for measuring the dispersion of liquid feed jet into a hot fluidized bed of coke. Although there were numerous particle-particle collisions in the fluidized bed, they found that the transfer of liquid feed among the particles was poor. However, at

lower L/S values it has been shown that heat transfer, as opposed to mass transfer, may be the limiting process (House et al., 2004).

In order to improve this transfer, Chan et al. (2006) have devised a draft tube mixer that is positioned co-axially downstream of an atomization nozzle and enhances the contact between the liquid spray droplets and the fluidized particles. Hulet et al. (2003) studied the entrainment and stability of a horizontal gas-liquid jet in a fluidized bed with a draft tube located downstream of the injection nozzle. They found that the optimal distance for entrainment occurred at a point when the liquid jet was touching the draft tube wall near its centre. House et al. (2004) proposed a model to illustrate the importance of the initial liquid-solid mixing on coker yields and developed an experimental technique to quantitatively determine the quality of the initial liquid-solid mixing. Tests were done using a conventional nozzle and a nozzle with a draft tube mounted co-axially downstream, similar to the one used by Hulet et al (2003). The use of the draft tube was shown to greatly improve the liquid-solid mixing by increasing the amount of wetted solids and creating a more uniform initial liquid-solid mixture.

Presently, there has not been a method developed to determine the local quality of solid-liquid mixing in a fluidized bed on a short time scale. The objective of this study is to develop a technique to determine the local, instantaneous quality of solid-liquid mixing when a gas-liquid spray jet is injected horizontally into a fluidized bed. The liquid-solid mixing when a conventional spray nozzle is injected into the bed is compared to the results obtained when a draft tube is located co-axially downstream of the spray nozzle. The effect of changing the distance between the draft tube and the spray nozzle is also investigated.

5.2 Experimental Setup

A unique technique was used to determine the local, instantaneous quality of solid-liquid mixing on a short time scale using cold liquid and thermocouples.

Experiments were conducted in a fluidized bed with a height of 3.2 m and a rectangular cross section of 1 m by 0.3 m, as shown in Figure 5.1. The bed was operated with 140 μm coke particles, which filled the bed to a height of 0.3 m. The bed was fluidized with air at a velocity of 4.6×10^{-2} m/s. Entrained particles were separated from

the gas stream by two cyclones in series and were returned to the fluidized bed by a dipleg.

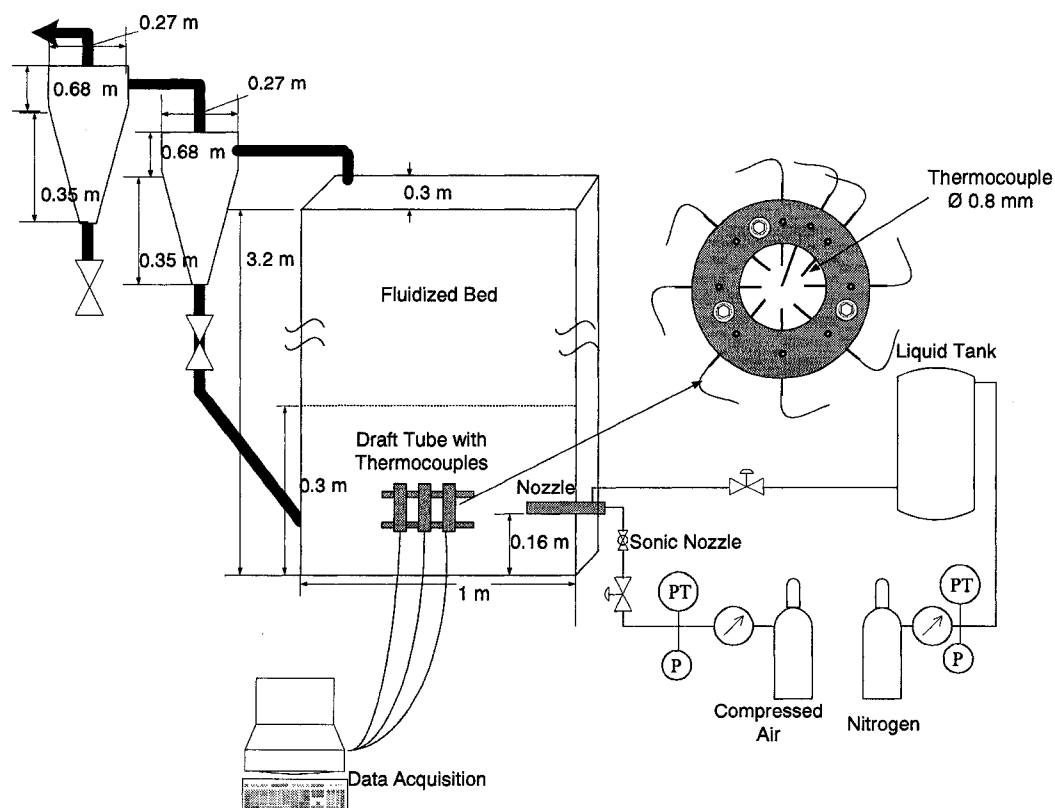


Figure 5.1: Experimental Set-Up

A gas-liquid nozzle was placed inside the bed at a distance of 1.6×10^{-1} m from the gas distributor, which injected a horizontal spray into the fluidized coke. The nozzle was a scaled-down model of a typical fluid coking nozzle, with an internal diameter of 2.4 mm as shown in Figure 5.2 (Base et al., 1999).

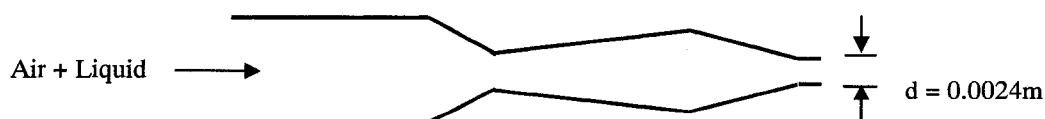


Figure 5.2: Injection Nozzle

A constant air mass flowrate from a high-pressure cylinder was supplied to the injection nozzle through a sonic nozzle in the upstream line. The liquid, ethanol, was supplied to the nozzle from a high-pressure tank. Adjusting the pressure of the liquid tank feeding the nozzle controlled the liquid flowrate to the nozzle. Ethanol was chosen as the injection liquid for two reasons. First, at room temperature, ethanol exhibits similar contact properties to bitumen at reaction temperatures. Second, ethanol evaporates relatively quickly and therefore, the time between successive experiments was reduced. The air and liquid flowrates were kept constant at 1 g/s and 67 g/s, respectively, resulting in an air-to-liquid ratio (ALR) of 1.5%. This air-to-liquid mass ratio was chosen in order to obtain the atomization quality and exit velocity that is similar to that of a commercial fluid coking nozzle.

The fluidized bed was pre-heated to 40°C by an immersion heater. The liquid, having a temperature of approximately -10°C, was then injected into the bed for 20 seconds. Fast response thermocouples with a diameter of 0.8 mm measured the local temperature. These thermocouples had a response-time (defined as the time it took the sensor to reach 63.2% of a step temperature change) of 20 ms in still water. Temperature signals were simultaneously recorded at a frequency of 2000 Hz.

Two sets of experiments were conducted. In the first set of experiments the spray was injected through a draft tube, which was mounted co-axially downstream of the spray nozzle. The draft tube had an internal diameter (d_i) of 1.9×10^{-2} m and a length (L) of 7×10^{-2} m. A special holder was used which allowed the distance from the draft tube to the exit of the nozzle (ℓ) to be easily varied, while ensuring that the centre of the nozzle was aligned with that of the draft tube (Figure 5.3).

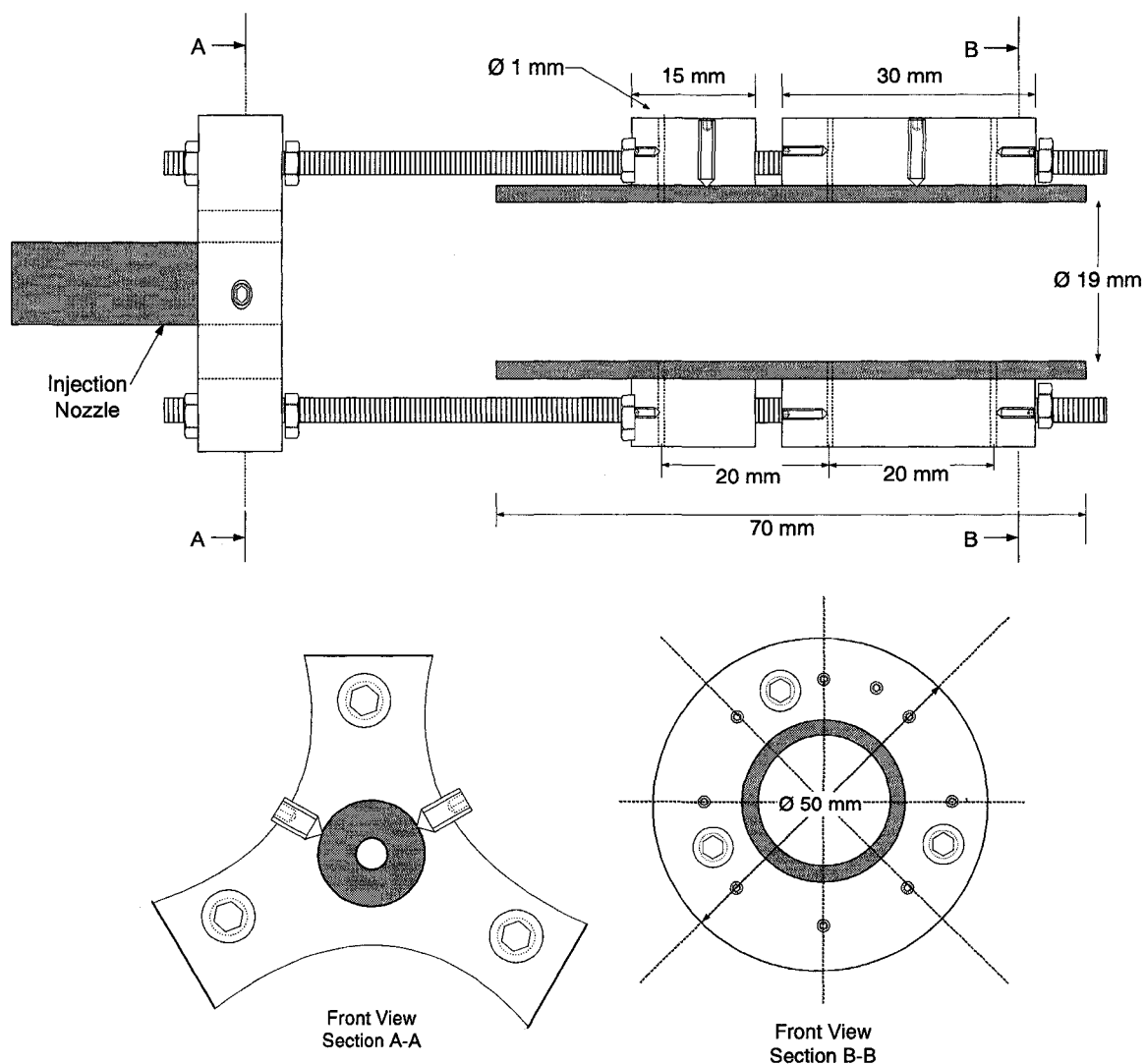


Figure 5.3: Holder Used to Align Draft Tube with Injection Nozzle and to Position Thermocouples Inside the Draft Tube

Distances ℓ of 12.7 mm, 25.4 mm, 38.1 mm, 50.8 mm, 63.5 mm and 76.2 mm were chosen for the experiments. The temperature was measured at 3 axial locations in the draft tube: A, B and C, which were spaced 20 mm from each other. Figure 5.4 shows the dimensions of the draft tube and the locations of A, B and C. A holder was placed around the draft tube that allowed the thermocouples to be inserted at 4 radial positions, 8 angular positions and one central location, resulting in a total of 33 temperature measurements at each axial location.

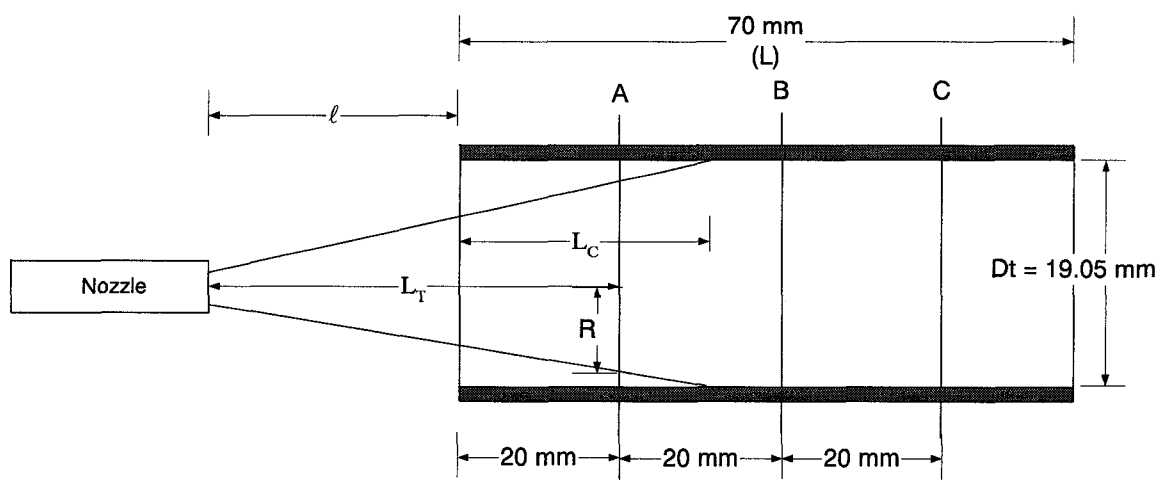


Figure 5.4: Dimensions of Draft Tube and Locations of Positions A, B and C.

In the second set of experiments the gas-liquid spray was injected into the fluidized bed as a free jet. Thermocouples were inserted into thin aluminum rings having an internal diameter of 70 mm. The rings were spaced so as to provide axial temperature measurements at the corresponding draft tube locations (L_T) of 32.7, 52.7, 72.7, 96.2, 116.2 and 136.2 mm.

5.2.1 Theory

When the cold liquid is injected into the fluidized bed of warm coke particles, the heat from the particles is transferred to the liquid. The liquid/solid distribution varies throughout the jet cross-section depending on the effectiveness of the mixing and the entrainment rate of solids into the liquid jet. In the case of perfect radial mixing, the temperature at each radial location should be equal. The mixing can be evaluated by obtaining the L/S, which is a function of the temperature, the specific heat capacity and the flowrate of the liquid and the solids. Using the time-averaged temperature, a heat balance can be performed on the mixture to obtain the liquid to solid ratio (L/S). Even if the gas surrounding the droplets becomes saturated with ethanol vapor, the resulting drop in liquid temperature would be well below 0.01°C , and, as a result, the effect of droplet

evaporation can be considered negligible. In addition, there would only be a 2°C drop in the temperature of the gas-liquid mixture due to the Joule-Thompson effect. Therefore:

$$F_L c_{p,L}(T_{Lin} - T) = F_S c_{p,S}(T - T_{Sin}) \quad (5.1)$$

and

$$\frac{L}{S} = \frac{c_{p,S}(T - T_{Sin})}{c_{p,L}(T_{Lin} - T)} \quad (5.2)$$

The information obtained from the temperature measurements provides the local ratio of liquid to solid flowrates. In order to effectively determine the quality of mixing, the local solids flowrate, or the local liquid flowrate within the liquid spray jet is required. A mixing model of a turbulent gas-liquid jet injected horizontally in a fluidized bed of coke particles, presented by Ariyapadi et al. (2005), was used to determine the local liquid flowrate and local solids flowrate within the liquid spray jet cross-section and, consequently, their ratio L/S.

The coefficient of variation was calculated at each location, L_T , for the experimental L/S values and the L/S values obtained with the mixing model.

$$C_v = \frac{\sqrt{\frac{1}{N} \sum_{j=1}^N \left(\left(\frac{L}{S} \right)_j - \frac{1}{N} \sum_{j=1}^N \left(\frac{L}{S} \right)_j \right)^2}}{\frac{1}{N} \sum_{j=1}^N \left(\frac{L}{S} \right)_j} \quad (5.3)$$

Despite some scattering, the model and the experimental data are well correlated, as shown in Figure 5.5. The mixing model does not predict as well for distances where the coefficients of variation are high and the mixing is poor. However, these cases are of little practical interest and only cases that produce good mixing results, are further examined and modeled. A simplified version of the above mentioned mixing model, which omits the effect of the draft tube, was used to estimate the local solids flowrate in the free jet. The local solids flowrate was obtained by adjusting the value of the model empirical parameter, the eddy diffusivity, in order to fit the local experimental (L/S)

obtained with the thermocouple measurements. The local liquid flowrate can, thus, be estimated from the product of the experimental L/S and the local solids flowrate given by the model.

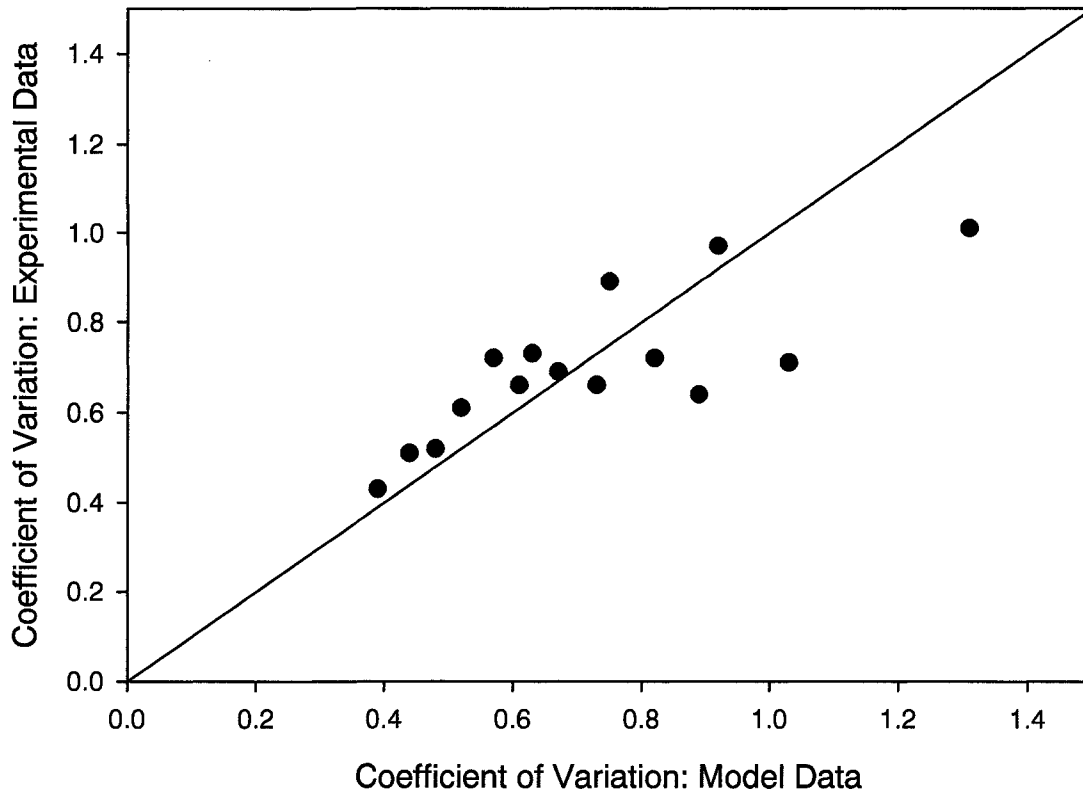


Figure 5.5: Comparison of the Coefficient of Variation Obtained with the Experimental Data and Model Data for Various L_T for the Draft Tube

5.3 Results and Discussion

Using the data obtained from the experiments, the quality of mixing in a free jet is compared to the quality of mixing when a draft tube mixer is introduced. The solid-liquid distribution depends on the distance from the nozzle to the draft tube (ℓ), the location in the draft tube where the jet impacts the wall (L_c) and the axial location in the draft tube. In order to compare the results, the mixing state at each location was defined by a mixing index that is based on the coefficient of variation of the L/S within the desired cross-section.

$$\text{Mixing Index} = 1 - \left[\frac{1 - e^{-0.25C_v}}{1 + e^{-0.25C_v}} \right] \quad (5.4)$$

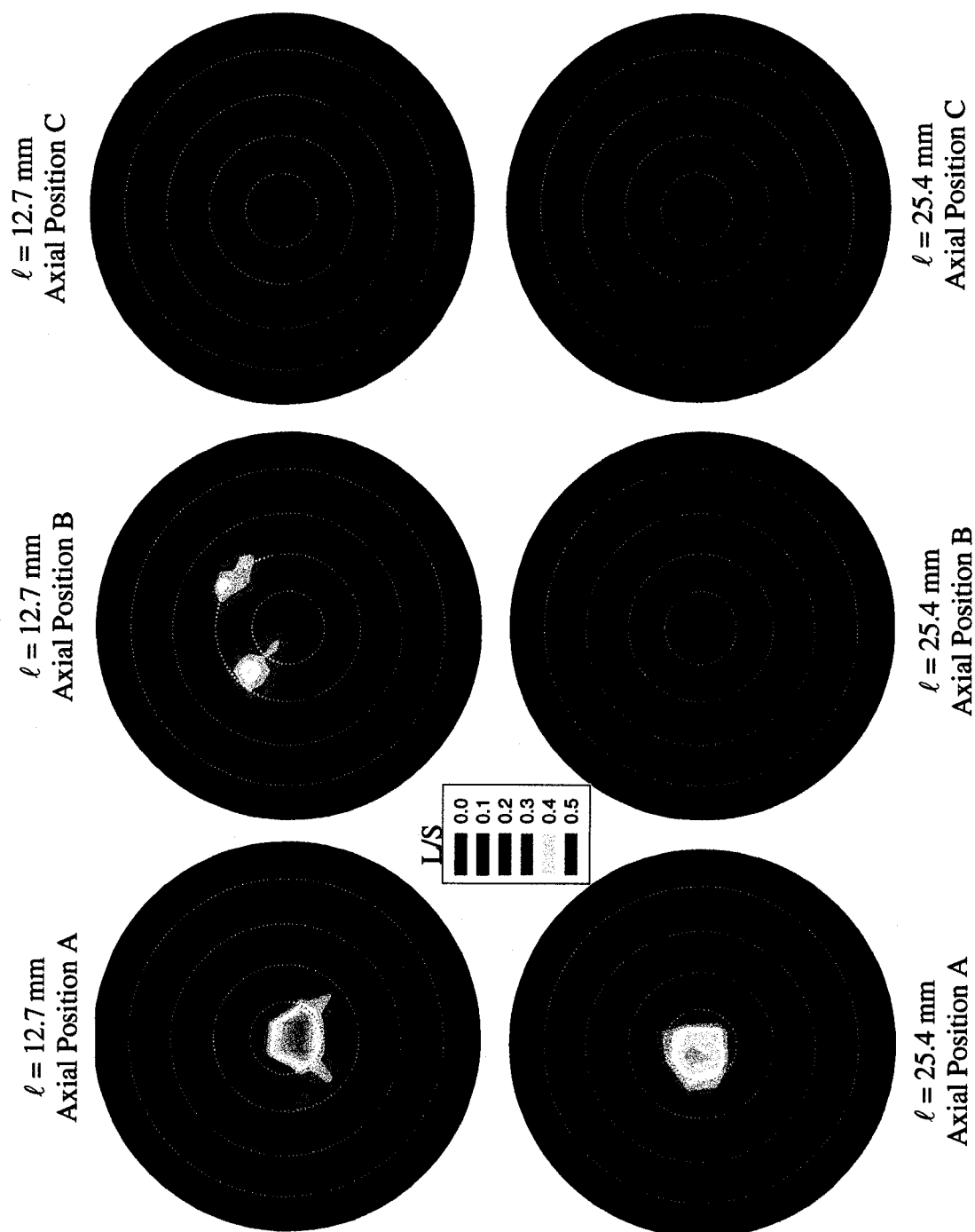
This equation was chosen since it provides enough definition in the range of mixing results obtained in this study. Table 5.1 summarizes the measurement locations and shows the mixing indices obtained. A high mixing index corresponds to a well mixed system, where a value of 1 indicates perfect mixing and 0 very poor mixing.

Table 5.1: Summary of Measurement Locations and Mixing Indices

ℓ (mm)	Position in Draft Tube	L_T (mm)	L_c (mm)	Mixing Index: Draft Tube	Mixing Index: Free Jet
12.7	A	32.7	42.5	0.88	0.82
12.7	B	52.7		0.91	0.84
12.7	C	72.7		0.92	0.85
25.4	A	45.4	30.5	0.87	
25.4	B	65.4		0.91	
25.4	C	85.4		0.92	
38.1	A	58.1	17.5	0.87	
38.1	B	78.1		0.91	
38.1	C	98.1		0.92	
5.08	A	70.8	4.5	0.88	
5.08	B	90.8		0.91	
5.08	C	110.8		0.92	

Contour plots of the liquid/solid distribution within the cross-sectional area of the jet spray were also created for each L_T . A computer program was used to generate additional points within the desired cross-sectional area. The L/S values for these points were determined using linear interpolation between the original 33 points.

Both the contour plots and the mixing indices were used to compare the mixing results in the draft tube for different distances. For the results obtained using the draft tube mixer, the dimensionless cross-sectional area of the contour plots corresponds to the diameter of the draft tube. Results for ℓ of 12.7, 25.4, 38.1 and 50.8 mm are shown in Figure 5.6. This figure shows the progression of mixing through the draft tube. For a distance of $\ell = 12.7$ mm, it can clearly be seen that the mixing improves along the length of the draft tube. The significance of the distance ℓ , can also be demonstrated in this figure. At $\ell = 25.4$ mm the mixing is nearly perfect at location C, whereas for the other distances, this is not the case. The mixing at location C starts to degrade beyond $\ell = 25.4$ mm. This could be explained by analyzing the location at which the jet impacts the draft tube wall. Hulet et al. (2003) found that the optimal distance, ℓ , occurs at a point where the jet impacts the draft tube wall 0.8 times into the length of the tube. In this study the jet contacts the draft tube wall 0.8 times into the length of the tube at a distance, $\ell = 25.4$ mm. The results observed in the contour plots agree well with the mixing indices. The mixing indices show that the quality of solid-liquid mixing increases as the axial distance in the draft tube is increased. At each ℓ , the mixing indices are the highest at location C, and the lowest at location A. The significance of ℓ can also be demonstrated from the mixing indices since the values for larger ℓ distances are higher than for lower ℓ distances. The effect of the jet interaction with the draft tube wall is particularly evident in the case when $\ell = 12.7$ mm. At location A, the L/S is very high and the liquid is not well distributed because the jet has not yet contacted the draft tube wall, and the spray behaves as a free jet. However, the jet comes into contact with the draft tube wall after location A, and the mixing at locations B and C improves significantly.



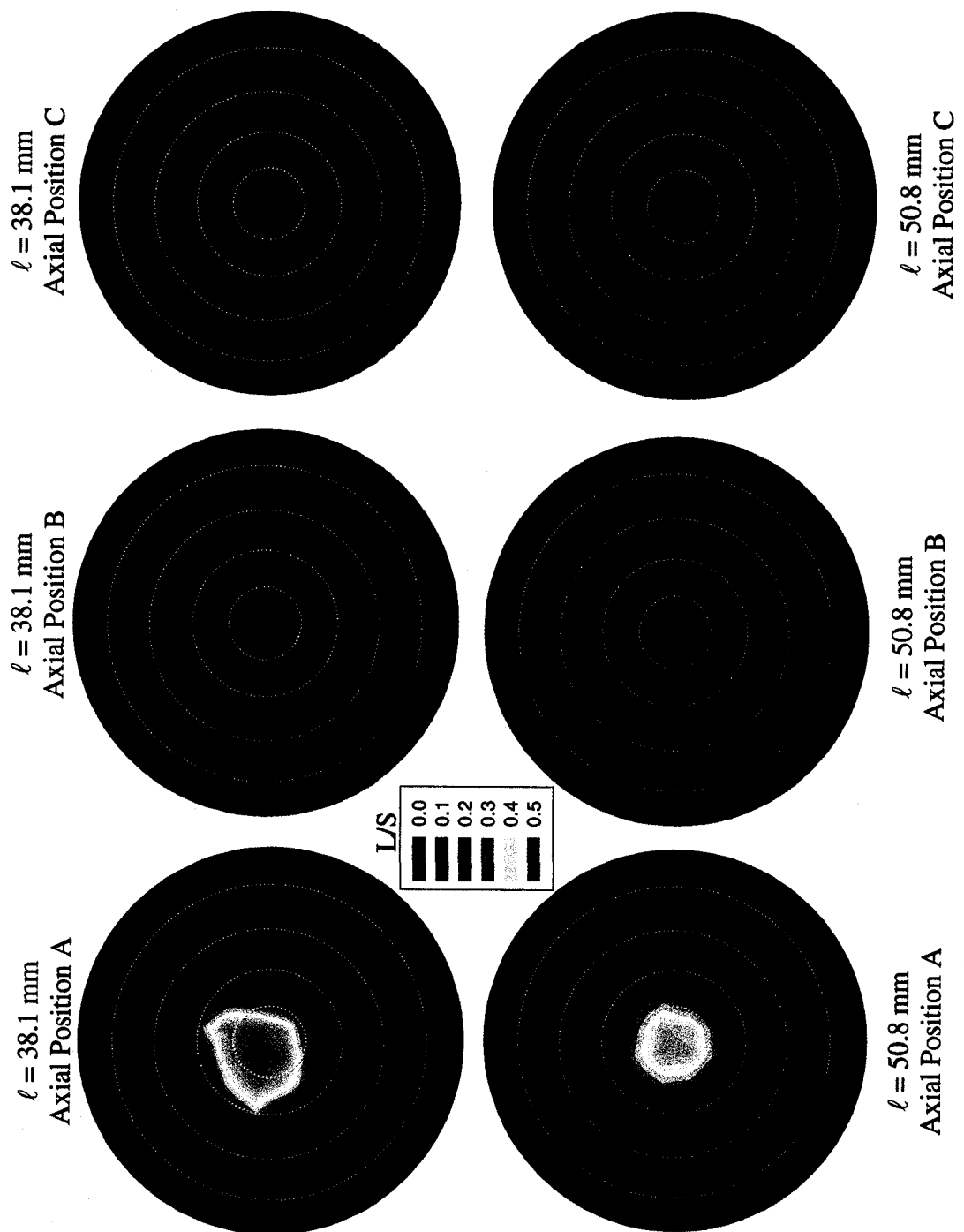
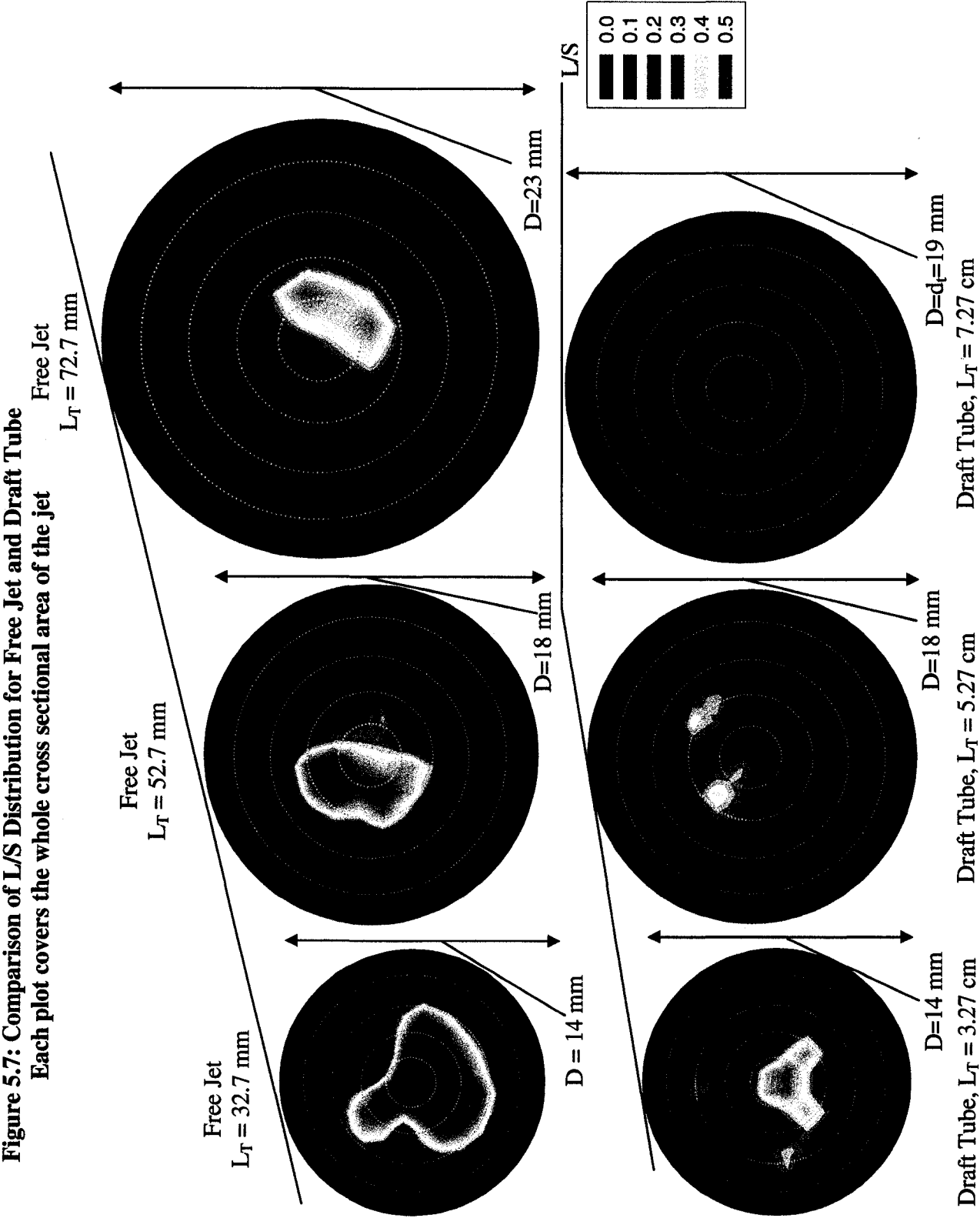


Figure 5.6: L/S Distribution at Locations A, B and C in the Draft Tube
Each plot covers the whole cross sectional area of the draft tube, $d_t = 1.9$ cm

In addition to studying the effect of ℓ on the liquid-solid mixing, the effect of using the draft tube mixer was compared to the results obtained in a free jet. For the results obtained in the free jet, the dimensionless cross-sectional area of the contour plots corresponds to the diameter of the liquid spray jet, which is calculated using a main jet expansion half angle of 6° and an initial jet expansion half angle of around 40° , which was based on the X-ray experiments performed by Ariyapadi et al. (2003b). However, in order to effectively compare the mixing in a free jet to the mixing in the draft tube, the results obtained from a draft tube were scaled accordingly to correspond to the dimensionless cross-sectional area of the liquid jet spray. Figure 5.7 shows a comparison of the contour results obtained with the free jet and the draft tube for L_T of 32.7, 52.7 and 72.7 mm. The size of each of the plots is representative of the area of the liquid spray jet. For a free jet at a distance of 32.7 mm the diameter of the spray is 14 mm, whereas at a distance of 72.7 mm the diameter of the spray is 23 mm. Both the contour plots and the mixing indices show that the liquid-solid mixing in the draft tube is superior to that obtained in the free jet. The mixing indices for the draft tube case are much higher than the results obtained with the free jet. The contour plots show that when a draft tube mixer is placed downstream of the nozzle, the L/S is more evenly distributed throughout the cross-section of the liquid jet radius, especially at location C. This is due to the fact that, as seen in Figure 5.7, the liquid spray hits the draft tube before location C. As a result, the diameter of this plot is the diameter of the draft tube as opposed to the 23 mm diameter of the liquid spray region that was used for the free jet result at the same distance from the nozzle.



Plots of the cumulative liquid distribution as a function of liquid to solid ratio (L/S) were also created in order to quantify the mixing, and its impact on the coking reaction. To achieve high yields of valuable products, it is important to minimize the amount of liquid which is exposed to a high liquid to solid ratio. The cumulative plot of the liquid distribution (e.g. Figure 5.8), should therefore be as vertical as possible indicating uniform mixing, and as much to the left as possible, indicating contact of the liquid with a large amount of solids. Figures 5.8 and 5.9 show the results for the case when a draft tube is used for ℓ of 12.7 mm and 25.4 mm, respectively. For both cases the liquid is more evenly distributed at location C than at location A.

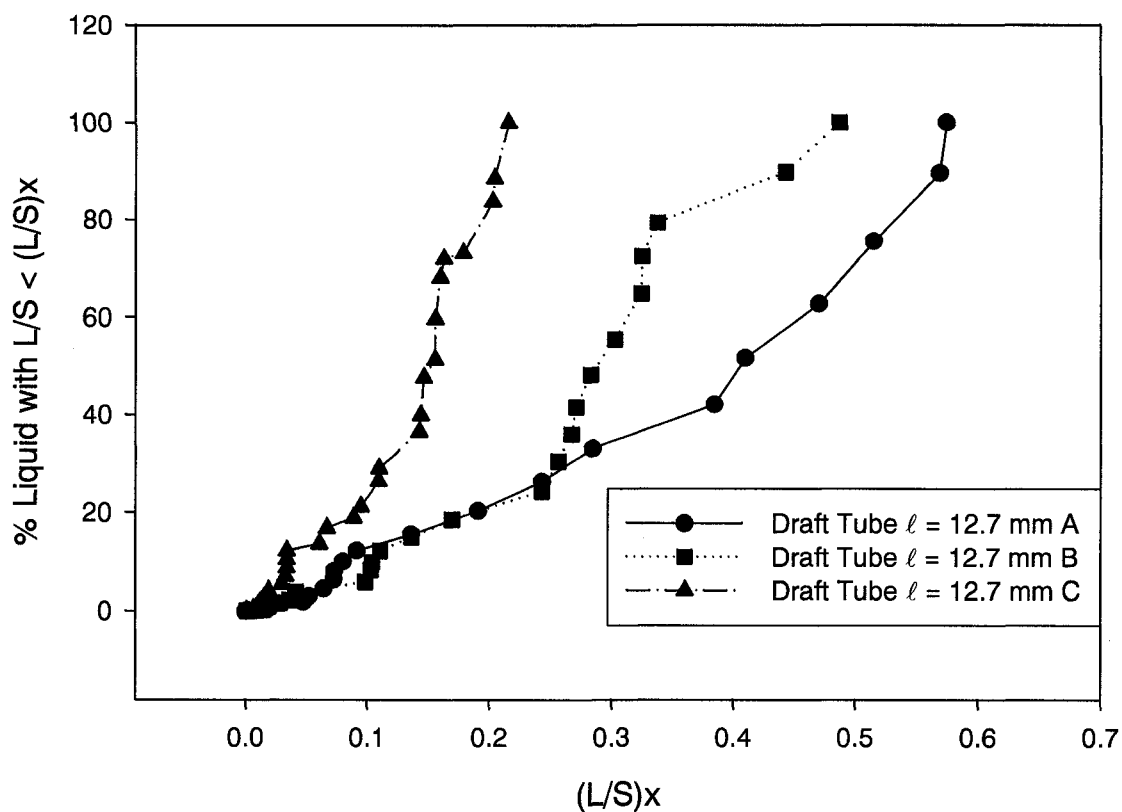


Figure 5.8: Cumulative Distribution of Liquid for Draft Tube $\ell = 12.7$ mm

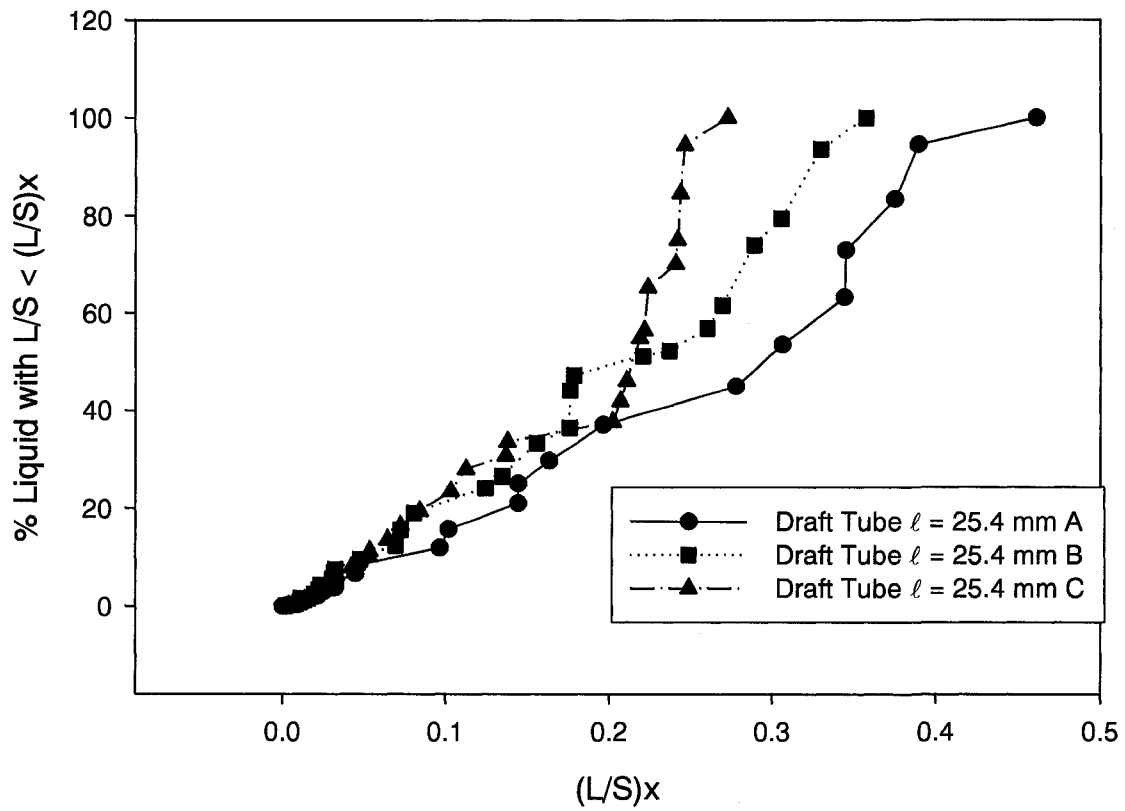


Figure 5.9: Cumulative Distribution of Liquid for Draft Tube $\ell = 25.4$ mm

Figures 5.10a, 5.10b and 5.10c compare the liquid distribution in the free jet and the draft tube for distances of 32.7, 52.7 and 72.7 mm, respectively.

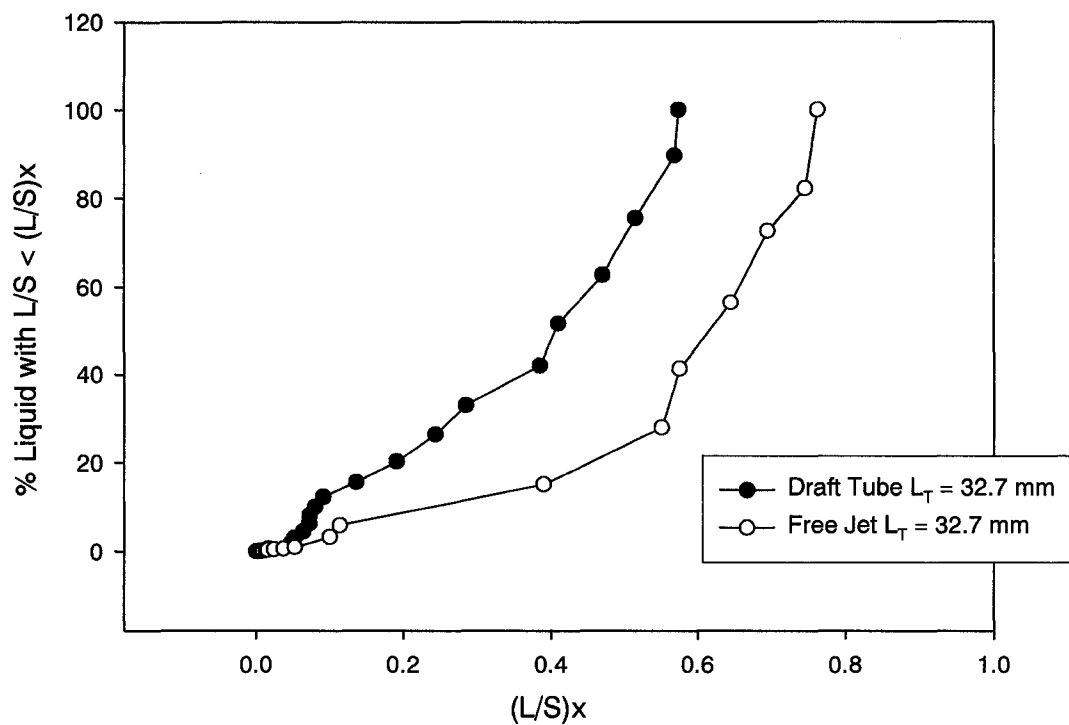


Figure 5.10a: Cumulative Distribution of Liquid for $L_T = 32.7$ mm

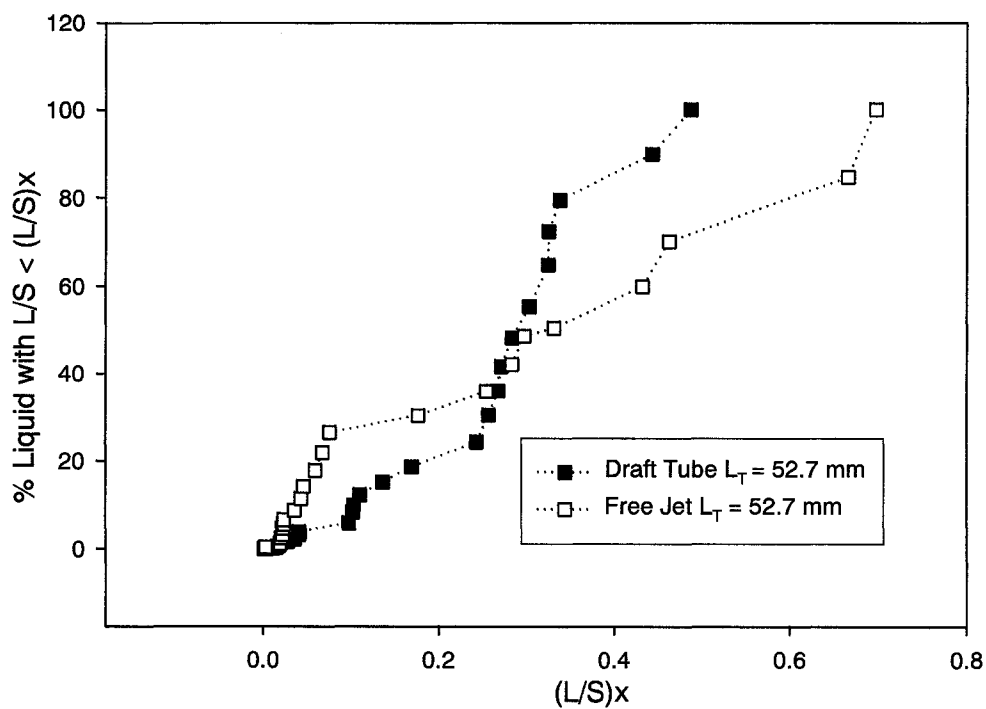


Figure 5.10b: Cumulative Distribution of Liquid for $L_T = 52.7$ mm

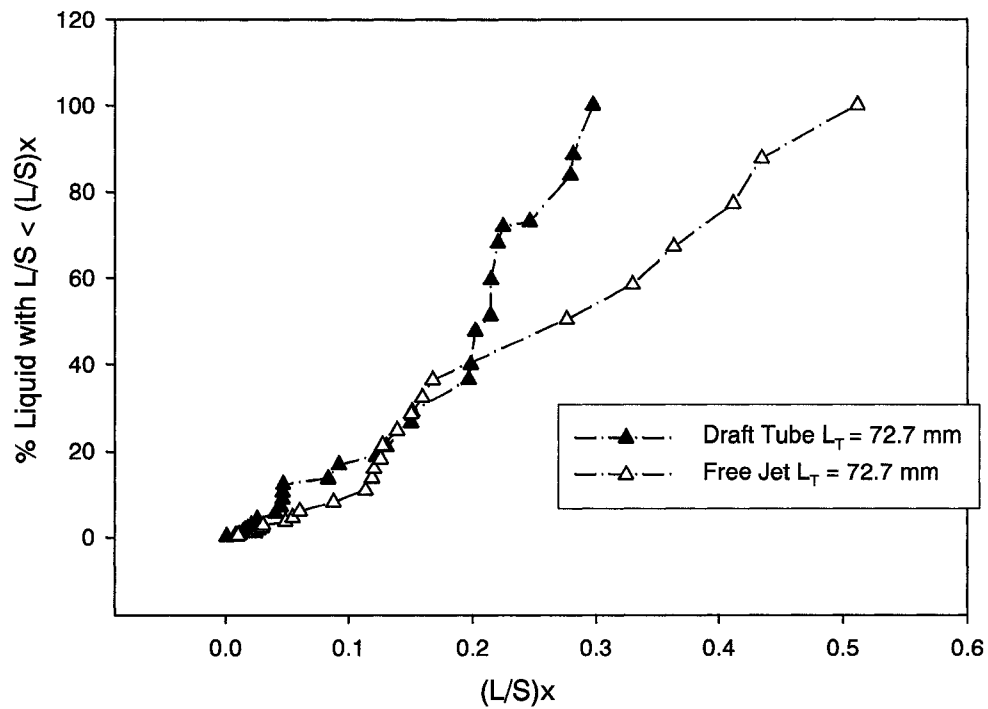


Figure 5.10c: Cumulative Distribution of Liquid for $L_T = 72.7$ mm

Figure 5.11 shows the cumulative liquid distribution obtained at location C for $\ell = 63.5$ mm for replicate experiments. The graph shows that the results are reproducible, as the liquid distribution is very similar for both cases.

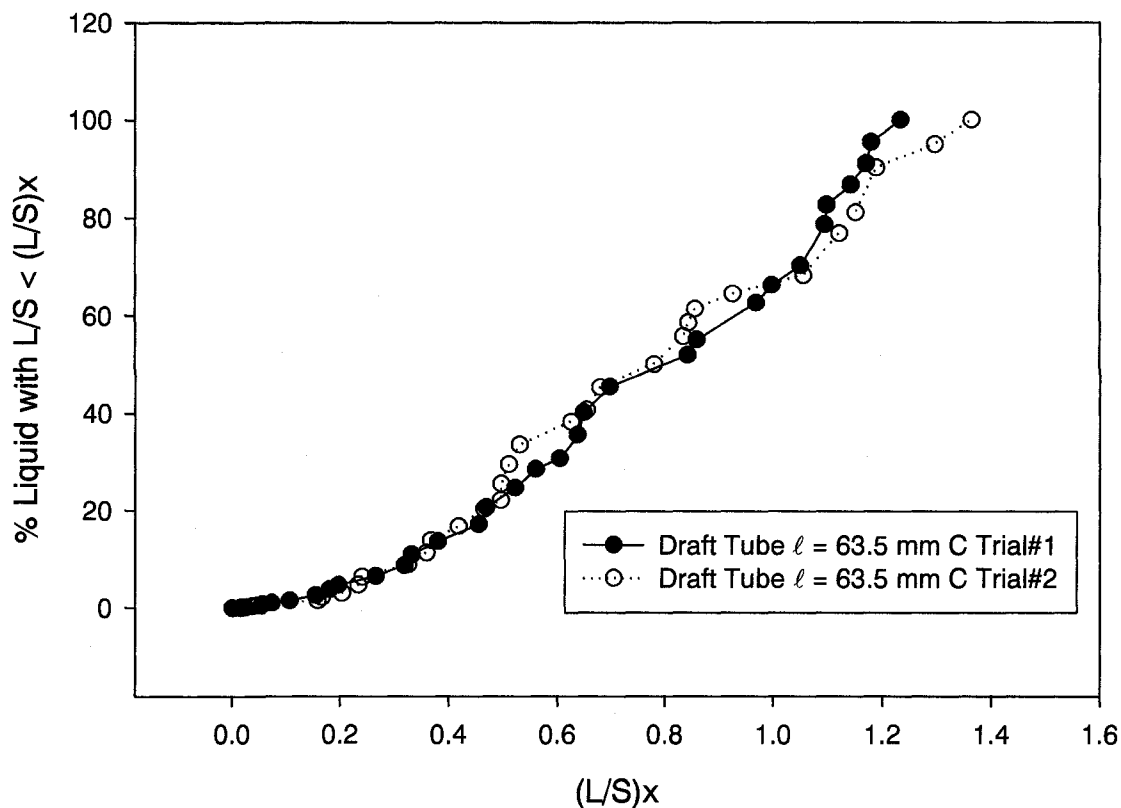


Figure 5.11: Reproducibility of Data: Cumulative Distribution of Liquid for Draft Tube $\ell = 63.5$ mm

For each distance, the liquid distribution is much more uniform when the draft tube mixer is used. Knapper et al. (2003) used the same sized feed nozzle as the one used in this study in a pilot plant fluid coker, under reacting conditions. They found that the average liquid to solid ratio (L/S) varied between 0.16 and 0.54. These values are comparable to the average L/S values using the measurement technique described in this paper. However, House et al. (2004) used a smaller scale nozzle and found the average L/S to be much lower than the L/S obtained from this study. This suggests that the nozzle scale could have a significant effect on the liquid-solid distribution, which was also confirmed by the model from Ariyapadi et al. (2005). A major advantage of the measurement technique developed in this paper is the fact that it can easily be applied to a commercial-scale nozzle, in order to verify the scale-up effects.

5.4 Conclusion

A measurement technique was developed to evaluate the solid-liquid mixing quality within the spray region of a liquid jet that was horizontally injected into a fluidized bed of particles. The technique is a convenient method to determine the liquid/solid distribution within the feed jet cavity. The mixing state was qualified by a mixing index that is based on the coefficient of variation of the ratio of the liquid flux to the solid flux within the desired cross-section. These mixing indices agree with the results observed in the contour plots of the liquid to solid ratio and in the cumulative distribution of the liquid on the particles. The results show that uniform and rapid contact between sprayed droplets and particles can be achieved by placing a horizontal draft tube downstream of the spray nozzle.

5.5 Acknowledgements

Financial support from Syncrude Canada Ltd. and the Ontario Graduate Scholarship Program is greatly appreciated. Thank you also to the Natural Sciences and Engineering Research Council (NSERC) for Discovery Grants to Professors Cedric Briens and Franco Berruti, as well as a Collaborative Research Development Grant. Special thanks to the University Machine Services for their help with the experimental apparatus.

5.6 Nomenclature

ALR	air-to-liquid ratio
$c_{p,L}$	specific heat capacity of liquid (kJ/kg°C)
$c_{p,S}$	specific heat capacity of solids (kJ/kg°C)
C_v	coefficient of variation (-)
d	diameter of nozzle (mm)
d_t	diameter of draft tube (m)
F_L	liquid mass flowrate (kg/s)
F_S	solids mass flowrate (kg/s)
ℓ	length from nozzle to draft tube (cm)
L	length of draft tube (cm)
L_C	location where jet contacts draft tube wall (cm)
L_T	distance from nozzle to location where measurements were taken (cm)
L/S	liquid to solid ratio (-)
N	number of data points within cross-section (-)
T	temperature of mixture (°C)

T_{Lin} initial temperature of liquid ($^{\circ}\text{C}$)
 T_{Sin} initial temperature of solids ($^{\circ}\text{C}$)

5.7 References

- Ariyapadi, S., Berruti, F., Briens, C., Griffith, P., Hulet, C., "Modeling the Injection of Gas-Liquid Jets into Fluidized Beds of Fine Particles", *Can. J. Chem. Eng.*, **81**, 891 – 899 (2003a).
- Ariyapadi, S., Holdsworth, D., Norley, C., Berruti, F., Briens, C., "Digital X-Ray Imaging Technique to Study the Horizontal Injection of Gas-Liquid Jets into Fluidized Beds", *Int. J. Chem. React. Eng.*, **1** (A56), 1114 (2003b).
- Ariyapadi, S., McMillan, J., Zhou, D., Berruti, F., Briens, C., Chan, E., "Modeling the Mixing of a Gas-Liquid Jet Injected into a Fluidized Bed: The Effect of a Draft Tube", *Chem. Eng. Sci.*, **60**, 5738 - 5750 (2005).
- Base, T., Chan, E., Kennett, R., Emberly, D., "Nozzle for Atomizing Liquid in Two Phase Flow", *United States Patent*: 6 003 789, (1999).
- Bruhns, S., Werther, J., "On the Mechanism of Liquid Injection into Fluidized Bed Reactors", *Fluidization XI*, U. Arena, R. Chirone, M. Miccio, P. Salatino, (Eds.) Engineering Conferences International, Brooklyn, NY: 2004, pp. 67 – 74.
- Chan, E., McDougall, S., Knapper, B., "Nozzle/Mixer Assembly", *United States Patent*: 7 025 874 (2004).
- Felli, V., "Solids Entrainment From a Fluidized Bed into a Gas-Liquid Jet". *MESc Thesis*, The University of Western Ontario, (2002).
- Gray, M., "Upgrading of Petroleum Residues and Heavy Oils", Marcel Dekker Inc., New York, NY, (1994).
- Gray, M., "Fundamentals of Bitumen Coking Processes Analogous to Granulations: A Critical Review", *Can. J. Chem. Eng.*, **80**, 393 – 401 (2002).
- House, P., Saberian, M., Briens, C., Berruti, F., Chan, E., "Injection of a Liquid Spray into a Fluidized Bed: Particle-Liquid Mixing and Impact on Fluid Coker Yields", *Ind. Eng. Chem. Res.*, **43**(18), 5663 – 5669 (2004).
- Hulet, C., Briens, C., Berruti, F., Chan, E., Ariyapadi, S., "Entrainment and Stability of a Horizontal Gas-Liquid jet in a Fluidized Bed", *Int. J. Chem. React. Eng.*, **1** (A60), 1127 (2003).

- Knapper, B., Gray, M., Chan, E., Mikula, R., "Measurement of Efficiency of Distribution of Liquid Feed in a Gas-Solid Fluidized Bed Reactor", *Int. J. Chem. React. Eng.*, **1**(A35), 1035 (2003).
- Leclere, K., Briens, C., Gauthier, T., Bergougnou, M., Bayle, J., Guigon, P., "Liquid Vaporization in a Fluidized Bed", *Ind. Eng. Chem. Res.*, **40**, 5415 - 5420 (2001a).
- Leclere, K., Briens, C., Gauthier, T., Bayle, J., Bergougnou, M., Guigon, P., "Experimental Study of Droplet Vaporization in a Fluidized Bed," *Can. J. Chem. Eng.*, **79**, 866 – 873 (2001b).
- Leclere, K., Briens, C., Gauthier, T., Bergougnou, M., Bayle, J., Guigon, P., "Experimental Measurement of Droplet Vaporization Kinetics in a Fluidized Bed", *Chem. Eng. Process.*, **43**, 693 – 699 (2004).
- Shakhova, N., Minaev, G., "Investigation of the Temperature Field in the Spray Zone of a Granulator with a Fluidized Bed", *Int. Chem. Eng.*, **13** (1), 65 - 68 (1973).
- Smith, P., Nienow, A., "On Atomising a Liquid Into a Gas Fluidized Bed", *Chem. Eng. Sci.*, **37** (6), 950-954 (1982).
- Wang, X., Zhu, C., "Concentric Evaporating Spray Jets in Dilute Gas-Solids Pipe Flows", *Powder Technol.*, **129**, 59 - 71 (2003).
- Zhu, C., Wang, X., Fan, L.-S., "Effect of Solids Concentration on Evaporative Liquid Jets in Gas-Solid Flows", *Powder Technol.*, **111**, 79 – 82 (2000).

CHAPTER 6

Measurement Techniques to Characterize the Contact Between Injected Liquid and Circulating Solids in a Downer Mixing Chamber

Jennifer McMillan, David Zhou, Mohammad Saberian,
Cedric Briens, Franco Berruti

*Department of Chemical and Biochemical Engineering
The University of Western Ontario
1151 Richmond Street
London, Ontario, Canada, N6A 5B9*

6.1 Introduction

Liquid injection into conventional and circulating gas-solid fluidized-bed reactors is encountered in many industrial applications such as fluid catalytic cracking and fluid coking. In such applications, the initial interaction of the liquid jet spray and the fluidized particles represents a crucial step in the process. In particular, the fluid coking and fluid catalytic cracking processes require uniform contact of the liquid droplets and particles in order to achieve efficient cracking and high yields. A poor initial distribution of the liquid feed on the particles can cause a thick liquid film to form on the solids surface, imposing a high resistance to mass and heat transfer, resulting in the formation of undesirable secondary products. To avoid slow cracking and prevent heat or mass transfer limitations, the feedstock must contact a large number of particles quickly and uniformly. Using a downer equipped with a mixing chamber located at its entrance may intensify this contact. This mixing chamber must ensure good initial contact between liquid and solids at the inlet to the downer.

Although spray nozzles are widely used to inject atomized feeds in industrial circulating fluidized bed reactors such as FCC risers, which could presumably be replaced by downers (Skouby, 1999; Chang et al., 2001; Gao et al., 2001; Gupta and Subba Rao, 2001; Tafreshi et al., 2002), they are not typically used in the published

Reprinted from *Powder Technology*, Vol 161, McMillan, J., Zhou, D., Saberian, M., Briens, C., Berruti, F., "Measurement Techniques to Characterize Contact Between Injected Liquid and Circulating Solids in a Downer Mixing Chamber", pp. 175 – 184, Copyright 2006, with permission from Elsevier.

studies of downer reactors. Therefore, it is important to evaluate the liquid-solid mixing in the downer reactor equipped with a nozzle injection system.

A previous investigation involved the injection of gas jets into down-flowing solid particles in a mixing chamber, very similar to the experimental set-up used in this study (Mirgain et al., 1998). Although their techniques provided direct, reliable results for the gas-solid system, the authors only measured the mixing between a gas jet and particles.

The majority of the work conducted to measure local solids flow and mixing patterns in circulating fluidized beds focuses on radiation absorption methods such as x-ray absorption tomography, and electrical capacitance methods (Wei et al., 1994; Soon et al., 1995; Schiewe et al., 1999; Hage and Werther, 2001). However, these techniques result in poor spatial resolution and long scan times, and cannot be easily adapted to a gas-liquid-solid system.

Temperature measurements have been widely used in circulating fluidized beds (White and Dry, 1991; Westphalen and Glicksman, 1995; Huilin et al., 2002; Wang and Zhu, 2003). In particular, Wang and Zhu (2003) developed a model for the hydrodynamic mixing between solids and evaporating spray jets in dilute gas-solids pipe flows and studied the effect of solids loading, inlet gas velocity, and spray mass. They acquired temperature measurements along the spray jet axis to obtain an averaged mixture temperature, from which information regarding each phase was obtained. However, temperature measurements have not been used to characterize the mixing between solids and non-evaporating liquids.

The use of tribo-electric probes to measure the flux of solids in a two-phase gas-solid flow has been employed in previous studies (Soo et al., 1964; Gajewski et al., 1993; Nieuwland et al., 1996). However, tribo-electric probes have not been used to measure the solids or liquid flux in gas-liquid-solid flows.

There have been several studies conducted that consider the interaction of evaporative liquid jets in gas-solid risers (Schuermans, 1980; Skouby, 1999; Liu, 2003). However, droplet evaporation is a key factor in the phase mixing and flow characteristics

of evaporating spray jets, and the same methods cannot be adapted to applications with a non-vaporizing liquid.

To date, there have been no studies done which investigate the injection of non-evaporative liquids into downer reactors equipped with a mixing chamber. The objective of this study was to develop a technique to determine the local, instantaneous quality of solid-liquid mixing when non-evaporative, gas-liquid spray jets are injected into a downer mixing chamber. The effects of using two different entrance configurations for the solids (a circular solids jet or an annular solids jet), and the geometry of the mixing chamber were examined using a mixing chamber equipped with either 4 or 8 injection nozzles.

6.2 Experimental Set-Up

A unique technique involving temperature measurements coupled with tribo-electric measurements was developed to characterize the initial contact between injected liquid and particles in a mixing chamber.

Experiments were conducted in a mixing chamber that was located at the entrance of a downer, as depicted in Figure 6.1. Coke particles with a Sauter mean diameter of 140 μm , which were stored in a silo, flowed down through an orifice plate into the mixing chamber before entering the 0.076 m diameter downer. An orifice plate was placed at the inlet of the mixing chamber in order to control and distribute the solids flow over the cross section.

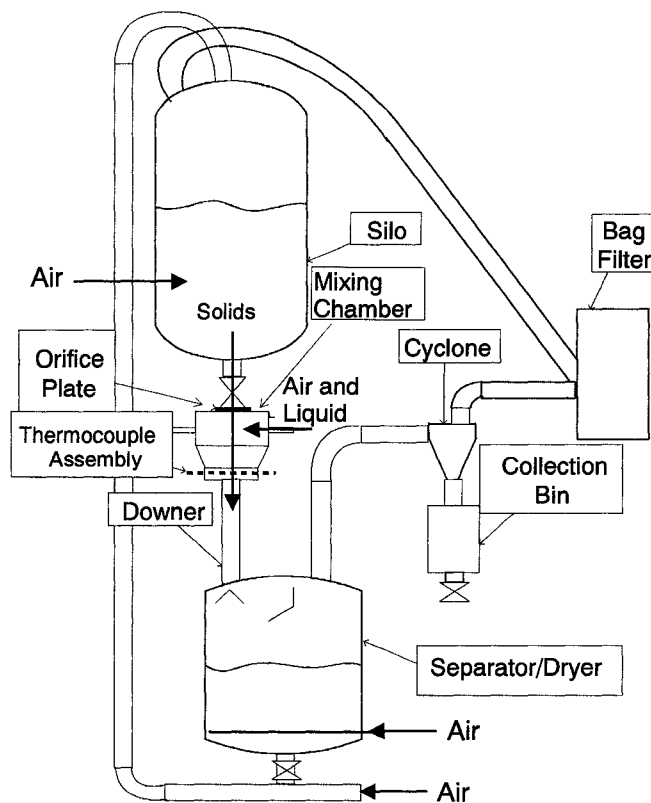


Figure 6.1 Experimental Apparatus

Two types of orifice plates were used in this study, which produced either a circular or an annular solids jet. The circular orifice plate had a diameter of 20 mm and the annular orifice consisted of 4 mm slots that had an outside diameter of 35 mm, as shown in Figure 6.2. In order to achieve the desired solids flowrate resulting in a liquid to solid ratio of approximately 5%, the silo was pressurized by delivering a constant flowrate of pressurization air. The solids flowrate when 4 injection nozzles were used was approximately 0.5 kg/s (110 kg/m²s) and 1 kg/s (220 kg/m²s) when 8 injection nozzles were used, to keep the solids to liquid ratio constant.

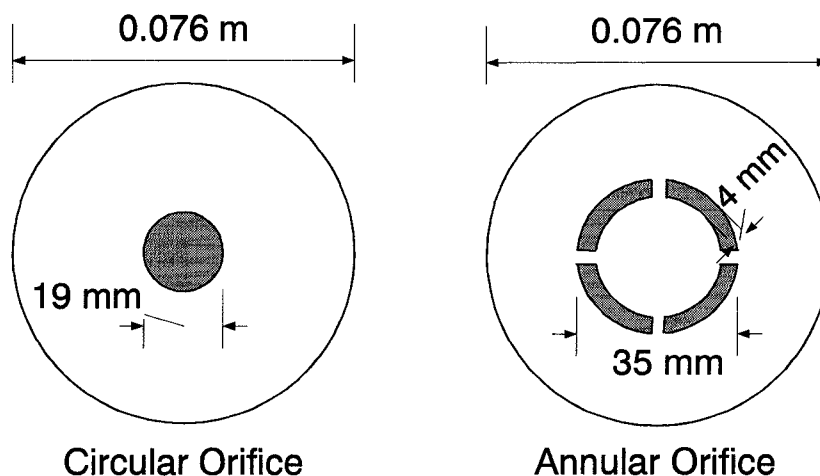


Figure 6.2: Orifice Dimensions

Liquid from two-phase spray nozzles was contacted with the down-flowing particles in a mixing chamber, which is shown in Figure 6.3. The mixing chamber consisted of a 0.145 m diameter cylindrical section followed by a conical section angled at 30° that led to the 0.076 m diameter downer. The mixing chamber used in this case was equipped with either 4 or 8 air-liquid injector nozzles. The injector nozzles could be oriented independently in both the horizontal and vertical planes. They could be angled in the horizontal plane to induce a swirl, and inclined to hit the solids jet near the top or bottom of the mixing chamber.

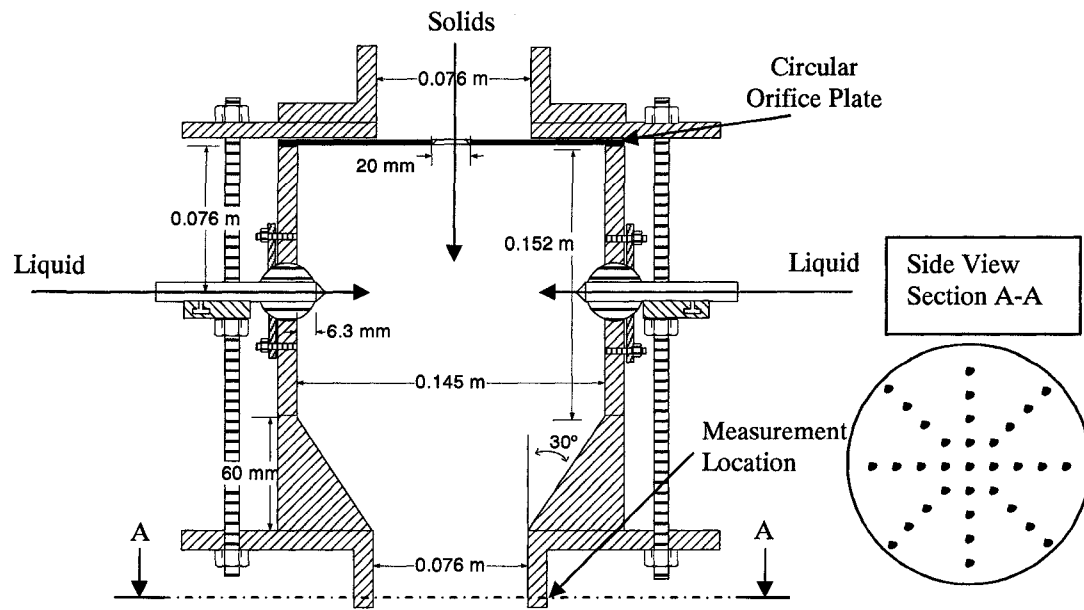


Figure 6.3: Mixing Chamber

Figure 6.4 depicts the geometry of spray nozzle that was used. The liquid was supplied to the nozzle through a centrally located hypodermic needle with an internal diameter of 1.5 mm, while the atomizing air flowed through an annular region. The liquid tube was offset by 2 mm towards the inside of the nozzle to allow for internal mixing of the two phases (Ariyapadi et al., 2003). Ethanol-water mixtures were used as liquid. A constant air mass flowrate from a high-pressure cylinder was supplied to each injection nozzle through a sonic nozzle located in the upstream line. The liquid was supplied to the nozzles from a tank pressurized by nitrogen in order to ensure uniform liquid flowrate to each injector nozzle. The air and liquid flowrates for each nozzle were kept constant at 0.43 g/s and 6.83 g/s, respectively, resulting in an average air-to-liquid ratio (ALR) of 5.9%.

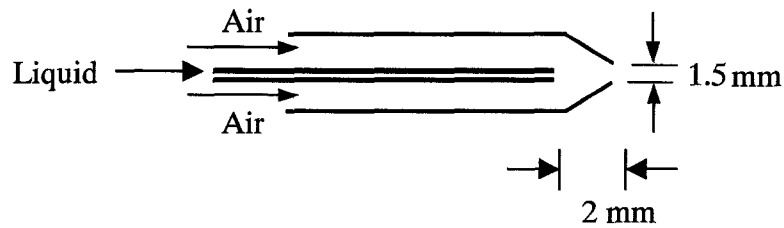


Figure 6.4: Spray Nozzle

The solid-liquid mixture flowed through the downer and entered a separator vessel where it was subsequently dried. A pneumatic line returned the dry solids to the silo.

6.2.1 Temperature Method

The first technique used temperature measurements to characterize the solid-liquid mixing. Cold ethanol at -10°C was injected into the mixing chamber and mixed with coke particles flowing at room temperature. An assembly of fast thermocouples located just below the exit of the mixing chamber provided temperature readings at 5 radial positions and 8 angular positions. The temperature signals were simultaneously recorded at a frequency of 1000 Hz for 60 s.

When the cold liquid is injected into the mixing chamber and is contacted with the warm coke particles, the heat from the particles is transferred to the liquid. In the case of perfect mixing, the temperature should be the same at each location in the downer cross-section. The mixing can be evaluated by obtaining the liquid to solid ratio (L/S), which is a function of the time-averaged values of the steady state temperatures, the specific heat capacities and the flowrates:

$$\frac{L}{S} = \frac{C_{p_s}(T - T_{sin})}{C_{p_L}(T_{Lin} - T)} \quad (6.1)$$

Even if the gas surrounding the droplets becomes saturated with ethanol vapour, the resulting drop in liquid temperature would be well below 0.01°C and, as a result, the effect of droplet evaporation is negligible and therefore not included in the energy

balance. In addition, there would only be a 2°C drop in the temperature of the gas-liquid mixture due to the Joule-Thompson effect and as a result, it also was not taken into consideration in the energy balance. In order to fully characterize the mixing quality, the local solids flowrate is also required.

6.2.2 *Tribo-Electric Method*

The second technique involved the use of tribo-electric probe measurements to determine the local solids flux in the downer cross-section. Friction between a flowing stream and a metal surface can cause the transfer of electrons between the two objects. If the metal surface is connected to the ground, a tribo-electric current is obtained. A metal probe inserted into a two or three-phase (gas-solid or gas-liquid-solid) flow will transfer an electrical current that is related to the local mass flux of particles hitting it (Soo et al., 1964). The probes used in this study were 0.185 m long, 2.5 mm diameter stainless steel rods. The probes were insulated with Teflon tubing so that only 2.5 mm of the tip of the probe was exposed and in direct contact with the liquid-solid mixture. The tribo-electric probes were inserted just below the exit of the mixing chamber and obtained data at the same 5 radial positions and 8 angular positions where the temperature measurements were recorded. The tribo-electric current generated by the friction of the particles and liquid on the metal probes was converted to voltage and amplified from 200nA input to 5V output. Data was obtained for 90s at a sampling frequency of 1000 Hz. The file was then cut to 20 000 points in order to eliminate the experimental start-up and shut-off times (the first 15 s and the last 55 s).

In order to determine the effect of the liquid on the tribo-electric signal, the concentration of water in the injected ethanol was varied. Three sets of data, containing 33 points within the cross section of the downer, were obtained for each mixing chamber nozzle configuration using ethanol with 0, 5 and 10 percent by weight of water. Since water has a much higher dielectric constant than ethanol (80.4 compared to 24.3), the mixture with the highest water concentration produced the strongest tribo-electric current. For a similar global solids flux the average of all of the tribo signals in the downer cross

section was 1.5 times the 0% water in ethanol case when 5 wt% water in ethanol was used, and 3 times the 0% water in ethanol case when 10 wt% water in ethanol was used.

Preliminary experiments by McMillan et al. (2005a) showed that injecting a liquid containing water greatly enhanced the tribo-electric current in proportion to the concentration of the water. However, injecting pure ethanol had a negligible effect on the triboelectric current. Therefore, data collected with pure ethanol were used to obtain the local solids flux at each of 33 locations in the downer for each nozzle configuration. There were several steps involved in obtaining the local liquid and solids fluxes in the downer cross-section. First, an equation was assumed which relates the solids flux, (W_s), to the tribo-electric current, (y):

$$y_i = \lambda W_{s,i}^\beta \quad (6.2)$$

A value for β was assumed, and then λ was determined by performing a mass balance on the solids, as shown in Equation (6.3).

$$\lambda = \left(\frac{\sum y_i^{1/\beta} \Delta A_i}{F_{S,\text{exp}}} \right)^\beta \quad (6.3)$$

where ΔA_i represents the incremental area in the radial direction, i.e. the cross-sectional area associated to the measurement location i .

Next, the local solids flowrate was determined for this cross-sectional area:

$$F_{S,i} = \left(\frac{y_i}{\lambda} \right)^{1/\beta} \Delta A_i \quad (6.4)$$

Then the global liquid flowrate was determined by using the experimental L/S values obtained with the temperature method.

$$F_{L,\text{calc}} = \sum F_{L,i} = \sum (L/S)_i F_{S,i} \quad (6.5)$$

The value of β was determined by minimizing the difference between the experimental and calculated liquid flowrates. The value of β was found to be about 1.1 for each configuration. The results from the present study thus agree well with findings from McMillan et al. (2005b) who obtained a value of about 1 for β . This yielded the following equation to obtain the local solids flux:

$$W_{s,i} = \left(\frac{y_i}{\lambda} \right)^{1/1.1} \quad (6.6)$$

Therefore, combining the results from the temperature measurements (Equation 6.1) with the triboelectric measurements performed with pure ethanol (Equation 6.6) provides the local liquid and solid fluxes. This combined temperature-tribo method provided accurate and reliable results.

In addition, a method was developed to obtain the local liquid flux that relied only on the use of the triboelectric measurements obtained with ethanol-water mixtures of various water concentrations. This method was verified by comparing the findings to the results obtained from the coupled temperature/tribo method. The moments, wavelet coefficients (using Daubechies 4), W statistics (Briens et al., 2003), V statistics (Peters, 1994), cycle times (Briens et al., 1997), and powers over specified frequency bands were calculated for the signals at each position in the downer, for each concentration of ethanol and, for all of the mixing chamber geometries. A multi-linear regression program was used to find a power law relationship between the local liquid flux and these signal characteristics for two of the best mixing chamber geometries (configurations #3 and #7) and the one poor mixing chamber geometry (configuration #13) (see Figure 6.6). The multi-linear regression program used data from 78 signal analysis values, from 3 different nozzle configurations each consisting of 33 points, and 3 different ethanol concentrations, and therefore over 20000 pieces of information were used to obtain the empirical expression. The multi-linear regression program determined which characteristics of the signal would best relate to the liquid flux, and the F statistic was applied to check whether the insignificant terms could be omitted from the equation.

The majority of the terms chosen by the multi-linear regression program were from the wavelet analysis. Wavelets are mathematical functions that divide the data into different frequency levels or octaves, and then each level is studied on a scale that matches its resolution. The number of levels depends on the size of the signal, and, in this case, 13 frequency levels have been used. The averages, μ , and the standard deviations, σ , of the wavelet coefficients were calculated at each frequency level. For example, one of the values used in the expression is the average of the wavelet coefficients at the 7th octave or level, and another one is the standard deviation of the wavelet coefficients at the 1st octave or level. These values provide information about the power and stationarity of the signal at certain frequency levels. Another signal property that was used to obtain the expression was the power spectrum. The complete power spectra over specific frequency ranges were extracted and the average values were obtained. For example, the average power of the signal at a frequency of 1.6 Hz was used in the expression. The third signal property that was used was the Wstatistic. The Wstatistic is related to wavelet analysis and its purpose is to characterize the relative amplitude of the small fluctuations of a signal. To obtain the Wstatistic, the raw signal was first smoothed to eliminate the small fluctuations. Then the small fluctuations component of the signal was recovered by subtracting the smoothed signal from the raw signal. Different compression ratios can be used when smoothing the signal in order to obtain the Wstatistic. For example, the average Wstatistic when a compression ratio of 99% is used in the expression.

The derived empirical expression was validated using data that had not been used for its derivation: the data from the remaining mixing chamber configuration (configuration #1). The cumulative distribution of liquid that was determined for this configuration from the triboelectric measurements with empirical expression was then compared to the cumulative liquid distribution calculated using the previous coupled temperature/tribo technique. Figure 6.5 shows that the two techniques provided similar results. Although the empirical expression is not a generalized expression and is not applicable to radically different mixing chamber designs (i.e. different scales or proportions), it has been shown to be reliable for the purpose of this study.

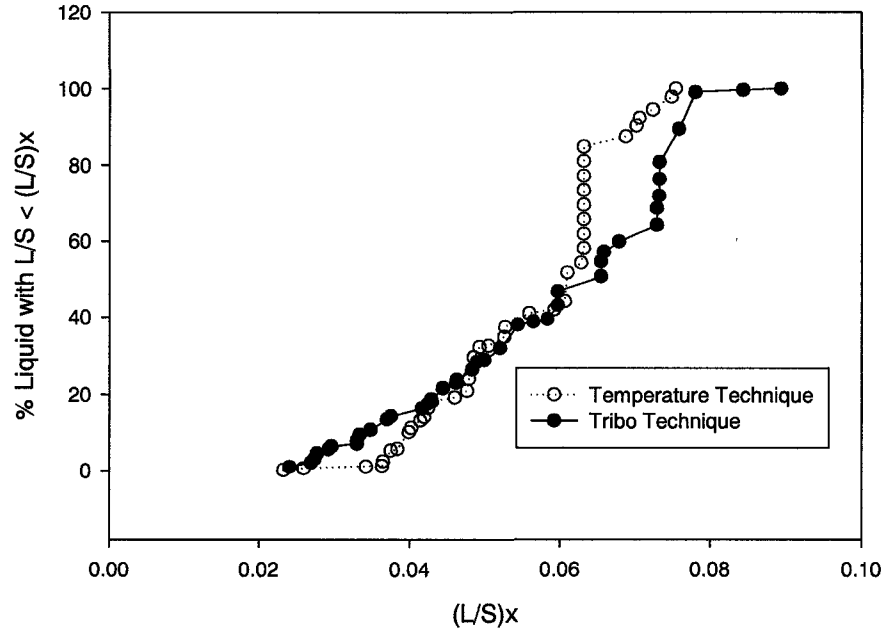


Figure 6.5: Cumulative Liquid Distribution for Configuration #1 – Comparison Between Temperature and Tribo-Electric Techniques

6.3 Results and Discussion

The solid-liquid distribution depends on the type of orifice, on the number of injection nozzles used and on their configuration. After performing many experiments, the best mixing configurations were narrowed down by a three-stage analysis process. First, in order to compare the results, the mixing state for each configuration was defined by a mixing index that was based on the coefficient of variation of the L/S within the desired cross-section, obtained with the temperature measurements, as shown in Equation 6.7.

$$\text{Mixing Index} = 100 \left[1 - \frac{\sqrt{\frac{1}{N} \sum_{i=1}^N \left(\frac{L}{S}, i - \frac{1}{N} \sum_{i=1}^N \frac{L}{S}, i \right)^2}}{\frac{1}{N} \sum_{i=1}^N \frac{L}{S}, i} \right] \quad (6.7)$$

A value of 100 indicates perfect mixing and 0 very poor mixing. Tables 6.1 and 6.2 show the results of the mixing indices for the 4-nozzle configurations and the 8-nozzle configurations, respectively. For the 4-nozzle configurations, using the circular orifice, the mixing indices ranged from 65.9 to 78.5. For the 4-nozzle configurations, using the annular orifice, the mixing indices ranged from 53.7 to 77.1. For the 8-nozzle configurations the mixing indices ranged from 69.5 to 86.3, when the circular orifice was used.

Table 6.1: Mixing Indices for 4-Nozzle Configurations

Configuration #	Mixing Index	
	Circular Orifice	Annular Orifice
1	78.5	77.1
3	76.4	74.9
7	75.7	67.8
12	71.0	54.9
11	65.9	53.7
13	45.5	49.7

Table 6.2: Mixing Indices for 8-Nozzle Configurations

Configuration #	Mixing Index for Circular Orifice
14	86.3
16	80.6
1	80.4
3	76.7
15	72.7
7	69.5

In addition, in the second stage of the analysis, contour plots of the liquid/solid distribution within the cross-sectional area of the downer were created for the nozzle configurations that showed the best mixing results based on the mixing indices, using linear interpolation between the original 33 points obtained using the temperature technique. Figure 6.6 shows the vertical and lateral views of the nozzle configurations and the corresponding contour plots for both the annular and circular orifice plates when 4 nozzles were used, with the diameter of the plots corresponding to the diameter of the downer.

Figure 6.7 shows the results when the circular orifice was used for the six 8-nozzle configurations. The results from both the contour and mixing indices indicate that the mixing is better with the circular orifice. Also, both the mixing indices and the contour plots show that the mixing when 8 nozzles are used is better than when 4 injection nozzles are used.

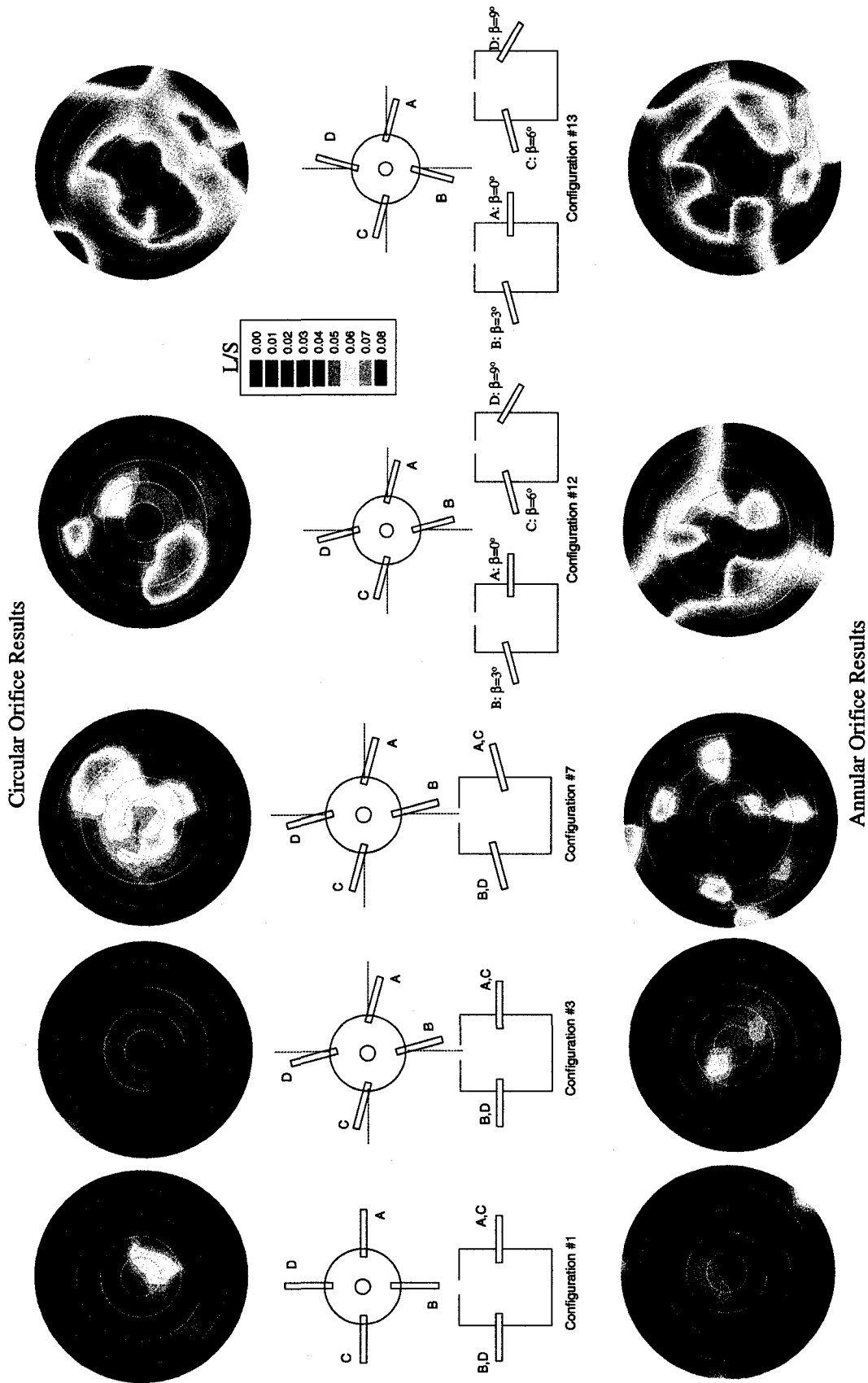


Figure 6.6: Contour Plots for 4-Nozzle Configurations

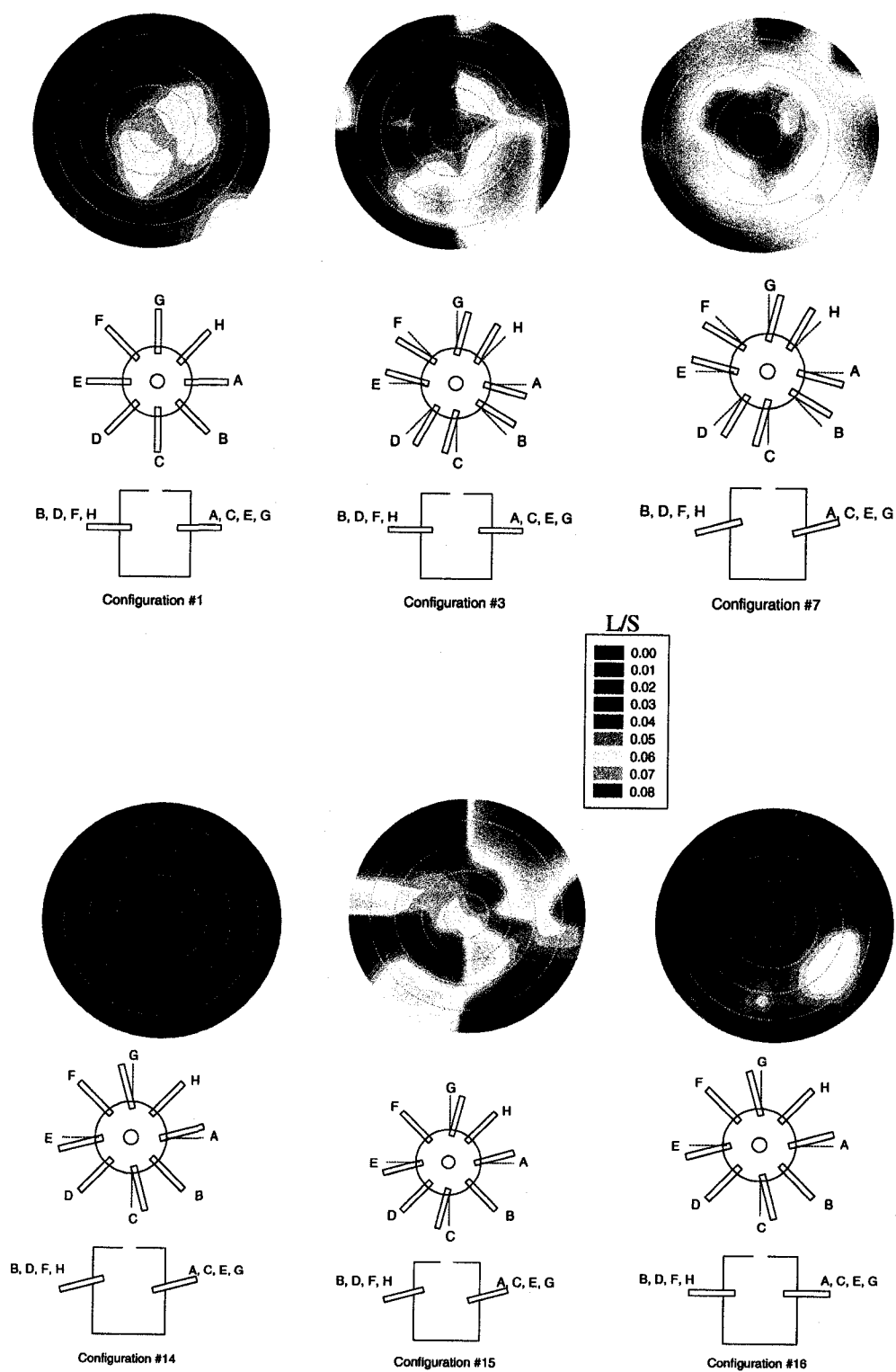


Figure 6.7: Contour Plots of 8-Nozzle Configurations

Finally, for the third stage, plots of the cumulative liquid distribution as a function of liquid to solid ratio (L/S) were also created in order to quantify the mixing. House et al. (2004) showed that such cumulative distribution could be used to quantify the impact of solid-liquid mixing on the coking reaction of bitumen in fluid cokers. To achieve high yields of valuable products, it is important to minimize the amount of liquid that is exposed to a high liquid to solid ratio. The cumulative plot of the liquid distribution should therefore be as vertical as possible indicating uniform mixing, and as much to the left as possible, indicating contact of the liquid with a large amount of solids. The values of the local fluxes used in these plots were obtained using Equation 6.6. Figures 6.8 and 6.9 show the results for the best cases for the 4-nozzle and 8-nozzle configurations, respectively.

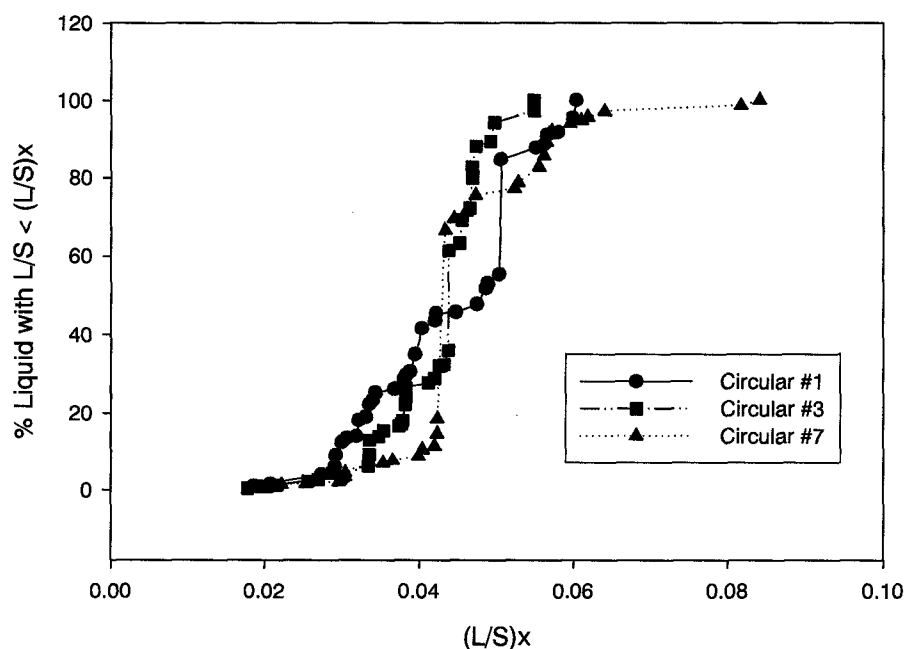


Figure 6.8: Cumulative Plots for 4-Nozzle Configurations Using the Circular Orifice Plate

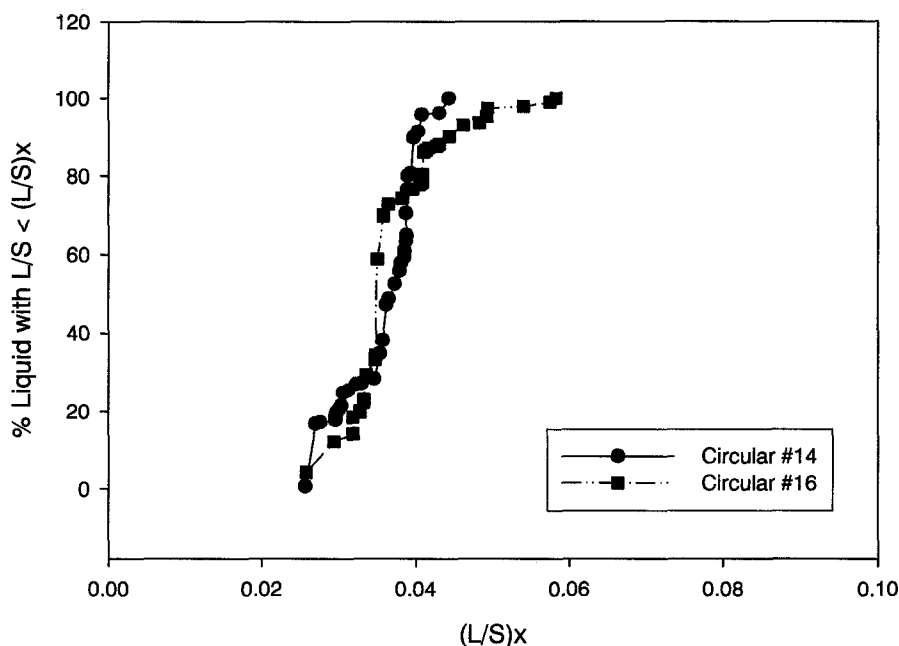


Figure 6.9: Cumulative Liquid Distribution for 8-Nozzle Configurations Using the Circular Orifice Plate

As shown in Figure 6.9, the solid liquid mixing for configuration #14 is more uniform than for configuration #16 since the line is more vertical. This agrees with what is shown in the contour plots, as there are more light green and blue regions in the contour plot for configuration #14, indicating that more liquid is in contact with a high concentration of solids.

The tribo-electric method using various concentrations of water in ethanol, as outlined above, was developed using three excellent mixing chamber geometries and one poor geometry, based on the above criteria. For simplicity sake, mixing chamber geometries were chosen for the cases where four injection nozzles were used. Configurations #1, 3 and 7 were chosen since they exhibited excellent mixing, and configuration #13 was chosen to demonstrate poor mixing conditions. Contour plots of the liquid/solid distribution within the cross-sectional area of the downer, based on the solid and liquid fluxes obtained using triboelectric measurements and the derived empirical expression, were created using linear interpolation among the 33 measurement points and are shown in Figure 6.10.

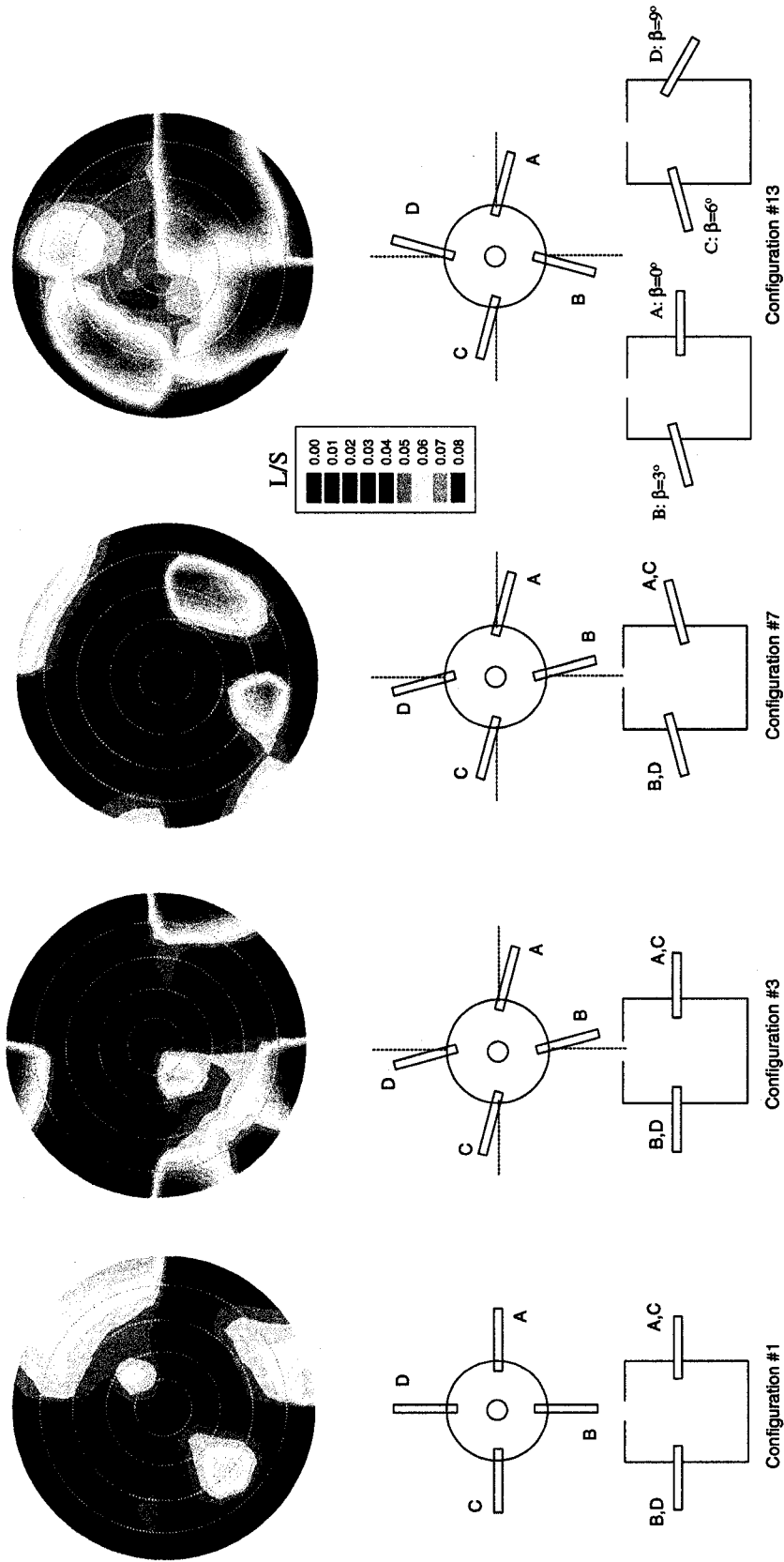


Figure 6.10: Contour Plots for 4-Nozzle Configurations Using Tribo-Electric Measurements

These results are slightly different from the results obtained using the temperature measurements seen in Figure 6.6. Although, the local L/S values seem to have shifted between the experiments conducted to obtain Figures 6.6 and 6.10, their spread is similar as confirmed by the cumulative distributions shown in Figure 6.5. These results suggest that local L/S values might shift with small changes in start-up conditions, and the stability of the system needs to be investigated further.

Plots of the cumulative liquid distribution as a function of liquid to solid ratio (L/S) were also created using the results obtained from the empirical expression. Figure 6.11 shows the results obtained for the 4 mixing chamber geometries tested. Solid-liquid mixing is better for configurations #1, #3 and #7 than for configuration #13, since the lines are more vertical. This agrees with what is shown in the contour plots, as there are more light green and blue regions in the contour plots for configurations #1, #3 and #7, indicating that a large proportion of the liquid comes in good contact with the solids. These results also agree with the results obtained with the temperature technique.

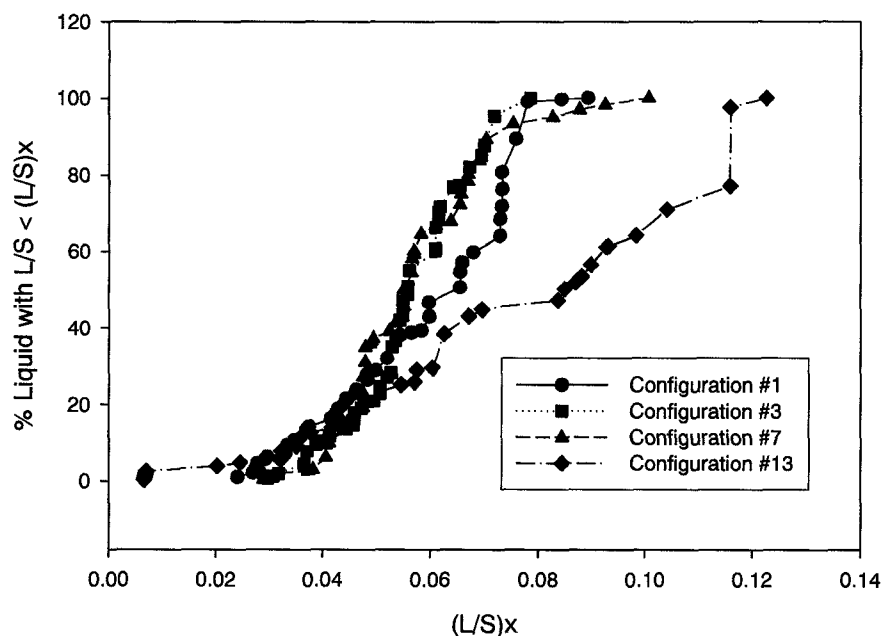


Figure 6.11: Cumulative Distribution Plots for 4-Nozzle Configurations Using Tribo-Electric Method

6.4 Conclusion

Measurement techniques were developed to evaluate the solid-liquid mixing quality within the cross sectional area of a downer when a mixing chamber was located at its entrance and liquid injected into down-flowing particles. The first technique used both temperature and tribo-electric measurements to determine the liquid/solid distribution within the downer. The second technique used only triboelectric signals obtained from liquids with varying concentrations of water to determine the liquid/solid distribution within the downer. The mixing state was qualified by a mixing index that is based on the coefficient of variation of the ratio of the liquid flux to the solid flux within the desired cross-section. These mixing indices agreed with the results observed in the contour plots of the liquid to solid ratio and in the cumulative distribution of the liquid on the particles. The results obtained using both techniques were comparable and indicated that certain mixing chamber geometries provided very good and rapid contact between sprayed droplets and particles.

A circular orifice provides better liquid-solid mixing than an annular orifice. Simple mixing chamber geometries where the spray jets impacted with each other near the axis of the mixing chamber provided the best mixing results when 4-nozzle mixing chambers were used. However, mixing chambers equipped with 8 nozzles, oriented in such a way that a swirling motion was created within the mixing chamber, were found to produce the best liquid/solid mixing results.

6.5 Acknowledgements

Financial support from Syncrude Canada Ltd. and the Ontario Graduate Scholarship Program is greatly appreciated. Thank you also to the Natural Sciences and Engineering Research Council (NSERC) for Discovery Grants to Professors Cedric Briens and Franco Berruti, as well as a Collaborative Research Development Grant. Special thanks to the University Machine Services for their help with the experimental apparatus.

6.6 Nomenclature

ALR air-to-liquid ratio
 C_{pL} specific heat capacity of liquid (kJ/kg°C)
 C_{pS} specific heat capacity of solids (kJ/kg°C)

ΔA_i	area (m^2)
F_L	liquid mass flowrate (kg/s)
$F_{L,\text{exp}}$	global experimental liquid mass flowrate (kg/s)
F_S	solids mass flowrate (kg/s)
$F_{S,\text{exp}}$	global experimental solids mass flowrate (kg/s)
L/S	liquid to solid ratio (-)
N	number of data points within cross-section (-)
T	temperature of mixture ($^{\circ}\text{C}$)
T_{Lin}	initial temperature of liquid ($^{\circ}\text{C}$)
T_{Sin}	initial temperature of solids ($^{\circ}\text{C}$)
W_L	liquid mass flux ($\text{kg/m}^2\text{s}$)
W_S	solids mass flux ($\text{kg/m}^2\text{s}$)
W_{stat}	W statistic
y	tribo-electric signal (V)

Greek Letters

β	tribo-electric exponent (-)
δ	L/S correction factor (-)
λ	tribo-electric signal constant ($\text{kg/Vm}^2\text{s}$)
μ	average
σ	standard deviation
σ_{abs}	absolute deviation

Subscripts

i	location in cross-section of downer
freq1.6	frequency of 1.6 Hz
freq8.6	frequency of 8.6 Hz
wav1	wavelet coefficient of the 1 st octave
wav2	wavelet coefficient of the 2 nd octave
wav4	wavelet coefficient of the 4 th octave
wav7	wavelet coefficient of the 7 th octave
wavn1	normalized wavelet coefficient of the 1 st octave
wavn3	normalized wavelet coefficient of the 3 rd octave
wavn5	normalized wavelet coefficient of the 5 th octave
wavn6	normalized wavelet coefficient of the 6 th octave
wavn10	normalized wavelet coefficient of the 10 th octave
0	0 wt% water in ethanol
5	5 wt% water in ethanol
10	10 wt% water in ethanol
99%comp	using a 99% compression ratio

6.7 References

- Ariyapadi, S., Holdsworth, D., Norley, C., Berruti, F., Briens, C., "Digital X-ray Imaging Technique to Study the Horizontal Injection of Gas-Liquid Jets into Fluidized Beds", *Int. J. Chem. React. Eng.*, **1** (A56)(2003).
- Briens, C., Briens, L., Hay, J., Hudson, C., Margaritis, A., "Hurst's Analysis to Detect Minimum Fluidization and Gas Maldistribution in Fluidized Beds", *AIChE J.*, **43**, 1904-1908 (1997).
- Briens, C., Mirgain, C., Bergougnou, M., Del Pozo, M., Loutaty, R., "Evaluation of Gas-Solids Mixing Chamber Through Cross Correlation and Hurst's Analysis", *AIChE J.*, **43**, 1469-1479 (1997).
- Briens, C., McDougal, S., Chan, E., "On-Line Detection of Bed Fluidity in a Fluidized Bed Coker", *Powder Technol.*, **138**, 160-168 (2003).
- Chang, S., Lottes, S., Zhou, C., Bowman, B., Petrick, M., "Numerical Study of Spray Injection Effects on the Heat Transfer and Product Yields of FCC Riser Reactors", *J. Heat Trans.*, **123**, 544-555 (2001).
- Gajewski, J., Glod, B., Kala, W., "Electrostatic Method for Measuring the Two-Phase Pipe Flow Parameters", *IEEE Trans. Ind. App.*, **29**, 650-655 (1993).
- Gao, J., Xu, C., Lin, S., Yang, G., Guo, Y., "Simulations of Gas-Liquid-Solid 3-Phase Flow and Reaction in FCC Riser Reactors", *AIChE J.*, **47**, 677-692 (2001).
- Gupta, A., Subba Rao, D., "Model for the Performance of a Fluid Catalytic Cracking (FCC) Riser Reactor: Effect of Feed Atomization", *Chem. Eng. Sci.*, **56**, 4489-4503 (2001).
- Hage, B., Werther, J., "The Guarded Capacitance Probe -- A Tool for the Measurement of Solids Flow Patterns in Laboratory and Industrial Fluidized Bed Combustors", *Powder Technol.*, **93**, 235-245 (2001).
- House, P., Saberian, M., Briens, C., Berruti, F., Chan, E., "Injection of a Liquid Spray Into a Fluidized Bed: Particle-Liquid Mixing and Impact on Fluid Coker Yields", *Ind.Eng. Chem. Res.*, **43**, 5663-5669 (2004).
- Huilin, L., Gidaspow, D., Bouillard, J., "Chaotic Behavior of Local Temperature Fluctuations in a Laboratory-Scale Circulating Fluidized Bed", *Powder Technol.*, **123**, 59-68 (2002).
- Liu, G., "Evaporating Crossflow Sprays in Gas-Solid Flows", *PhD Thesis*. New Jersey Institute of Technology, (2003).

- McMillan, J., Zhou, D., Saberian, M., Briens, C., Berruti, F., "Enhancement of Liquid-Solids Contact in a Downer Mixing Chamber: Effect of Liquid Spray Nozzle Orientation and Solids Jet Geometry", Presented at the *7th World Congress of Chemical Engineering*, Glasgow, Scotland, June (2005a).
- McMillan, J., Zhou, D., Saberian, M., Briens, C., Berruti, F., "Mixing Between Injected Liquid Feed and Circulating Solids in a Downer Mixing Chamber", *Circulating Fluidized Bed Technology VIII*, K. Cen. (Ed.) Beijing: International Academic Publishers/World Publishing Corporation, 2005, pp. 697-703.
- Mirgain, C., Briens, C., Del Pozo, M., Loutaty, R., Bergougnou, M., "New Technique for the Evaluation of a Circulating Fluidized Bed Mixing Chamber with a Central Solids Jet", *Powder Technol.*, **96**, 202-210 (1998).
- Nieuwland, J., Meijer, R., Kuipers, J., Van Swaaij, W., "Measurements of Solids Concentration and Axial Solids Velocity in Gas-Solid Two-Phase Flows", *Powder Technol.*, **87**, 127-139 (1996).
- Peters, E., *Fractal Market Analysis : Applying Chaos Theory to Investment and Economics*, New York: Wiley, 1994.
- Schiewe, T., Wirth, K., Molerus, O., Tuzla, K., Sharma, A., Chen, J., "Measurements of Solid Concentration in a Downward Vertical Gas-Solid Flow", *AIChE J.*, **45**, 949-955 (1999).
- Schuermans, H., "Measurements in a Commercial Catalytic Cracking Unit", *Ind. Eng. Chem. Proc. Des. Dev.*, **19**, 267-271 (1980).
- Skouby, D., "Hydrodynamic Studies in a 0.45m Riser with Liquid Feed Injection" *AIChE Symp.*, **95**, 67-70 (1999).
- Soo, S., Trezek, G., Dimick, R., Hohnstreiter, G., "Concentration and Mass Flow Distribution in Gas-Solid Suspension", *Ind. Eng. Chem. Fund.*, **3**, 98-106 (1964).
- Soong, C., Tuzla, K., Chen, J., "Experimental Determination of Cluster Size and Velocity in Circulating Fluidized Bed", *Fluidization VIII*, J.-F. Large, C. Laguerie (Eds.), Engineering Foundation: New York, 1995, pp. 219 - 227.
- Tafreshi, Z., Kirpalani, D., Bennett, A., McCracken, T., "Improving the Efficiency of Fluid Cokers by Altering Two-Phase Feed Characteristics", *Powder Technol.*, **125**, 234-241 (2002).
- Wang, X., Zhu, C., "Concentric Evaporating Spray Jets in Dilute Gas-Solids Pipe Flows", *Powder Technol.*, **129**, 59-71 (2003).

- Wei, F., Wang, Z., Jin, Y., Yu, Z., Chen, W., "Dispersion of Lateral and Axial Solids in a Cocurrent Downflow Circulating Fluidized Bed", *Powder Technol.*, **81**, 25-30 (1994).
- Westphalen, D., Glicksman, L., "Lateral Solid Mixing Measurements in Circulating Fluidized Beds", *Powder Technol.*, **82**, 153-167 (1995).
- White, C., Dry, R., "The Effect of Particle Size on Gas-Solid Contact Efficiency in a Circulating Fluidized Bed", *Circulating Fluidized Bed Technology III*, A. Avidan, (Ed.), Pergamon Press: New York, 1991, pp. 569 – 574.

CHAPTER 7

Flow Stability in a Downer Mixing Chamber

Jennifer McMillan, Cedric Briens, Franco Berruti

*Department of Chemical and Biochemical Engineering
The University of Western Ontario
1151 Richmond Street
London, Ontario, Canada, N6A 5B9*

7.1 Introduction

Liquid injection into conventional gas-solid fluidized beds and circulating fluidized-bed reactors is encountered in many industrial applications such as fluid catalytic cracking and fluid coking. In such applications, the initial interaction of the liquid jet spray and the fluidized particles represents a crucial step in the process. In particular, the fluid coking process requires uniform contact of the liquid droplets and entrained particles in order to achieve efficient thermal cracking and high yields of valuable products. A poor distribution of the liquid feed on the particles can cause either a thick liquid film to form on the solids surface or promote the formation of wet agglomerates, imposing a high resistance to mass and heat transfer between the feed and the particles, thus decreasing the yield of valuable products. To prevent the slow cracking associated with heat or mass transfer limitations, the feedstock must contact a large number of particles quickly and uniformly. A downer equipped with a mixing chamber located at its entrance may be used to intensify this contact.

A good mixing chamber must ensure good initial contact between liquid and solids while providing a continuous, uniform, stable dispersion at the inlet to the downer. An ideal mixing chamber should also provide a stable mixing quality on a time scale smaller than the average gas residence time in the downer (around 50 ms). An

experimental technique which could be used to determine the stability of this type of system would be extremely useful.

Previous studies have investigated the stability of liquid sprays into conventional fluidized beds. Ariyapadi et al. (2004) developed a simple and reliable technique for characterizing the stability of sprays injected in open-air, based on the V statistic for cycle detection and analysis. This technique was then applied to determine whether the stability of a spray changes when introduced into a fluidized bed. A transducer measured the pressure in the gas line upstream of the nozzle, and a tribo-electric probe was used to characterize the spray downstream of the nozzle. Hulet et al. (2003) also studied jet stability using tribo probes and the V-statistic when a horizontal gas-liquid spray was injected into a fluidized bed. However, there have not been any studies done which investigated the stability of gas-liquid jets injected into a circulating fluidized bed.

Previous investigations involved the injection of gas jets into down-flowing solid particles in a mixing chamber, very similar to the experimental set-up used in this study (Briens et al., 1997; Mirgain et al., 1998). Effective and stable gas-solids mixing chambers were identified from the signals of simple and robust momentum probes. The signals were analyzed using cross correlation and Hurst analysis. A stability index was determined which indicated the changes of the detected overall flow structure. Although these techniques provided direct, reliable results for the gas-solid system, they can only approximate the stability and mixing between a sprayed liquid and particles.

McMillan et al. (2005a, 2005b) studied the liquid solid mixing quality when a liquid was injected into a mixing chamber and contacted with down-flowing particles. A combination of measurements from thermocouples and tribo-electric probes were used to obtain the liquid to solid ratio within the cross-section of the downer. However, the stability of this flow was not investigated.

The use of tribo-electric probes to measure the flux of solids in a two-phase gas-solid flow has been employed in previous studies (Soo et al., 1964; Gajewski et al., 1993; Nieuwland et al., 1996; Yan and Byrne, 1997). More recently they have been used in three-phase gas-liquid-solids flows to measure the local solids flux (McMillan et al.,

2005a, 2005b) and moisture content (Portoghese, 2005). However, tribo-electric probes have not been used to measure the stability of gas-liquid-solid flows.

To date, there has been no investigation of the flow stability in a downer when a gas-liquid spray is injected into downer reactors equipped with a mixing chamber. The objective of this study was to develop a technique for such an investigation. The effects of changing the start-up conditions as well as using different liquids were, then, examined.

7.2 Experimental Set-Up

Experiments were conducted in a mixing chamber that was located at the entrance of a downer. Coke particles with a Sauter mean diameter of $140\text{ }\mu\text{m}$, which were stored in a silo, flowed down through an orifice plate into the mixing chamber before entering the 0.076 m diameter downer. A 0.02 m diameter circular orifice plate was placed at the inlet to the mixing chamber in order to control and distribute the solids flow over the cross section. In order to achieve the desired solids flowrate resulting in a liquid to solid ratio of approximately 5%, the silo was pressurized by delivering a constant flowrate of pressurization air. The instantaneous pressure drop through the orifice of the solids feeder was measured and the instantaneous solids flowrate could be determined from a calibration curve. During a run the solids flowrate was kept constant at approximately 0.5 kg/s ($110\text{ kg/m}^2\text{s}$).

Liquid from spray nozzles was contacted with the down-flowing particles in a mixing chamber, which is shown in Figure 7.1.

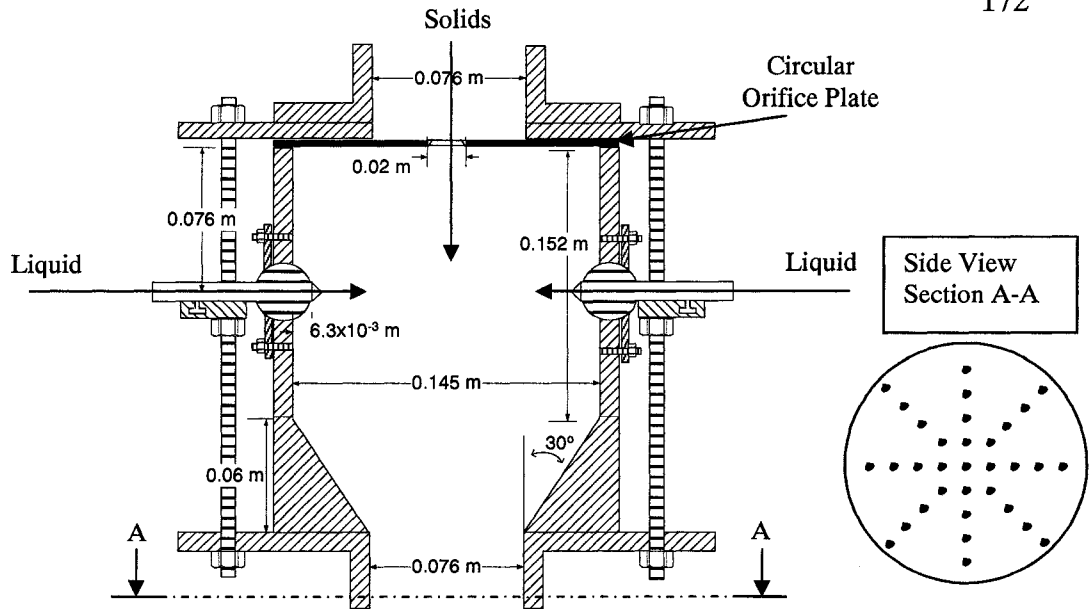


Figure 7.1: Mixing Chamber

The mixing chamber consisted of a 0.145 m diameter cylindrical section followed by a conical section angled at 30° that led to the 0.076 m diameter downer. The mixing chamber used in this study was equipped with 4 gas-liquid injector spray nozzles, which could be independently oriented in both the horizontal and vertical planes. An injection nozzle configuration that had provided good mixing between the solids and liquid in a previous study (McMillan et al., 2005a) was chosen in order to test the stability of the system, and is shown in Figure 7.2.

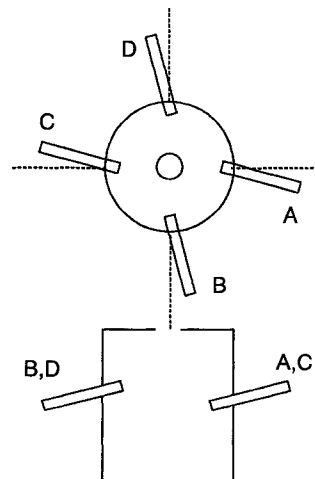


Figure 7.2: Mixing Chamber Configuration

Figure 7.3 depicts the geometry of the spray nozzle that was used. The liquid was supplied to a nozzle through a centrally located hypodermic needle with an internal diameter of 0.0015 m, while the atomizing air flowed through an annular region. The liquid tube was offset by 0.002 m towards the inside of the nozzle to allow for internal mixing of the two phases (Ariyapadi et al., 2003).

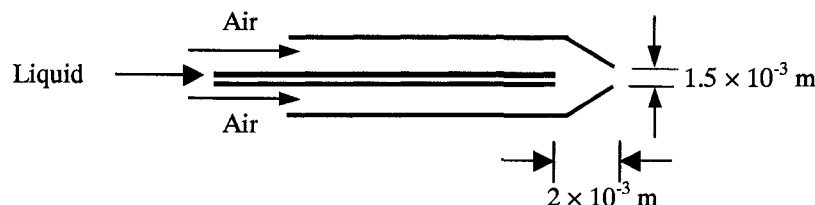


Figure 7.3: Gas-Liquid Injection Nozzle

Pure ethanol was chosen as the injection liquid for most of the runs because it has a negligible effect on the tribo-electric current, and therefore the solids flux can be directly measured (McMillan et al., 2005b). A constant air mass flowrate from a high-pressure cylinder was supplied to each injection nozzle through a dedicated sonic nozzle in the upstream line. The liquid was supplied to the nozzles from a tank pressurized by nitrogen in order to ensure uniform liquid flowrate to each injector nozzle. The air and liquid flowrates for each nozzle were kept constant at 0.43 g/s and 6.83 g/s, respectively, resulting in an air-to-liquid ratio (ALR) of 5.9%.

The solid-liquid mixture flowed through the downer and entered a separator where it was dried. A pneumatic line returned the dry solids to the silo.

7.2.1 Tribo-Electric Measurement Procedure

Friction between particles and a metal surface can result in the transfer of electrons between the two objects. If the metal surface is connected to the ground during this charge transfer, a tribo-electric current is obtained. A probe inserted into a particle flow will develop an electrical charge at a rate that is proportional to the solids mass flow (e.g. the higher the solids flux the greater the tribo-electric signal). The probes used in

this study were 2.5×10^{-3} m diameter stainless steel rods that were 0.185 m long. Each probe was insulated with Teflon tubing so that only 2.5×10^{-3} m of the tip of the probe was exposed and in direct contact with the liquid-solid mixture. The tribo-electric probes were inserted just below the exit of the mixing chamber, as indicated in section A-A of Figure 7.1, and obtained data at 4 different radial locations, as shown in Figure 7.4.

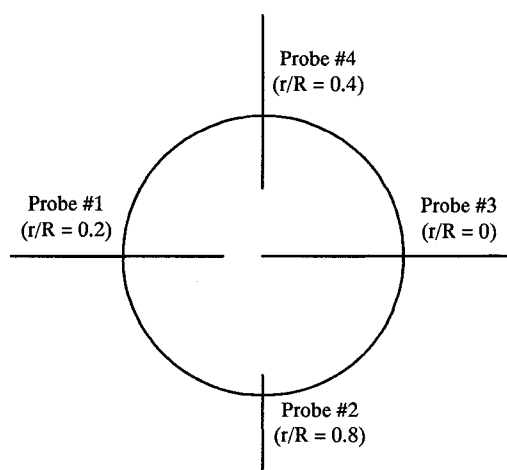


Figure 7.4: Probe Locations

Two different sets of experiments were performed. The first set consisted of 5 replicate runs, called base case runs #1-5, under normal start-up conditions (flowrates through each nozzle of 0.43 g/s for the gas and 6.83 g/s for the liquid) and used pure ethanol as the injection liquid. One extra run, called base case run 5%, was performed that took place under normal start-up conditions, but used ethanol which contained 5% water.

The second set of experiments consisted of 5 different runs in which the startup conditions were varied slightly before the system reached steady state:

- For the case called Liquid Valve A, the valve supplying liquid to injection nozzle A was initially closed (see Figure 7.2).
- For the case called Liquid Valve B, the valve supplying liquid to injection nozzle B was initially closed (see Figure 7.2).

- For the case High F_s , the silo was initially pressurized to a higher value, resulting in a higher solids flowrate at the beginning of the run.
- For the case Low F_s , the silo was not pressurized at the start of the run, resulting in a lower solids flowrate at the beginning of the run.
- For the case No Air, no atomization air was supplied to the injection nozzles, resulting in a pure liquid stream exiting from the nozzles for the initial part of the run.

For all five cases, the alternate start-up condition was maintained for 10 seconds before resuming normal operating conditions. As shown below in section 7.3.3, the system took less than 10 seconds to reach steady state after the normal operating conditions were applied, and data was then collected for 50 seconds at a frequency of 1000 Hz.

7.3 Results and Discussion

Various signal analysis techniques were used in order to determine the variability of the tribo-electric signals within each run as well as the variability of the tribo-electric signals among runs.

7.3.1 Raw Signals

For each run, the absolute values of the tribo-electric signals for each of the 4 probes were plotted vs time (Figures 7.5-7.8). The respective solids flowrate, obtained from the pressure drop across the solids feeder orifice, was also plotted on each graph.

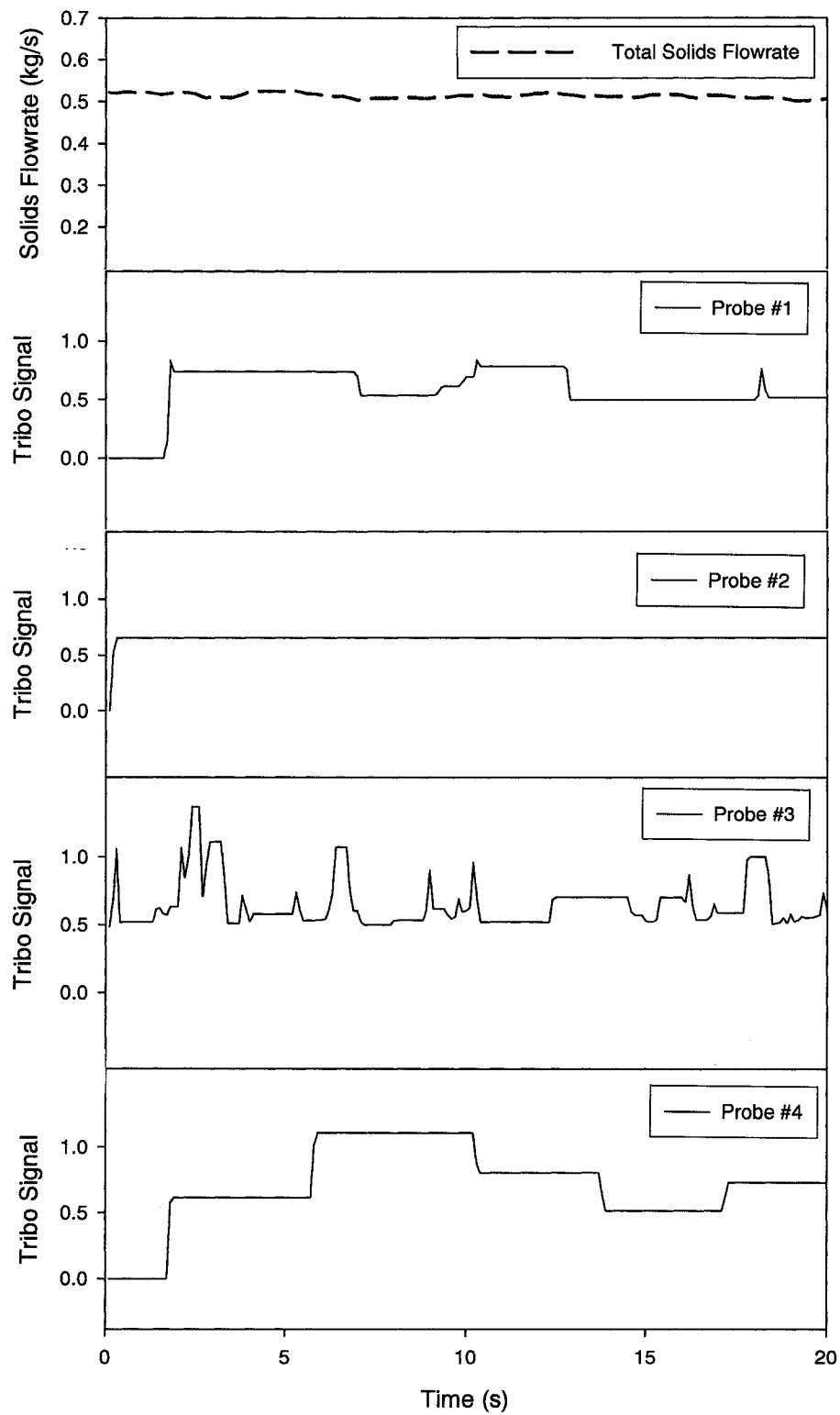


Figure 7.5: Raw Data for Base Case 5% Water

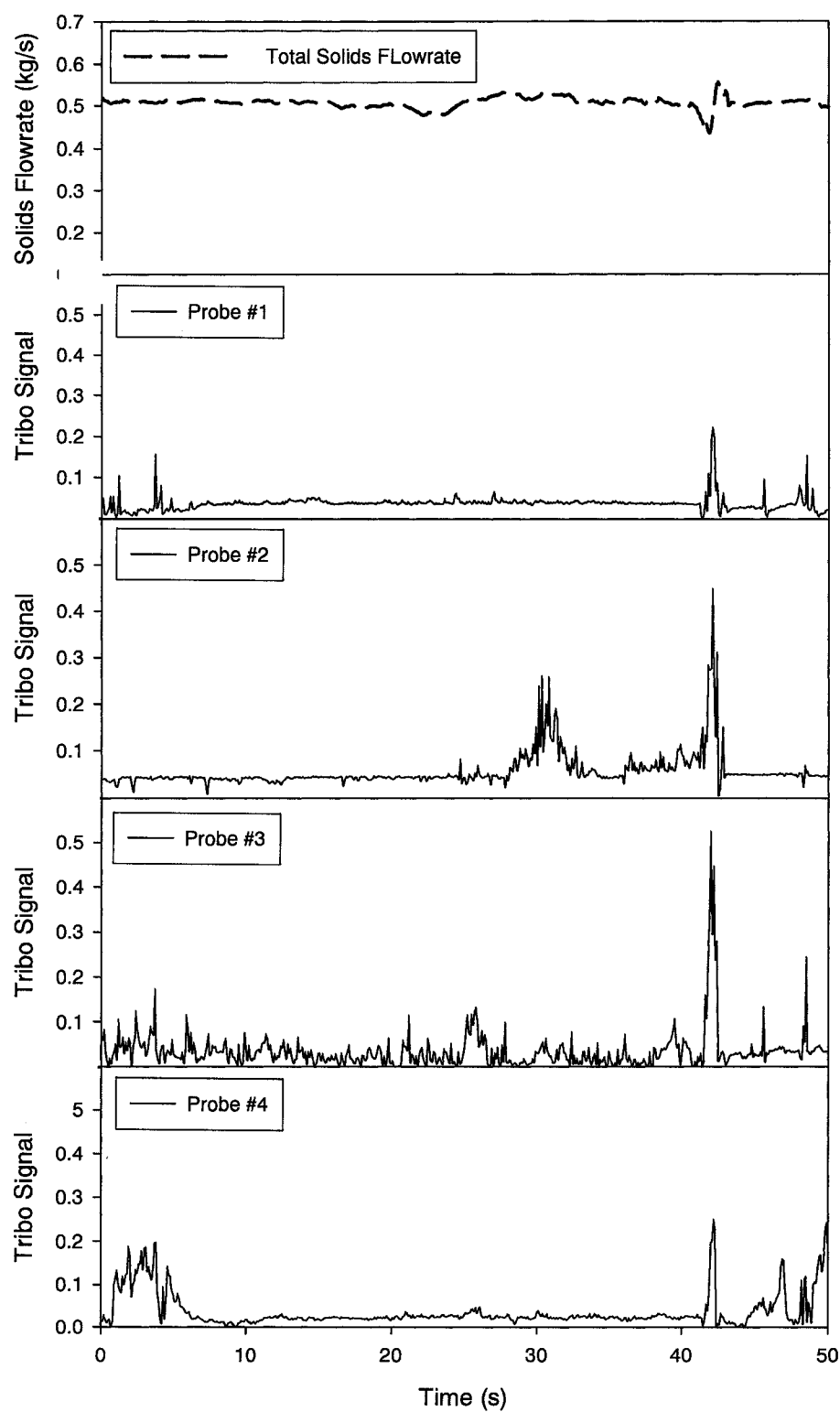


Figure 7.6: Raw Data for Replicate Run #5

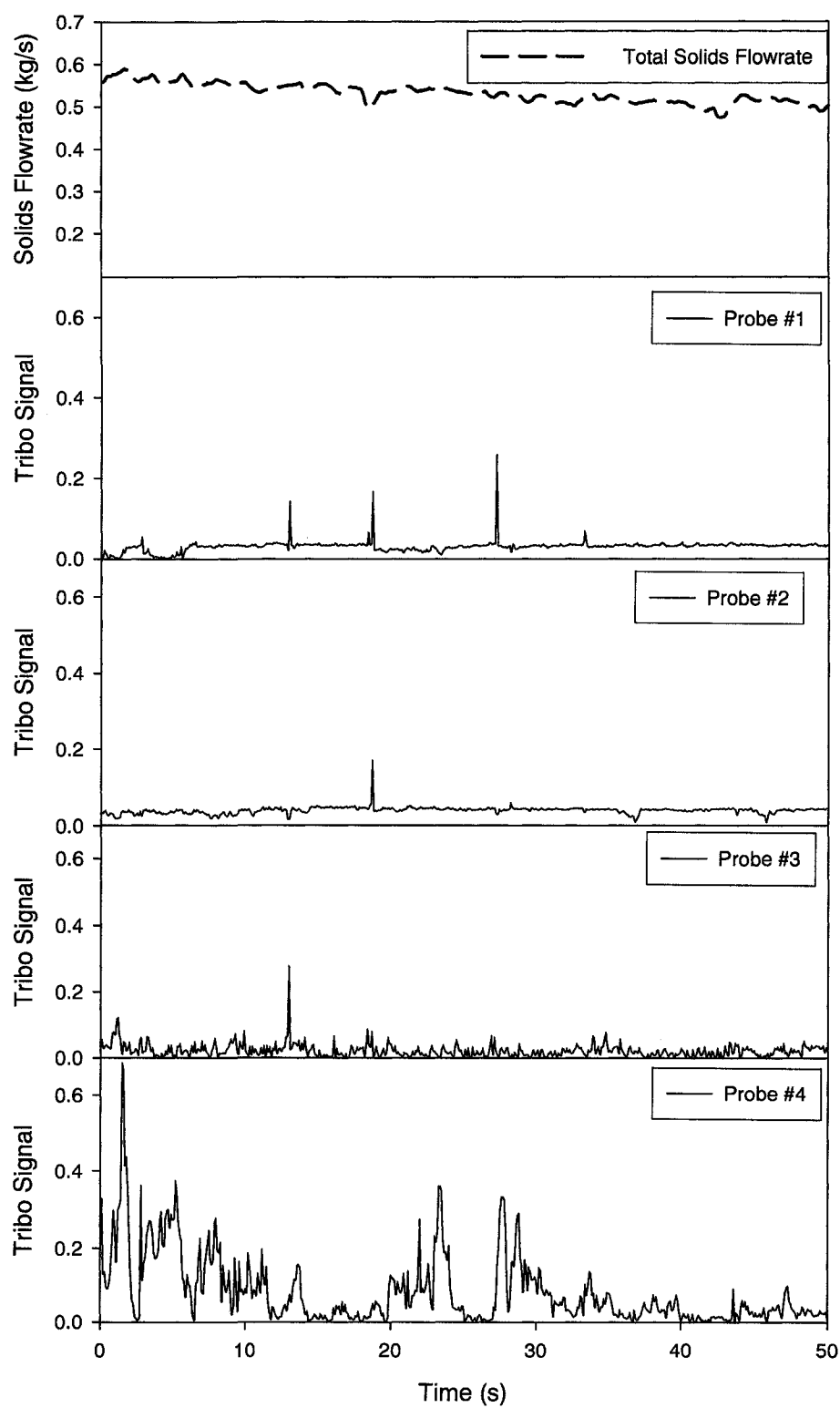


Figure 7.7: Raw Data for High Fs Case

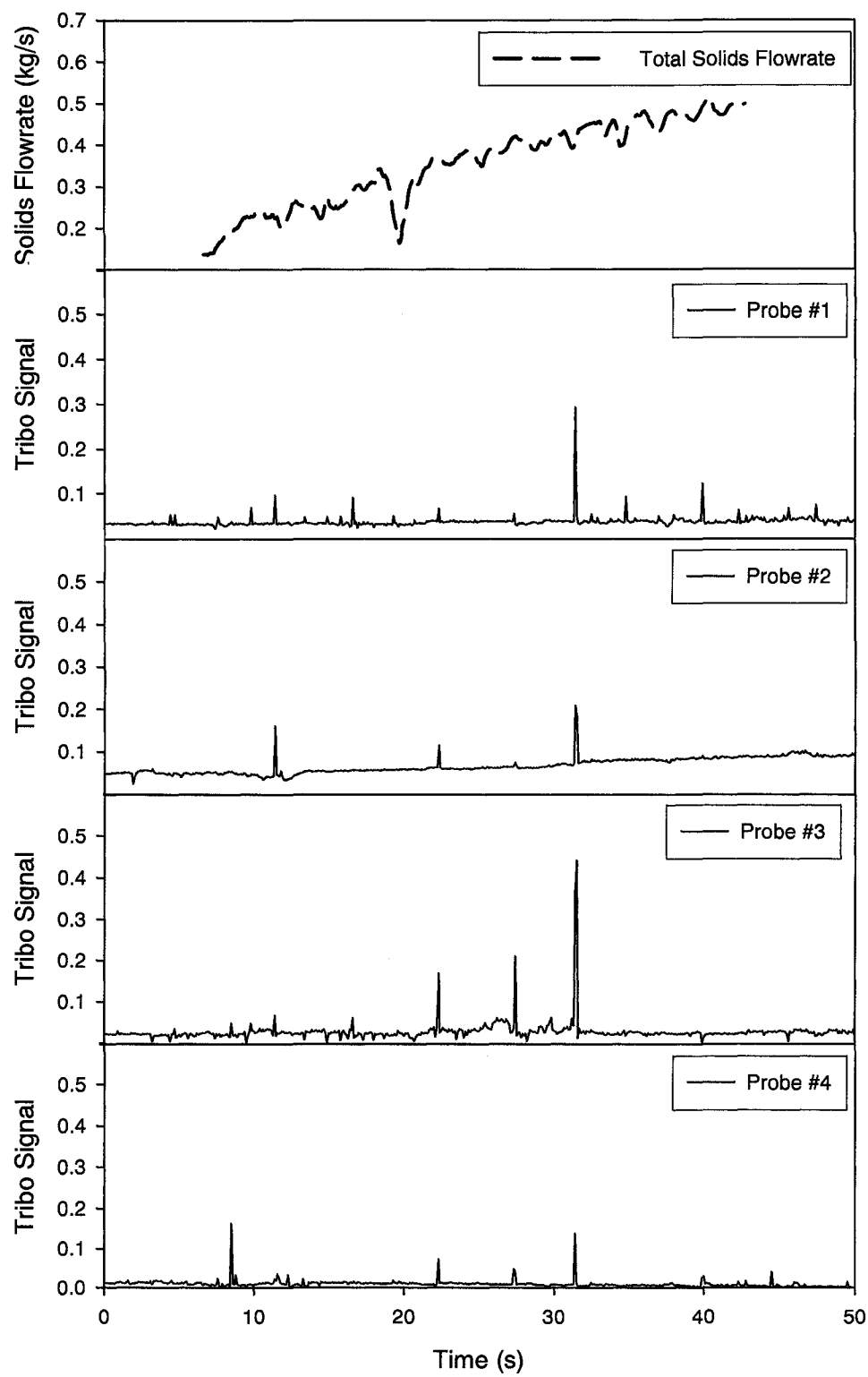


Figure 7.8: Raw Data for Low F_s Case

Several conclusions can be drawn from the raw signals:

- First, the fluctuations seem greatly amplified when a liquid is used to which the tribo probes respond. Figure 7.5 shows a plot of the results when ethanol containing 5% water was injected into the system. The signals are much stronger than the signals obtained when pure ethanol was injected into the system, as shown in Figure 7.6. This confirms previous results (McMillan et al., 2005b).
- Second, the fluctuations for probe #2 are much lower than the fluctuations from the other 3 probes for most runs, as can be seen from Figure 7.6. Probe #2 is located in a region of low turbulence, near the wall of the downer (see Figure 7.4).
- Third, the solids flowrate has a strong effect on the tribo-electric signal, as can be seen from the results of Run #5, shown in Figure 7.6. At 42 seconds there is a solids flowrate perturbation, which had a very large effect on most of the probes. In Figure 7.7, High F_s , the gradual decrease in solids flowrate is reflected in the tribo probe signals, as there are more peaks during the first 25 seconds of the run when the solids flux is higher. The same is true for the Low F_s case, Figure 7.8. The average tribo-electric signals are higher during the last 25 seconds of the run when the solids flux is higher.

Since sudden fluctuations in solids flowrate can affect the tribo signals, it is important to monitor the solids flowrate and minimize the fluctuations. The fluctuations of the solids flowrate meter, which consisted of an orifice and a differential pressure transducer, are very small, although its response is very fast. Mirgain et al. (1998) found that the average fluctuations of the solids flow, which were estimated by the standard deviation of the pressure-drop signal were less than 5% on a 10 ms scale.

7.3.2 Cross Correlation

To further determine the effects of the solids flowrate on the system, the signals were analyzed by calculating the cross-correlation coefficient between each probe and the solids flowrate signal. The normalized cross-correlation coefficient, R_{xy} , for a lag time τ , was determined by Equation 7.1.

$$R_{xy}(\tau) = \frac{1}{t_2 - t_1} \int_{t_1}^{t_2} \left(\frac{x(t) - x_m}{\sigma_x} \right) \left(\frac{y(t + \tau) - y_m}{\sigma_y} \right) dt \quad (7.1)$$

The coefficients were found to be very small, with values ranging between 0 and 0.46, and therefore, most of the fluctuations of the probes signals do not result from fluctuations in the solids flowrate. This confirms that the control of the solids flux achieved in this study was excellent.

7.3.3 Standard Deviations

The individual signals from each probe were also analyzed to characterize the stability of the system. In order to determine the length of time it took for the system to stabilize, the signals for each base case replicate run were divided in “chunks” or intervals of the same length, and the standard deviation was calculated for each time interval. Figure 7.9 shows an example of the standard deviation versus the “chunk” length for replicate run #1, and indicates that the system becomes stable after approximately 4 seconds.

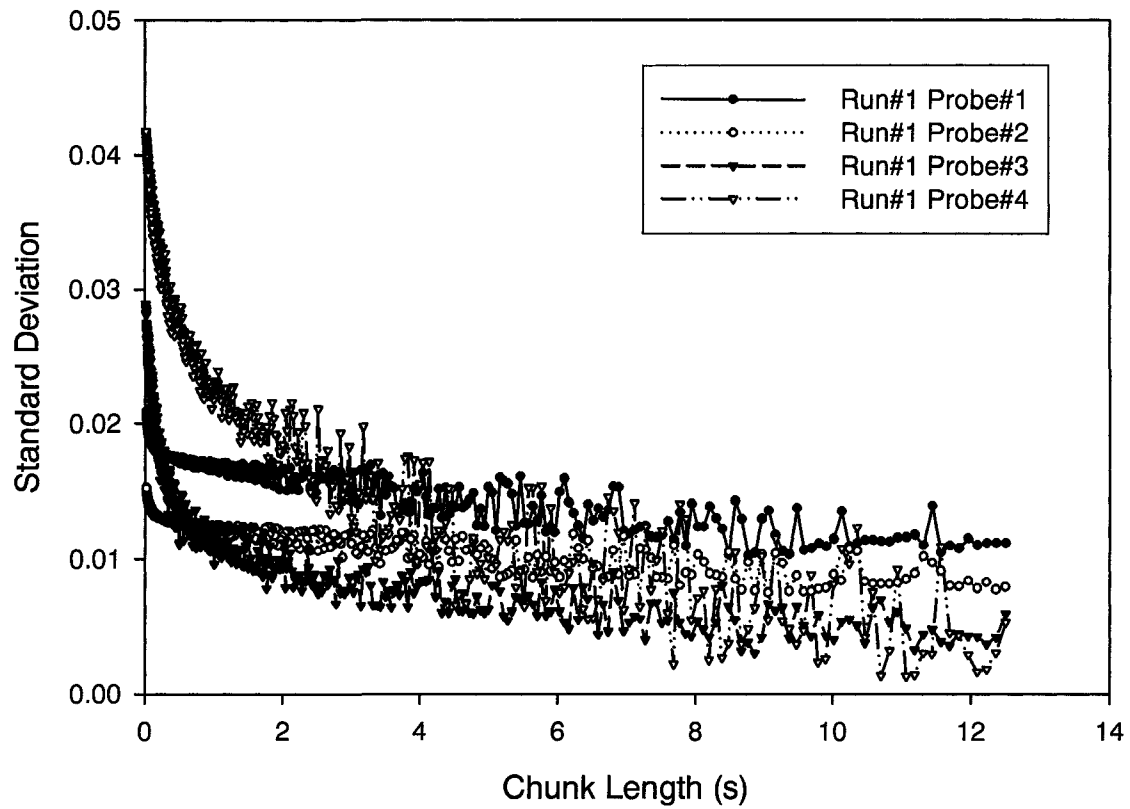


Figure 7.9: Standard Deviation vs Chunk Length for Each Probe of Replicate Run #1

7.3.4 Power Spectrum

The power spectral density for each replicate run was also calculated and plotted against frequency. Figure 7.10 shows the results for replicate run #1. This figure shows that the power is very low at high frequencies and that the signals did not display a regular periodicity. This indicates that the signals, and therefore the L/S, fluctuate with time and are not affected by electrical noise, which would show up at 60 Hz.

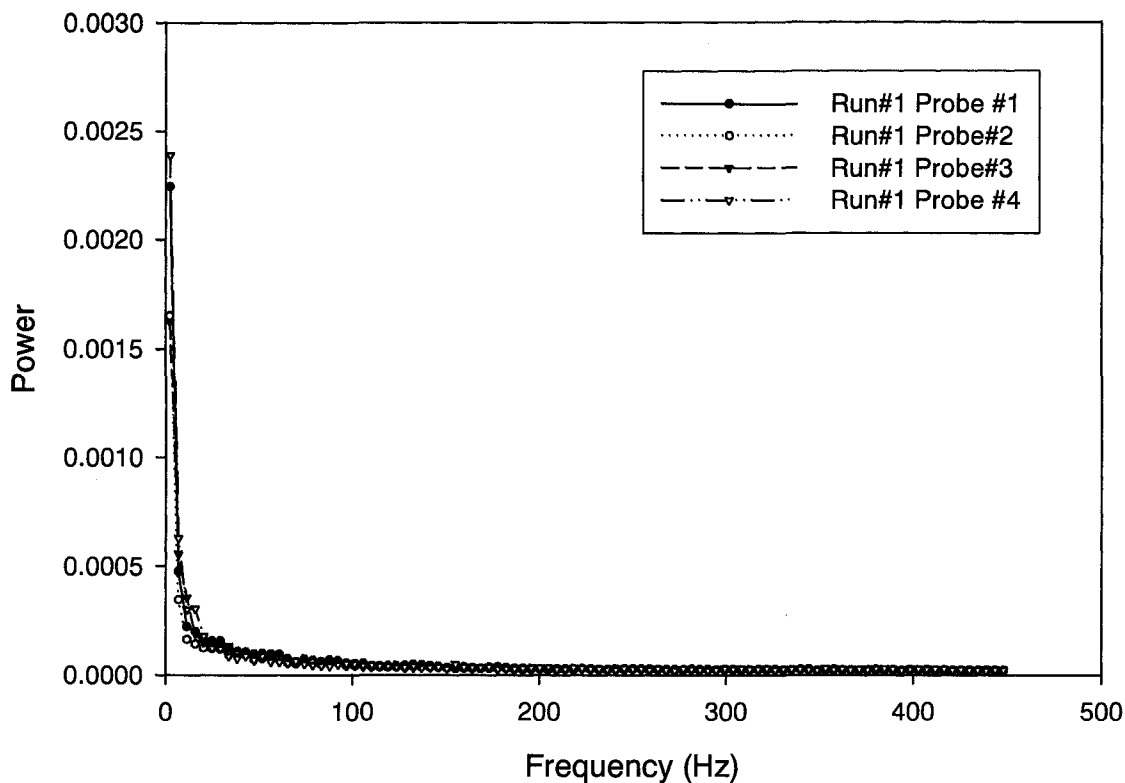


Figure 7.10: Power Spectrum for Replicate Run #1

7.3.5 Correlation Dimension

In order to determine whether the system was chaotic or not the correlation dimension was calculated. A high correlation dimension corresponds to a complex structure, which indicates a chaotic system. The calculation procedure involves calculating a correlation integral for various distances for increasing dimensional phase space. The correlation integral was calculated for a specified range of embedding dimensions. The lags required for the calculation were determined by using the cycle times, which were calculated by using the P statistic (Briens, 2000). The P statistic was used to identify non-periodic cycles and was used since the V-statistic and power spectrum failed to identify a cycle time. The correlation dimension values for each run are fairly small, with values ranging between 0.38 and 2.9, indicating that the system is not very chaotic.

7.3.6 Hölder Exponent

Fractal noise is characterized by trends and discontinuities that give a particular geometric shape to the signal. The rapid changes in the time series are called singularities of the signal and their strength is measured by a Hölder exponent (Scafetta et al., 2003). The Hölder exponent of a singularity can be evaluated by using the wavelet transform and describes the continuity qualities of a signal. The Hölder exponents that were calculated range between -0.8 and -0.33, and are all negative, indicating that the fluctuations in the system are accidental.

7.3.7 Time Averaged Solids Dispersion Over the Downer Cross Section

McMillan et al. (2005a) performed experiments under the same conditions as the base case replicate runs and obtained data using the tribo-electric probes at 33 locations within the downer cross-section. A relationship between solids flux and triboprobe signal developed by McMillan et al. (2005) was used to calculate the local values of the solid flux.

$$W_s = \lambda i^{1/1.1} \quad (7.2)$$

From linear interpolation of the 33 points, contour plots of the solids dispersion within the downer cross-section were created for replicate run #1 and replicate run #2, and are shown in Figures 7.11 and 7.12, respectively.

$$W_s = 5.02 \times 10^{-3} \text{ kg/m}^2\text{s}$$

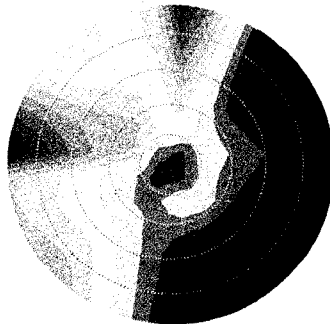


Figure 7.11: Contour Plot of W_s for Run #1

$$W_s = 5.09 \times 10^{-3} \text{ kg/m}^2\text{s}$$

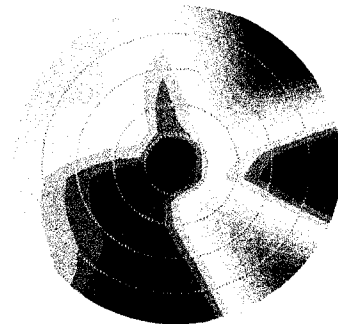
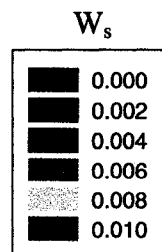


Figure 7.12: Contour Plot of W_s for Run #2



Although the contour maps are completely different for both cases and the regions containing a high and low concentrations of solids are situated in different locations within the downer cross section, the average solid flux values are approximately the same. The average solids flux for replicate run #1 is $5.02 \times 10^{-3} \text{ kg/m}^2\text{s}$ and the average solids flux for replicate run #2 is $5.09 \times 10^{-3} \text{ kg/m}^2\text{s}$. A plot of the cumulative solid distribution within the downer cross section was created for these two replicate runs, as well as for the Liquid Valve A case, and is shown in Figure 7.13. The cumulative distributions for the two replicate cases are approximately the same. However, the cumulative distribution for the Liquid Valve A case is different from the distributions for the repeat cases, which indicates that changing the startup conditions changes the solids distribution in the mixing chamber significantly.

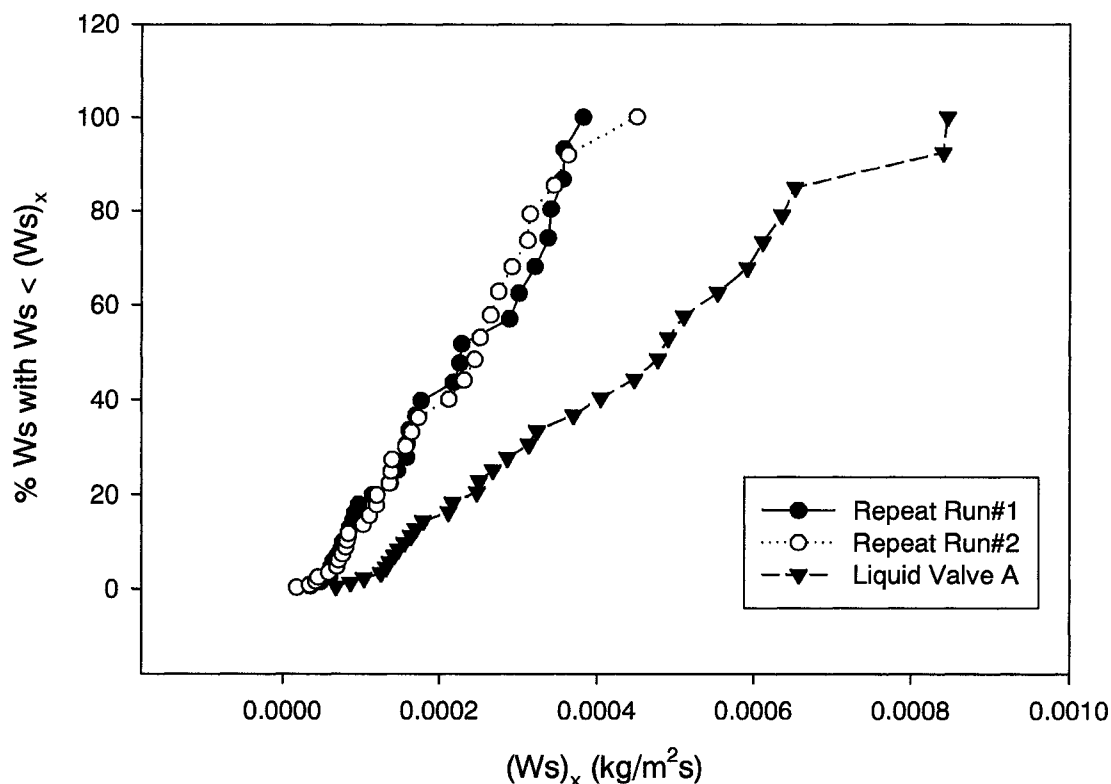
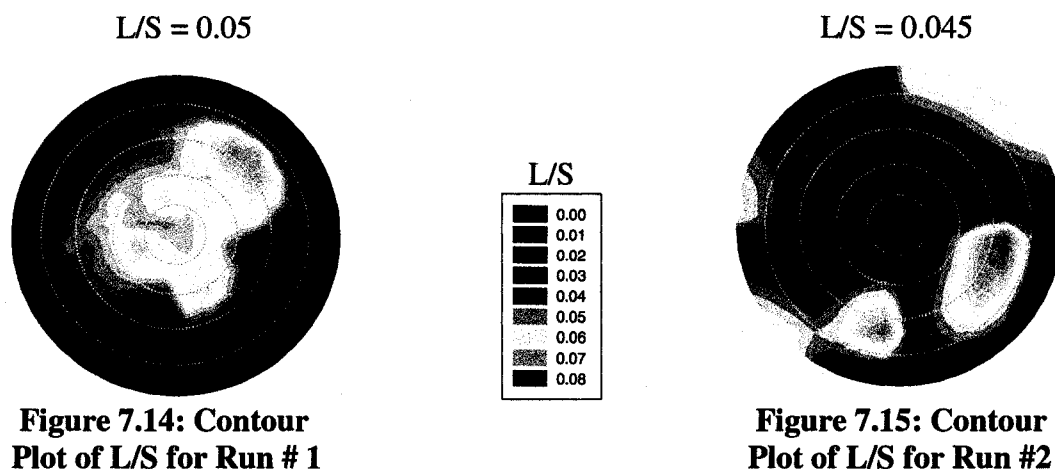


Figure 7.13: Cumulative Solid Distribution

7.3.8 Time Averaged Liquid-Solid Dispersion Over the Downer Cross Section

A different measurement technique, which had been used in a previous study (McMillan et al., 2005), involving the use of temperature and tribo probes was used to obtain contour plots of the time averaged L/S in the downer cross section. These plots are shown in Figures 7.14 and 7.15, and show the results for two of the base case replicate runs. The two plots show that although the contour maps are completely different due to the fact that the local L/S values are shifted within the downer cross section, both plots have the same global average L/S. The average L/S values for repeat run #1 and repeat run#2 are 0.05 and 0.045, respectively.



Another way to illustrate this point is to plot the cumulative liquid distribution as a function of liquid to solid ratio (L/S). Figure 7.16 shows the cumulative distribution for the replicate run cases and Figure 7.17 shows the cumulative distribution for the different start-up conditions cases. As can be seen in Figure 7.16, the cumulative liquid distributions for repeat run #1 and repeat run #2 are very similar. It is interesting to note that with the exception of the Low F_s case, the cumulative liquid distribution plots for the different start-up conditions show less variability than the plots for the replicate cases. This may suggest that a disruption of the steady state operation of the mixing chamber may in fact improve the liquid-solid contact in the downer.

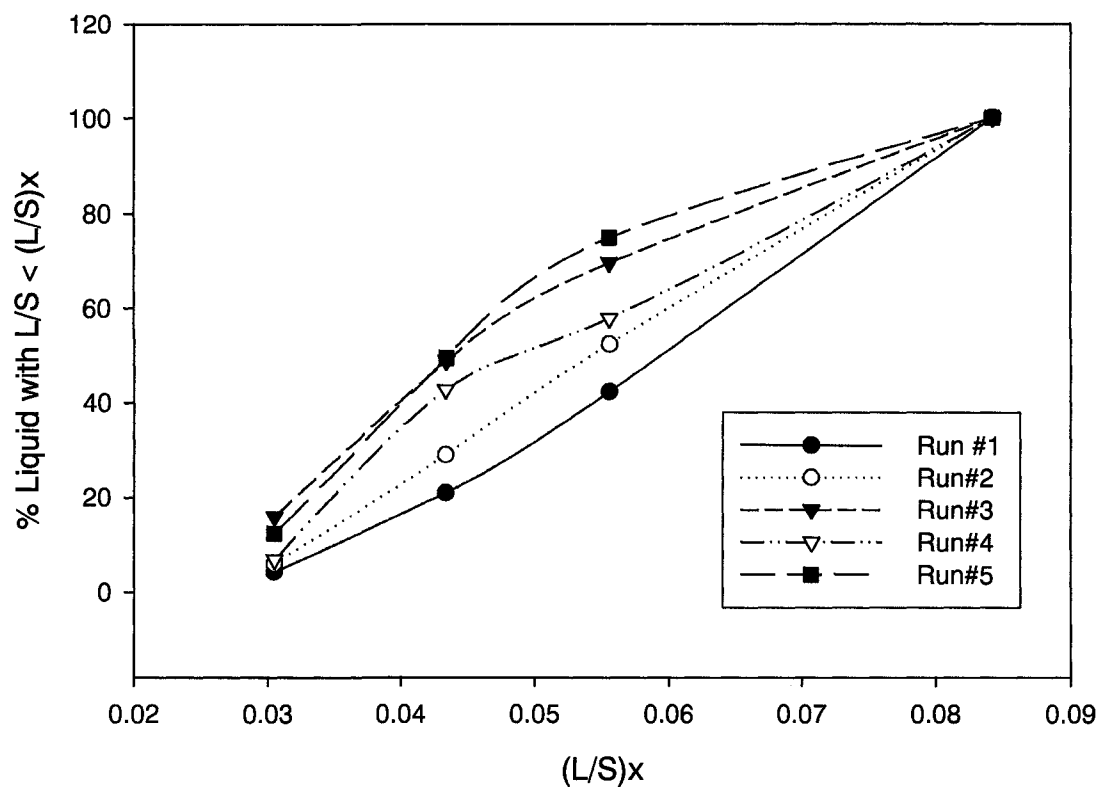


Figure 7.16: Cumulative Liquid Distribution for Replicate Runs

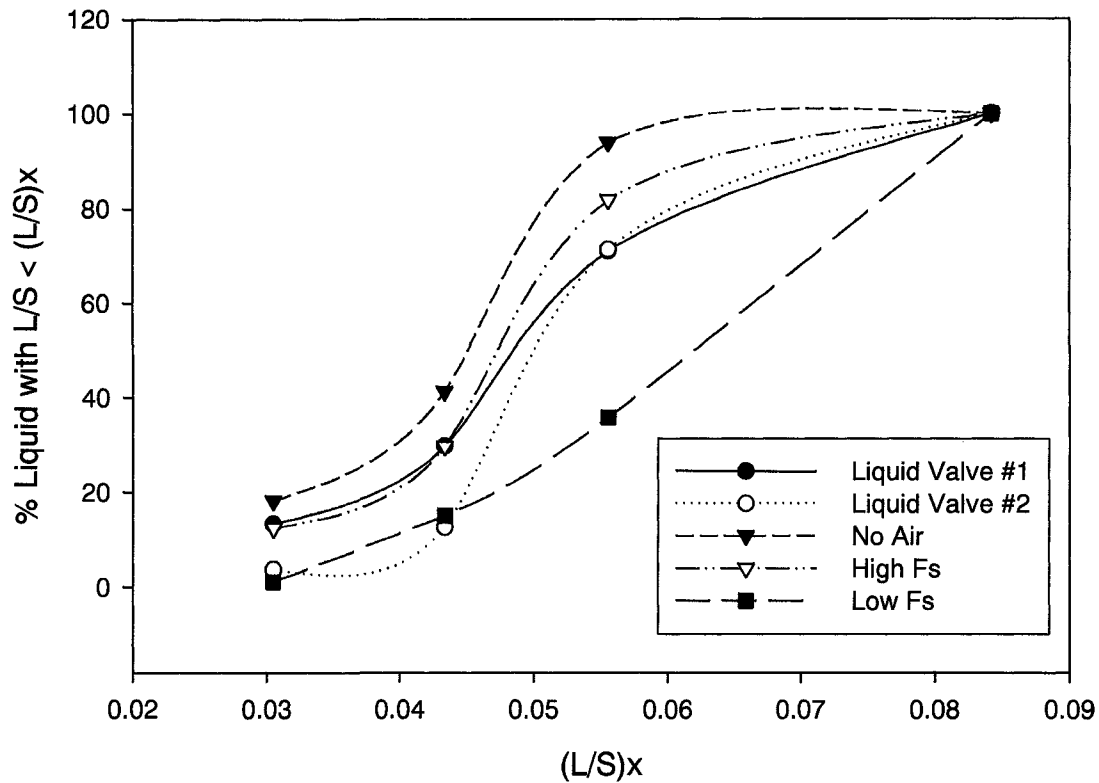


Figure 7.17: Cumulative Liquid Distribution for Different Startup Conditions

The residence time in the mixing chamber is approximately 100ms (Mirgain et al., 1998) and as a result, replicate run #1 was used as an example and divided into chunks of 1 second intervals. The cumulative liquid distribution for each 1 second chunk was determined and plotted in Figure 7.18. The variation between chunks is relatively small, indicating that the average spread of liquid within the mixing chamber is fairly constant for the entire run and that there is a stable mixing quality on a time scale that is close to the average residence time.

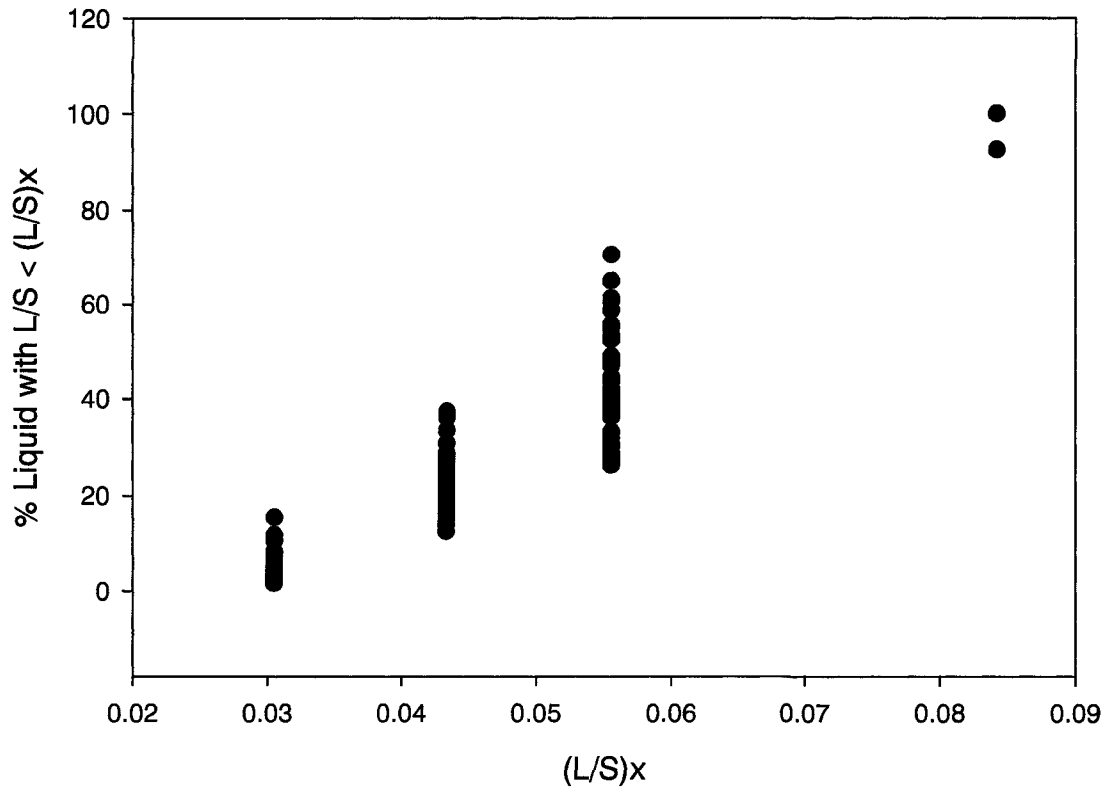


Figure 7.18: Cumulative Liquid Distribution for 1 Second Chunk Intervals for Run #1

7.4 Conclusion

A measurement technique was developed to evaluate the stability of flow within the cross sectional area of a downer when a mixing chamber was located at its entrance and liquid injected into down-flowing particles. The technique uses tribo-electric measurements to determine the stability of the system as well as the effects of changing the startup conditions.

Results from the various signal analysis techniques indicate that the system is non-chaotic and non-cyclic. The local standard deviations for each run are fairly large, indicating that the system is not very stable locally. However, similar structures are observed between runs, which suggests that the system is stable globally. Although the

regions containing high and low liquid to solid ratios are situated in different locations within the downer cross section, each replicate run has approximately the same average distribution of the liquid to solid ratio over the whole downer cross-section. This indicates that between runs the liquid to solid ratio values are shifted within the downer cross section, and the overall performance remains stable. The same comments apply to the solids flux: its local value changes with time but the distribution of its values over the whole downer cross-section remain the same. As a result a Lagrangian as opposed to an Eulerian approach to modeling should be used.

It was also found that the system is very sensitive to changes in the initial startup conditions and the effects of the changes remain in the system for up to 1 minute after startup.

7.5 Acknowledgements

Financial support from Syncrude Canada Ltd. and the Ontario Graduate Scholarship Program is greatly appreciated. Thank you also to the Natural Sciences and Engineering Research Council (NSERC) for Discovery Grants to Professors Cedric Briens and Franco Berruti, as well as a Collaborative Research Development Grant. Special thanks to the University Machine Services for their help with the experimental apparatus.

7.6 Nomenclature

i	tribo signal
L/S	liquid to solid ratio (-)
n	sample size
r	population size
R_{xy}	cross-correlation coefficient (-)
S_x	sample standard deviation
S_y	population standard deviation
t	time (s)
W_s	solids mass flux ($\text{kg/m}^2\text{s}$)
\bar{X}	sample mean
\bar{Y}	population mean
y	tribo-electric signal (V)

Greek Letters

λ	tribo-electric constant
τ	time lag of the cross-correlation function (s)
σ_x	sample standard deviation
σ_y	population standard deviation

7.7 References

- Ariyapadi, S., Holdsworth, D., Norley, C., Berruti, F., Briens, C., "Digital X-Ray Imaging Technique to Study the Horizontal Injection of Gas-Liquid Jets into Fluidized Beds", *Int. J. Chem. React. Eng.*, **1**, 1114-1130 (2003).
- Ariyapadi, S., Berruti, F., Briens, C., "Stability of Horizontal Gas-Liquid Sprays in Open Air and in a Gas-Solid Fluidized Bed", *Powder Technol.*, **155**, 161-174 (2004).
- Briens, C., Mirgain, C., Bergougnou, M., Del Pozo, M., Loutaty, R., "Evaluation of Gas-Solids Mixing Chamber Through Cross Correlation and Hurst's Analysis", *AIChE J.*, **43**, 1469-1479 (1997).
- Briens, L. "Identification of Flow Regimes in Multiphase Reactors by Time Series Analysis", *Ph.D. Thesis*, The University of Western Ontario, (2000).
- Gajewski, J., Glod, B., Kala, W., "Monitoring Electrostatic Flow Noise for Mass Flow and Mean Velocity Measurement in Pneumatic Transport", *IEEE Trans. Ind. App.*, **29**, 650-655 (1993).
- Hulet, C., Briens, C., Berruti, F., Chan, E., Ariyapadi, S., "Entrainment and Stability of a Horizontal Gas-Liquid Jet in a Fluidized Bed", *Int. J. Chem. React. Eng.*, **1**(A60) (2003).
- McMillan, J., Zhou, D., Saberian, M., Briens, C., Berruti, F., "Mixing Between Injected Liquid Feed and Circulating Solids in a Downer Mixing Chamber", *Circulating Fluidized Bed Technology VIII*, K. Cen, (Ed.), Beijing: International Academic Publishers/World Publishing Corporation, 2005a, pp. 697 – 703.
- McMillan, J., Zhou, D., Saberian, M., Briens, C., Berruti, F., "Measurement Techniques to Characterize the Contact Between Injected Liquid and Circulating Solids In a Downer Mixing Chamber", *Powder Technol.*, **161**, 175-184 (2005b).
- Mirgain, C., Briens, C., Del Pozo, M., Loutaty, R., Bergougnou, M., "A New Technique for the Evaluation of a Circulating Fluidized Bed Mixing Chamber with a Central Solids Jet", *Powder Technol.*, **96**, 202-210 (1998).

- Nieuwland, J., Meijer, R., Kuipers, J., Van Swaaij, W., "Measurements of Solids Concentration and Axial Solids Velocity in Two-Phase Flows", *Powder Technol.*, **87**, 127-139 (1996).
- Portoghese, F., Berruti, F., Briens, C., "Use of Triboelectric Probes for On-Line Monitoring of Liquid Concentration in Wet Gas-Solid Fluidized Beds", *Chem. Eng. Sci.*, **60** (22), 6043 - 6048 (2005).
- Scafetta, N., Griffin, L., West, B., "Hölder Exponent Spectra for Human Gait", *Phys. A.*, **328**, 561-583 (2003).
- Soo, S., Trezek, G., Dimick, R., Hohnstreiter, G., "Concentration and Mass Flow Distributions in a Gas-Solid Suspension", *Ind. Eng. Chem. Fund.*, **3**, 98-106 (1964).
- Yan, Y., Byrne, B., "Measurement of Solids Deposition in Pneumatic Conveying", *Powder Technol.*, **91**, 131-139 (1997).

CHAPTER 8

GENERAL DISCUSSION

This chapter discusses the results and contributions of the research work, and illustrates the connections between each of the individual studies. Where applicable, the relevance of this research work to the commercial fluid coking operation will also be discussed.

8.1 Key Contributions and Links Between Chapters

8.1.1 Chapter 2

Chapter 2 presents a study of attrition nozzles in fluidized beds. For some industrial applications, such as fluid coking, controlling the size distribution of the particles in a fluidized bed is extremely important in order to avoid poor fluidization. One method to control the size of the particles in the bed is to use attrition nozzles, which inject high velocity gas jets into the bed creating high shear regions and grinding particles together. Several studies have been published focusing on the effects of injecting subsonic jets on the attrition of particles in fluidized beds (Chen et al., 1980; Pacek and Nienow, 1991; Werther and Xi, 1993; Ghadiri et al., 1994; Wu et al., 1999; Boerefijn et al., 2000; Bentham et al., 2004). In addition, most of the experimental research on jet grinding is believed to have been done using straight tube nozzles. Only one experimental research study has been done using a nozzle with the contraction-expansion geometry typical of Laval nozzles (Benz et al., 1996). However, tests were required to determine the effects of nozzle geometry and gas properties on particle attrition when sonic velocity jets are injected into a fluidized bed.

An investigation on jet grinding characteristics using nozzles with an expansion section and operating at sonic conditions was performed. Different high velocity attrition nozzles and operating conditions were tested in order to determine the effects of fluidization velocity, nozzle size, nozzle geometry, bed material and attrition gas properties on the grinding efficiency. An empirical correlation was developed to estimate the grinding efficiency, which takes these factors into account.

$$\eta = 7.81 \times 10^{-7} \alpha \beta d_N^{1.131} U_{\text{sound,eq}}^{0.55} (\rho U_{\text{sound,eq}}^2)^{1.635} \left(\frac{U_g - U_{mf}}{U_{mf}} \right)^{0.494} \quad (8.1)$$

The predictions from this correlation were validated using the experimental data, and it was found that there was excellent agreement between the calculated values and the experimental values. The highest grinding efficiencies were obtained when larger diameter nozzles were used with an expansion region at the tip, operating at high flowrates using lower density gases with higher equivalent speeds of sound.

8.1.2 Chapter 3

An important aspect of particle attrition is the understanding and modeling of the particle breakage mechanisms. Austin (1971) developed a model introduced by Epstein (1948) and Reid (1965) to estimate the particle size distribution of ground particles after a known grinding time, given the initial size distribution. Most particle attrition models are based upon this model. These models developed for jet attritors are quite complex and require many empirical parameters that have to be experimentally determined. Baddour and Briens (2006) developed a simple, two-parameter model to describe jet milling of carbon nanotubes. However, as all the other models, it applies only to small fluidized beds where there is intense solids mixing.

A simple model was developed to describe the attrition mechanism when a sonic velocity gas jet is used to grind particles in a fluidized bed. This model uses a minimum of empirical parameters and takes into account the effect of solids mixing. The model, predicts two parameters, the proportion of unground particles in the fluidized bed, β , and grinding symmetry coefficient, γ , which represents the ratio of the volume of the small daughter particle to the volume of the large daughter particle. The model also predicts the particle size distribution of ground particles, and the particle breakage frequency, which can be applied to any sized fluidized bed. The results from this model were verified with experimental data that was obtained in Chapter 2. In addition, an empirical correlation was developed to predict the particle breakage frequency, F_m .

$$F_m = 3.33 \times 10^{-7} \alpha \beta^{-1.406} d_N^{2.918} U_{sound,eq}^{0.434} (\rho U_{sound,eq}^2)^{0.306} \left(\frac{V_g - U_{mf}}{V_g} \right)^{0.278} \quad (8.2)$$

This correlation uses the proportion of unground particles in the bed, as well as the same parameters that were used to predict the grinding efficiencies in Chapter 2. The experimental fraction of ground particles was found to be in good agreement with the values calculated using Equation 8.2. Both the particle breakage frequency, F_m , and the grinding efficiency, η , were dependent on the nozzle diameter, exit velocity, jet momentum and the fluidization velocity.

8.1.3 Chapter 4

Simple jet attritors require large amounts of gas to grind the particles effectively, and in fact, consume a large proportion of the overall steam requirements in the fluid cokers. If these attrition jets were improved, they may be able to achieve the same attrition rates while operating at a much lower gas flowrate. Previously, it had been found that simple jet attrition can be enhanced through the use of a target (Dunlop et al., 1958; Tasirin et al., 1999), opposing jets (Yates et al., 1991; Tasirin et al., 1999) or a draft tube accelerator (Smith et al., 1992). However, there may be other modifications and designs of attrition nozzles, not yet investigated, that could improve the grinding efficiency of particles in a fluidized bed.

In Chapter 2 it was found that attrition was improved when nozzles with larger diameters were used that created a larger cavity within the fluidized bed, and allowed for more particles to be entrained into the jet. In addition, it was found that higher fluidization velocities that increased particle entrainment also increased the grinding efficiencies.

As a result, nozzle designs which enhanced attrition by promoting the entrainment into the gas jet of particles and accelerating them to high speed have been developed and tested. It was found that when a target, draft tube, shroud, nozzle inserts, or spiral flow was used to enhance particle entrainment and mixing, the grinding efficiency was greatly increased.

In addition, the model developed in Chapter 3 was used to verify that the attrition mechanism did not change when either the draft tube or shroud were used. When compared to the Type C nozzle, the proportion of unground particles in the bed, β , was significantly lower for both the draft tube and shroud cases. In addition, the particle breakage frequency was significantly higher for the draft tube and shroud cases, when compared to the Type C nozzle. Various values of the grinding symmetry coefficient, γ , were tested for all three cases. The value of γ did not change when either the draft tube, or shroud were used; all three cases had a grinding symmetry coefficient of approximately 0.8. Since the grinding symmetry coefficient is fairly high, and the mother particle is splitting into two particles of fairly equal size, the primary attrition mechanism occurring in the bed is fragmentation, as opposed to abrasion, for both the Type C nozzle, as well as when either the draft tube or shroud are used.

Since it was found in Chapter 2 that particle entrainment played an important role in the particle grinding efficiency, tests were done which measured the particle entrainment for three types of nozzles: the Type C nozzle, the Type A nozzle and the shrouded nozzle. It was found that although the shrouded nozzle had the highest grinding efficiency, the Type A nozzle actually had a higher solids entrainment rate. Therefore, it can be concluded that the way in which the particles are entrained affects the particle grinding rate more than the amount of solids that are entrained into the jet. The reason that the shroud was superior to the Type A nozzle was not that it entrained more solids, but that it entrained more solids closer to the nozzle tip where the momentum is the greatest, allowing the particles to be accelerated to a higher velocity and, therefore, resulting in more efficient grinding.

8.1.4 Chapter 5

In addition to particle attrition, the initial contact between the injected bitumen and fluidized coke particles is an important aspect of the fluid coking process. Uniform contact between the liquid droplets and entrained particles is essential for high yields. To prevent slow cracking and to avoid heat or mass transfer limitations, the bitumen must contact a large number of coke particles quickly and uniformly. Therefore, the greater the number of hot coke particles with which the liquid comes into contact and the better

the dispersion of the liquid both on the surface and between the particles, the better the yield. As a result, methods to improve the mixing between the liquid feed and the fluidized particles are required.

In Chapter 4 one technology that was found to improve the grinding efficiency significantly, was a draft tube that was placed downstream of the nozzle. The draft tube enhanced the migration of particles from the low velocity peripheral region to the high velocity central region of the jet. Particles in the central region were accelerated to higher velocities and were much more likely to fragment when hitting the dense bed of particles at the tip of the jet. The increased mixing and acceleration of the particles resulted in an increased grinding efficiency. This technology which increased the particle mixing and acceleration was applied to a gas-liquid-solid system to improve the contact between injected liquid and fluidized particles.

Chan et al. (2004) devised a draft tube mixer similar to the one used in the attrition nozzle study. This draft tube was positioned co-axially downstream of an atomization nozzle and enhanced the contact between the liquid spray droplets and the fluidized particles. However, a measurement technique was required to characterize the solid-liquid contact when a gas-liquid jet was injected into a fluidized bed either as a free jet or into a draft tube mixer. There have been several studies done which used temperature measurements to investigate the injection of evaporative liquid jets into fluidized beds (Shakhova and Mineav, 1973; Smith and Nienow, 1982; Zhu et al., 2000; Wang and Zhu, 2003; Bruhns and Werther, 2004). However, droplet evaporation was a key factor in the phase mixing and flow characteristics of these evaporating spray jets, and these methods could not be adapted to applications with a non-vaporizing liquid.

As a result, a technique was developed to determine the local, instantaneous quality of solid-liquid mixing when a gas-liquid spray jet was injected horizontally into a fluidized bed. A thermal tracer technique was developed in which cold liquid was injected into the bed and thermocouples obtained time averaged temperature readings. A heat balance was performed and the local liquid to solid ratio (L/S) was determined at various locations within the spray region. It was found that the draft tube resulted in better mixing between the liquid and the solids than the free jet. The draft tube created turbulence within the draft tube and increased the solid-liquid mixing.

8.1.5 Chapter 6

The use of a draft tube helped to improve the solid-liquid mixing when a horizontal jet was injected into a fluidized bed. However, another revolutionary technology was developed in Chapter 6 which improved the solid-liquid mixing even further. Downers operate under stable, almost plug-flow conditions. Therefore, a uniform dispersion of solids and liquid must be performed in a mixing chamber upstream of the downer. A downer equipped with a mixing chamber at its entrance was found to greatly improve the solid-liquid mixing. A measurement technique was required in order to characterize the quality of mixing between injected liquid and fluidized particles. The majority of the work conducted to measure local solids flow and mixing patterns in fluidized beds focused on radiation absorption methods such as x-ray absorption tomography, and electrical capacitance methods (Wei et al., 1994; Soong et al., 1995; Schiewe et al., 1999; Hage and Werther, 2001). However, these techniques resulted in poor spatial resolution and could not be easily adapted to a gas-liquid-solid system.

Therefore, an efficient method was developed to determine the local quality of solid-liquid mixing on a short time scale. The measurement technique used two types of measurements in order to obtain the cross-sectional distribution of liquid-to-solid ratios. First, temperature measurements, similar to the measurement technique used in Chapter 5 were used to characterize the solid/liquid distribution and, second, tribo-electric probes were used to obtain the local solids fluxes. These techniques were used to determine the mixing chamber geometries which provided the best solid-liquid mixing. When four spray nozzles were used, the nozzle configuration that resulted in the best mixing results occurred when all the nozzles were impacting each other at a focal point. This force broke up the dense phase of solids in the centre of the mixing chamber and dispersed the solids more evenly throughout the downer cross section. For the case when eight injection nozzles were used, the best mixing results occurred when some of the spray nozzles were impacting with each other, and some were creating a swirling pattern within the mixing chamber. These technologies developed in Chapter 6 may be applied to the fluid coking process in the future in order to improve the initial contact between the injected bitumen and fluidized coke particles.

8.1.6 Chapter 7

To achieve the best mixing results, the mixing chamber should provide a stable solid-liquid dispersion. A measurement technique to measure the stability of the solid-liquid flow in the downer was developed. Previous studies had investigated the stability of liquid sprays into conventional fluidized beds. However, there had not been any studies done which investigated the stability of gas-liquid jets injected into a circulating fluidized bed. Therefore, a novel technique was developed to determine the stability of the flow in the downer, which applied the tribo-electric technique that was previously used in Chapter 6 to characterize the solid-liquid contact.

The tribo-electric probes were used to obtain the local solids flowrates and their signals were then analyzed to determine the stability of the solids flow. A variety of different startup conditions and injection liquids were tested in order to determine their effects on the stability of the system. It was found that the system was non-chaotic and non-cyclic. The local standard deviations for each run were fairly large, indicating that the system was not very stable locally. However, similar structures were observed between runs, which suggested that the system was stable globally.

8.1.7 Appendix A

In Appendix A, a novel half jet was injected into a fluidized bed, which allowed for qualitative observations of the effect of the shroud. By conducting visualization tests with both a free jet (Type C nozzle) and a shrouded jet, the flow patterns and the behaviour of the solids in the vicinity of the jet could be understood. It was found that when the shrouded nozzle was used the gas jet entrained a larger amount of solids while entraining a significantly lower volume of gas. The shrouded jet was narrower, more stable, and penetrated less, as a result of the increased solids entrainment rate. It was observed that while the solids moved in intermittent waves towards the free jet, the solids moved in a smooth continuous manner towards the shrouded jet at a faster rate. These findings help to explain why the shrouded nozzle had a higher grinding efficiency than any of the other nozzle geometries.

8.1.8 Appendix B

During the experimental work performed for the study in Chapters 2 and 4, some of the particles in the fluidized bed would become very fine after a significant number of experiments. As a result, the solids needed to be changed frequently. It would be extremely useful to have a method to continuously monitor the proportion of fines in a fluidized bed. Therefore, a study was conducted in which tribo-electric measurements were taken at different fluidization velocities while varying the proportion of fines in the bed. It was noted that the tribo-electric signal increased with the fluidization velocity and the proportion of fines in the bed.

A correlation was developed to predict the proportion of fines in the bed by using the mean value of the tribo-electric signal and the fluidization velocity of the bed. This was the first online bed fines detection method reported in the literature. Currently, the most common method of measuring for fines in a fluidized bed is to take a particle sample and use a laser diffraction analyzer to get the particle size distribution. Another method is to collect fines in a cyclone or filter during fluidization, which are then weighed to give the weight percentage of fines relative to the mass of the bed. Both of these methods are slow, labor-intensive, and require direct access to the particles in the fluidized bed system. Knowledge of the proportion of fines in a fluidized bed is an important parameter needed to maintain good fluidization quality in the bed, and to prevent too many particles from leaving the cyclones in the gas stream. Furthermore, in an experimental setting, the measurement of the proportion of fines in a fluidized bed can also be a useful tool to evaluate the performance of nozzles or devices that increase or decrease the particle size.

8.1.9 Appendix C

Another technology from Chapter 4 that was found to improve particle attrition considerably was the shroud. The shroud enhanced solids entrainment into the jet by creating a dense region of non-fluidized solids near the tip of the injection nozzle. The particles were constantly being entrained into the jet and replenished with fresh solids.

An additional piece was added to the tip of the gas-liquid injection nozzle used in Chapter 5 in order to simulate the shroud apparatus that was previously used in the

attrition nozzle study. The measurement technique which was developed in Chapter 5 was applied to the case when a shrouded nozzle was used. Tests were conducted with the shrouded nozzle, as a free jet and in conjunction with the draft tube mixer, and the results were compared to the values obtained with the nozzle used in Chapter 5. The shrouded nozzle resulted in more uniform contact between the solids and the liquid, especially at distances further downstream of the nozzle tip. When the shrouded nozzle was used, the momentum of the jet was increased and re-circulation eddies were created near the nozzle tip. As a result, more solids were entrained into the jet and, therefore, the liquid came into contact with more solids, minimizing areas with high liquid-to-solid ratios.

8.2 Comparison Between the Downer and the Draft Tube Mixer

In order to demonstrate that the mixing in the downer mixing chamber (Chapter 6) was superior to the mixing in the conventional fluidized bed equipped with a draft tube mixer (Chapter 5), a comparison between the two studies was done. Table 8.1 shows a summary of the results obtained in both the downer and the draft tube.

Table 8.1: Table of Data Comparing Downer to Draft Tube

Parameter	Downer	Draft Tube
Diameter (mm)	76	19
Flowrate of Solids, F_s (kg/s)	1	0.68
Flowrate of Liquid, F_L (kg/s)	0.05	0.067
F_L/F_s	0.05	0.1
Measured Average L/S in Cross-Section	0.04	0.35

As shown in Table 8.1, the draft tube diameter was 4 times smaller than the diameter of the downer, and slightly more liquid was injected into the draft tube. Therefore, it would be expected that the mixing in the draft tube would be superior to the downer, due to the extra turbulence that would be created. However, due to the small entrainment of solids into the draft tube, the average L/S in the draft tube was relatively high, when compared to the downer. This indicates that solids entrainment into the gas-liquid jet is a very important parameter. The downer mixing chamber configuration allowed more solids to be in contact with the liquid, thus improving the solid-liquid mixing.

The importance of solids entrainment into the spray was also observed in the studies involving gas-only jets. The attrition nozzles tested in Chapter 4, such as the nozzle inserts, helped to entrain more particles into the jet, which helped to increase their grinding efficiencies. In future work, these nozzle geometries could be used with a gas-liquid spray nozzle to increase particle entrainment and improve the solid-liquid mixing.

To illustrate the importance of the initial liquid-solid mixing, House et al. (2004) developed a simple model to predict its effect on coker yields, and found that the coke yield increased with increasing L/S. This model can be used to show the effects on coker yields when using either a draft tube or a downer. A plot (Figure 8.1) of the cumulative liquid distribution as a function of liquid to solid ratio (L/S) was created for the free jet, the draft tube and the downer case in order to quantify the mixing, and its impact on the coking reaction. As shown in this figure the downer greatly improves the liquid/solid mixing by increasing the amount of wetted solids and achieving a more uniform liquid/solid mixture. Using this cumulative liquid distribution plot, the average L/S for each case was then calculated. The free jet resulted in an average L/S of 0.269, the draft tube resulted in an average L/S of 0.175, and the downer resulted in an average L/S of 0.052. The model from House et al. (2004) was then applied to these three cases in order to determine the percent coke yield, and it was found that the free jet resulted in a coke yield of 22.4%, the draft tube resulted in a coke yield of 17.8% and the downer resulted in a coke yield of 11.9%. The model suggests that the downer will reduce the coke yield by approximately 33% when compared to the case when a draft tube is used, and by 47% when compared to the case when a free jet is used.

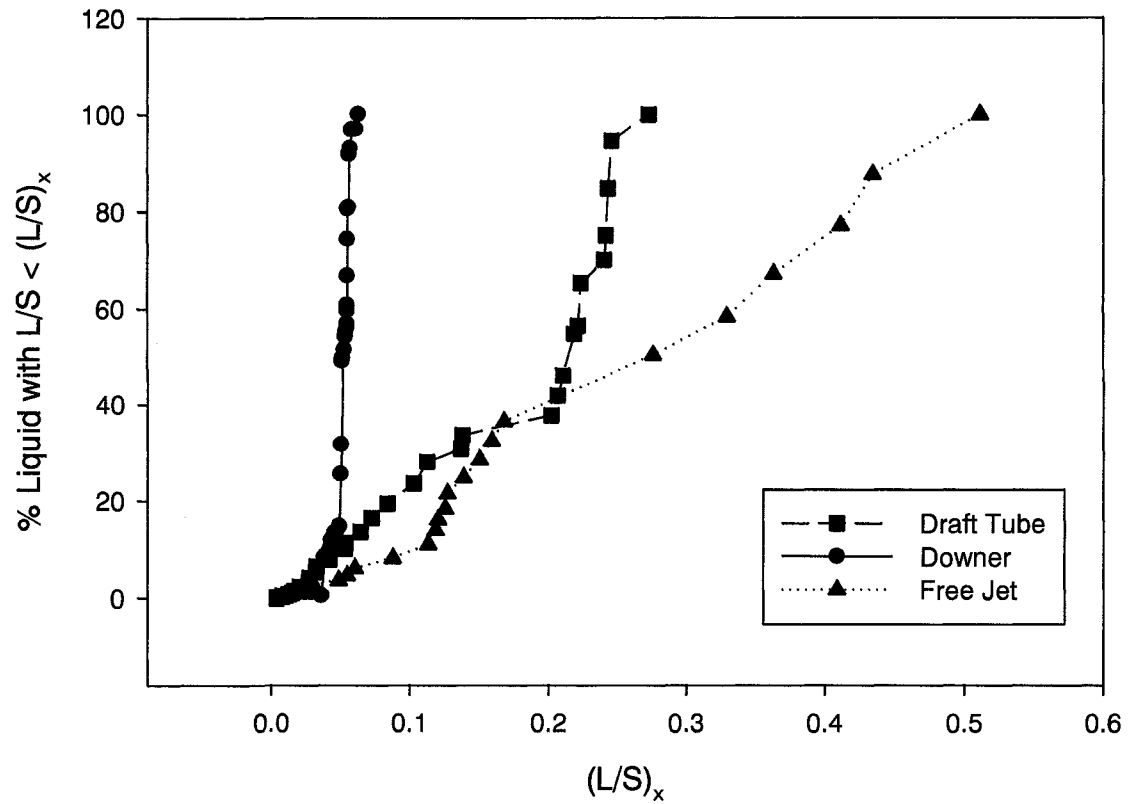


Figure 8.1: Cumulative Liquid Distribution for the Free Jet, Draft Tube and Downer

8.3 Nomenclature

d_N	Nozzle diameter (m)
F_L	Liquid mass flowrate (kg/s)
F_m	Particle breakage rate (mass of particles/s)
F_S	Solids mass flowrate (kg/s)
L/S	Liquid to solid ratio (-)
$U_{\text{sound,eq}}$	Equivalent speed of sound (m/s)
U_g	Fluidization velocity (m/s)
U_{mf}	Minimum fluidization velocity (m/s)

Greek Letters

α	Solid coefficient (-)
β	Equation 8.1: Geometry coefficient (-); Equation 8.2: Proportion of original particles that have not been ground (%)
η	Grinding efficiency (m ² /kg)
ρ	Gas density at nozzle throat (kg/m ³)

8.4 References

- Austin, L., "A Review: Introduction to the Mathematical Description of Grinding As a Rate Process", *Powder Technol.*, **5**, 1-17 (1971).
- Baddour, C., Briens, C., "Modeling the Grinding Process of Carbon Nanotubes", Manuscript Submitted to *AIChE J.*, (2006).
- Bentham, A., Kwan, C., Boerefijn, R., Ghadiri, M., "Fluidised-Bed Jet Milling of Pharmaceutical Powders", *Powder Technol.*, **161**, 233-238 (2004).
- Benz, M., Herold, H., Ulfik, B., "Performance of a Fluidized Bed Jet Mill as a Function of Operating Parameters, *Int. J. Miner. Process.*, **44-45**, 507-519 (1996).
- Boerefijn, R., Gudde, N., Ghadiri, M., "Review of Attrition of Fluid Cracking Catalyst Particles", *Adv. Powder Tech.*, **11**, 145-174 (2000).
- Bruhns, S., Werther, J., "On the Mechanism of Liquid Injection into Fluidized Bed Reactors", *Fluidization XI*, U. Arena, R. Chirone, M. Miccio, P. Salatino, (Eds.) Engineering Conferences International, Brooklyn, NY: 2004, pp. 67 – 74.
- Chan, E., McDougall, S., Knapper, B., "Nozzle/Mixer Assembly", *United States Patent*: 7 025 874 (2004).
- Chen, T., Sishtla, C., Punwani, D., Arastoopour, H., "A Model for Attrition In Fluidized Beds", in: J. Grace, J. Matsen, (Eds.), *Fluidization*, Engineering Foundation, New York, NY: 1980, pp. 445 – 452.
- Dunlop, D., Griffin, L., Moser, J., "Particle Size Control in Fluid Coking", *Chem. Eng. Prog.*, **54**, 39-43 (1958).
- Epstein, B., "Logarithmico-Normal Distribution in Breakage of Solids", *Ind. Eng. Chem.*, **40**, 2289-2291 (1948).
- Ghadiri, M., Cleaver, J., Tuponogov, V., Werther, J., "Attrition of FCC Powder in the Jetting Region of a Fluidized Bed", *Powder Technol.*, **80**, 175-178 (1994).
- Hage, B., Werther, J., "The Guarded Capacitance Probe -- A Tool for the Measurement of Solids Flow Patterns in Laboratory and Industrial Fluidized Bed Combustors", *Powder Technol.*, **93**, 235-245 (2001).
- House, P., Saberian, M., Briens, C., Berruti, F., Chan, E., "Injection of a Liquid Spray into a Fluidized Bed: Particle-Liquid Mixing and Impact on Fluid Coker Yields", *Ind. Eng. Chem. Res.*, **43**(18), 5663 – 5669 (2004).
- Pacek, A., Nienow, A., "Application of Jet Grinding to Fluidised Bed Granulation", *Powder Technol.*, **65**, 305-310 (1991).

- Reid, K., "A Solution to the Batch Grinding Equation", *Chem. Eng. Sci.*, **20**, 953-963 (1965).
- Schiewe, T., Wirth, K., Molerus, O., Tuzla, K., Sharma, A., Chen, J., "Measurements of Solid Concentration in a Downward Vertical Gas-Solid Flow", *AIChE J.*, **45**, 949-955 (1999).
- Shakhova, N., Minaev, G., "Investigation of the Temperature Field in the Spray Zone of a Granulator with a Fluidized Bed", *Int. Chem. Eng.*, **13** (1), 65 - 68 (1973).
- Smith, P., Nienow, A., "On Atomising a Liquid Into a Gas Fluidized Bed", *Chem. Eng. Sci.*, **37** (6), 950 - 954 (1982).
- Smith, L., Mastalski, H., "Throughput Efficiency Enhancement of Fluidized Bed Jet Mill", *United States Patent*, 5 133 504 (1992).
- Soong, C., Tuzla, K., Chen, J., "Experimental Determination of Cluster Size and Velocity in Circulating Fluidized Bed", *Fluidization VIII*, J.-F. Large, C. Laguerie (Eds.), Engineering Foundation: New York, 1995, pp. 219 - 227.
- Tasirin, S., Geldart, D., "Experimental Investigation on Fluidized Bed Jet Grinding", *Powder Technol.* **105**, 337-341 (1999).
- Wang, X., Zhu, C., "Concentric Evaporating Spray Jets in Dilute Gas-Solids Pipe Flows", *Powder Technol.*, **129**, 59 - 71 (2003).
- Wei, F., Wang, Z., Jin, Y., Yu, Z., Chen, W., "Dispersion of Lateral and Axial Solids in a Cocurrent Downflow Circulating Fluidized Bed", *Powder Technol.*, **81**, 25-30 (1994).
- Werther, J., Xi, W., "Jet Attrition of Catalyst Particles in Gas Fluidized Beds", *Powder Technol.*, **76**, 39-46 (1993).
- Wu, S., Baeyens, J., Chu, C., "Effect of the Grid-Velocity on Attrition in Gas Fluidized Beds", *Can. J. Chem. Eng.*, **77**, 738-744 (1999).
- Yates, J., Cobbinah, S., Cheesman, D., Jordan, S., "Particle Attrition in Fluidized Beds Containing Opposing Jets", *AIChE Symposium Series* **87**, 13-19 (1991).
- Zhu, C., Wang, X., Fan, L.-S., "Effect of Solids Concentration on Evaporative Liquid Jets in Gas-Solid Flows", *Powder Technol.*, **111**, 79 - 82 (2000).

CHAPTER 9

CONCLUSIONS AND RECOMMENDATIONS

A summary of the results, the major findings and conclusions drawn from this work are outlined below. In addition, several suggestions are proposed for future studies.

9.1 Conclusions

1. Fluidization velocity, nozzle size, nozzle geometry, bed material and attrition gas properties all have an effect on the particle grinding efficiency when a sonic gas jet is injected into a fluidized bed. Larger diameter nozzles with an expansion region at the tip, operating at high flowrates using lower density gases with higher equivalent speeds of sound, resulted in the highest grinding efficiencies. In these cases more particles were entrained into the jet and had a higher probability of grinding with each other and with particles located in the dense phase surrounding the jet cavity, thus resulting in an increased grinding efficiency.
2. An empirical correlation was developed to estimate the grinding efficiency when a sonic gas jet was injected into a fluidized bed. This correlation, which took into account solid properties, nozzle scale, nozzle geometry, fluidization velocity and gas properties, was able to accurately predict the grinding efficiencies for nozzles operating at sonic conditions at the nozzle throat.
3. A model was developed which predicts the particle breakage rate, the proportion of original particles that were not ground, and the size distribution of particles in a fluidized bed after they have been ground by the injection of a sonic velocity gas jet. The results were verified using experimental data obtained using various nozzle designs and different operating conditions. The particle breakage rate increased as the fluidization velocity and nozzle diameter were increased. The mass of particles broken per unit time remained constant as the grinding time, the mass of solids in the bed and the column size increased. Therefore, once the

particle breakage frequency is known for a given nozzle design and size, it can be used to predict the attrition results in larger beds.

4. A significant increase in the grinding efficiency was observed when either a target, draft tube, shroud, nozzle inserts, or spiral flow was used to enhance particle entrainment and mixing. The best grinding efficiencies were obtained when the shroud and draft tube were used in conjunction with each other. The best results, without the addition of internals to the bed, were obtained with the Laval-type nozzle equipped with 3 nozzle inserts.
5. Although the average solids entrainment into the jet was a significant factor contributing to the grinding efficiency for each nozzle type, other factors such as the mechanism of solids entrainment into the jet, and the location at which the solids were entrained played a significant role. For example, the reason that the shroud has a higher grinding efficiency than the Type A nozzle is not that it entrains more solids, but that it entrains solids as close to the nozzle tip as possible, causing them to accelerate to higher velocities and, therefore, grind more effectively.
6. A measurement technique was developed to evaluate the solid-liquid mixing quality within the spray region of a liquid jet that was horizontally injected into a fluidized bed of particles. This technique is an efficient method to determine the liquid/solid distribution within the feed jet cavity, as well as within a draft tube mixer placed downstream of the nozzle.
7. Uniform and rapid contact between sprayed droplets and particles can be achieved by placing a horizontal draft tube downstream of a gas-liquid spray nozzle in a fluidized bed. Using a nozzle with a shrouded tip also enhances the solid-liquid mixing, when compared to the mixing in a free jet.
8. Measurement techniques were developed to evaluate the solid-liquid mixing quality within the cross sectional area of a downer when a mixing chamber was located at its entrance and liquid injected into down-flowing particles. The first

technique used both temperature and tribo-electric measurements to determine the liquid/solid distribution within the downer. The second technique used only tribo-electric signals obtained from liquids with varying concentrations of water to determine the liquid/solid distribution within the downer. The results obtained using these techniques indicated that certain mixing chamber geometries provided very good and rapid contact between sprayed droplets and particles. A circular orifice provided better liquid-solid mixing than an annular orifice. Simple mixing chamber geometries where the spray jets impacted with each other near the axis of the mixing chamber provided the best mixing results when four nozzles were used. However, mixing chambers equipped with eight nozzles, oriented in such a way that a swirling motion was created within the mixing chamber, were found to produce the best liquid/solid mixing results.

9. A measurement technique was developed to evaluate the stability of flow within the cross sectional area of a downer when a mixing chamber was located at its entrance and liquid injected into down-flowing particles. The technique used tribo-electric measurements to determine the stability of the system as well as the effects of changing the startup conditions. Results from the various signal analysis techniques indicated that the system was non-chaotic and non-cyclic. The local standard deviations for each run were fairly large, indicating that the system was not very stable locally. However, similar structures were observed between runs, which suggests that the system was stable globally. Although the regions containing high and low liquid to solid ratios were situated in different locations within the downer cross section, each replicate run had approximately the same average distribution of the liquid to solids ratio (L/S) over the whole downer cross-section. This indicated that although between runs the L/S values were shifted within the downer cross section, the overall performance remained stable.

9.2 Recommendations

1. It was found that placing a shroud on the tip of a sonic velocity gas attrition jet greatly improved the grinding efficiency in a fluidized bed. However, this shroud has not been completely optimized. Future work should be done to fully optimize the shroud and determine the effects of parameters such as the distance between the nozzle tip and the base of the shroud, shroud depth, shroud diameter and shroud shape. In addition, the draft tube which was also found to increase the particle grinding efficiency has not been completely optimized. Parameters such as distance between the draft tube and the nozzle tip, draft tube length, diameter and shape should be studied to determine their effects on particle attrition.
2. Tests should be performed at large scale using the various attrition nozzles both as a free jet and in conjunction with the shroud and draft tube to confirm the effect of scale on the grinding efficiency. Attrition tests should also be performed at high temperatures to determine if particle attrition properties change with temperature.
3. Various enhancements to the attrition nozzle such as nozzle inserts helped to increase the grinding efficiency by increasing the particle entrainment into the jet. These nozzles might help to improve the contact in solid-liquid systems. Further tests could be performed using these nozzles as gas-liquid injectors.
4. The thermal tracer technique developed to quantify the liquid-solid mixing when a gas-liquid jet was injected into a fluidized bed should be applied to a large scale bed to verify the results found at a small scale. Devices such as the draft tube mixer and the shrouded nozzle tip should be tested to determine their benefits at a commercial scale. In addition, tests with the draft tube and shrouded nozzle should be performed at high temperatures to determine if temperature has an impact on their performance.
5. Since a large proportion of the total steam flowrate is used in the commercial fluid cokers for particle attrition, methods to decrease the steam consumption would be very useful. One way to decrease the amount of steam entering the fluid coker

would be to couple the attrition nozzles with the feed dispersion nozzles. Quite often agglomerates are formed at the tip of the gas-liquid feed jet. By injecting both the liquid feed and the high velocity gas attrition nozzles in the vicinity of each other, the attrition nozzles could help to break up the agglomerates before they are formed. The extra attrition gas could also help to entrain more particles into the liquid jet, thus increasing the solid-liquid mixing.

6. A downer equipped with a mixing chamber at its entrance was found to provide excellent solid-liquid mixing when certain mixing chamber geometries were used. However, only one type of injection nozzle was tested; a simple centrally located hypodermic needle of liquid surrounded by an annular flow of atomization gas. The effects of nozzle geometry should be tested to determine if different nozzle designs and geometries would result in better mixing between the solids and liquid.
7. The tests performed in the downer mixing chamber were all performed at a constant global liquid to solid ratio of 0.05. The liquid flowrate through the injection nozzles, and the solids flowrate entering the mixing chamber should be varied to determine the effects of the global liquid to solid ratio on the mixing quality. Certain mixing chamber geometries may perform better at a different global liquid to solid ratio.

APPENDIX A

Visualization of the Effect of a Shroud on Entrainment of Fluidized Solids into a Gas Jet

Craig Hulet¹, Jennifer McMillan¹, Cedric Briens¹, Franco Berruti¹, Edward W. Chan²

*¹Department of Chemical and Biochemical Engineering
The University of Western Ontario
1151 Richmond Street
London, Ontario, Canada N6A 5B9*

*²Synchrude Canada Ltd
Edmonton Research Centre
9421 – 17 Avenue
Edmonton, Alberta, Canada T6N 1H4*

A.1 Introduction

Submerged gas jets issuing into fluidized beds are used in many different industries including drying, particle coating, granulation, scrubbing, heating and cooling of solids, solids mixing, shale pyrolysis, coal gasification, combustion, and attrition or grinding (Zhong et al., 2006). Gas jets are also used in multiple industries to transport solid particles via eductors (Bohnet and Teifke, 1985) to other fluidized beds via “L”, “J” or “V” valves or particulate products to storage hoppers. One critical component that all these systems have in common is the requirement that particulate solids are entrained by the motive gas, whether to be attrited, combusted, coated, heated or cooled, or dried. Therefore, it is important to have a fundamental understanding of how the gas and surrounding medium interact – to understand the flow patterns and how the solids behave in the vicinity of the nozzle jet.

A.1.1 Theory

The benchmark review of Massimilla (1985) provides an excellent overview of the considerable body of work that exists on the interaction of free gas jets in fluidized beds. However, the majority of studies concern vertical jets typically found in the grid region of industrial units (Ariyapadi, 2003). Generally, most models of gas jets submerged in fluidized beds are based on the theory of turbulent jets proposed by Abromovich (1963) such as those of De Michele et al. (1976), Donadono et al. (1980) and Xuereb et al. (1991a, 1991b). Figure A.1 illustrates the three main regions of a typical axisymmetrical submerged turbulent jet, which include the potential core region, the transition region, and the fully developed region.

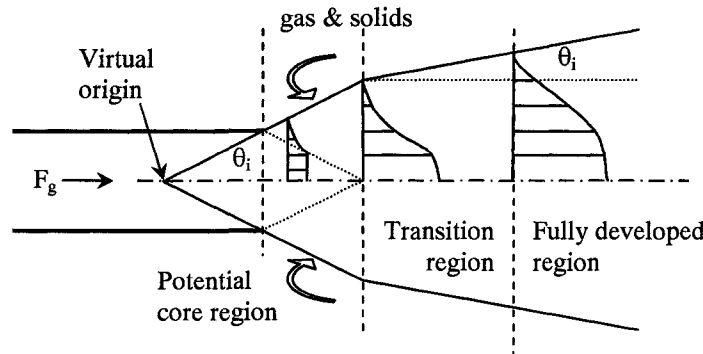


Figure A.1: Illustration of a Typical Turbulent Submerged Jet (Ariyapadi et al., 2003)

A submerged jet issuing from a nozzle into a fluidized bed acts as a source of momentum and energy (Sharpe, 1994). Many distinctions need to be made in order to characterize their behaviour within fluidized beds, such as whether the flow is laminar or turbulent, subsonic or sonic, and as to the density of the jet in relation to that of the surrounding medium. In general, the flow field may be characterized by superimposing fluctuating motion onto the steady mean flow field using the so-called statistical approach (Equation A.1):

$$u = \bar{u} + u' \quad (\text{A.1})$$

where u is the axial velocity comprised of the mean velocity \bar{u} and the fluctuating component u' . The fluctuating component is a result of the presence of unsteady eddies

and vortices. A submerged jet may be considered turbulent, when the jet Reynolds number exceeds 3000 (Equation A.2)

$$N_{Re} = \frac{\rho V d}{\mu} \quad (A.2)$$

where ρ , μ , and V are the motive gas density, viscosity, and velocity at the nozzle exit, respectively, and d is the nozzle outlet diameter.

For a turbulent submerged jet $\partial u / \partial y$, where y is the radial dimension, is large due to the relatively high velocity of the entering gas and the relative stagnation of the surrounding medium this shear layer. It has been generally proven that the axial momentum may be considered constant and does not depend on how the jet disperses. Therefore, when the conservation of mass is taken into consideration fluid must be entrained into the jet from the surroundings (Sharpe, 1994) as the turbulent shear layers transfer momentum to the surrounding medium, which also causes the jet to expand. This expansion may also create a slight depressurized zone which would draw even more fluidization gas towards the jet, especially near the potential zone where the rate of shear is the greatest. It has been observed in previous studies that the majority of entrainment occurs near the nozzle tip in the potential zone region (Merry, 1971; Xuereb et al., 1991; Felli, 2002). The fluid that is drawn towards the jet as a result of the shear forces combined with the presence of a depressurized zone create drag on the fluidized particles and entrain them towards the jet as well. Where the solids enter the jet, and how deep they penetrate, will affect the solids acceleration and the jet expansion (Bohnet & Teifke, 1985). Particle size and density, as well as the jet momentum, will affect the entrainment rate and jet penetration (Merry, 1971; Ariyapadi, 2003). For horizontal jets, the effects of gravity, buoyancy, and cross-flow between the jet and fluidization gas that acts perpendicular to the jet may influence the jet behaviour. Xuereb et al. (1992) and Ariyapadi et al. (2003), among others, have developed models to predict gas and solids entrainment into horizontal jets.

The behaviour described above will be altered by the presence of any walls, sudden contractions (e.g. the entrance to the ESE draft tube described by Hulet et al., 2003) or sudden enlargements. Idelchek (1994) provides a thorough discussion of the

flow patterns and methods of reducing the resistance to flow at the entrance into tubes and conduits. In such situations, the sudden expansions or contractions create strong recirculation zones, which may create relative low pressure regions.

Following the discussions of Bohnet and Teifke (1985) and Idelchek (1994) it was decided to investigate the effects of altering the region surrounding the jet in order to affect the method of contact between the jet and the fluidized bed. This was accomplished using several different configurations of “shrouds” that formed physical barriers either around the nozzle tip or draft tube inlet, or both. Videos were recorded using a special transparent plate on the wall of the fluidized bed of the gas and solids flow patterns for a half-jet with and without a shroud. Presented below are the original videos and observations derived from the two simple experiments.

A.2 Materials and Methods

The videos were created using a fluidized bed having a rectangular cross section (1.2 m x 0.1 m) and 1.2 m tall as shown in Figure A.2. Typically, this fluidized bed is used for measuring the entrainment rate of fluidized solids into a submerged gas or gas-liquid jet and into a cylindrical draft located axially downstream from the nozzle (Hulet et al., 2003). This is the reason why the fluidized bed (including the plenum chamber) is divided into 2 separate compartments of equal cross section. The access portals shown in Figure A.2 allowed for access to the nozzle and draft tube. A Canon 4 MP digital camera was used to record the video images which are viewable as mpg files.

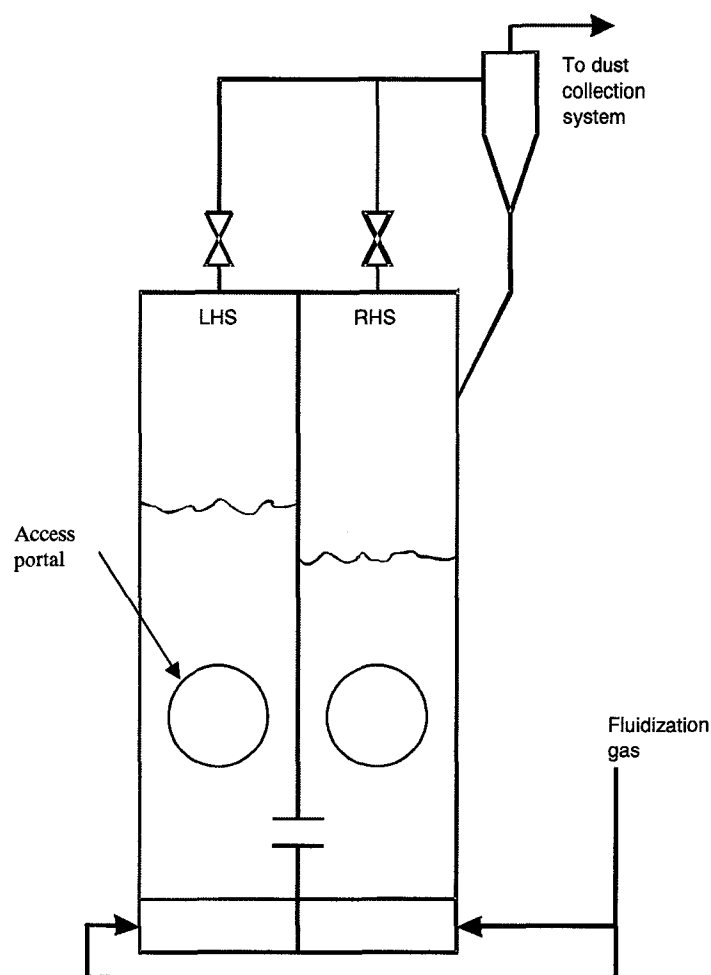


Figure A.2: Side View of 2.5D Fluidized Bed Used for the Half-Jet Study

The half-jet videos were made by replacing one of the circular access portals with a special circular plate (refer to Figure A.3). In the centre of the round plate a rectangular glass plate, approximately 0.0635 m by 0.15 m and 0.0127 m thick has been embedded flush to the inside surface (the overall plate thickness is approximately 0.0191 m). This glass plate serves two purposes: it provides resistance to the strong erosion forces from the entrained solids and provides for easier observation into the bed. From the outside, the nozzle traverses the access portal normal to the glass plate. A 90° elbow directs the nozzle tube parallel to the inside face. The nozzle orifice diameter (0.0016 m i.d.) is completely round so as not to create a distorted velocity distribution in the gas exiting the nozzle, with the centerline located 0.0016 m from the inner plate surface.

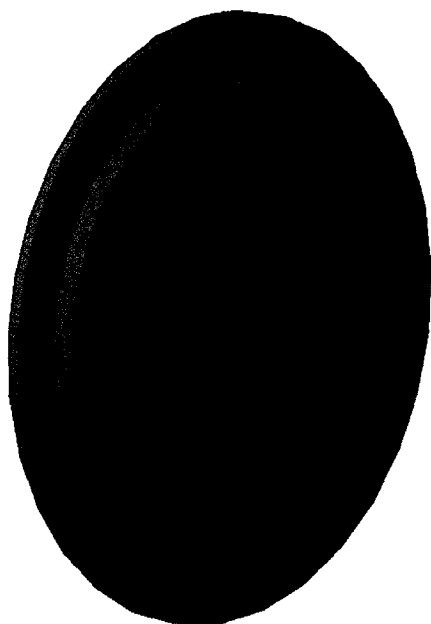
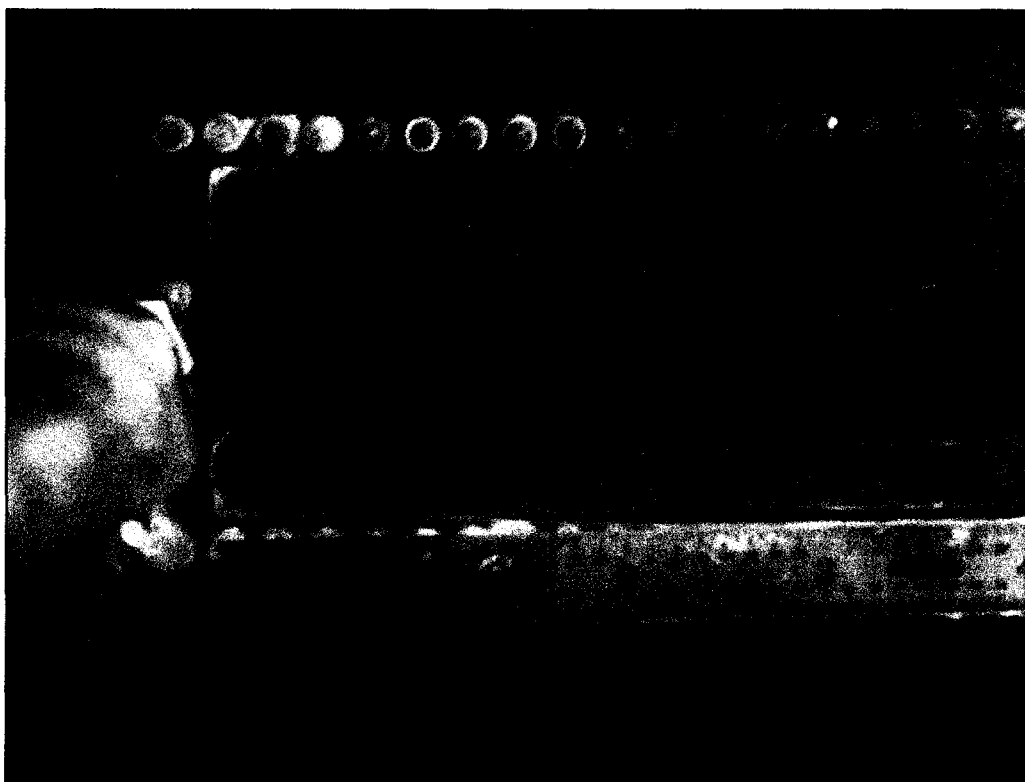


Figure A.3: Half-Jet Nozzle Assembly Showing the Glass Plate, Nozzle and Semi-Cylindrical Shroud

Fluid coke particles ($135\ \mu\text{m}$ Sauter mean diameter and particle density $1450\ \text{kg/m}^3$) were used for bed material and air was used for both the motive and fluidization gas. The superficial fluidization velocity U_0 was maintained at $0.11\ \text{m/s}$. The motive gas flow was in the sonic regime with a mass flow rate F_g of $0.0039\ \text{kg/s}$ and an upstream pressure of approximately 200 psig. All flow rates were controlled using calibrated sonic nozzles and pressure transducers. The semi-cylindrical shroud length and inner diameter were $0.0428\ \text{m}$ and $0.0349\ \text{m}$, respectively.

A.3 Results and Discussion

The videos with and without the shroud may be accessed by [double] clicking on the corresponding links below.



MOV00958_free jet.MPG

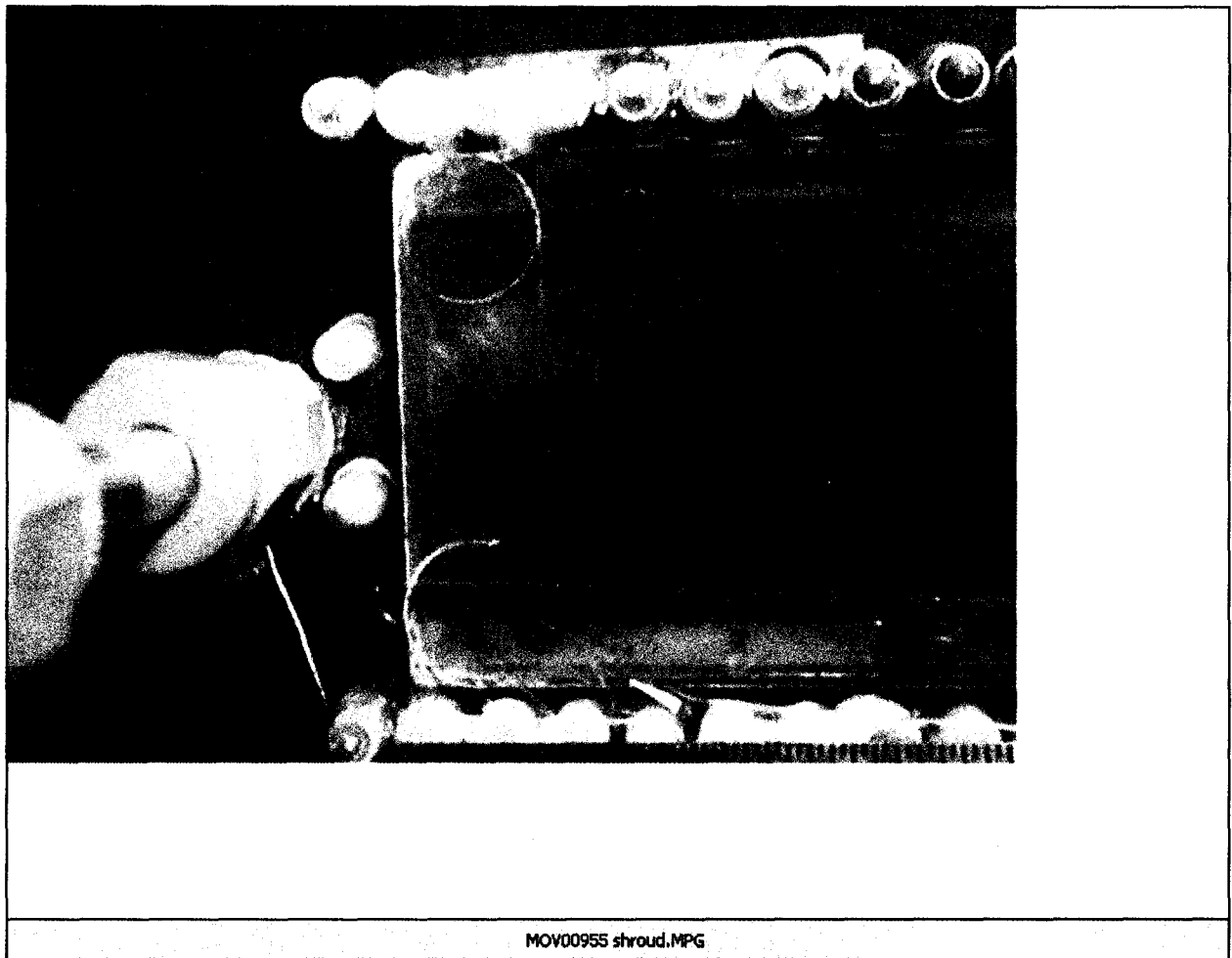


Figure A.4 illustrates the general behaviour associated for both experiments: (a) without a shroud and (b) with a shroud. The discussion below mimics that from Hulet et al. (2006). The discussion is summarized below in Table A.1.

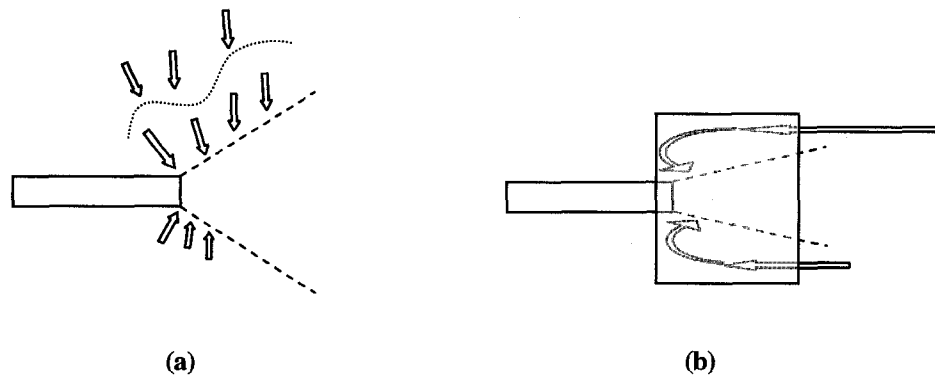


Figure A.4: Illustration of Entrainment into Horizontal Gas Jet (a) Without Shroud and (b) With Shroud. The Arrows Indicate the Direction of Solids Flow and the Relative Velocity (The Jet Expansion Angle Has Been Exaggerated for the Illustration).

A.3.1 Free Jet

When there is no shroud, the solids were observed to move in “waves” or “pulses” towards the jet. The solids enter primarily at the nozzle tip (at a relatively higher velocity) but are also observed entering along the entire length of the jet (the solids movement above the jet being the most visible) (Chen and Weinstein, 1993; Xuereb et al., 1991a,b). The non-shrouded jet is relatively less stable as it interacts with the cross flow of fluidization gas and encounters rising bubbles, which divert the jet.

A.3.2 Shrouded Jet

The change in flow patterns when the shroud is installed is quite striking. In this experiment the solids were observed to move horizontally, countercurrent to the motive gas jet – even those solids already near the jet boundary – to the nozzle tip before entering. The solids definitely moved faster above the jet than those below the jet (the movement of which is clearly visible) and the solids flow pattern was smooth and constant. While no bubbles were observed being diverted by the shroud, the shrouded jet was observed to be narrower and more stable. No completely defluidized zones within the shroud were evident from visual observation. The jet penetration length of the shrouded jet was lower than that of the non-shrouded jet. This is attributed to the increased rate of solids entrainment into the shrouded jet, which would cause it to decelerate more rapidly.

Table A.1: Differences Between Free Jet and Shrouded Jet

Parameter	Free Jet	Shrouded Jet
Motion	“Wave”-like	Smooth/continuous
Direction	Radial	Axial
Stability	Less stable	More stable
Entrainment Zone	Entire jet	Nozzle tip
Penetration	Greater	Lower

A.4 Concluding Remarks

Videos of a half-jet with and without a nozzle shroud indicate quite clearly that the flow patterns of gas and solids are strongly affected by the presence of the shroud. With the shroud, the gas jet entrains a larger amount of solids while entraining a significantly lower volume of gas. The shrouded jet is narrower, more stable, and penetrates less as a result of the deflection of bubbles and the increased solids entrainment rate. It was observed that while the solids move in intermittent waves towards the free jet, the solids move in a smooth continuous manner towards the shrouded jet at a faster rate.

A.5 Acknowledgements

The authors gratefully acknowledge the financial support of Syncrude Canada Ltd. and of the Natural Sciences and Engineering Research Council (NSERC) of Canada, in the form of an Industrial Post-Graduate Scholarship and of a Collaborative Research Development Grant.

A.6 Nomenclature

d	nozzle outlet diameter, m
F_g	motive gas mass flow rate, kg/s
N_{Re}	jet Reynolds number
u	axial velocity, m/s
\bar{u}	mean velocity component in the axial direction, m/s
u'	fluctuating component of the axial velocity, m/s
U_0	superficial fluidization gas velocity, m/s
V	motive gas velocity at the nozzle tip, m/s

Greek Letters

μ	motive gas viscosity, kg/m.s
ρ	motive gas density, kg/m ³

A.7 References

- Abromovich, G., *The Theory of Turbulent Jets*, Massachusetts: M.I.T. Press, 1963.
- Ariyapadi, S., Berruti, F., Briens, C., Griffith, P., Hulet, C., "Modeling the Injection of Gas-Liquid Jets into Fluidized Beds of Fine Particles", *Can. J. Chem. Eng.*, **81**, 891 – 899 (2003).
- Bohnet, M., Teifke, J., "New Results on the Efficiency Transformation in Gas-Solids-Injectors", *Proceedings - Reliable Flow of Particulate Solids: EFCE Publication Series (European Federation of Chemical Engineering)*, **49**, 383 – 400 (1985).
- Chen, L., Weinstein, H., "Shape and Extent of the Void Formed By a Horizontal Jet in a Fluidized Bed", *AIChE J.*, **39** (12), 1901 – 1909 (1993).
- De Michele, G., Elia, A., Massimilla, L., "The Interaction Between Jets and Fluidized Beds", *Ing. Chim. Ital.*, **12**, 155 – 162 (1976).
- Donadono, S., Maresca, A., Massimilla, L., "Gas Injection in Shallow Beds of Fluidized Coarse Solids", *Ing. Chim. Ital.*, **16**, 1 – 10 (1980).
- Felli, V., "Solids Entrainment From a Fluidized Bed into a Gas-Liquid Jet". *MESc Thesis*, The University of Western Ontario, (2002).
- Hulet, C., Briens, C., Berruti, F., Chan, E., Ariyapadi, S., "Entrainment and Stability of a Horizontal Gas-Liquid jet in a Fluidized Bed", *Int. J. Chem. React. Eng.*, **1** (A60), 1127, (2003).
- Idelchek, I., *Handbook of Hydraulic Resistance*, Boca Raton: CRC Press, 1994.
- Massimilla, L., "Gas Jets in Fluidized Beds", *Fluidization*, J. Davidson, R. Clift, D. Harrison, (Eds.), Academic Press: London, 1985, pp. 133 – 172.
- Merry, J., "Penetration of a Horizontal Gas Jet into a Fluidised Bed", *Trans. Instn. Chem. Engrs.*, **49**, 189 – 195 (1971).
- Sharpe, G., *Solving Problems in Fluid Dynamics*, New York: Wiley, 1994.

- Xuereb, C., Laguerie, C., Baron, T., "Etude du Comportement de Jets Continus Horizontaux ou Inclines Introduits Dans un Lit Fluidise Par un Gaz. II : Profiles de Vitesse du Gaz Dans Les Jets Horizontaux", *Powder Technol.*, **64**, 271 – 283 (1991a).
- Xuereb, C., Laguerie, C., Baron, T., "Etude du Comportement de Jets Continus Horizontaux ou Inclines Introduits Dans un Lit Fluidise Par un Gaz. I : Morphologie des Jets", *Powder Technol.*, **67**, 43 – 56 (1991b).
- Zhong, W., Xiao, R., Zhang, M., "Experimental Study of Gas Mixing in Spout-Fluid Bed", *AIChE J.*, **52** (3), 924 – 930 (2006).

APPENDIX B

Measurement Technique for the On-Line Detection of Fines in a Fluidized Bed

Matthew Dawe, Jennifer McMillan, Cedric Briens, Franco Berruti

*Department of Chemical and Biochemical Engineering
The University of Western Ontario
1151 Richmond Street
London, Ontario, Canada N6A 5B9*

B.1 Introduction

During the operation of fluidized beds, the size distribution of the particles in the bed is an important operating parameter. Specifically, knowledge of the proportion of fines, which are particles that are below an acceptable particle diameter, is important to maintain good fluidization quality in the bed, and to prevent too many particles from leaving the cyclones in the gas stream. Furthermore, in an experimental setting, the measurement of the proportion of fines in a fluidized bed can be a useful tool to evaluate the performance of nozzles or devices that increase or decrease the particle size.

Currently, one of the most common methods of monitoring particle size in a laboratory situation is to take a sample of particles from the fluidized bed and using equipment such as a laser diffraction device to analyze the sample. This method can be cumbersome, especially when the fluidized bed is not equipped with easy access to the particles in order to take the sample. Another measurement method used when the generation of fines is of interest is to weigh the fines collected by a cyclone and/or filter in the fluidized bed system. This technique can also be inconvenient, since long run times are often required to accumulate enough particles in the cyclone or filter for accurate weight measurements, and it can be difficult to collect all of the solids to be weighed from the cyclone or filter. Also, neither of these methods can be used for continuous processes, and so, during operation, the size characteristics of the bed particles are unknown.

The objective of this study was to develop a method to monitor the proportion of fines in a fluidized bed that does not require a stop in operation of the system. In order to achieve this objective, triboelectric probes were chosen as the measurement apparatus. Triboelectric probes have been used to monitor solids flow in cyclones (Da Silva et al., 2003), in fluidized beds (Lee et al., 1995), and in jets in fluidized beds (Dawe et al., 2006). The present study adapts these methods to the on-line monitoring of the proportion of fines in a fluidized bed.

Triboelectricity occurs when friction between a flowing stream and a metal surface causes the transfer of electrons between the two objects. If the metal surface is connected to the ground, a triboelectric current is obtained as electrons flow from the ground to the metal surface. A metal surface inserted into a two-phase, gas-solid flow will transfer an electrical current that is related to the local mass flux of particles hitting it (Soo et al., 1964). The intensity of the electrical current will vary, depending on the average size of the particles hitting the probe.

B.2 Experimental Setup

Experiments were conducted in a fluidized bed with a height of 3.2 m and a rectangular cross section of 1.0 m by 0.3 m, as shown in Figure B.1. The solids were silica sand particles with a density of 2650 kg/m^3 and an initial Sauter-mean diameter of $200 \text{ }\mu\text{m}$, which filled the column to a height of approximately 0.3 m. The bed was normally fluidized with air at a velocity of 0.09 m/s and entrained particles were separated from the gas stream by two cyclones in series. Particles from the primary cyclone were continuously returned to the fluidized bed by a dipleg. Particles from the secondary cyclone were collected after each run: under most of the studied conditions, their contribution to the new particle surface was negligible.

An attrition nozzle, with an internal diameter of 2.4 mm, was placed inside the bed at a distance of 0.16 m above the gas distributor, and injected air horizontally into the fluidized particles in order to grind the particles. A constant gas mass flow rate of 0.019 kg/s was supplied from a high-pressure cylinder to the injection nozzle during the grinding process. The mass gas flow rate was controlled by a pressure regulator and was

verified after each run by comparing the cylinder pressure before and after an injection, using a transducer connected to a data acquisition system.

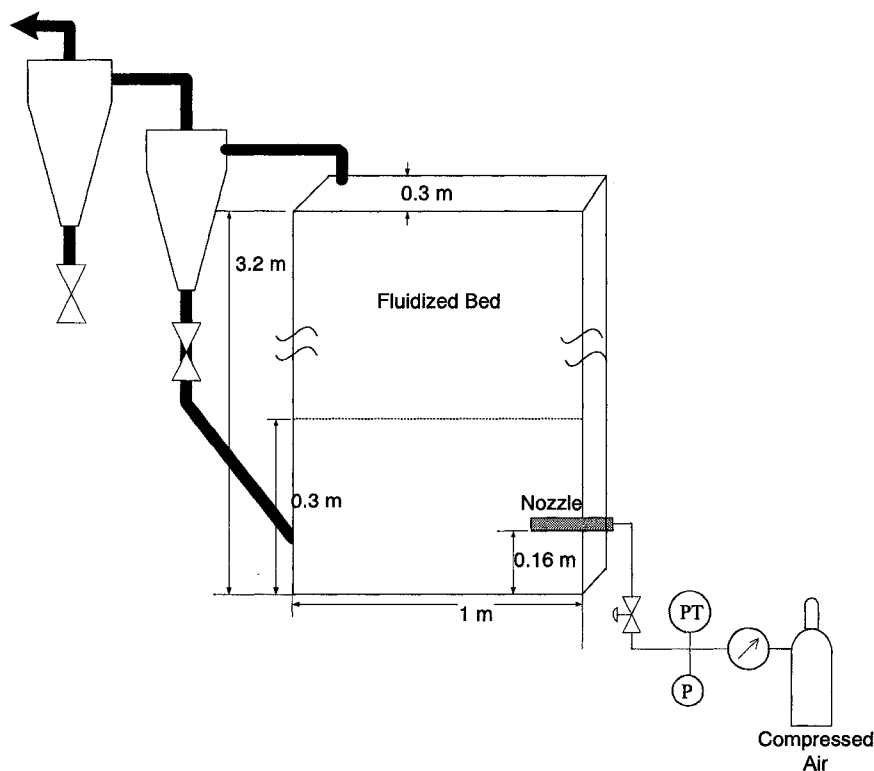


Figure B.1: Schematic Diagram of Fluidized Bed System

After each injection, the fluidization gas was stopped in order to slump the bed. The fluidization gas was then turned on again at a velocity just above the minimum bubbling velocity for approximately 5 minutes in order to mix the particles (separate experiments indicated that background particle attrition in the fluidized bed, in the absence of an attrition jet, was negligible when compared to the attrition observed with the nozzles). A sample of solids was taken from the bed before and after each injection and analyzed using a Malvern laser diffraction apparatus in order to obtain the size distribution of the bed particles.

To detect the proportion of fines in the bed after each injection, a measurement technique was developed, which used triboelectric probes. After each injection, the bed was fluidized using four different fluidization velocities; 0.065 m/s, 0.09 m/s, 0.12 m/s and 0.18 m/s, and triboelectric signals were obtained at each velocity.

The triboelectric probes used in this study were made from plain insulated copper wire with a diameter of 1.5 mm. A 5 mm piece of insulation was removed from the middle of each wire, creating an exposed section that acted as the actual probe. Twenty-eight triboelectric probes were strung through the fluidized bed so that they were in the same horizontal plane as the attrition nozzle. Fittings on each side of the column could be tightened on the wires to ensure that the wires remained taut and that the exposed section of each probe was positioned directly in the centre of the bed throughout the duration of each test. Signals from each probe traveled through the wire to an amplifier and then to the data acquisition system. A simplified diagram of the triboelectric probes can be seen in Figure B.2.

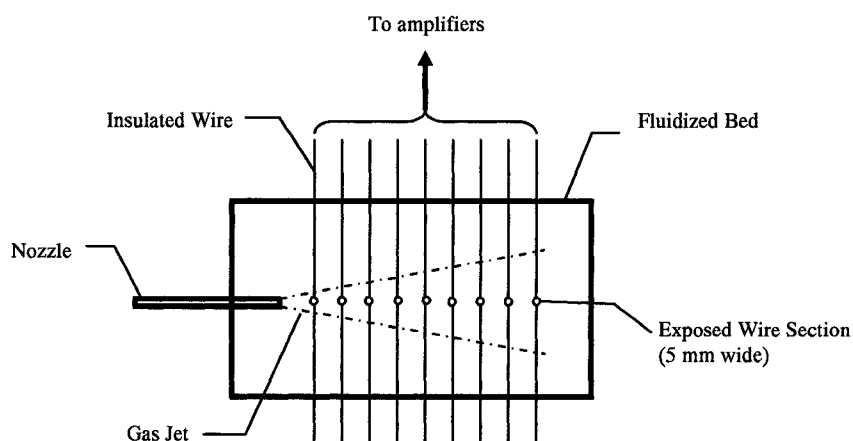


Figure B.2: Simplified Overhead View of Triboelectric Probe Setup

The triboelectric current generated by the friction of the particles on the metal probes was converted to voltage and amplified from a 0 - 200nA input to a 0 - 5V output. Data was obtained for 30 seconds at a sampling frequency of 1000 Hz.

B.3 Results and Discussion

Each triboelectric measurement yielded a raw signal of a voltage corresponding to the current between the ground and each triboelectric probe. Figures B.3 and B.4 show examples of raw triboelectric data obtained from a triboelectric probe. Figure B.3 shows the effect of fluidization velocity on the triboelectric signal, and Figures B.4 and B.5

show the effect of average particle size on the triboelectric signal. The intensity of the signal increases as the fluidization velocity increases, as the particle size decreases, and as the proportion of fines in the bed is increased. Also, a fluctuation of the signal was observed, which was attributed to the bubbles which are present in the fluidized bed.

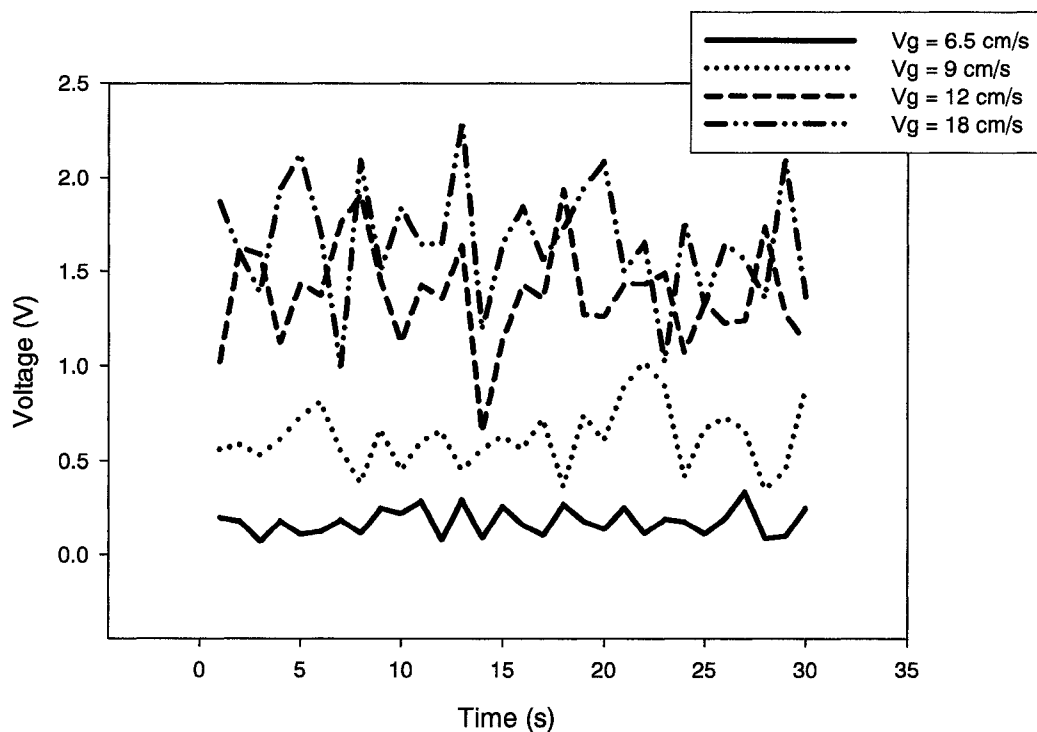


Figure B.3: Effect of Fluidization Velocity on Triboelectric Signal: $d_{psm} = 132 \mu\text{m}$

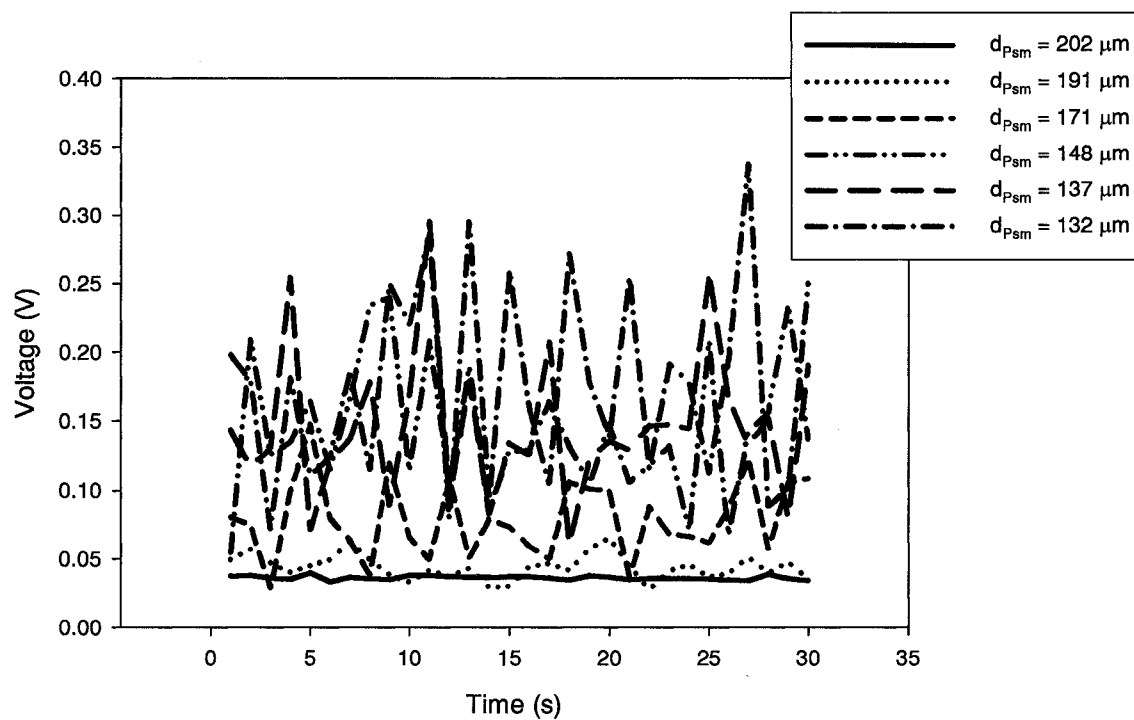
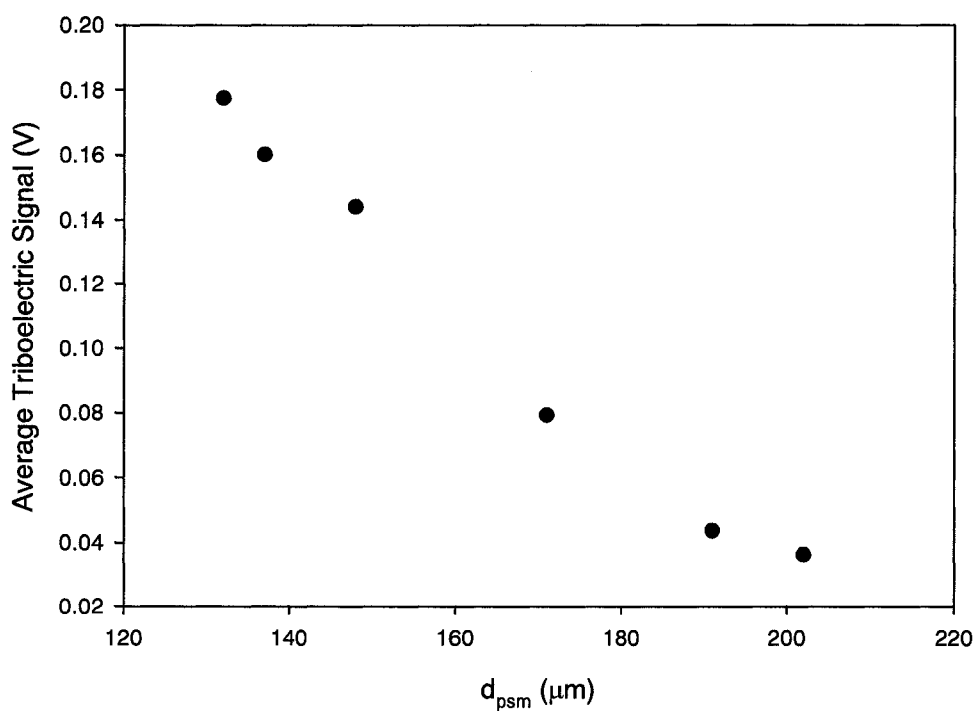


Figure B.4: Effect of Particle Diameter on Triboelectric Signal: $V_g = 0.065$ m/s



**Figure B.5: Effect of Particle Diameter on the Average Triboelectric Signal:
 $V_g = 0.065$ m/s**

A correlation was developed to estimate the proportion of fines in the bed from the triboelectric signals. Using multi-linear regression, a power law relationship was determined, which related the proportion of fines in the bed with a diameter less than 90 μm to the signal characteristics of the triboelectric probes. For each average bed particle diameter and fluidization velocity, the mean, absolute deviation, standard deviation, coefficient of variation, skewness and kurtosis of each signal from each of the 28 probes in the bed were calculated. In addition, the wavelet coefficients (using Daubechies 4), W statistics (Briens et al., 2003), and powers over specified frequency bands were calculated for each signal. The multi-linear regression program determined which characteristics of the signal would best relate to the proportion of fines in the bed, and the F statistic was applied to omit statistically insignificant terms from the equation. A simple equation which uses the mean value of the 28 triboelectric signals and the fluidization velocity of the bed was found to predict the proportion of fines in the bed with a diameter less than 90 μm quite well:

$$wt\% < 90\mu\text{m} = 0.936V_g^{-0.895} \bar{i}^{1.27} \quad (\text{B.1})$$

Where V_g is the fluidization velocity and \bar{i} is the mean triboelectric signal. Figure B.6 compares the experimental and calculated proportion of fines less than 90 μm .

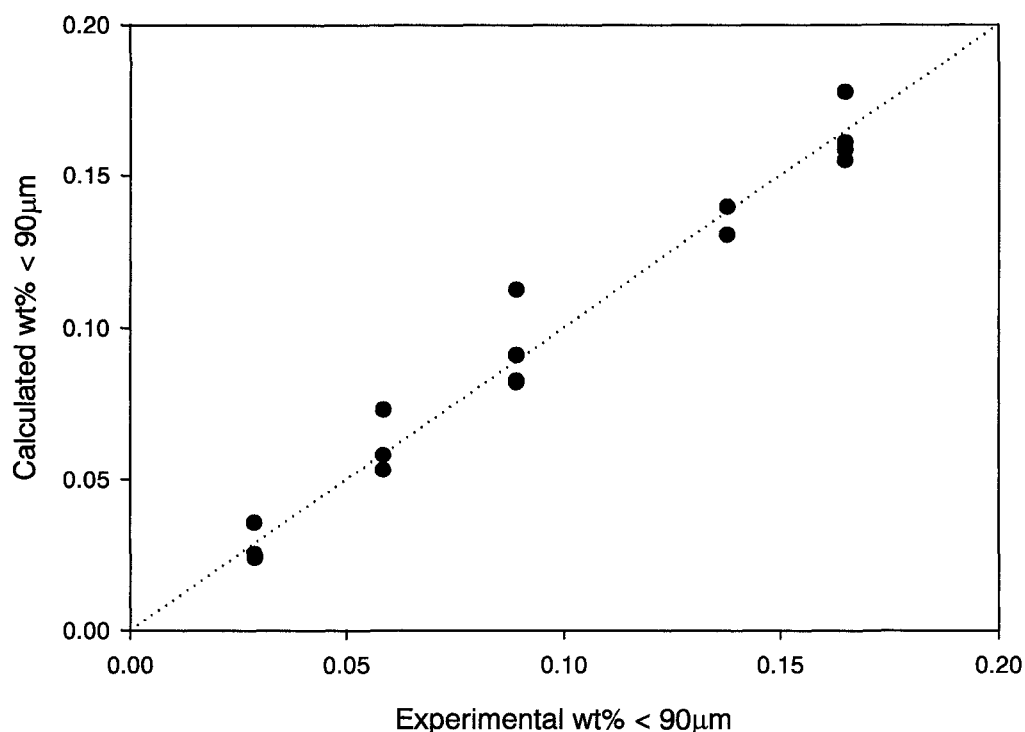


Figure B.6: Comparison Between Experimental and Calculated Results

In order to validate the expression, two critical tests were performed. The particles were ground to reduce the Sauter-mean diameter to 124 μm , and then triboelectric measurements were recorded at the four fluidization velocities. This Sauter-mean diameter of 124 μm was well below the Sauter-mean diameter in the bed for the runs used to determine the correlation. As a result, the proportion of fines in the bed was outside the range of values used to develop the correlation. However, the experimentally observed proportion of fines less than 90 μm matched quite well with the calculated value obtained using Equation B.1. For the second critical test, fresh solids were then added to the bed to increase the Sauter-mean diameter in the bed to 174 μm , and triboelectric measurements were once again recorded at the four fluidization velocities. Although the Sauter-mean diameter was similar to its values in some of the runs used to develop the correlation, the proportion of fines was quite different and the triboelectric signal was also quite different. When Equation B.1 was applied to these two critical tests, the experimental and calculated values were very similar, as shown in Figure B.7. Therefore, the empirical correlation that has been developed can be used to predict the

proportion of fines in the bed, and does not necessarily predict the average particle size in the bed.

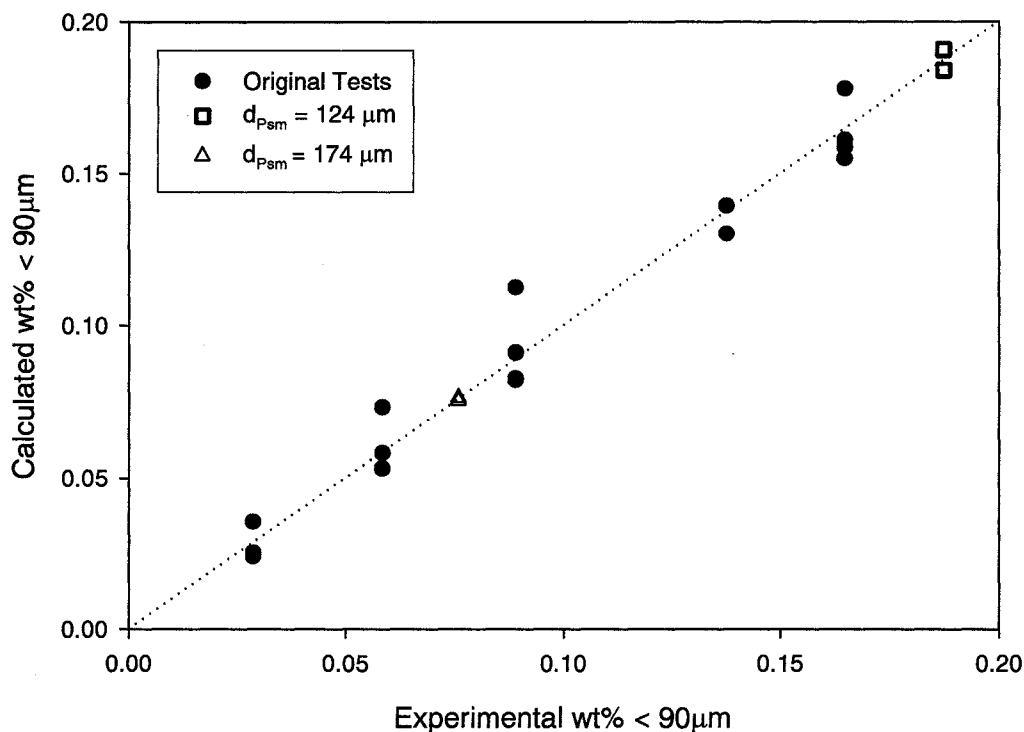


Figure B.7: Comparison Between Experimental and Calculated Results Including the Results of Two Critical Tests

B.4 Conclusion

In this study, a correlation was developed that can be used to calculate the proportion of fines in a fluidized bed based on triboelectric signals obtained within the bed. The correlation parameters will vary with the solid type. Simple, on-line monitoring of the proportion of fines can, thus, be performed.

B.5 Nomenclature

d_{psm}	Sauter-mean diameter (m)
\bar{i}	mean triboelectric signal (V)
V_g	fluidized bed superficial velocity (m/s)

B.6 References

- Briens, C., McDougall, S., Chan, E., "On-Line Detection of Bed Fluidity in a Fluidized Bed Coker", *Powder Technol.*, **138**, 160-168 (2003).
- Da Silva, P., Briens, C., Bernis, A., "Development of a New Rapid Method to Measure Erosion Rates in Laboratory and Pilot Plant Cyclones", *Powder Technol.*, **131**, 111-119 (2003).
- Dawe, M., Briens, C., Berruti, F., "Study of Gas-Liquid Jet Boundaries in a Gas-Solid Fluidized Bed", Submitted to *Powder Technol.*, (2006).
- Lee, S., Wang, B., "Effect of Particle-Tube Collision Frequency on Material Wastage of In-Bed Tubes in the Bubbling Fluidized Bed Combustor", *Wear*, **184**, 223-229 (1995).
- Soo, S., Trezek, G., Dimick, R., Hohnstreiter, G., "Concentrations and Mass Flow Distributions in a Gas-Solid Suspension", *I&EC Fund.*, **3**, 98-106 (1964).

APPENDIX C

Solid-Liquid Mixing Results Obtained with a Shrouded Gas-Liquid Nozzle

C.1 Introduction

The objective of this study was to test a modified version of the gas-liquid nozzle used in Chapter 5, and determine the quality of solid-liquid mixing. This modified nozzle has a shroud type device located on the nozzle tip. For proprietary reasons, a more detailed description of the nozzle cannot be provided. The original nozzle, used in Chapter 5, will be referred to as nozzle X, and the shrouded nozzle will be referred to as nozzle Y. The liquid-solid mixing when a free jet was injected into the bed was compared to the results obtained when a draft tube was located co-axially downstream of the spray nozzle. The effect of changing the distance between the draft tube and the spray nozzle was investigated as well. In addition, the results obtained with the type Y nozzle were compared to the results obtained with nozzle X.

C.2 Experimental Setup and Theory

The experimental technique that was used in Chapter 5 was applied to the case when nozzle Y was used. Figure C.1 shows the dimensions of the draft tube, and the measurement locations. A heat balance was used to obtain the local ratio of the liquid to solid flowrates. A mixing model of a turbulent gas-liquid jet injected horizontally in a fluidized bed of coke particles, presented by Ariyapadi et al. (2005), was used to determine the local liquid flowrate and local solids flowrate within the liquid spray jet cross-section and, consequently, their L/S ratio.

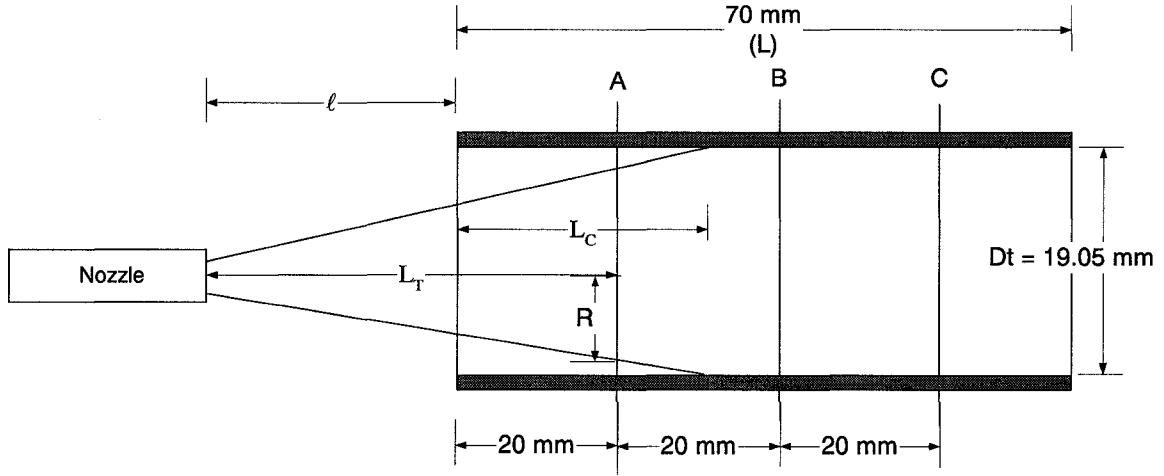


Figure C.1: Dimensions of Draft Tube and Locations of Positions A, B and C

C.3 Results and Discussion

Using the data obtained from the experiments, the quality of mixing in a free jet was compared to the quality of mixing when a draft tube mixer was introduced. The solid-liquid distribution depended on the distance from the nozzle to the draft tube (ℓ), the location in the draft tube where the jet impacted the wall (L_c) and the axial location in the draft tube. In order to compare the results, the mixing state at each location was defined by a mixing index that was based on the coefficient of variation of the L/S within the desired cross-section.

$$\text{Mixing Index} = 100 \left[1 - \frac{\sqrt{\frac{1}{N} \sum_{i=1}^N \left(\frac{L}{S}, i - \frac{1}{N} \sum_{i=1}^N \frac{L}{S}, i \right)^2}}{\frac{1}{N} \sum_{i=1}^N \frac{L}{S}, i} \right] \quad (\text{C.1})$$

This equation was chosen since it provides enough definition in the range of mixing results obtained in this study. Table C.1 summarizes the measurement locations and shows the mixing indices obtained with the Type Y nozzle when a draft tube mixer was placed downstream of the nozzle. Table C.2 shows a comparison of the Type X and Type Y nozzles when they are injected into the fluidized bed as a free jet. A high mixing

index corresponds to a well mixed system, where a value of 1 indicates perfect mixing and 0 very poor mixing.

Table C.1: Summary of Mixing Indices for Nozzle Y with a Draft Tube

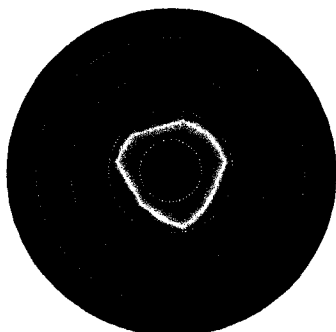
ℓ (mm)	Position in Draft Tube	L_T (mm)	L_c (mm) Nozzle Y	Mixing Index: Draft Tube Nozzle Y
12.7	A	32.7		0.23
12.7	B	52.7		0.72
12.7	C	72.7	58.4	0.8
25.4	A	45.4		0.5
25.4	B	65.4	45.7	0.64
25.4	C	85.4		0.75
38.1	A	58.1	33.	0.38
38.1	B	78.1		0.67
38.1	C	98.1		0.74
50.8	A	70.8	20.3	0.62
50.8	B	90.8		0.71
50.8	C	110.8		0.8
63.5	A	83.5	7.6	0.48
63.5	B	103.5		0.69
63.5	C	123.5		0.77
76.2	A	96.2	-	0.63
76.2	B	116.2		0.74
76.2	C	136.2		0.81

Table C.2: Comparison Between Nozzle X and Y

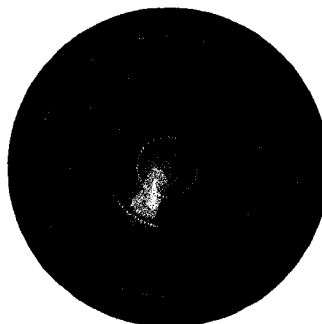
ℓ (mm)	L_T (mm)	Mixing Index: Free Jet Nozzle X	Mixing Index: Free Jet Nozzle Y
12.7	32.7	0.83	0.83
12.7	52.7	0.85	0.86
12.7	72.7	0.81	0.83
76.2	96.2	0.54	0.73
76.2	116.2	0.51	0.63
76.2	136.2	0.59	0.76

Contour plots of the liquid/solid distribution within the cross-sectional area of the jet spray were also created to compare the mixing results in the draft tube for different axial distances for the Type Y nozzle. For the results obtained using the draft tube mixer, the dimensionless cross-sectional area of the contour plots corresponded to the diameter of the draft tube. Results for ℓ of 12.7, 25.4, 38.1 and 50.8 mm are shown in Figure C.2.

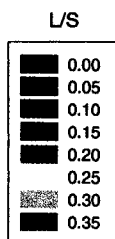
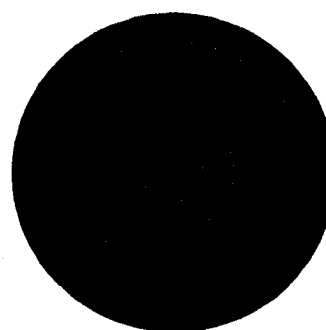
Type Y Nozzle
 $\ell = 12.7$ mm
Axial Position A



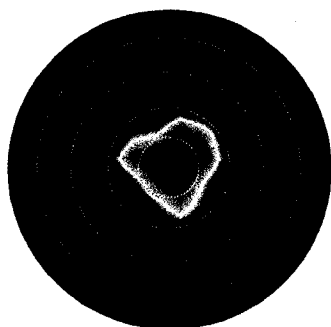
Type Y Nozzle
 $\ell = 12.7$ mm
Axial Position B



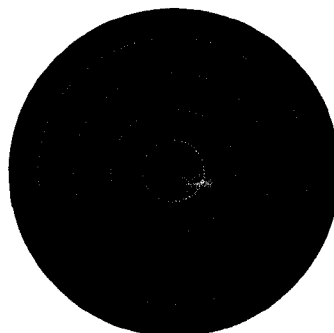
Type Y Nozzle
 $\ell = 12.7$ mm
Axial Position C



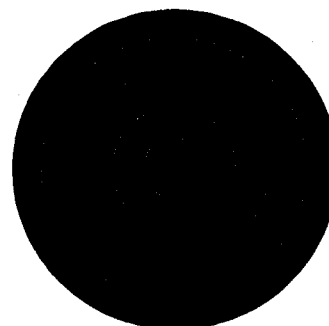
Type Y Nozzle
 $\ell = 25.4$ mm
Axial Position A



Type Y Nozzle
 $\ell = 25.4$ mm
Axial Position B



Type Y Nozzle
 $\ell = 25.4$ mm
Axial Position C



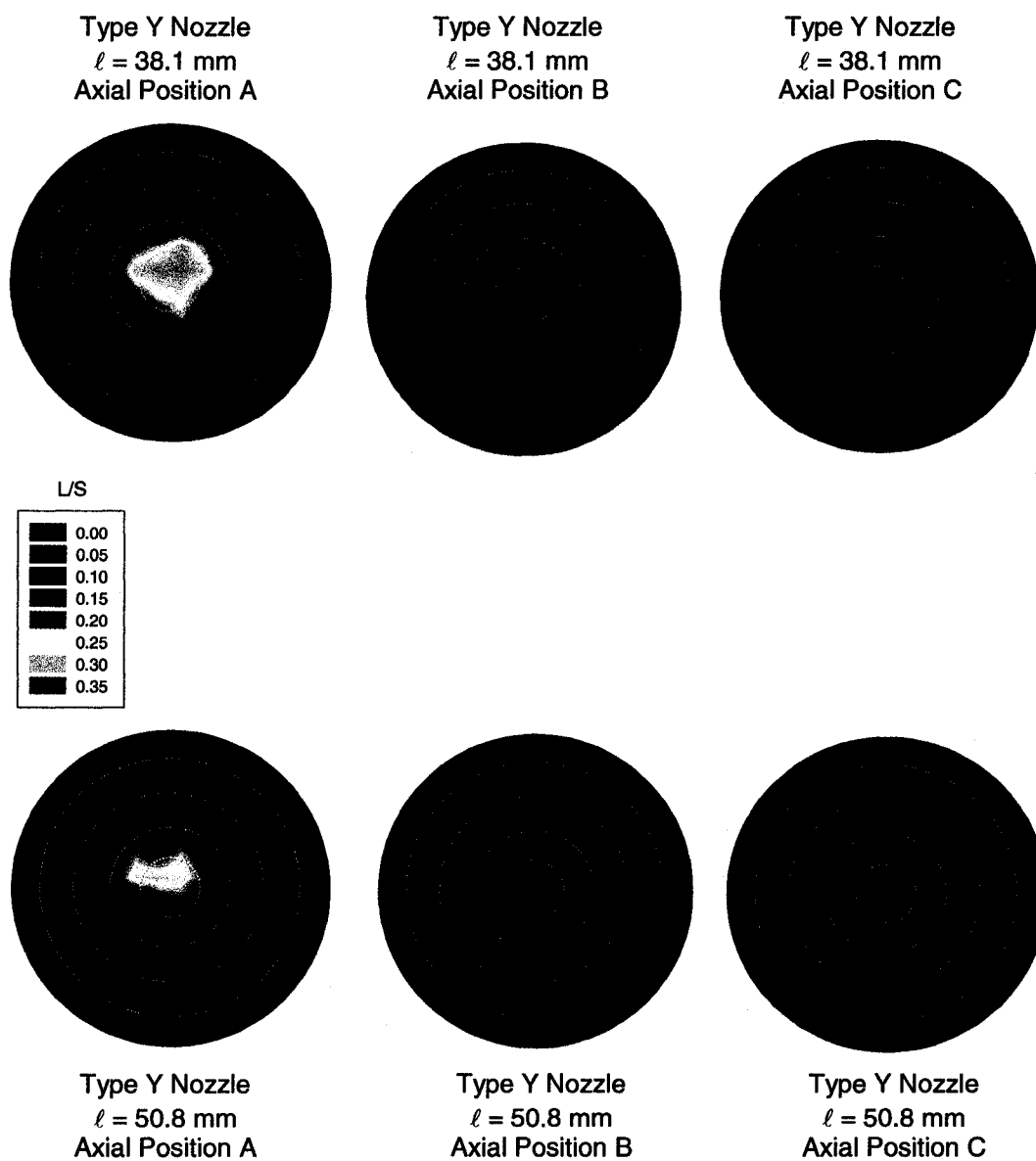


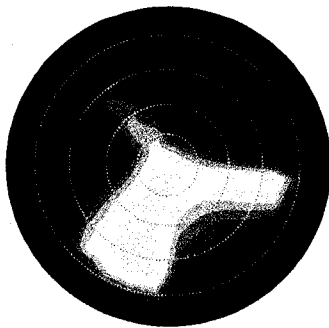
Figure C.2: Contour Plots of the L/S Distribution Within the Draft Tube at Locations A, B and C for the Type Y Nozzle

This figure shows the progression of mixing through the draft tube. For a distance of $\ell = 12.7$ mm, it can clearly be seen that the mixing improves along the length of the draft tube. There is a very high liquid-to-solid ratio in the centre of the draft tube at location A. However, as the axial distance inside the draft tube is increased, more solids are entrained into the jet, and the mixing is improved. In addition, there is a significant improvement in the mixing after the point that the jet impacts the draft tube wall. At an ℓ distance of 12.7 mm, the jet impacts the draft tube wall between axial positions B and C, and the mixing at axial position C, is significantly better than the mixing at location B. The significance of the distance ℓ , can also be demonstrated in this figure. At $\ell = 38.1$ mm the mixing is nearly perfect at location C, whereas for the distances of 12.7 and 25.4 mm, this is not the case. This could be explained by analyzing the location at which the jet impacts the draft tube wall. Hulet et al. (2003) found that the optimal distance, ℓ , occurs at a point where the jet impacts the draft tube wall 0.8 times into the length of the tube. In this study the jet contacts the draft tube wall 0.8 times into the length of the tube at a distance, $\ell = 38.1$ mm. As observed in Chapter 5, the jet hits the draft tube wall at 0.8 times the length of the draft tube at an ℓ distance of 25.4 mm for the type X nozzle. As a result, the best mixing is obtained at an ℓ distance of 25.4 mm for the type X nozzle, whereas the best mixing occurs at an ℓ distance of 38.1 mm for the type Y nozzle. The type Y nozzle has a smaller angle of expansion and, therefore, penetrates further before hitting the draft tube wall (Ariyapadi, 2003, 2004). The results observed in the contour plots agree well with the mixing indices. The mixing indices show that the quality of solid-liquid mixing increases as the axial distance in the draft tube is increased. At each ℓ distance, the mixing indices are the highest at location C, and the lowest at location A. The significance of ℓ can also be demonstrated from the mixing indices since the values for larger ℓ distances are higher than for lower ℓ distances. The effect of the jet interaction with the draft tube wall is particularly evident in the case when $\ell = 12.7$ mm. At location A, and B the L/S is very high and the liquid is not well distributed because the jet has not yet contacted the draft tube wall, and the spray behaves

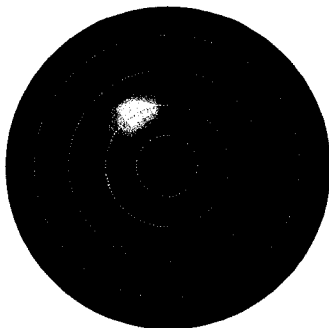
as a free jet. However, the jet comes into contact with the draft tube wall after location B, and the mixing at location C improves significantly.

In addition to studying the effect of using the draft tube mixer, data was obtained using a free jet with the Type Y nozzle, and the results were compared to the results obtained in a free jet using the Type X nozzle. For the results obtained in the free jet, the dimensionless cross-sectional area of the contour plots corresponds to the diameter of the liquid spray jet, which, for the Type Y nozzle, is calculated using a main jet expansion half angle of 3° and an initial jet expansion half angle of approximately 30° , which was based on the X-ray experiments performed by Ariyapadi et al. (2003). However, for the Type X nozzle, the main jet expansion half angle is 6° and the initial jet expansion half angle is 40° , which results in a much wider jet than the Type Y nozzle. In order to effectively compare the mixing between the two nozzles, the results obtained using the Type X nozzle were scaled accordingly to correspond to the dimensionless cross-sectional area of the liquid jet spray for the Type Y nozzle at the same axial position. Figure C.3 shows a comparison of the contour results obtained with the free jet for both the Type X and Type Y nozzles for L_T distances of 32.7, 52.7, 72.7, 96.2, 116.2 and 136.2 mm.

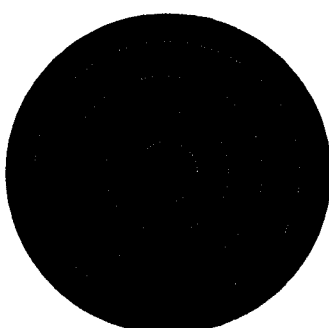
Type X Nozzle
Free Jet
 $L_T = 32.7$ mm



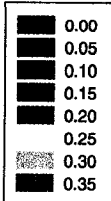
Type X Nozzle
Free Jet
 $L_T = 52.7$ mm



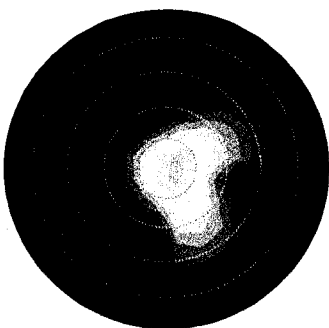
Type X Nozzle
Free Jet
 $L_T = 72.7$ mm



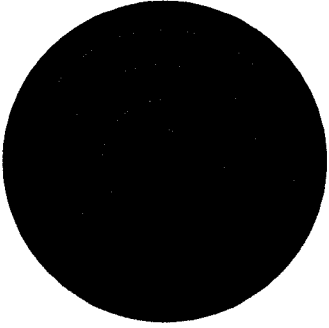
L/S



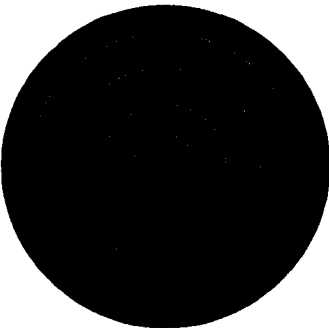
Type Y Nozzle
Free Jet
 $L_T = 32.7$ mm



Type Y Nozzle
Free Jet
 $L_T = 52.7$ mm



Type Y Nozzle
Free Jet
 $L_T = 72.7$ mm



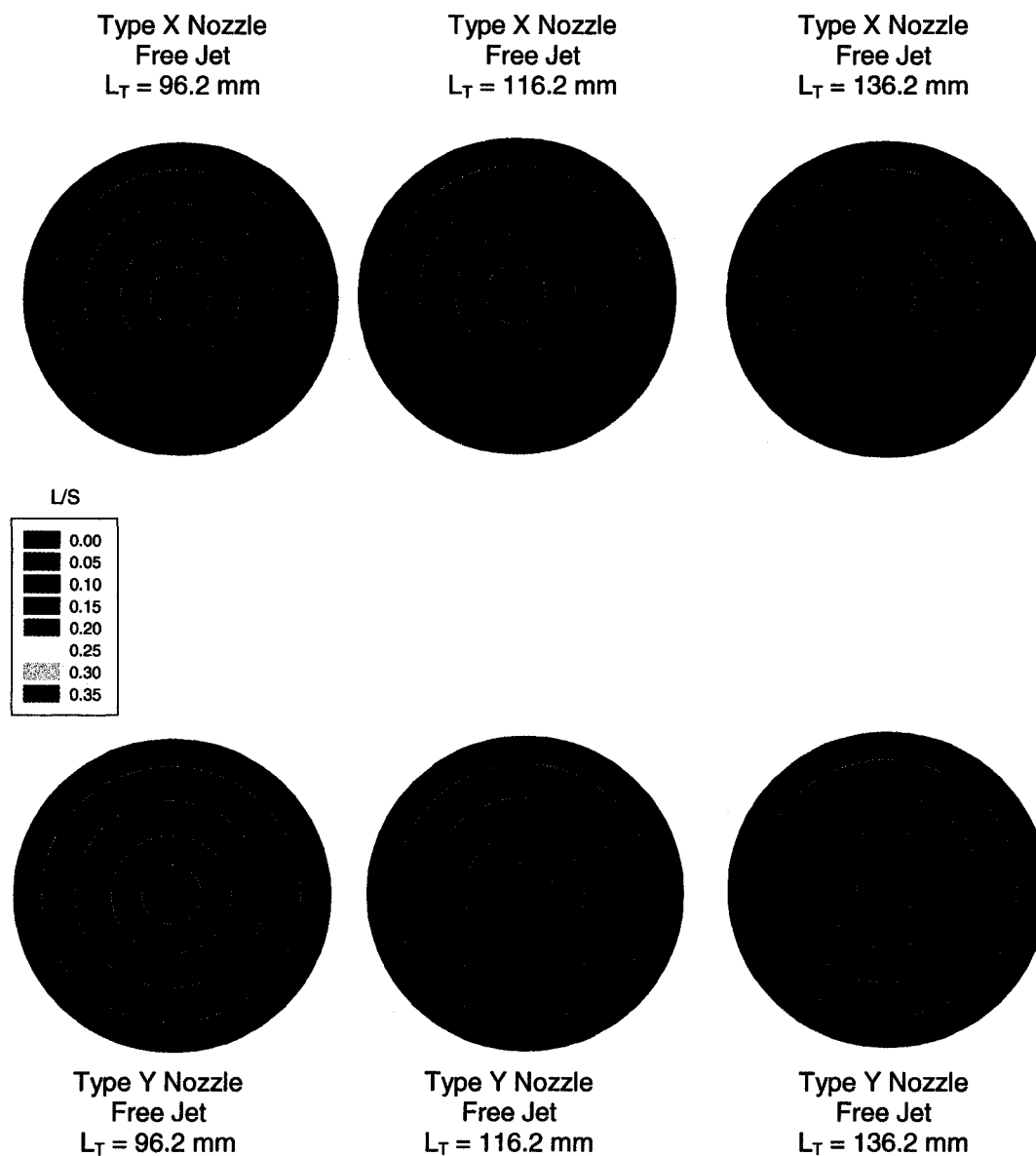


Figure C.3: Contour Plots of the L/S Distribution Within the Free Jet for the Type Y and Type X Nozzles

Both the contour plots and the mixing indices show that the liquid-solid mixing for both nozzles is very similar at distances closer to the nozzle tip. However, at distances further from the nozzle tip the mixing indices for the Type Y nozzle are much higher than the results obtained with the Type X nozzle. This is due to the fact that the extra shroud on nozzle Y increases the momentum of the jet and creates gas re-circulation zones near the nozzle tip, which help increase the particle entrainment into the jet. In addition, the Type Y nozzle penetrates further than the Type X nozzle (Ariyapadi et al., 2004), and therefore the Type Y's jet momentum is higher than the Type X nozzle, at the same axial distance. However, there is no significant impact of the extra solids entrainment apparent at locations closer to the nozzle tip, as there is a significant liquid core at these locations when the Type Y nozzle is used. This dense liquid core prevents the entrained solids from penetrating into the centre of the spray jet, thus decreasing the solid-liquid mixing.

Plots of the cumulative liquid distribution as a function of liquid to solid ratio (L/S) were also created in order to quantify the mixing and its impact on the coking reaction. To achieve high yields of valuable products, it is important to minimize the amount of liquid which is exposed to a high liquid to solid ratio. The cumulative plot of the liquid distribution (e.g. Figure C.4), should, therefore, be as vertical as possible indicating uniform mixing, and as much to the left as possible, indicating contact of the liquid with a large amount of solids. Figure C.4 shows the results for the case when a draft tube is used for ℓ distances of 25.4 mm.

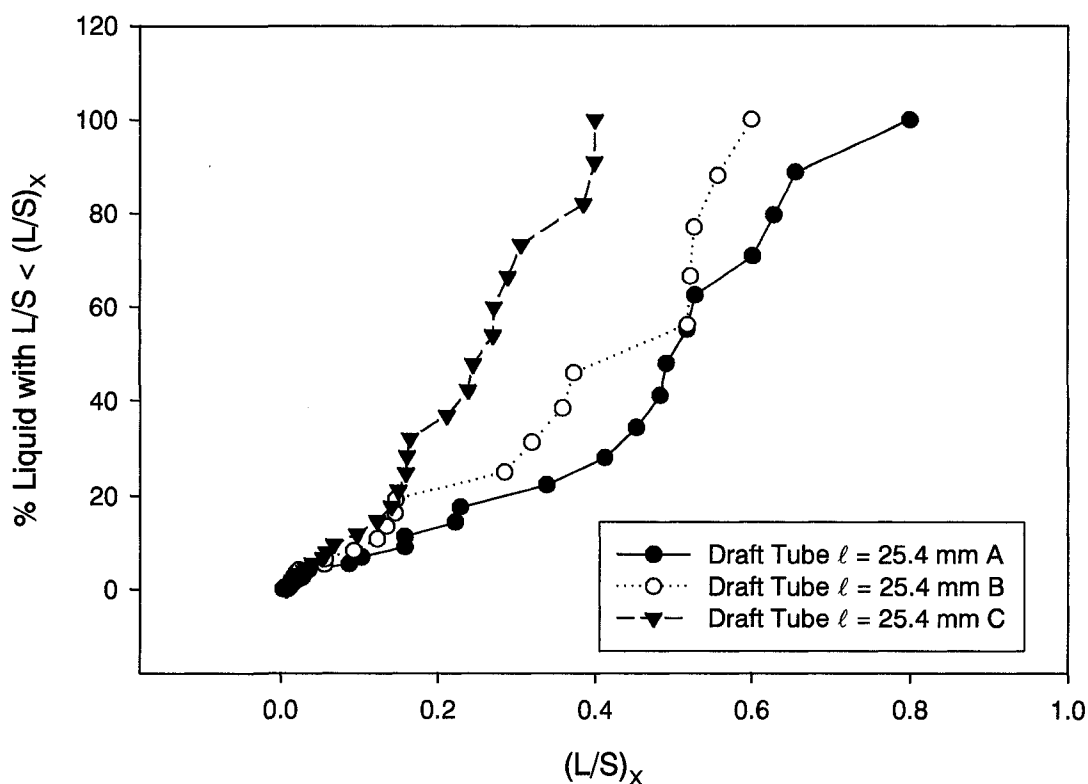


Figure C.4: Cumulative Distribution of Liquid Within the Draft Tube $\ell = 25.4$ mm for the Type Y Nozzle

As shown in Figure C.4, the mixing improves as the axial distance in the draft tube is increased. The significance of the interaction between the jet and the draft tube wall can also be observed in Figure C.4. At this particular ℓ distance, the jet hits the draft tube wall between locations B and C. The line in the graph corresponding to location C is much more vertical than for locations A and B, indicating that the mixing at this location is much more uniform.

Figures C.5a, C.5b and C.5c compare the liquid distribution in the free jet for the Type X and Type Y nozzles for distances (L_T) of 96.2, 116.2 and 136.2 mm, respectively. For each distance, the liquid distribution is much more uniform when the Type Y nozzle is used. The presence of the shroud on the Type Y nozzle enhances the shear rate of the fluid, which increases the drag force exerted on the particles. In addition, the shear forces create vortices within the jet cavity, which cause recirculation eddies, which results in an increase in particle entrainment. Moreover, due to the increased momentum of the Type

Y nozzle, momentum loss due to the fluidization gas is minimized. All of the results show that when the shrouded type nozzle (Type Y) was used, the liquid-solid mixing was improved, especially at distances further downstream from the nozzle tip.

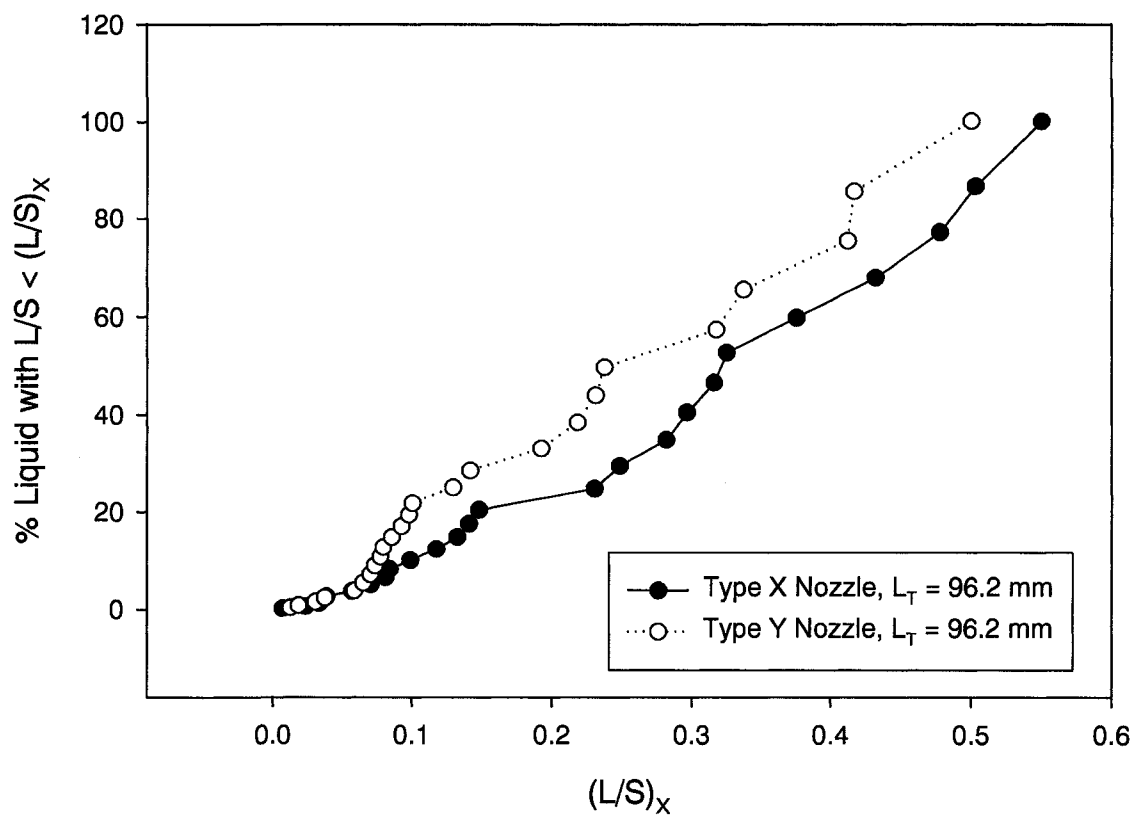


Figure C.5a: Cumulative Distribution of Liquid for a Free Jet at $L_T = 96.2$ mm

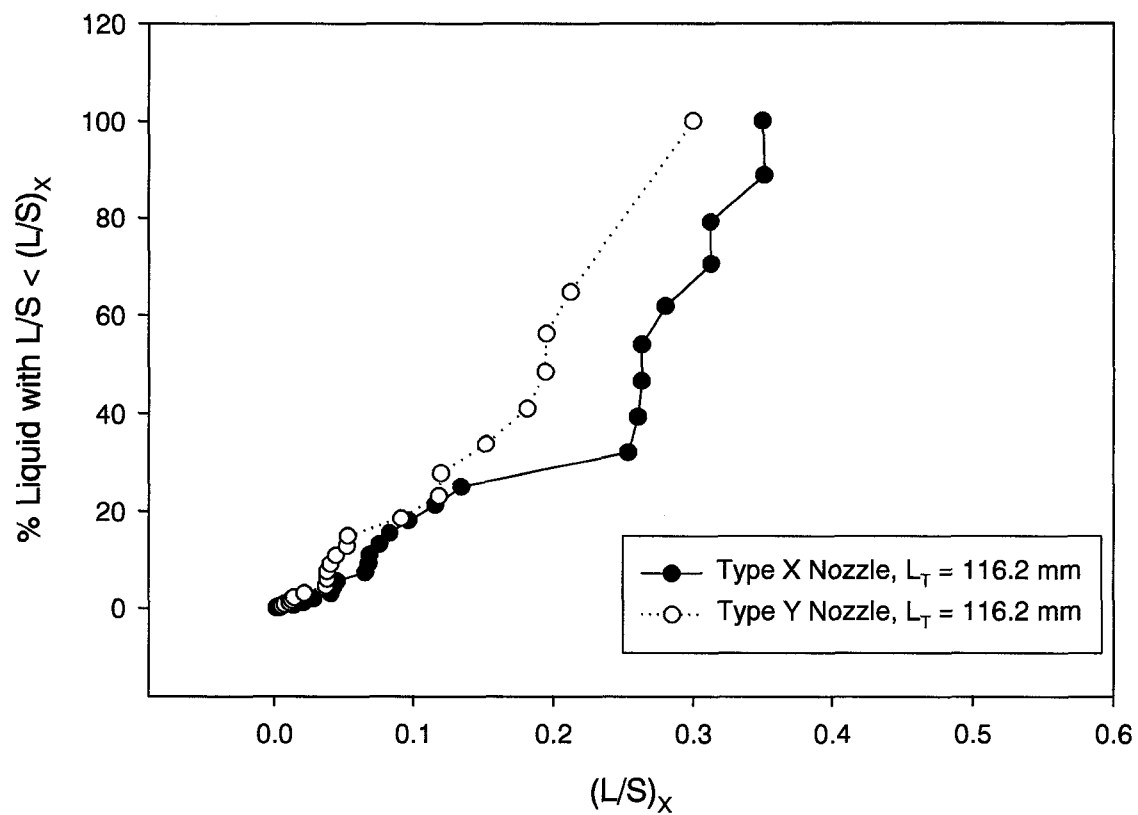


Figure C.5b: Cumulative Distribution of Liquid for a Free Jet at $L_T = 116.2$ mm

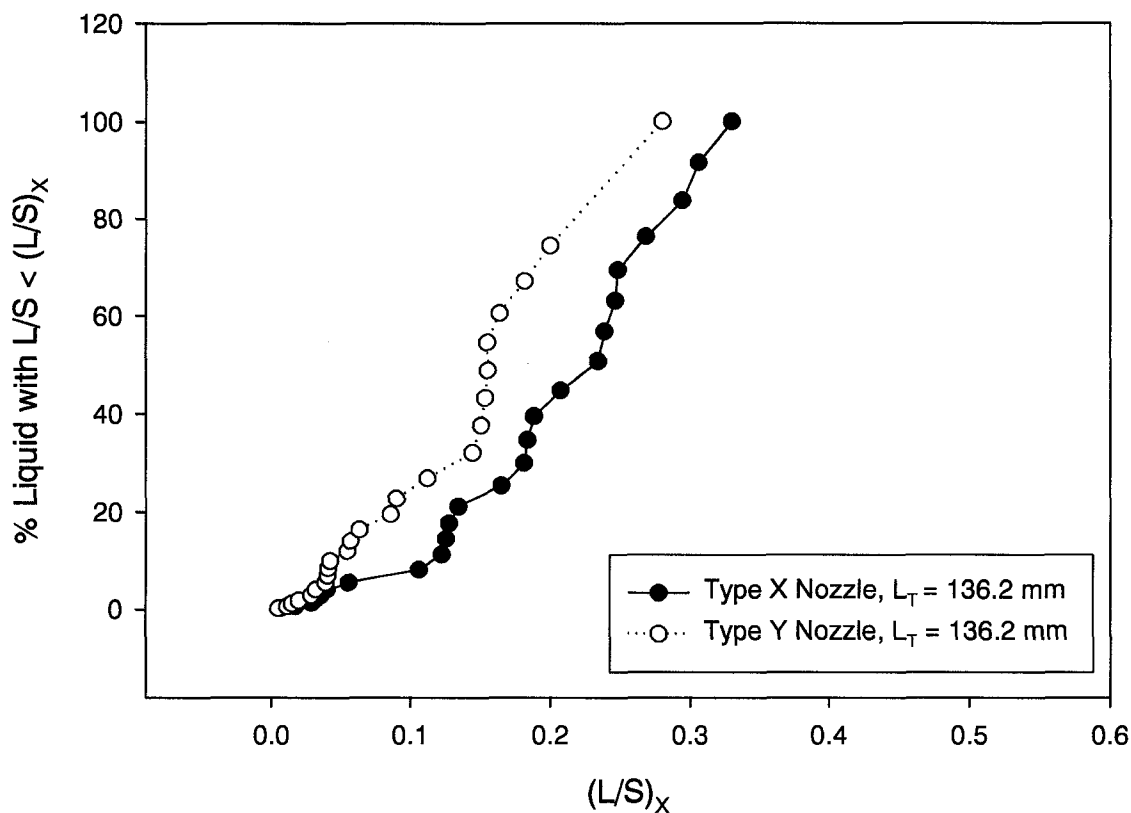


Figure C.5c: Cumulative Distribution of Liquid for a Free Jet at $L_T = 136.2$ mm

C.4 Nomenclature

d	diameter of nozzle (mm)
d_t	diameter of draft tube (m)
ℓ	length from nozzle to draft tube (cm)
L	length of draft tube (cm)
L_C	location where jet contacts draft tube wall (cm)
L_T	distance from nozzle to location where measurements were taken (cm)
L/S	liquid to solid ratio (-)
N	number of data points within cross-section (-)
R	Radius of jet (cm)

C.5 References

Ariyapadi, S., Holdsworth, D., Norley, C., Berruti, F., Briens, C., "Digital X-Ray Imaging Technique to Study the Horizontal Injection of Gas-Liquid Jets into Fluidized Beds", *Int. J. Chem. React. Eng.*, 1 (A56), 1114 (2003).

- Ariyapadi, S., Berruti, F., Briens, C., McMillan, J., Zhou, D. "Horizontal Penetration of Gas-Liquid Spray Jets in Gas-Solid Fluidized Beds", *Int. J. Chem. React. Eng.* **2**: (A22) (2004).
- Ariyapadi, S., McMillan, J., Zhou, D., Berruti, F., Briens, C., Chan, E., "Modeling the Mixing of a Gas-Liquid Jet Injected into a Fluidized Bed: The Effect of a Draft Tube", *Chem. Eng. Sci.*, **60**, 5738 - 5750 (2005).
- Hulet, C., Briens, C., Berruti, F., Chan, E., Ariyapadi, S., "Entrainment and Stability of a Horizontal Gas-Liquid jet in a Fluidized Bed", *Int. J. Chem. React. Eng.*, **1** (A60), 1127 (2003).

APPENDIX I

COPYRIGHT PERMISSION



American Chemical Society

Publications Division
Copyright Office

1155 Sixteenth Street, NW
Washington, DC 20036
Phone: (1) 202-872-4368 or -4367
Fax: (1) 202-776-8112 E-mail: copyright@acs.org

DATE: October 24, 2006

TO: Jennifer McMillan, Department of Chemical and Biochemical Engineering
The University of Western Ontario, London, ON, Canada

FROM: C. Arleen Courtney, Copyright Associate

Thank you for your request for permission to include your paper(s) or portions of text from your paper(s) in your thesis. Permission is now automatically granted; please pay special attention to the implications paragraph below. The Copyright Subcommittee of the Joint Board/Council Committees on Publications approved the following:

Copyright permission for published and submitted material from theses and dissertations

ACS extends blanket permission to students to include in their theses and dissertations their own articles, or portions thereof, that have been published in ACS journals or submitted to ACS journals for publication, provided that the ACS copyright credit line is noted on the appropriate page(s).

Publishing implications of electronic publication of theses and dissertation material

Students and their mentors should be aware that posting of theses and dissertation material on the Web prior to submission of material from that thesis or dissertation to an ACS journal may affect publication in that journal. Whether Web posting is considered prior publication may be evaluated on a case-by-case basis by the journal's editor. If an ACS journal editor considers Web posting to be "prior publication", the paper will not be accepted for publication in that journal. If you intend to submit your unpublished paper to ACS for publication, check with the appropriate editor prior to posting your manuscript electronically.

If your paper has not yet been published by ACS, we have no objection to your including the text or portions of the text in your thesis/dissertation in print and microfilm formats; please note, however, that electronic distribution or Web posting of the unpublished paper as part of your thesis in electronic formats might jeopardize publication of your paper by ACS. Please print the following credit line on the first page of your article: "Reproduced (or 'Reproduced in part') with permission from [JOURNAL NAME], in press (or 'submitted for publication'). Unpublished work copyright [CURRENT YEAR] American Chemical Society." Include appropriate information.

If your paper has already been published by ACS and you want to include the text or portions of the text in your thesis/dissertation in print or microfilm formats, please print the ACS copyright credit line on the first page of your article: "Reproduced (or 'Reproduced in part') with permission from [FULL REFERENCE CITATION.] Copyright [YEAR] American Chemical Society." Include appropriate information.

Submission to a Dissertation Distributor: If you plan to submit your thesis to UMI or to another dissertation distributor, you should not include the unpublished ACS paper in your thesis if the thesis will be disseminated electronically, until ACS has published your paper. After publication of the paper by ACS, you may release the entire thesis (not the individual ACS article by itself) for electronic dissemination through the distributor; ACS's copyright credit line should be printed on the first page of the ACS paper.

Use on an Intranet: The inclusion of your ACS unpublished or published manuscript is permitted in your thesis in print and microfilm formats. If ACS has published your paper you may include the manuscript in your thesis on an intranet that is not publicly available. Your ACS article cannot be posted electronically on a publicly available medium (i.e. one that is not password protected), such as but not limited to, electronic archives, Internet, library server, etc. The only material from your paper that can be posted on a public electronic medium is the article abstract, figures, and tables, and you may link to the article's DOI or post the article's author-directed URL link provided by ACS. This paragraph does not pertain to the dissertation distributor paragraph above.

06/07/06

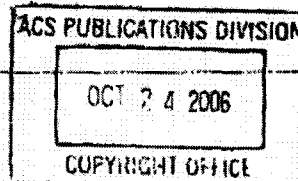
Arleen Courtney

From:

Sent: Monday, October 23, 2006 2:02 PM

To: Copyright

Subject: Permission to Reprint Article



I would like permission to reprint the entire article from your publication:

McMillan, J., Zhou, D., Ariyapadi, S., Briens, C., Berruti, F., Chan, E., "Characterization of the Contact Between Liquid Spray Droplets and Particles in a Fluidized Bed", *Industrial and Engineering Chemistry Research*, Vol 44, Issue 14, pp 4931 - 4939, 2005.

This material is to appear in my PhD dissertation at the University of Western Ontario, London, Ontario, Canada.

Sincerely,

Jennifer McMillan

Dear Ms McMillan

We hereby grant you permission to reproduce the material detailed below at no charge in your thesis subject to the following conditions:

1. If any part of the material to be used (for example, figures) has appeared in our publication with credit or acknowledgement to another source, permission must also be sought from that source. If such permission is not obtained then that material may not be included in your publication/copies.

2. Suitable acknowledgement to the source must be made, either as a footnote or in a reference list at the end of your publication, as follows:

"Reprinted from Publication title, Vol number, Author(s), Title of article, Pages No., Copyright (Year), with permission from Elsevier".

3. Reproduction of this material is confined to the purpose for which permission is hereby given.

4. This permission is granted for non-exclusive English rights only. For other languages please reapply separately for each one required. Permission excludes use in an electronic form. Should you have a specific electronic project in mind please reapply for permission.

5. This includes permission for the Library and Archives of Canada to supply single copies, on demand, of the complete thesis. Should your thesis be published commercially, please reapply for permission.

Yours sincerely

Marion Moss
Senior Rights Assistant
Elsevier Ltd
The Boulevard
Langford Lane
Kidlington
Oxford
OX5 1GB

This Email was sent from the Elsevier Corporate Web Site and is related
to Obtain Permission form:

To use the following material:

ISSN/ISBN:

Title: Powder Technology

Author(s): J. McMillan, D. Zhou, M. Saberian, C. Briens, ...

Volume: 161

Issue: 3

Year: 2006

Pages: 175 - 184

Article title: Measurement Techniques to Characterize Contact...

How much of the requested material is to be used:

The entire article

Are you the author: Yes

Author at institute: Yes

How/where will the requested material be used: [how_used]

Details:

I would like permission to reprint the entire article to include in my
PhD dissertation at the University of Western Ontario.

Additional Info:

- end -

For further info regarding this automatic email, please contact:
WEB APPLICATIONS TEAM (esweb.admin@elsevier.co.uk)

Subject RE: Obtain Permission
From
Date Tuesday, October 24, 2006 5:48 am
To

Dear Ms McMillan

We hereby grant you permission to reproduce the material detailed below at no charge in your thesis subject to the following conditions:

1. If any part of the material to be used (for example, figures) has appeared in our publication with credit or acknowledgement to another source, permission must also be sought from that source. If such permission is not obtained then that material may not be included in your publication/copies.

2. Suitable acknowledgement to the source must be made, either as a footnote or in a reference list at the end of your publication, as follows:

"Reprinted from Publication title, Vol number, Author(s), Title of article, Pages No., Copyright (Year), with permission from Elsevier".

3. Reproduction of this material is confined to the purpose for which permission is hereby given.

4. This permission is granted for non-exclusive English rights only. For other languages please reapply separately for each one required. Permission excludes use in an electronic form. Should you have a specific electronic project in mind please reapply for permission.

5. This includes permission for the Library and Archives of Canada to supply single copies, on demand, of the complete thesis. Should your thesis be published commercially, please reapply for permission.

Yours sincerely

Marion Moss
Senior Rights Assistant
Elsevier Ltd
The Boulevard
Langford Lane
Kidlington
Oxford
OX5 1GB

This Email was sent from the Elsevier Corporate Web Site and is related to Obtain Permi

To use the following material:

ISSN/ISBN:

Title: Chemical Engineering and Processing

Author(s): J. McMillan, C. Briens, F. Berruti

Volume: 45

Issue: 9

Year: 2006

Pages: 798 - 805

Article title: Flow Stability in a Downer Mixing Chamber

How much of the requested material is to be used:

The entire article

Are you the author: Yes

Author at institute: Yes

How/where will the requested material be used: In a thesis or dissertation

Details:

I would like permission to reprint the entire article in my PhD dissertation at the University of Western Ontario.

Additional Info:

- end -

For further info regarding this automatic email, please contact:
WEB APPLICATIONS TEAM (esweb.admin@elsevier.co.uk)

CURRICULUM VITAE

Name:	Jennifer McMillan
Post-secondary Education and Degrees:	The University of Western Ontario London, Ontario, Canada 1999 – 2003 B.E.Sc.
Honours and Awards:	NSERC Industrial Postgraduate Scholarship (IPS-2) 2005 – 2006 UWO Graduate Tuition Scholarship Award 2003 - 2006 Ontario Graduate Scholarship 2004 - 2005 Dean's Honour List 1999-2003 Four-Year Continuing Admission Scholarship 1999 – 2003 Faculty of Engineering Alexander Charles Spenser Scholarship 1999
Related Work Experience:	Visiting Engineer Syncrude Canada Limited, Edmonton Jan 2005 - May 2005, Apr 2006 – Sept 2006 Society of Graduate Students (SOGS) Councillor The University of Western Ontario, London Jan 2004 – Dec 2004 Teaching Assistant The University of Western Ontario, London 2003 – 2006 Research Assistant The University of Western Ontario, London May 2003 – Aug 2003

Patents and Publications:

McMillan, J., Briens, C., Berruti, F., Chan, E., “Study of High Velocity Attrition Nozzles in Fluidized Beds”, Accepted for publication in: *Fluidization XII*, Harrison Hot Springs, Canada, May, 2007.

McMillan, J., C. Briens, F. Berruti, E. Chan (2006) “High Velocity Attrition Nozzles in Fluidized Beds”, Submitted to *Powder Technology*.

McMillan, J., C. Briens, F. Berruti, E. Chan (2006) “Modeling the Particle Attrition Mechanism of a Sonic Gas Jet Injected into a Fluidized Bed”, Submitted to *Chemical Engineering Science*.

McMillan, J., C. Briens, F. Berruti (2006) “Flow Stability in a Downer Mixing Chamber”. *Chemical Engineering and Processing*, 45, 798-805.

McMillan, J., D. Zhou, M. Saberian, C. Briens, F. Berruti (2006) “Measurement Techniques to Characterize the Contact Between Injected Liquid and Circulating Solids in a Downer Mixing Chamber”. *Powder Technology*, 161, 175-184.

McMillan, J., D. Zhou, S. Ariyapadi, C. Briens, F. Berruti, E. Chan (2005) “Characterization of the Contact Between Liquid Spray Droplets and Particles in a Fluidized Bed”. *Industrial and Engineering Chemistry Research*, 44(14), 4931-4939.

McMillan, J., D. Zhou, M. Saberian, C. Briens, F. Berruti (2005) “Mixing Between Injected Liquid Feed and Circulating Solids in a Mixing Chamber Downer”. *Proceedings from the 8th International Conference on Circulating Fluidized Beds*, 697-703.

Ariyapadi, S., J. McMillan, D. Zhou, F. Berruti, C. Briens, E. Chan (2004) “Modeling the Mixing of a Gas-Liquid Spray Jet Injected in a Gas-Solid Fluidized Bed: The Effect of the Draft Tube”. *Chemical Engineering Science*, 60(21), 5738-5750.

Ariyapadi, S., F. Berruti, C. Briens, J. McMillan, D. Zhou, (2004) “Horizontal Penetration of Gas-Liquid Spray Jets in Gas-Solid Fluidized Beds”. *International Journal of Chemical Reactor Engineering*, 2 (A22), 1148-1166.

McMillan, J., Briens, C., Berruti, F., Floryan, J., “Attrition Nozzles with Inserts”; pending patent.

Hulet, C., McMillan, J., Briens, C., Berruti, F., “Shrouded Attrition Nozzle”; pending patent.

Dawe, M., McMillan, J., Briens, C., Berruti, F., “Probe for Monitoring the Proportion of Fine Particles in a Fluidized Bed”; pending patent.